

ADVANCEMENT OF HAZARD-CONSISTENT GROUND MOTION
SELECTION METHODOLOGY

A DISSERTATION
SUBMITTED TO THE DEPARTMENT OF CIVIL AND
ENVIRONMENTAL ENGINEERING
AND THE COMMITTEE ON GRADUATE STUDIES
OF STANFORD UNIVERSITY
IN PARTIAL FULFILLMENT OF THE REQUIREMENTS
FOR THE DEGREE OF
DOCTOR OF PHILOSOPHY

Ting Lin
August 2012

© 2012 by Ting Lin. All Rights Reserved.

Re-distributed by Stanford University under license with the author.



This work is licensed under a Creative Commons Attribution-Noncommercial 3.0 United States License.

<http://creativecommons.org/licenses/by-nc/3.0/us/>

This dissertation is online at: <http://purl.stanford.edu/fg174sf6778>

I certify that I have read this dissertation and that, in my opinion, it is fully adequate in scope and quality as a dissertation for the degree of Doctor of Philosophy.

Jack Baker, Primary Adviser

I certify that I have read this dissertation and that, in my opinion, it is fully adequate in scope and quality as a dissertation for the degree of Doctor of Philosophy.

Gregory Deierlein

I certify that I have read this dissertation and that, in my opinion, it is fully adequate in scope and quality as a dissertation for the degree of Doctor of Philosophy.

Eduardo Miranda

I certify that I have read this dissertation and that, in my opinion, it is fully adequate in scope and quality as a dissertation for the degree of Doctor of Philosophy.

Curt Haselton

Approved for the Stanford University Committee on Graduate Studies.

Patricia J. Gumport, Vice Provost Graduate Education

This signature page was generated electronically upon submission of this dissertation in electronic format. An original signed hard copy of the signature page is on file in University Archives.

Abstract

Performance-based earthquake engineering (PBEE) quantifies the seismic hazard, predicts the structural response, and estimates the damage to building elements, in order to assess the resulting losses in terms of dollars, downtime, and deaths. This dissertation focuses on the ground motion selection that connects seismic hazard and structural response, the first two elements of PBEE, to ensure that the ground motion selection method to obtain structural response results is consistent with probabilistic seismic hazard analysis (PSHA).

Structure- and site-specific ground motion selection typically requires information regarding the system characteristics of the structure (often through a structural model) and the seismic hazard of the site (often through characterization of seismic sources, their occurrence frequencies, and their proximity to the site). As the ground motion intensity level changes, the target distribution of important ground motion parameters (e.g., magnitude and distance) also changes. With the quantification of contributing ground motion parameters at a specific spectral acceleration (S_a) level, a target response spectrum can be computed using a single or multiple ground motion prediction models (GMPMs, previously known as attenuation relations). Ground motions are selected from a ground motion database, and their response spectra are scaled to match the target response spectrum. These ground motions are then used as seismic inputs to structural models for nonlinear dynamic analysis, to obtain structural response under such seismic excitations. This procedure to estimate structural response results at a specific intensity level is termed an intensity-based assessment. When this procedure is repeated at different intensity levels to cover the frequent to rare levels of ground motion (expressed in terms of S_a), a risk-based assessment can be performed by integrating the structural response results at each intensity level with their corresponding seismic hazard occurrence (through the seismic hazard curve).

This dissertation proposes that a more rigorous ground motion selection methodology will carefully examine the aleatory uncertainties from ground motion parameters, incorporate the epistemic uncertainties from multiple GMPMs, make adaptive changes to ground motions at various intensity levels, and use the Conditional Spectrum (CS) as the new target spectrum. The CS estimates the distribution (with mean and standard deviation) of the response spectrum, conditioned on the occurrence of a target Sa value at the period of interest. By utilizing the correlation of Sa values across periods, the CS removes the conservatism from the Uniform Hazard Spectrum (which assumes equal probabilities of exceedance of Sa at all periods) when used as a target for ground motion selection, and more realistically captures the Sa distributions away from the conditioning period. The variability of the CS can be important in structural response estimation and collapse prediction. To account for the spectral variability, aleatory and epistemic uncertainties can be incorporated to compute a CS that is fully consistent with the PSHA calculations upon which it is based. Furthermore, the CS is computed based on a specified conditioning period, whereas structures under consideration may be sensitive to multiple periods of excitation. Questions remain regarding the appropriate choice of conditioning period when utilizing the CS as the target spectrum.

To advance the computation and the use of the CS in ground motion selection, contributions have been made in the following areas:

- The computation of the CS has been refined by incorporating multiple causal earthquakes and GMPMs.
- Probabilistic seismic hazard deaggregation of GMPMs provides the essential input for such refined CS computation that maintains the rigor of PSHA.
- It is shown that when utilizing the CS as the target spectrum, risk-based assessments are relatively insensitive to the choice of conditioning period when ground motions are carefully selected to ensure hazard consistency.
- Depending on the conditioning period, the structural analysis objective, and the target response spectrum, conclusions regarding appropriate procedures for selecting ground motions may differ.

Acknowledgements

This work is funded by the U.S. Geological Survey (USGS) external grants program, the Pacific Earthquake Engineering Research Center (PEER), the Applied Technology Council (ATC), and the John A. Blume Engineering Graduate Fellowship. The generous support from the funding agencies is graciously acknowledged. These funding opportunities also allow me to collaborate with government research scientists, university professors, and industrial practitioners, who share similar passion for probabilistic seismic hazard analysis and ground motion selection. Their insightful perspectives have motivated me to connect research and practice while tackling the challenges of computing and applying the Conditional Spectrum. Without the USGS seismic hazard interactive deaggregation team, the implementation of the Ground Motion Prediction Model deaggregation and the Conditional Mean Spectrum computation for U.S. sites would not be possible. It is a pleasure to work with my co-authors Steve Harmsen and Nico Luco who make the USGS implementation a reality and teach me lots along the way. Also, thanks to Eric Martinez for his assistance on the USGS implementation. I enjoy the lively presentations and discussions with the PEER Ground Motion Selection and Modification group and the Consortium of Organizations for Strong Motion Observation Systems at numerous meetings. It is an honor to be part of the ATC-82 project team working together on the NIST (2011) report. I would like to thank my co-author Curt Haselton for sharing his structural models, as well as his challenging question of “what does this mean for building code?” followed by incredible inputs. I would also like to acknowledge the contributions of Jared DeBock and Fortunato Enriquez in conducting the structural analyses used in this study. I am grateful to Jon Heintz, Andrew Whittaker, Norm Abrahamson, Bob Bachman, Charlie Kircher, Ron Hamburger, Jon Stewart, Jon Bray, Jack Moehle, Gail Atkinson, John Hooper, Bill Holmes, and many others

for their leadership and encouragements. My gratitude also goes to Racquel Hagen, Kim Vonner, Brenda Sampson, Jill Nomura, Sandra Wetzels, Heidi Faison, and Ayse Hortacsu for their administrative support.

I am indebted to my dissertation oral defense and reading committee, Greg Deierlein, Eduardo Miranda, and Curt Haselton, for the exciting discussions and thoughtful comments that keep me nerdily entertained. Thanks to my oral defense chair, Eric Dunham, for orchestrating one of the most enjoyable events of my life. I am grateful to many Cornell professors and Ronnie Borja for enticing me to PhD at Stanford, Anne Kiremidjian for serving on my qualifying exam committee, Sarah Billington for allowing me to design fracture experiments, and Kincho Law for the computational dynamics fun. The PhD years have been memorable encircled by the collegiality of past and present Blume Center fellows and the Baker Research Group members – you know who you are! I would also like to thank Brendon Bradley, Gabriel Toro, Ned Field, Ivan Wong, and anonymous reviewers for their helpful reviews that improve the quality of the manuscript. Last but not least, I very much appreciate the outstanding guidance in research and generous advice in teaching and many other aspects offered by my academic father, Jack Baker – what a rare fortunate event to follow a role model for n years! Thank you for smiling through the tougher patches with me. What you have taught me would remain extremely valuable in many years to come. The intellectual interactions with all of you are so enlightening that I look forward to more in the future.

I would like to dedicate this dissertation to my family and friends for their unconditional love and support, and the late Prof. Allin Cornell, Prof. Steve Schneider, and Prof. Helmut Krawinkler for their inspirational work.

Contents

Abstract	iv
Acknowledgements	vi
1 Introduction	1
1.1 Background and motivation	1
1.2 Objectives and scope	4
1.3 Contributions and chapter organization	7
2 Deaggregation of ground motion prediction models	10
2.1 Abstract	10
2.2 Introduction	11
2.3 Methodology	12
2.3.1 Probabilistic seismic hazard analysis	13
2.3.2 Parameters for ground motion prediction	13
2.3.3 Deaggregation of magnitude, distance, and epsilon	14
2.3.4 Deaggregation of other parameters	16
2.3.5 Deaggregation of ground motion prediction models	17
2.3.6 Deaggregation of GMPM-specific parameters	17
2.4 Example application	18
2.4.1 Description of site and events	18
2.4.2 PSHA computation	19
2.4.3 Deaggregation of events	19
2.4.4 Deaggregation of GMPMs	20

2.4.5	Deaggregation of ground motion parameters	20
2.5	Availability of GMPM deaggregation	20
2.6	Conclusions	21
3	Refinements to the Conditional Spectrum computation	29
3.1	Abstract	29
3.2	Introduction	30
3.2.1	Basic Conditional Spectrum computation	31
3.2.2	Deaggregation	33
3.3	Conditional Spectrum calculation approaches	34
3.3.1	Method 1: Approximate CS using mean M/R and a single GMPM	35
3.3.2	Method 2: Approximate CS using mean M/R and GMPMs with logic-tree weights	35
3.3.3	Method 3: Approximate CS using GMPM-specific mean M/R and GMPMs with deaggregation weights	36
3.3.4	Method 4: “Exact” CS using multiple causal earthquake M/R and GMPMs with deaggregation weights	37
3.3.5	Aggregation approach to Method 4 (exact CS)	39
3.4	Example calculations for three sites	40
3.4.1	Description of example sites and GMPMs	40
3.4.2	Deaggregation information	41
3.4.3	Conditional Spectra results	42
3.5	Impact of approximations on ground motion selection	45
3.6	Conditional Spectrum calculation tools from USGS	46
3.6.1	Description of calculation tool	47
3.6.2	Current implementation issues	48
3.6.3	Future features	49
3.7	Conclusions	49
4	Hazard consistency for risk-based assessments	56
4.1	Abstract	56
4.2	Introduction	57

4.3	Conditional-Spectrum-based ground motion selection	60
4.3.1	Seismic hazard analysis and deaggregation	60
4.3.2	Target spectrum computation	61
4.3.3	Ground motion selection to match target spectrum	64
4.4	Hazard consistency of ground motion response spectra	64
4.4.1	Linking ground motion response spectra to seismic hazard	65
4.4.2	Comparison of approximate and exact Conditional Spectra	67
4.4.3	Response spectra refinement	68
4.5	Structural analysis	69
4.5.1	Risk-based assessment procedure	69
4.5.2	Varying conditioning periods	71
4.5.3	Significance of hazard consistency	71
4.6	Additional engineering demand parameters	72
4.7	Conclusions	76
5	Intensity-based assessments and evaluation of alternative target spectra	87
5.1	Abstract	87
5.2	Introduction	88
5.3	Analysis objectives	90
5.3.1	Risk-based assessments	90
5.3.2	Intensity-based assessments	91
5.4	Impact of conditioning period on intensity-based assessments using the Conditional Spectrum	92
5.5	Alternative target spectra	95
5.5.1	Uniform Hazard Spectrum and Conditional Mean Spectrum	96
5.5.2	Impact of target spectra on intensity-based assessments	96
5.5.3	Impact of target spectra on risk-based assessments	97
5.6	Additional structures	100
5.7	Conclusions	101
6	Summary, implications, and future work	112
6.1	Summary and conclusions	112

6.1.1	Deaggregation of ground motion prediction models	113
6.1.2	Refined computation of Conditional Spectrum	114
6.1.3	Hazard consistency in risk-based assessments	115
6.1.4	Intensity-based assessments and evaluation of alternative target spectra	116
6.2	Implications for buildings codes and performance-based earthquake engineering	117
6.2.1	Risk-based assessments	117
6.2.2	Intensity-based assessments	118
6.2.3	Selection of target spectrum	118
6.3	Limitations and future work	119
6.3.1	Automation of exact Conditional Spectrum computation	119
6.3.2	Linking performance goals and design checks	120
6.3.3	Refinements for bidirectional ground motion inputs	121
6.3.4	Engineering demand parameters, structures, and systems	121
6.3.5	Sources of ground motion inputs	122
6.3.6	Integration of ground motion hazard and structural modeling uncertainties	123
6.3.7	Sites	124
6.3.8	Other effects not captured in elastic response spectra	124
6.4	Concluding remarks	125
A	Additional structures	126
A.1	Conditional Spectra for perimeter frames	127
A.1.1	20-story perimeter frame	127
A.1.2	12-story perimeter frame	130
A.1.3	8-story perimeter frame	131
A.1.4	4-story perimeter frame	131
A.1.5	2-story perimeter frame	132
A.1.6	1-story perimeter frame	132
A.2	Conditional Spectra for space frames	133

A.2.1	20-story space frame	133
A.2.2	12-story space frame	133
A.2.3	8-story space frame	133
A.2.4	4-story space frame	133
A.2.5	2-story space frame	134
A.2.6	1-story space frame	134
A.3	Additional spectral amplitudes	135
A.4	Other target spectra	135

List of Tables

2.1	Parameters used for the Ground Motion Prediction Models considered in Coastal California	23
4.1	Summary of selected structural response results from risk-based assessments using ground motions selected to match the CS.	80
5.1	Summary of selected structural response results from intensity-based assessments using ground motions selected to match the CS.	110
5.2	Summary of selected structural response results from intensity-based assessments using ground motions selected to match the CS, the CMS, and the UHS.	111
5.3	Summary of selected structural response results from risk-based assessments using ground motions selected to match the CS, the CMS, and the UHS.	111

List of Figures

1.1	Response spectra of ground motions selected and scaled with (a) UHS, (b) CMS and (c) CS as target spectra for $Sa(2.6s)$ associated with 2% in 50 years probability of exceedance for an illustrative 20-story perimeter frame located in Palo Alto, CA.	9
2.1	Uncertainties in USGS PSHA logic tree for Coastal California. (from Petersen et al., 2008)	23
2.2	Probability density function of epsilons demonstrating the deaggregation difference between ϵ^* conditioned on $Sa = y$ in McGuire (1995) and $\bar{\epsilon}$ conditioned on $Sa > y$ in Bazzurro and Cornell (1999).	24
2.3	Layout of an example site dominated by two earthquake events A and B.	24
2.4	Hazard curves for the example site.	25
2.5	Deaggregation of events given $Sa(1s) > y$ for the example site.	25
2.6	Deaggregation of GMPMs given $Sa(1s) > y$ for the example site.	26
2.7	Deaggregation of magnitudes given $Sa(1s) > y$ for the example site.	26
2.8	Deaggregation of distances given $Sa(1s) > y$ for the example site.	27
2.9	Deaggregation of epsilons given $Sa(1s) > y$ for the example site.	27
2.10	USGS implementation of GMPM deaggregation. (from USGS, 2012)	28
3.1	Deaggregation for $Sa(0.2s)$ with 10% probability of exceedance in 50 years at Stanford, Bissell, and Seattle (a, b, and c respectively) and for $Sa(1s)$ with 2% probability of exceedance in 50 years at Stanford, Bissell, and Seattle (d, e, and f respectively) (adapted from USGS, 2012).	51

3.2	CMS at Stanford, Bissell and Seattle (a, b, and c respectively) and conditional standard deviation spectra at Stanford, Bissell, and Seattle (d, e, and f respectively) using Methods 1 to 4, for $Sa(0.2s)$ with 10% probability of exceedance in 50 years.	52
3.3	Conditional standard deviation spectra with contribution from σ_{lnSa} (variance in $lnSa$ for a given M_j/R_j & $GMPM_k$) and μ_{lnSa} (due to variation in M_j/R_j & $GMPM_k$) at Stanford, Bissell, and Seattle (a, b, and c respectively) and CMS for each considered M_j/R_j & $GMPM_k$ at Stanford, Bissell, and Seattle (d, e, and f respectively) using Methods 2 to 4, for $Sa(0.2s)$ with 10% probability of exceedance in 50 years.	53
3.4	CS computed using Methods 2 and 4, for $Sa(0.2s)$ with 10% probability of exceedance in 50 years at Stanford, Bissell, and Seattle (a, b, and c respectively) and $Sa(1s)$ with 2% probability of exceedance in 50 years at Stanford, Bissell, and Seattle (d, e, and f respectively).	54
3.5	Response spectra of ground motions selected match CS obtained using (a) Method 4 and (b) Method 2 at Bissell site for $Sa(0.2s)$ with 10% probability of exceedance in 50 years.	55
3.6	Interface for USGS online interactive deaggregations, including options to request GMPM deaggregation and CMS computation (from USGS, 2012).	55
4.1	(a) Seismic hazard curve for $Sa(2.6s)$ and (b) deaggregation for $Sa(2.6s)$ amplitude with 2% in 50 years probability of exceedance.	79
4.2	Target response spectra of (a) CMS at $T^* = 2.6s$ at multiple intensity levels (from 50% in 20 years to 1% in 200 years) and (b) CMS at multiple conditioning periods (0.45s, 0.85s, 2.6s, and 5s with UHS superimposed) at the 2% in 50 years intensity level.	79
4.3	Response spectra of selected ground motions with CS as target spectra for $Sa(2.6s)$ associated with 2% in 50 years probability of exceedance (a) in log scale and (b) in linear scale.	80

4.4	(a) Ground motion response spectra for ground motions selected at $T^* = 2.6s$, to match the CS μ and σ (at all intensity levels). (b) Ground motion response spectra for ground motions selected at $T^* = 0.85s$, to match the CS μ and σ (at all intensity levels). (c) Sa distribution at $Sa(2.6s)$ for ground motions selected at four conditioning periods, CS μ and σ . (d) Sa distribution at $Sa(5s)$ for ground motions selected at four conditioning periods, CS μ and σ . (e) Sa distribution at four periods for ground motions selected at $T^* = 0.85s$, CS μ and σ	81
4.5	Exact and approximate CS, given $Sa(T^*)$ with 2% probability of exceedance in 50 years. Exact results are denoted “4: Exact” and approximate results are denoted “2: Mean M/R, logic tree weights” in the legend. (a) CS using $T^* = 0.2s$. (b) CS using $T^* = 1s$. Results from Lin et al. (2012).	82
4.6	Comparison of selected ground motion spectra at 4 periods (in solid lines) versus corresponding ground motion hazard curves (in dashed lines) (a) Ground motions selected with $T^* = 0.45s$ and using basic approximate CS. (b) Ground motions selected with $T^* = 0.45s$ and using approximate CS with conditional standard deviations inflated by 10% (“1.1 σ ”).	82
4.7	(a) $PSDR$ distribution for $Sa(2.6s)$. (b) Collapse fragility for Sa at four conditioning periods. (c) Risk-based assessments of $PSDR$ for Sa at four conditioning periods using approximate CS.	83
4.8	(a) Collapse fragility function and (b) risk-based assessments of $PSDR$ obtained from ground motions with an approximate conditional standard deviation and inflated conditional standard deviations for the case of $Sa(0.45s)$	84
4.9	Risk-based assessments of $PSDR$ obtained with four choices of T^* using an inflated conditional standard deviation for the case of $Sa(0.45s)$	84
4.10	Sa distribution at four periods for ground motions selected at (a) $T^* = 2.6s$, CS μ and σ , (b) $T^* = 2.6s$, CS μ and 1.3σ , (c) $T^* = 5s$, CS μ and σ , and (d) $T^* = 5s$, CS μ and 1.3σ	85
4.11	Risk-based assessments of PFA obtained with four choices of T^* using (a) an approximate conditional standard deviation and (b) an inflated conditional standard deviation for the cases of $Sa(2.6s)$ and $Sa(5s)$	86

4.12	Rates of exceedance of drift ratios and floor accelerations on the 15th story of the building.	86
5.1	Statistics of structural responses from intensity-based assessments of the 20-story perimeter frame (Building No.1020) using the CS (a) median <i>PSDR</i> , (b) logarithmic standard deviation of <i>PSDR</i> , (c) median <i>PFA</i> , (d) logarithmic standard deviation of <i>PFA</i> , and (e) probability of collapse.	103
5.2	Response spectra of selected ground motions with (a) UHS, (b) CMS and (c) CS as target spectra for <i>Sa</i> (2.6 <i>s</i>) associated with 2% in 50 years probability of exceedance for the 20-story perimeter frame (Building No.1020). .	104
5.3	Statistics of structural responses from intensity-based assessments of the 20-story perimeter frame (Building No.1020) (a) median <i>PSDR</i> , (b) logarithmic standard deviation of <i>PSDR</i> , (c) median <i>PFA</i> , (d) logarithmic standard deviation of <i>PFA</i> , and (e) probability of collapse.	105
5.4	Risk-based assessments of <i>PSDR</i> of the 20-story perimeter frame (Building No.1020) obtained from ground motions selected to match the CS (all four conditioning periods) as well as the CMS and the UHS for (a) $T^* = 2.6s$ and (b) $T^* = 0.45s$	106
5.5	<i>Sa</i> distribution at four periods for ground motions selected at (a) $T^* = 2.6s$, UHS; (b) $T^* = 0.45s$, UHS; (c) $T^* = 2.6s$, CMS; and (d) $T^* = 0.45s$, CMS. .	107
5.6	Risk-based assessments of (a) <i>PSDR</i> and (b) <i>PFA</i> of the 20-story perimeter frame (Building No.1020) obtained from ground motions selected to match the CS, the CMS, and the UHS.	108
5.7	Risk-based assessments of <i>PSDR</i> of the 4-story perimeter frame (Building No.1008) obtained from ground motions with (a) approximate CS with approximate conditional standard deviations and (b) refined CS with inflated conditional standard deviations.	108
5.8	Statistics of structural responses from intensity-based assessments of the 4-story perimeter frame (Building No.1008) using the CS (a) median <i>PSDR</i> , (b) logarithmic standard deviation of <i>PSDR</i> , (c) median <i>PFA</i> , (d) logarithmic standard deviation of <i>PFA</i> , and (e) probability of collapse.	109

A.1	20-story perimeter frame (Building No.1020) <i>Sa</i> distribution at four periods for ground motions selected at (a) $T^* = T_3$, CS μ and σ , (b) $T^* = T_3$, CS μ and 1.1σ , (c) $T^* = T_2$, CS μ and σ , (d) $T^* = T_1$, CS μ and σ , and (e) $T^* = 2T_1$, CS μ and σ	137
A.2	20-story perimeter frame (Building No.1020) (a-b) probability of collapse, (c-d) <i>PSDR</i> hazard, and (e-f) <i>PFA</i> hazard for “basic” ground motions selected to match CS μ and σ ($T_3, T_2, T_1, 2T_1$) at (a, c, e) and “improved” ground motions selected to match CS μ and σ ($T_2, T_1, 2T_1$) and CS μ and 1.1σ (T_3) at (b, d, f).	138
A.3	20-story perimeter frame (Building No.1020) <i>PSDR</i> at (a) $T^* = T_3$, (b) $T^* = T_2$, (c) $T^* = T_1$, and (d) $T^* = 2T_1$ for “improved” ground motions selected to match CS μ and σ ($T_2, T_1, 2T_1$) and CS μ and 1.1σ (T_3).	139
A.4	20-story perimeter frame (Building No.1020) <i>PFA</i> at (a) $T^* = T_3$, (b) $T^* = T_2$, (c) $T^* = T_1$, and (d) $T^* = 2T_1$ for “improved” ground motions selected to match CS μ and σ ($T_2, T_1, 2T_1$) and CS μ and 1.1σ (T_3).	140
A.5	20-story perimeter frame (Building No.1020) (a) median <i>PSDR</i> , (b) logarithmic standard deviation of <i>PSDR</i> , (c) median <i>PFA</i> , (d) logarithmic standard deviation of <i>PFA</i> , and (e) probability of collapse given return period for “improved” ground motions selected to match CS μ and σ ($T_2, T_1, 2T_1$) and CS μ and 1.1σ (T_3).	141
A.6	12-story perimeter frame (Building No.1013) <i>Sa</i> distribution at four periods for ground motions selected at (a) $T^* = T_3$, CS μ and σ , (b) $T^* = T_3$, CS μ and 1.2σ , (c) $T^* = T_2$, CS μ and σ , (d) $T^* = T_1$, CS μ and σ , and (e) $T^* = 2T_1$, CS μ and σ	142
A.7	12-story perimeter frame (Building No.1013) (a-b) probability of collapse, (c-d) <i>PSDR</i> hazard, and (e-f) <i>PFA</i> hazard for “basic” ground motions selected to match CS μ and σ ($T_3, T_2, T_1, 2T_1$) at (a, c, e) and “improved” ground motions selected to match CS μ and σ ($T_2, T_1, 2T_1$) and CS μ and 1.2σ (T_3) at (b, d, f).	143

A.8	12-story perimeter frame (Building No.1013) <i>PSDR</i> at (a) $T^* = T_3$, (b) $T^* = T_2$, (c) $T^* = T_1$, and (d) $T^* = 2T_1$ for “improved” ground motions selected to match CS μ and $\sigma (T_2, T_1, 2T_1)$ and CS μ and $1.2\sigma (T_3)$	144
A.9	12-story perimeter frame (Building No.1013) <i>PFA</i> at (a) $T^* = T_3$, (b) $T^* = T_2$, (c) $T^* = T_1$, and (d) $T^* = 2T_1$ for “improved” ground motions selected to match CS μ and $\sigma (T_2, T_1, 2T_1)$ and CS μ and $1.2\sigma (T_3)$	145
A.10	12-story perimeter frame (Building No.1013) (a) median <i>PSDR</i> , (b) logarithmic standard deviation of <i>PSDR</i> , (c) median <i>PFA</i> , (d) logarithmic standard deviation of <i>PFA</i> , and (e) probability of collapse given return period for “improved” ground motions selected to match CS μ and $\sigma (T_2, T_1, 2T_1)$ and CS μ and $1.2\sigma (T_3)$	146
A.11	8-story perimeter frame (Building No.1011) <i>Sa</i> distribution at four periods for ground motions selected at (a) $T^* = T_3$, CS μ and σ , (b) $T^* = T_3$, CS μ and 1.2σ , (c) $T^* = T_2$, CS μ and σ , (d) $T^* = T_2$, CS μ and 1.1σ , (e) $T^* = T_1$, CS μ and σ , and (f) $T^* = 2T_1$, CS μ and σ	147
A.12	8-story perimeter frame (Building No.1011) (a-b) probability of collapse, (c-d) <i>PSDR</i> hazard, and (e-f) <i>PFA</i> hazard for “basic” ground motions selected to match CS μ and $\sigma (T_3, T_2, T_1, 2T_1)$ at (a, c, e) and “improved” ground motions selected to match CS μ and $\sigma (T_1, 2T_1)$, CS μ and $1.1\sigma (T_2)$, and CS μ and $1.2\sigma (T_3)$ at (b, d, f).	148
A.13	8-story perimeter frame (Building No.1011) <i>PSDR</i> at (a) $T^* = T_3$, (b) $T^* = T_2$, (c) $T^* = T_1$, and (d) $T^* = 2T_1$ for “improved” ground motions selected to match CS μ and $\sigma (T_1, 2T_1)$, CS μ and $1.1\sigma (T_2)$, and CS μ and $1.2\sigma (T_3)$	149
A.14	8-story perimeter frame (Building No.1011) <i>PFA</i> at (a) $T^* = T_3$, (b) $T^* = T_2$, (c) $T^* = T_1$, and (d) $T^* = 2T_1$ for “improved” ground motions selected to match CS μ and $\sigma (T_1, 2T_1)$, CS μ and $1.1\sigma (T_2)$, and CS μ and $1.2\sigma (T_3)$	150
A.15	8-story perimeter frame (Building No.1011) (a) median <i>PSDR</i> , (b) logarithmic standard deviation of <i>PSDR</i> , (c) median <i>PFA</i> , (d) logarithmic standard deviation of <i>PFA</i> , and (e) probability of collapse given return period for “improved” ground motions selected to match CS μ and $\sigma (T_1, 2T_1)$, CS μ and $1.1\sigma (T_2)$, and CS μ and $1.2\sigma (T_3)$	151

A.16	4-story perimeter frame (Building No.1008) <i>Sa</i> distribution at four periods for ground motions selected at (a) $T^* = T_3$, CS μ and σ , (b) $T^* = T_3$, CS μ and 1.3σ , (c) $T^* = T_2$, CS μ and σ , (d) $T^* = T_2$, CS μ and 1.2σ , (e) $T^* = T_1$, CS μ and σ , and (f) $T^* = 2T_1$, CS μ and σ	152
A.17	4-story perimeter frame (Building No.1008) (a-b) probability of collapse, (c-d) <i>PSDR</i> hazard, and (e-f) <i>PFA</i> hazard for “basic” ground motions selected to match CS μ and σ ($T_3, T_2, T_1, 2T_1$) at (a, c, e) and “improved” ground motions selected to match CS μ and σ ($T_1, 2T_1$), CS μ and 1.2σ (T_2), and CS μ and 1.3σ (T_3) at (b, d, f).	153
A.18	4-story perimeter frame (Building No.1008) <i>PSDR</i> at (a) $T^* = T_3$, (b) $T^* = T_2$, (c) $T^* = T_1$, and (d) $T^* = 2T_1$ for “improved” ground motions selected to match CS μ and σ ($T_1, 2T_1$), CS μ and 1.2σ (T_2), and CS μ and 1.3σ (T_3).154	
A.19	4-story perimeter frame (Building No.1008) <i>PFA</i> at (a) $T^* = T_3$, (b) $T^* = T_2$, (c) $T^* = T_1$, and (d) $T^* = 2T_1$ for “improved” ground motions selected to match CS μ and σ ($T_1, 2T_1$), CS μ and 1.2σ (T_2), and CS μ and 1.3σ (T_3).155	
A.20	4-story perimeter frame (Building No.1008) (a) median <i>PSDR</i> , (b) logarithmic standard deviation of <i>PSDR</i> , (c) median <i>PFA</i> , (d) logarithmic standard deviation of <i>PFA</i> , and (e) probability of collapse given return period for “improved” ground motions selected to match CS μ and σ ($T_1, 2T_1$), CS μ and 1.2σ (T_2), and CS μ and 1.3σ (T_3).	156
A.21	2-story perimeter frame (Building No.2064) <i>Sa</i> distribution at three periods for ground motions selected at (a) $T^* = T_2$, CS μ and σ , (b) $T^* = T_2$, CS μ and 1.3σ , (c) $T^* = T_1$, CS μ and σ , and (d) $T^* = 2T_1$, CS μ and σ	157
A.22	2-story perimeter frame (Building No.2064) (a-b) probability of collapse, (c-d) <i>PSDR</i> hazard, and (e-f) <i>PFA</i> hazard for “basic” ground motions selected to match CS μ and σ ($T_2, T_1, 2T_1$) at (a, c, e) and “improved” ground motions selected to match CS μ and σ ($T_1, 2T_1$) and CS μ and 1.3σ (T_2) at (b, d, f).	158
A.23	2-story perimeter frame (Building No.2064) <i>PSDR</i> at (a) $T^* = T_2$, (b) $T^* = T_1$, and (d) $T^* = 2T_1$ for “improved” ground motions selected to match CS μ and σ ($T_1, 2T_1$) and CS μ and 1.3σ (T_2).	159

A.24	2-story perimeter frame (Building No.2064) <i>PFA</i> at (a) $T^* = T_2$, (b) $T^* = T_1$, and (d) $T^* = 2T_1$ for “improved” ground motions selected to match CS μ and $\sigma (T_1, 2T_1)$ and CS μ and $1.3\sigma (T_2)$	160
A.25	2-story perimeter frame (Building No.2064) (a) median <i>PSDR</i> , (b) logarithmic standard deviation of <i>PSDR</i> , (c) median <i>PFA</i> , (d) logarithmic standard deviation of <i>PFA</i> , and (e) probability of collapse given return period for “improved” ground motions selected to match CS μ and $\sigma (T_1, 2T_1)$ and CS μ and $1.3\sigma (T_2)$	161
A.26	1-story perimeter frame (Building No.2069) <i>Sa</i> distribution at two periods for ground motions selected at (a) $T^* = T_1$, CS μ and σ and (b) $T^* = 2T_1$, CS μ and σ	162
A.27	1-story perimeter frame (Building No.2069) (a) probability of collapse, (b) <i>PSDR</i> hazard, and (c) <i>PFA</i> hazard for “basic” ground motions selected to match CS μ and σ	163
A.28	1-story perimeter frame (Building No.2069) <i>PSDR</i> at (a) $T^* = T_1$ and (b) $T^* = 2T_1$ for “basic” ground motions selected to match CS μ and σ	164
A.29	1-story perimeter frame (Building No.2069) <i>PFA</i> at (a) $T^* = T_1$ and (b) $T^* = 2T_1$ for “basic” ground motions selected to match CS μ and σ	164
A.30	1-story perimeter frame (Building No.2069) (a) median <i>PSDR</i> , (b) logarithmic standard deviation of <i>PSDR</i> , (c) median <i>PFA</i> , (d) logarithmic standard deviation of <i>PFA</i> , and (e) probability of collapse given return period for “basic” ground motions selected to match CS μ and σ	165
A.31	20-story space frame (Building No.1021) <i>Sa</i> distribution at four periods for ground motions selected at (a) $T^* = T_3$, CS μ and σ , (b) $T^* = T_3$, CS μ and 1.1σ , (c) $T^* = T_2$, CS μ and σ , (d) $T^* = T_1$, CS μ and σ , and (e) $T^* = 2T_1$, CS μ and σ	166
A.32	20-story space frame (Building No.1021) (a-b) probability of collapse, (c-d) <i>PSDR</i> hazard, and (e-f) <i>PFA</i> hazard for “basic” ground motions selected to match CS μ and $\sigma (T_3, T_2, T_1, 2T_1)$ at (a, c, e) and “improved” ground motions selected to match CS μ and $\sigma (T_2, T_1, 2T_1)$ and CS μ and $1.1\sigma (T_3)$ at (b, d, f).	167

A.33	20-story space frame (Building No.1021) <i>PSDR</i> at (a) $T^* = T_3$, (b) $T^* = T_2$, (c) $T^* = T_1$, and (d) $T^* = 2T_1$ for “improved” ground motions selected to match CS μ and $\sigma (T_2, T_1, 2T_1)$ and CS μ and $1.1\sigma (T_3)$	168
A.34	20-story space frame (Building No.1021) <i>PFA</i> at (a) $T^* = T_3$, (b) $T^* = T_2$, (c) $T^* = T_1$, and (d) $T^* = 2T_1$ for “improved” ground motions selected to match CS μ and $\sigma (T_2, T_1, 2T_1)$ and CS μ and $1.1\sigma (T_3)$	169
A.35	20-story space frame (Building No.1021) (a) median <i>PSDR</i> , (b) logarithmic standard deviation of <i>PSDR</i> , (c) median <i>PFA</i> , (d) logarithmic standard deviation of <i>PFA</i> , and (e) probability of collapse given “improved” return period for ground motions selected to match CS μ and $\sigma (T_2, T_1, 2T_1)$ and CS μ and $1.1\sigma (T_3)$	170
A.36	12-story space frame (Building No.1014) <i>Sa</i> distribution at four periods for ground motions selected at (a) $T^* = T_3$, CS μ and σ , (b) $T^* = T_3$, CS μ and 1.1σ , (c) $T^* = T_2$, CS μ and σ , (d) $T^* = T_1$, CS μ and σ , and (e) $T^* = 2T_1$, CS μ and σ	171
A.37	12-story space frame (Building No.1014) (a-b) probability of collapse, (c-d) <i>PSDR</i> hazard, and (e-f) <i>PFA</i> hazard for “basic” ground motions selected to match CS μ and $\sigma (T_3, T_2, T_1, 2T_1)$ at (a, c, e) and “improved” ground motions selected to match CS μ and $\sigma (T_2, T_1, 2T_1)$ and CS μ and $1.1\sigma (T_3)$ at (b, d, f).	172
A.38	12-story space frame (Building No.1014) <i>PSDR</i> at (a) $T^* = T_3$, (b) $T^* = T_2$, (c) $T^* = T_1$, and (d) $T^* = 2T_1$ for “improved” ground motions selected to match CS μ and $\sigma (T_2, T_1, 2T_1)$ and CS μ and $1.1\sigma (T_3)$	173
A.39	12-story space frame (Building No.1014) <i>PFA</i> at (a) $T^* = T_3$, (b) $T^* = T_2$, (c) $T^* = T_1$, and (d) $T^* = 2T_1$ for “improved” ground motions selected to match CS μ and $\sigma (T_2, T_1, 2T_1)$ and CS μ and $1.1\sigma (T_3)$	174
A.40	12-story space frame (Building No.1014) (a) median <i>PSDR</i> , (b) logarithmic standard deviation of <i>PSDR</i> , (c) median <i>PFA</i> , (d) logarithmic standard deviation of <i>PFA</i> , and (e) probability of collapse given return period for “improved” ground motions selected to match CS μ and $\sigma (T_2, T_1, 2T_1)$ and CS μ and $1.1\sigma (T_3)$	175

A.41	8-story space frame (Building No.1012) <i>Sa</i> distribution at four periods for ground motions selected at (a) $T^* = T_3$, CS μ and σ , (b) $T^* = T_3$, CS μ and 1.2σ , (c) $T^* = T_2$, CS μ and σ , (d) $T^* = T_2$, CS μ and 1.1σ , (e) $T^* = T_1$, CS μ and σ , and (f) $T^* = 2T_1$, CS μ and σ	176
A.42	8-story space frame (Building No.1012) (a-b) probability of collapse, (c-d) <i>PSDR</i> hazard, and (e-f) <i>PFA</i> hazard for “basic” ground motions selected to match CS μ and σ ($T_3, T_2, T_1, 2T_1$) at (a, c, e) and “improved” ground motions selected to match CS μ and σ ($T_1, 2T_1$), CS μ and 1.1σ (T_2), and CS μ and 1.2σ (T_3) at (b, d, f).	177
A.43	8-story space frame (Building No.1012) <i>PSDR</i> at (a) $T^* = T_3$, (b) $T^* = T_2$, (c) $T^* = T_1$, and (d) $T^* = 2T_1$ for “improved” ground motions selected to match CS μ and σ ($T_1, 2T_1$), CS μ and 1.1σ (T_2), and CS μ and 1.2σ (T_3).	178
A.44	8-story space frame (Building No.1012) <i>PFA</i> at (a) $T^* = T_3$, (b) $T^* = T_2$, (c) $T^* = T_1$, and (d) $T^* = 2T_1$ for “improved” ground motions selected to match CS μ and σ ($T_1, 2T_1$), CS μ and 1.1σ (T_2), and CS μ and 1.2σ (T_3).	179
A.45	8-story space frame (Building No.1012) (a) median <i>PSDR</i> , (b) logarithmic standard deviation of <i>PSDR</i> , (c) median <i>PFA</i> , (d) logarithmic standard deviation of <i>PFA</i> , and (e) probability of collapse given return period for “improved” ground motions selected to match CS μ and σ ($T_1, 2T_1$), CS μ and 1.1σ (T_2), and CS μ and 1.2σ (T_3).	180
A.46	4-story space frame (Building No.1003) <i>Sa</i> distribution at four periods for ground motions selected at (a) $T^* = T_3$, CS μ and σ , (b) $T^* = T_3$, CS μ and 1.2σ , (c) $T^* = T_2$, CS μ and σ , (d) $T^* = T_2$, CS μ and 1.2σ , (e) $T^* = T_1$, CS μ and σ , and (f) $T^* = 2T_1$, CS μ and σ	181
A.47	4-story space frame (Building No.1003) (a-b) probability of collapse, (c-d) <i>PSDR</i> hazard, and (e-f) <i>PFA</i> hazard for “basic” ground motions selected to match CS μ and σ ($T_3, T_2, T_1, 2T_1$) at (a, c, e) and “improved” ground motions selected to match CS μ and σ ($T_1, 2T_1$) and CS μ and 1.2σ (T_3, T_2) at (b, d, f).	182

A.48	4-story space frame (Building No.1003) <i>PSDR</i> at (a) $T^* = T_3$, (b) $T^* = T_2$, (c) $T^* = T_1$, and (d) $T^* = 2T_1$ for “improved” ground motions selected to match CS μ and $\sigma (T_1, 2T_1)$ and CS μ and $1.2\sigma (T_3, T_2)$	183
A.49	4-story space frame (Building No.1003) <i>PFA</i> at (a) $T^* = T_3$, (b) $T^* = T_2$, (c) $T^* = T_1$, and (d) $T^* = 2T_1$ for “improved” ground motions selected to match CS μ and $\sigma (T_1, 2T_1)$ and CS μ and $1.2\sigma (T_3, T_2)$	184
A.50	4-story space frame (Building No.1003) (a) median <i>PSDR</i> , (b) logarithmic standard deviation of <i>PSDR</i> , (c) median <i>PFA</i> , (d) logarithmic standard deviation of <i>PFA</i> , and (e) probability of collapse given return period for “improved” ground motions selected to match CS μ and $\sigma (T_1, 2T_1)$ and CS μ and $1.2\sigma (T_3, T_2)$	185
A.51	2-story space frame (Building No.1001) <i>Sa</i> distribution at three periods for ground motions selected at (a) $T^* = T_2$, CS μ and σ , (b) $T^* = T_2$, CS μ and 1.3σ , (c) $T^* = T_1$, CS μ and σ , and (d) $T^* = 2T_1$, CS μ and σ	186
A.52	2-story space frame (Building No.1001) (a-b) probability of collapse, (c-d) <i>PSDR</i> hazard, and (e-f) <i>PFA</i> hazard for “basic” ground motions selected to match CS μ and $\sigma (T_2, T_1, 2T_1)$ at (a, c, e) and “improved” ground motions selected to match CS μ and $\sigma (T_1, 2T_1)$ and CS μ and $1.3\sigma (T_2)$ at (b, d, f).	187
A.53	2-story space frame (Building No.1001) <i>PSDR</i> at (a) $T^* = T_2$, (b) $T^* = T_1$, and (d) $T^* = 2T_1$ for “improved” ground motions selected to match CS μ and $\sigma (T_1, 2T_1)$ and CS μ and $1.3\sigma (T_2)$	188
A.54	2-story space frame (Building No.1001) <i>PFA</i> at (a) $T^* = T_2$, (b) $T^* = T_1$, and (d) $T^* = 2T_1$ for “improved” ground motions selected to match CS μ and $\sigma (T_1, 2T_1)$ and CS μ and $1.3\sigma (T_2)$	189
A.55	2-story space frame (Building No.1001) (a) median <i>PSDR</i> , (b) logarithmic standard deviation of <i>PSDR</i> , (c) median <i>PFA</i> , (d) logarithmic standard deviation of <i>PFA</i> , and (e) probability of collapse given return period for “improved” ground motions selected to match CS μ and $\sigma (T_1, 2T_1)$ and CS μ and $1.3\sigma (T_2)$	190

A.56	1-story space frame (Building No.2061) <i>Sa</i> distribution at two periods for ground motions selected at (a) $T^* = T_1$, CS μ and σ and (b) $T^* = 2T_1$, CS μ and σ	191
A.57	1-story space frame (Building No.2061) (a) probability of collapse, (b) <i>PSDR</i> hazard, and (c) <i>PFA</i> hazard for “basic” ground motions selected to match CS μ and σ	192
A.58	1-story space frame (Building No.2061) <i>PSDR</i> at (a) $T^* = T_1$ and (b) $T^* = 2T_1$ for “basic” ground motions selected to match CS μ and σ	193
A.59	1-story space frame (Building No.2061) <i>PFA</i> at (a) $T^* = T_1$ and (b) $T^* = 2T_1$ for “basic” ground motions selected to match CS μ and σ	193
A.60	1-story space frame (Building No.2061) (a) median <i>PSDR</i> , (b) logarithmic standard deviation of <i>PSDR</i> , (c) median <i>PFA</i> , (d) logarithmic standard deviation of <i>PFA</i> , and (e) probability of collapse given return period for “basic” ground motions selected to match CS μ and σ	194
A.61	20-story perimeter frame (Building No.1020) (a) probability of collapse and (b) <i>PSDR</i> hazard for “basic” ground motions selected to match CS μ and σ ($T_3, T_2, T_1, 2T_1$), additional ground motions selected to match CS μ and σ ($T_3, T_2, T_1, 2T_1$) with higher Intensity Measures (IMs), i.e., higher spectral amplitudes, and “improved” ground motions selected to match CS μ and σ ($T_2, T_1, 2T_1$) and CS μ and 1.1σ (T_3).	195
A.62	20-story perimeter frame (Building No.1020) <i>Sa</i> distribution at four periods for (a) $T^* = T_3$, (b) $T^* = T_2$, (c) $T^* = T_1$ and (d) $T^* = 2T_1$ for ground motions selected to match Conditional Mean Spectrum (CMS), i.e., CS μ ($T_3, T_2, T_1, 2T_1$).	196
A.63	20-story perimeter frame (Building No.1020) (a) probability of collapse, (b) <i>PSDR</i> hazard, and (c) <i>PFA</i> hazard for ground motions selected to match CMS, i.e., CS μ ($T_3, T_2, T_1, 2T_1$).	197
A.64	20-story perimeter frame (Building No.1020) <i>PSDR</i> at (a) $T^* = T_3$, (b) $T^* = T_2$, (c) $T^* = T_1$, and (d) $T^* = 2T_1$ for ground motions selected to match CMS, i.e., CS μ ($T_3, T_2, T_1, 2T_1$).	198

A.65	20-story perimeter frame (Building No.1020) <i>PFA</i> at (a) $T^* = T_3$, (b) $T^* = T_2$, (c) $T^* = T_1$, and (d) $T^* = 2T_1$ for ground motions selected to match CMS, i.e., $CS \mu (T_3, T_2, T_1, 2T_1)$	199
A.66	20-story perimeter frame (Building No.1020) (a) median <i>PSDR</i> , (b) logarithmic standard deviation of <i>PSDR</i> , (c) median <i>PFA</i> , (d) logarithmic standard deviation of <i>PFA</i> , and (e) probability of collapse given return period for ground motions selected to match CMS, i.e., $CS \mu (T_3, T_2, T_1, 2T_1)$	200
A.67	20-story perimeter frame (Building No.1020) <i>Sa</i> distribution at four periods for (a) $T^* = T_3$, (b) $T^* = T_2$, (c) $T^* = T_1$ and (d) $T^* = 2T_1$ for ground motions selected to match Uniform Hazard Spectrum (UHS).	201
A.68	20-story perimeter frame (Building No.1020) (a) probability of collapse, (b) <i>PSDR</i> hazard, and (c) <i>PFA</i> hazard for ground motions selected to match UHS.	202
A.69	20-story perimeter frame (Building No.1020) <i>PSDR</i> at (a) $T^* = T_3$, (b) $T^* = T_2$, (c) $T^* = T_1$, and (d) $T^* = 2T_1$ for ground motions selected to match UHS.	203
A.70	20-story perimeter frame (Building No.1020) <i>PFA</i> at (a) $T^* = T_3$, (b) $T^* = T_2$, (c) $T^* = T_1$, and (d) $T^* = 2T_1$ for ground motions selected to match UHS.	204
A.71	20-story perimeter frame (Building No.1020) (a) median <i>PSDR</i> , (b) logarithmic standard deviation of <i>PSDR</i> , (c) median <i>PFA</i> , (d) logarithmic standard deviation of <i>PFA</i> , and (e) probability of collapse given return period for ground motions selected to match UHS.	205
A.72	4-story perimeter frame (Building No.1008) <i>Sa</i> distribution at four periods for (a) $T^* = T_3$, (b) $T^* = T_2$, (c) $T^* = T_1$ and (d) $T^* = 2T_1$ for ground motions selected to match CMS, i.e., $CS \mu (T_3, T_2, T_1, 2T_1)$	206
A.73	4-story perimeter frame (Building No.1008) (a) probability of collapse, (b) <i>PSDR</i> hazard, and (c) <i>PFA</i> hazard for ground motions selected to match CMS, i.e., $CS \mu (T_3, T_2, T_1, 2T_1)$	207
A.74	4-story perimeter frame (Building No.1008) <i>PSDR</i> at (a) $T^* = T_3$, (b) $T^* = T_2$, (c) $T^* = T_1$, and (d) $T^* = 2T_1$ for ground motions selected to match CMS, i.e., $CS \mu (T_3, T_2, T_1, 2T_1)$	208

A.75 4-story perimeter frame (Building No.1008) <i>PFA</i> at (a) $T^* = T_3$, (b) $T^* = T_2$, (c) $T^* = T_1$, and (d) $T^* = 2T_1$ for ground motions selected to match CMS, i.e., $CS \mu (T_3, T_2, T_1, 2T_1)$	209
A.76 4-story perimeter frame (Building No.1008) (a) median <i>PSDR</i> , (b) logarithmic standard deviation of <i>PSDR</i> , (c) median <i>PFA</i> , (d) logarithmic standard deviation of <i>PFA</i> , and (e) probability of collapse given return period for ground motions selected to match CMS, i.e., $CS \mu (T_3, T_2, T_1, 2T_1)$	210
A.77 4-story perimeter frame (Building No.1008) <i>Sa</i> distribution at four periods for (a) $T^* = T_3$, (b) $T^* = T_2$, (c) $T^* = T_1$ and (d) $T^* = 2T_1$ for ground motions selected to match UHS.	211
A.78 4-story perimeter frame (Building No.1008) (a) probability of collapse, (b) <i>PSDR</i> hazard, and (c) <i>PFA</i> hazard for ground motions selected to match UHS.	212
A.79 4-story perimeter frame (Building No.1008) <i>PSDR</i> at (a) $T^* = T_3$, (b) $T^* = T_2$, (c) $T^* = T_1$, and (d) $T^* = 2T_1$ for ground motions selected to match UHS.	213
A.80 4-story perimeter frame (Building No.1008) <i>PFA</i> at (a) $T^* = T_3$, (b) $T^* = T_2$, (c) $T^* = T_1$, and (d) $T^* = 2T_1$ for ground motions selected to match UHS.	214
A.81 4-story perimeter frame (Building No.1008) (a) median <i>PSDR</i> , (b) logarithmic standard deviation of <i>PSDR</i> , (c) median <i>PFA</i> , (d) logarithmic standard deviation of <i>PFA</i> , and (e) probability of collapse given return period for ground motions selected to match UHS.	215

Chapter 1

Introduction

1.1 Background and motivation

The performance of structures under earthquake loading is critical to public safety and societal functionality. To quantify the seismic performance of structures, Cornell (1968) introduced the concept of probabilistic seismic hazard analysis (PSHA) (Kramer, 1996; McGuire, 2004) and its subsequent risk assessment termed performance-based earthquake engineering (PBEE) (Cornell and Krawinkler, 2000; Deierlein, 2004; Krawinkler and Miranda, 2004; Moehle and Deierlein, 2004). This framework has helped the construction of the United States national seismic hazard map (Petersen et al., 2008), enabled site- and structure-specific hazard analysis that resulted in more optimized structural design and analysis, and facilitated engineering communication with stakeholders and decision makers.

Performance-based earthquake engineering quantifies the seismic hazard, predicts the structural response, estimates the damage to building elements (structural, non-structural, and content), in order to assess the resulting losses in terms of dollars, downtime, and deaths (e.g., Cornell and Krawinkler, 2000; Krawinkler et al., 2003; Deierlein, 2004). One key input to seismic design and analysis of structures is earthquake ground motion. Ground motion selection provides the necessary link between seismic hazard and structural response, the first two components in PBEE. It determines ground motion input for a structure at a specific site for nonlinear dynamic analysis (i.e., response history analysis). As nonlinear

dynamic analysis becomes more common in research and practice, there is an increased need for clear guidance on appropriate ground motion selection methods. Ground motion selection has a significant impact on conclusions regarding structural safety, since ground motion uncertainty contributes significantly to uncertainty in structural analysis output.

The source of ground motion inputs can come from (1) simulations, either physics-based, stochastic, or hybrid; (2) spectral matching; (3) selection and scaling of recorded ground motions from ground motion databases. Simulations of ground motions are often used in regions where recorded ground motions are extremely limited (see Douglas and Aochi, 2008, for an overview of simulation techniques). Physics-based simulations attempt to depict the physical phenomenon of earthquake fault rupture and wave propagation using analytical models (e.g., Moczo et al., 2007; Aagaard et al., 2010; Graves et al., 2011) while stochastic simulations rely heavily on empirical calibration with an attempt to generate ground motions using fewer random variables (e.g., Thrainsson and Kiremidjian, 2002; Rezaeian and Kiureghian, 2008; Rezaeian and Der Kiureghian, 2010; Yamamoto and Baker, 2011; Vetter and Taflanidis, 2012). Hybrid simulations (e.g., Hartzell et al., 1999; Mai and Beroza, 2003; Graves and Pitarka, 2010), on the other hand, combine the two by utilizing physics-based simulations for low-frequency components and stochastic simulations for high-frequency components. A semi-artificial ground motion modification technique is spectral matching that changes the frequency content of the response spectra to be compatible with the target (e.g., Silva and Lee, 1987; Hancock et al., 2006). Another modification technique is selection and scaling of recorded ground motions (e.g., Stewart et al., 2001; Haselton et al., 2009; Katsanos et al., 2010; NIST, 2011) that involves selecting recorded ground motions from ground motion databases (e.g., Chiou et al., 2008; Aoi et al., 2011) and applying amplitude scaling to match the target.

To ensure the proper quantification of ground motion uncertainty, it is important to link ground motion selection to probabilistic seismic hazard analysis. PSHA is commonly used in structural dynamic analysis (e.g., Chopra, 2012) and geotechnical earthquake engineering (e.g., Kramer, 1996) to identify the ground motion hazard for which structural and geotechnical systems are analyzed and designed. PSHA accounts for the aleatory uncertainties (which are inherently random) of causal earthquakes with different magnitudes and distances with predictions of resulting ground motion intensity in order to compute

seismic hazard at a site (McGuire, 2004). PSHA also incorporates epistemic uncertainties (which are due to limited knowledge) in ground motion predictions, by considering multiple ground motion prediction models (GMPMs, previously known as attenuation relations, and also known as ground motion prediction equations, ground motion models, and ground motion relations) (e.g., Boore and Atkinson, 2008; Campbell and Bozorgnia, 2008; Chiou and Youngs, 2008; Abrahamson et al., 2008) using a logic tree that also includes seismic source models (e.g., Scherbaum et al., 2005; Petersen et al., 2008; Bommer and Scherbaum, 2008).

Ground motion selection is often associated with a target response spectrum (e.g., Shantz, 2006; Watson-Lamprey and Abrahamson, 2006; Beyer and Bommer, 2007; ASCE, 2010; ATC, 2011; Buratti et al., 2011). For instance, the target response spectrum in current building codes (e.g., ICC, 2003; CEN, 2005; ASCE, 2010) is based on the Uniform Hazard Spectrum (UHS), which assumes equal probabilities of exceedance of spectral accelerations (S_a) at all periods. However, no single ground motion is likely to produce a response spectrum as high as that of the UHS over a wide range of periods (Reiter, 1990; Naeim and Lew, 1995; Bommer et al., 2000; Baker and Cornell, 2006a). The Conditional Mean Spectrum (CMS), a target spectrum proposed for ground motion selection, utilizes the correlation of S_a across periods (T) (e.g., Baker and Jayaram, 2008) to more realistically compute the expected S_a values at all periods given a target S_a value at a period of interest (Baker, 2005; Baker and Cornell, 2006a; Baker, 2011). One notable work is that of Gulerce and Abrahamson (2011), who extend the CMS concept to vertical ground motions. A generalized conditional intensity measure approach is also developed by Bradley (2010a) to include intensity measures other than S_a . With its explicit probabilistic hazard-consistent characteristics and potential resulting cost savings (from considering for many periods S_a values that are lower than those of the UHS), the CMS method has gained popularity in engineering applications over the past few years (e.g., Somerville and Hamburger, 2009; Abrahamson and Al Atik, 2010; Abrahamson and Yunatci, 2010; Somerville and Thio, 2011; Ebrahimian et al., 2012).

Due to the limited number of recorded ground motions, modifications to the ground motions, often through amplitude scaling, are used to match the target response spectrum, especially for extreme intensity levels. One common state-of-the-art practice in

performance-based earthquake engineering is Incremental Dynamic Analysis that scales the same suite of ground motions up and down to cover a range of ground motion intensity levels (Vamvatsikos and Cornell, 2002, 2004). The scaling of ground motions, however, raise concerns that different ground motion characteristics (e.g., frequency content) are associated with different intensity levels (e.g., Han and Wen, 1994), and that distributions of the scaled ground motions are different from those of the unscaled ground motions from a random vibration perspective (Grigoriu, 2010). In some cases scaling introduces bias in structural response (e.g., Luco and Bazzurro, 2005) whereas in other cases scaled ground motions may produce similar structural response as unscaled ground motions (e.g., Shome et al., 1998; Iervolino and Cornell, 2005). Recent work by Baker (2005) shows that potential problems in scaling are mainly due to the discrepancies in spectral shape between the recorded ground motion and the target ground motion. When this spectral shape is characterized by ε , the number of logarithmic standard deviation of Sa of recorded ground motion from the predicted median ground motion, scaling can be used without introducing bias in structural response (Baker, 2007). It follows that if a target response spectrum captures a realistic spectral shape (and relevant ground motion properties) at various intensity levels, then ground motions can be selected and scaled to such a spectrum for unbiased structural response prediction (to the extent that elastic response spectra describe the relationship between ground motions and structural responses).

1.2 Objectives and scope

The focus of this dissertation is on advancing hazard-consistent selection and scaling methodology of recorded ground motions for nonlinear dynamic analysis and design as well as building codes and guidelines. PSHA-consistent ground motion selection needs to consider the aleatory and epistemic uncertainties in ground motions. Moreover, the concept of the CMS can be taken further with refined computation addressing spectral variability as well as application in ground motion selection for nonlinear dynamic analysis.

The Conditional Spectrum (CS) quantifies the conditional distribution of Sa at all periods given Sa at a conditioning period (T^*) of interest. The CS builds upon the CMS (which focuses on the mean), and includes a measure of the variance in addition to the mean. The

UHS, the CMS, and the CS are illustrated in Figure 1.1a, 1.1b, and 1.1c respectively. The consideration of the variability in the CS is important to capture the full distribution of the target S_a and its subsequent structural response analysis based on a target response spectrum, as briefly investigated in the “Impact of matching spectrum variance on structural response” section in Jayaram et al. (2011) and more thoroughly examined in this dissertation. While typical CMS calculations to date are produced for a single earthquake scenario using a single GMPM, a refined computation of the CS can incorporate multiple causal earthquakes from PSHA deaggregation and multiple GMPMs that are often considered in a PSHA computation. This refined computation also requires the extension of deaggregation from causal earthquakes to GMPMs so as to provide the intermediate inputs.

In addition to the refined computation of the CS, the recent availability of selection algorithms and structural models have facilitated ground motion selection and scaling to match the CS (with variability in addition to mean) for nonlinear dynamic analysis. One such algorithm has been developed by Jayaram et al. (2011) to enable computationally efficient selection of ground motions to match a target spectrum mean and variance. Alternative selection algorithms include those by e.g., Kottke and Rathje (2008), Wang (2011), and Bradley (2012a). Two-dimensional structural models have also been developed in OpenSEES (2011) for the recent FEMA P695 (ATC-63) project (Haselton and Deierlein, 2007; ATC, 2009), with strength deterioration (both cyclic and in-cycle) and stiffness deterioration (Ibarra et al., 2005). While the Jayaram et al. (2011) selection algorithm and the Haselton and Deierlein (2007) structural models are employed to illustrate the CS-based ground motion selection in this dissertation, these can be substituted by other algorithms and models.

Unlike the UHS, the CS has a varied spectral shape at different conditioning periods. Unlike the CMS, the CS additionally considers the spectral uncertainty about the mean. Several issues arise, however, when utilizing the CS as the target spectrum to select ground motions for structural performance assessments, and these issues are investigated in the following list:

- First, the computation of the CS requires the specification of a conditioning period. However, structures typically have responses that are sensitive to excitation over a

range of periods, including both higher-mode periods and “lengthened periods” associated with nonlinear behavior (e.g., Taghavi and Miranda, 2003; Haselton and Baker, 2006; Bradley et al., 2010a; Shome and Luco, 2010). Furthermore, when a structural design is not yet finalized, it is difficult to identify a single conditioning period. A question that follows may be: “What is the impact of conditioning period on structural response estimates?”

- Second, before running the structural analysis or even selecting ground motions, it is important to ask the question: “What is the objective of the structural analysis?” Nonlinear dynamic analysis can be an intensity-based assessment, which estimates structural response given ground motions with a specified intensity level (e.g., ATC, 2011). It can also be a risk-based assessment, which estimates the mean annual rate of exceeding a specified structural response amplitude. A risk-based assessment is also known as the first step of the “PEER Integral” in Cornell and Krawinkler (2000), a “drift hazard” calculation in Krawinkler and Miranda (2004), and “time-based assessment” in ATC (2011). The structural responses of interest may include Peak Story Drift Ratio (*PSDR*), Peak Floor Acceleration (*PFA*), member forces, or any other *EDP* of interest. Additionally, for intensity-based assessments, the objective could be prediction of mean response or also variability in response. It is perhaps not surprising that changing the structural analysis objective changes the appropriateness of different procedures for selecting ground motions.
- Third, to consider the use of the CS in practice, one may ask: “What difference does it make, if any, if other target response spectra are used instead?” Alternative target spectra may include most commonly the UHS, and more recently the CMS (which is the mean of the CS, without variability) that accounts for the correlations between S_a values across periods. A comparison of structural response results, obtained using ground motions selected and scaled to match different target spectra, will be useful for determining the practical impact of changing the target spectrum.

To advance the understanding of ground motion selection based on the CS, this dissertation proposes a more rigorous ground motion selection methodology which will carefully

examine the aleatory uncertainties from ground motion parameters, incorporate the epistemic uncertainties from multiple GMPMs, make adaptive changes to ground motions at various intensity levels, and typically use the CS as the new target spectrum. Depending on the conditioning period (which may range from high-mode periods to “lengthened periods”), the structural analysis objective (e.g., intensity-based and risk-based assessments of *PSDR* and *PFA*), and the target response spectrum (e.g., the UHS, the CMS, and the CS), conclusions regarding structural performance may differ. It is important to investigate such impacts, as well as the consistency with seismic hazard, to provide ground motion selection insights for future nonlinear dynamic analysis.

1.3 Contributions and chapter organization

This dissertation addresses various challenges of hazard-consistent ground motion selection. All chapters are designed to be autonomous, each being a self-contained paper that has either appeared in a publication or is in review for a future journal publication.

Chapter 2 presents the methodology of probabilistic seismic hazard deaggregation of GMPMs, which quantifies the probability that the exceedance of a given S_a level is predicted by a specific GMPM. A hypothetical site is used to illustrate the methodology and its underlying mathematics. Chapter 3 refines the CS calculation by incorporating the aleatory uncertainties from causal earthquakes and the epistemic uncertainties from GMPMs. The deaggregation of GMPMs from Chapter 2 provides the essential input information for this refined calculation. The methodology for the refined calculations with varying levels of complexity and accuracy are presented and illustrated through example sites from the western U.S.

Chapter 4 performs nonlinear dynamic analysis and risk-based assessments on a 20-story reinforced concrete frame structure using ground motions selected based on the CS. This CS-based ground motion selection utilizes the computation of the CS and the selection algorithm to match the target spectrum mean and variance. The conditioning period for the CS is varied to investigate its effect on structural response risk-based assessments. The CS, regardless of its conditioning period, essentially provides a robust link between the implied distribution of the selected ground motions and the site ground motion hazard, in

order to maintain hazard consistency. Chapter 5 then applies the CS-based ground motion selection methodology to structural analysis with an alternative objective of intensity-based assessments and evaluates the impact of such alternative target spectra as the UHS and the CMS. The findings from these analyses have potentially important implications for seismic assessments in both future building codes and performance-based earthquake engineering.

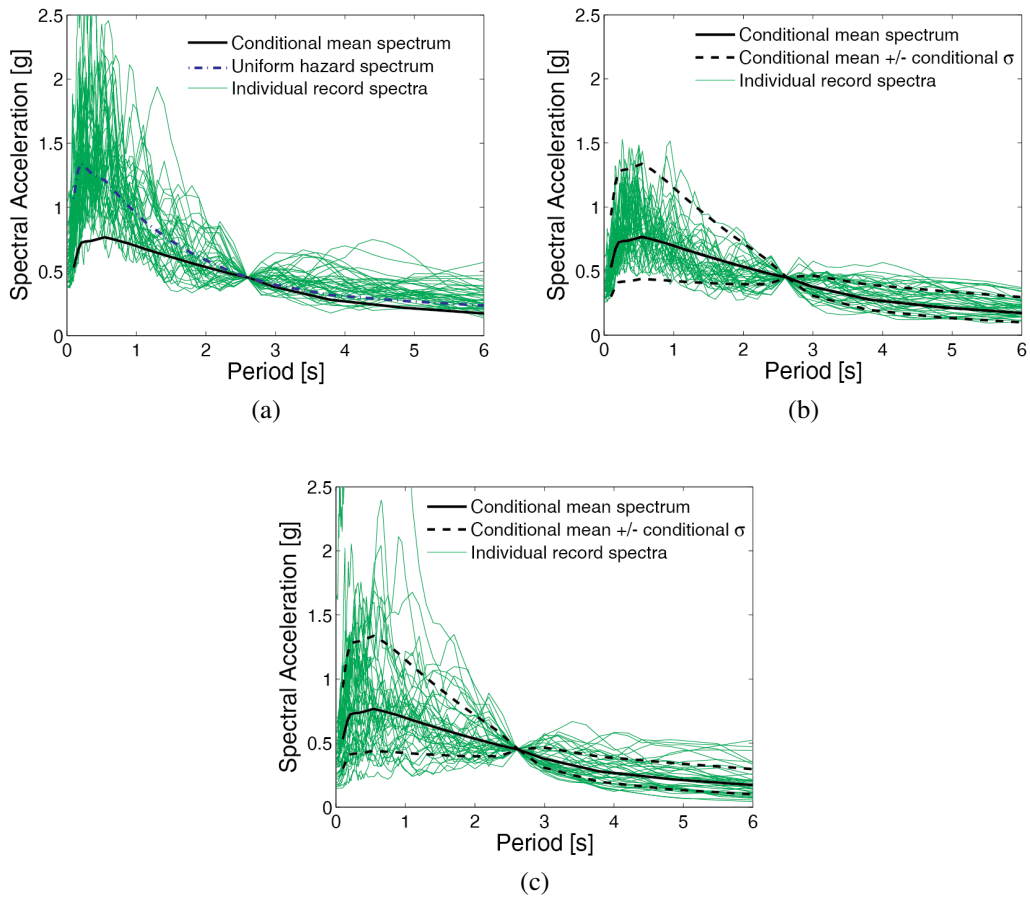


Figure 1.1: Response spectra of ground motions selected and scaled with (a) UHS, (b) CMS and (c) CS as target spectra for $Sa(2.6s)$ associated with 2% in 50 years probability of exceedance for an illustrative 20-story perimeter frame located in Palo Alto, CA.

Chapter 2

Probabilistic seismic hazard deaggregation of ground motion prediction models

Adapted from Lin, T. and J. W. Baker (2011). Probabilistic seismic hazard deaggregation of ground motion prediction models. In *5th International Conference on Earthquake Geotechnical Engineering*, Santiago, Chile.

2.1 Abstract

Probabilistic seismic hazard analysis (PSHA) combines the probabilities of all earthquake scenarios with different magnitudes and distances with predictions of resulting ground motion intensity, in order to compute seismic hazard at a site. PSHA also incorporates uncertainties in ground motion predictions, by considering multiple ground motion prediction models (GMPMs). Current ground motion selection utilizes probabilistic seismic hazard deaggregation to identify the distribution of earthquake scenarios that contribute to exceedance of a given spectral acceleration (S_a) level. That calculation quantifies effects of the aleatory uncertainties in earthquake events, but does not describe the epistemic uncertainties from multiple GMPMs. This chapter describes ways to calculate contributions of multiple GMPMs to S_a exceedance using deaggregation calculations. Deaggregation

of GMPMs plays an important role in the proposed target response spectrum computation for ground motion selection, in a similar way as logic tree weights of GMPMs do in PSHA computation. Just as the deaggregation of magnitude and distance identifies the relative contribution of each earthquake scenario to Sa exceedance, the deaggregation of GMPMs tells us the probability that the exceedance of that Sa level is predicted by a specific GMPM. We can further extend deaggregation to other ground motion parameters, such as earthquake fault mechanism, to more fully quantify the parameters that contribute to Sa values of interest. The proposed methodology for deaggregation of prediction models can be immediately applicable to other procedures which require multiple prediction models in an earlier stage of total prediction and a later stage of new target computation.

2.2 Introduction

Probabilistic seismic hazard analysis (PSHA) is commonly used in geotechnical earthquake engineering (e.g., Kramer, 1996) and structural dynamic analysis (e.g., Chopra, 2012) to identify the ground motion hazard for which geotechnical and structural systems are analyzed and designed. PSHA combines the probabilities of all earthquake scenarios with different magnitudes and distances with predictions of resulting ground motion intensity in order to compute seismic hazard at a site (e.g., McGuire, 2004). PSHA also incorporates uncertainties in ground motion predictions, by considering multiple ground motion prediction models (GMPMs) (e.g., Boore and Atkinson, 2008). In PSHA, aleatory uncertainties, which are inherently random, are accounted for by considering earthquake events with all possible magnitudes and distances; epistemic uncertainties, which are due to the lack of knowledge, can come from the uncertainty in identifying correct models such as GMPMs. GMPMs have inputs such as magnitude and distance, and outputs in terms of logarithmic mean and standard deviation of spectral acceleration (Sa) for various periods of vibration. When multiple GMPMs are considered in PSHA to represent our epistemic uncertainty, we use a logic tree to assign weights (equal or unequal) to each GMPM (Petersen et al., 2008; Scherbaum et al., 2005). PSHA then estimates seismic hazard at a site incorporating uncertainties in both earthquake scenarios and GMPMs.

As a key step in defining the seismic load input to nonlinear dynamic analysis, ground

motion selection often involves specification of a target spectrum such as the Conditional Mean Spectrum (CMS), which consists of the expected Sa values at all periods conditional on the Sa value at the period of interest, or its associated Conditional Spectrum (CS) that additionally includes variability (e.g., Baker and Cornell, 2006a; Abrahamson and Al Atik, 2010; Baker, 2011; Lin et al., 2012). The computation of the CMS or the CS requires specification of a GMPM. Current implementation of this ground motion selection approach uses the information from earthquake scenarios without considering multiple GMPMs. While PSHA computes the total seismic hazard using total probability theorem, PSHA deaggregation (McGuire, 1995; Bazzurro and Cornell, 1999; Harmsen, 2001) computes the relative contribution of earthquake parameters to the total hazard using Bayes' rule (Benjamin and Cornell, 1970). Current ground motion selection utilizes deaggregation results of magnitude and distance to identify causal events for a given Sa value associated with an annual rate of exceedance. In this chapter we consider ways to incorporate multiple GMPMs into ground motion selection techniques using refinements to PSHA deaggregation.

2.3 Methodology

PSHA deaggregation links the computation of a target spectrum to the total hazard prediction. Computation of a target CMS or CS requires deaggregation to identify the causal parameters, along with the choice of a GMPM. Multiple GMPMs are typically used for PSHA computation. For instance, the United States Geological Survey (USGS) specifies three models (Boore and Atkinson, 2008; Campbell and Bozorgnia, 2008; Chiou and Youngs, 2008) with equal weights for Coastal California (Petersen et al., 2008) in the logic tree, as highlighted in Figure 2.1. These models can be adjusted up or down to reflect additional epistemic uncertainties, as illustrated in the right-most branch in Figure 2.1. When multiple GMPMs are used in the total hazard prediction, PSHA deaggregation can be extended to include the relative contribution of GMPMs to the computation of a target spectrum for ground motion selection. This section will discuss the issues associated with obtaining this deaggregation.

2.3.1 Probabilistic seismic hazard analysis

PSHA integrates over all j potential earthquake sources with their associated annual rates of occurrence, v_j , and aleatory uncertainties such as magnitudes (M), distances (R), and epsilons (ϵ) in order to compute the annual rate of exceedance of a Sa level of interest, $v(Sa > y)$ (Kramer, 1996). Equation 2.1 depicts the conventional PSHA computation:

$$v(Sa > y) = \sum_j v_j \iiint f_{M,R,E}(m, r, \epsilon) P(Sa > y | m, r, \epsilon) dm dr d\epsilon \quad (2.1)$$

where $f_{M,R,E}(m, r, \epsilon)$ is the joint probability density function for magnitude m , distance r , and epsilon ϵ , and $P(Sa > y | m, r, \epsilon)$ is the probability of Sa exceeding a value y given m , r , ϵ with the underlying assumption of using a single GMPM.

PSHA is usually performed, however, with multiple GMPMs, an epistemic source of uncertainties. For instance, Figure 2.1 depicts the uncertainties in PSHA calculation through a logic tree with various weights assigned to magnitude range and GMPMs. We explicitly consider the epistemic uncertainty in PSHA by incorporating k GMPMs with their associated weights, $P(GMPM_k)$, into Equation 2.2, to compute the total hazard rate using the total probability theorem:

$$v(Sa > y) = \sum_k \sum_j v_j \iiint f_{M,R,E}(m, r, \epsilon) P(Sa > y | m, r, \epsilon, GMPM_k) dm dr d\epsilon P(GMPM_k) \quad (2.2)$$

where $P(Sa > y | m, r, \epsilon, GMPM_k)$ is the probability of Sa exceeding a value y given m , r , ϵ , and $GMPM_k$. The incorporation of GMPMs is directly related to the computation of a target spectrum, e.g. the CMS or the CS, as such computation requires the predictions from GMPMs.

2.3.2 Parameters for ground motion prediction

Equation 2.2 is the standard simplified equation for describing a PSHA calculation. As multiple GMPMs are used, variations in the parameters used must be considered. For instance, the models may differ in their distance definitions, as well as how they group and classify fault mechanisms; Table 2.1 illustrates these differences for the three models

used to predict ground motions from Coastal California crustal earthquakes in the USGS hazard maps. This variation presents challenges for the deaggregation process. When different definitions or groupings are used for similar ground motion properties, we need to convert one definition to another (e.g., using the distance conversion approaches proposed in Scherbaum et al., 2004) or re-group the inputs (e.g., sorting fault mechanisms according to dip and rake angles), in order to facilitate consistent deaggregation across GMPMs.

2.3.3 Deaggregation of magnitude, distance, and epsilon

Now we have computed the total hazard rate in Equation 2.2, we can find the distribution of magnitudes, distances, and epsilons that cause $Sa > y$ through deaggregation using Bayes' rule. For instance, the conditional distribution of magnitude given $Sa > y$, $f_{M|Sa>y}(m, y)$, can be computed as follows:

$$f_{M|Sa>y}(m, y) = \frac{1}{v(Sa > y)} \sum_k \sum_j v_j \iint f_{M,R,E}(m, r, \epsilon) P(Sa > y | m, r, \epsilon, GMPM_k) dr d\epsilon P(GMPM_k) \quad (2.3)$$

Since these parameters of interest are usually discretized in practice, the corresponding conditional distribution is expressed in terms of a percentage contribution to $Sa > y$, e.g., $P(M = m_j | Sa > y)$, instead of $f_{M|Sa>y}(m, y)$. The associated deaggregated mean magnitude, \bar{M} , can also be calculated as follows:

$$\bar{M} = E(M | Sa > y) = \sum_j m_j P(M = m_j | Sa > y) \quad (2.4)$$

The deaggregation of distance is similar in theory to the deaggregation of magnitude, except for the complication of sometimes differing definitions of distance in different GMPMs as discussed in 2.3.2. The deaggregated distribution of distance, $f_{R|Sa>y}(r, y)$, can be found as

follows, similar to Equation 2.3:

$$f_{R|Sa>y}(r, y) = \frac{1}{v(Sa > y)} \sum_k \sum_j v_j \iint f_{M,R,E}(m, r, \varepsilon) P(Sa > y | m, r, \varepsilon, GMPM_k) dm d\varepsilon P(GMPM_k) \quad (2.5)$$

The deaggregation of epsilon, ε , is an important step for the CMS or the CS computation, since the CMS or the CS utilizes the correlation between ε values across periods. Although it is similar in concept to the deaggregation of magnitude and distance, we should pay additional attention to the difference between the approach of McGuire (1995) and that of Bazzurro and Cornell (1999). McGuire's deaggregation is conditioned on $Sa = y$, so there is a single value of epsilon, ε^* , that corresponds to each Sa level (for a given magnitude and distance). On the other hand, Bazzurro and Cornell's deaggregation is conditioned on $Sa > y$, so the epsilon value, ε^* , that corresponds to $Sa = y$ is the lower bound value that marks the beginning of exceedance (Figure 2.2). For each event ($M = m_j, R = r_j$), to get an equivalent mean value of epsilon that corresponds to $Sa > y$, we can find a centroidal value of epsilon, $\bar{\varepsilon}$, integrated from the lower bound value, ε^* to infinity with respect to epsilon (Equations 2.6 and 2.7). Note that the tail of the ε distribution does not contribute significantly to this mean, so we can sometimes truncate the distribution at $\varepsilon = 4$ to 6, instead of infinity, without causing a significant difference in the numerical results (Strasser et al., 2008).

$$\bar{\varepsilon} | (Sa > y, M = m_j, R = r_j) = \int_{-\infty}^{\infty} \varepsilon f_E(\varepsilon | Sa > y, M = m_j, R = r_j) d\varepsilon \quad (2.6)$$

where $f_E(\varepsilon | Sa > y, M = m_j, R = r_j)$ is the conditional distribution of ε given $Sa > y$ and $M = m_j, R = r_j$, as shown in Figure 2.2 and defined by the following equation:

$$f_E(\varepsilon | Sa > y, M = m_j, R = r_j) = \begin{cases} \frac{\phi(\varepsilon)}{1 - \Phi(\varepsilon^*)} & \varepsilon \geq \varepsilon^* \\ 0 & \varepsilon < \varepsilon^* \end{cases} \Bigg| (Sa > y, M = m_j, R = r_j) \quad (2.7)$$

The deaggregated distribution of epsilon, $f_{E|Sa>y}(\epsilon, y)$, can be found as follows, similar to Equations 2.3 and 2.5:

$$f_{E|Sa>y}(\epsilon, y) = \frac{1}{v(Sa > y)} \sum_k \sum_j v_j \iint f_{M,R,E}(m, r, \epsilon) P(Sa > y | m, r, \epsilon, GMPM_k) dm dr P(GMPM_k) \quad (2.8)$$

Conditional distributions and mean values of magnitudes, distances, and epsilons given Sa , e.g., $f_{M|Sa>y}(m, y)$, are standard outputs of nearly all PSHA software, and are easily obtainable from the USGS interactive deaggregation web tool (USGS, 2012).

2.3.4 Deaggregation of other parameters

Magnitude, distance, and epsilon are currently the ground motion parameters that are of most interest, and deaggregation results for these parameters can be easily obtained from standard PSHA software. In certain regions or special applications, other uncertain parameters may also be of interest. The total hazard, $v(Sa > y)$, can be computed if other uncertain parameters, expressed as θ , are considered:

$$v(Sa > y) = \sum_k \sum_j v_j \iiint f_{M,R,E,\Theta}(m, r, \epsilon, \theta) P(Sa > y | m, r, \epsilon, \theta, GMPM_k) dm dr d\epsilon d\theta P(GMPM_k) \quad (2.9)$$

Deaggregation can be extended to other parameters in a similar fashion:

$$f_{\Theta|Sa>y}(\theta, y) = \frac{1}{v(Sa > y)} \sum_k \sum_j v_j \iiint f_{M,R,E,\Theta}(m, r, \epsilon, \theta) P(Sa > y | m, r, \epsilon, \theta, GMPM_k) dm dr d\epsilon P(GMPM_k) \quad (2.10)$$

For instance, θ could represent fault mechanism. Fault mechanism can be treated as discrete random variables, sometimes with several types lumped into one group. In practice,

this distribution is often inferred instead of explicitly calculated, by computing contributions of each earthquake source to exceedance of a given Sa value, and identifying typical mechanisms associated with that source.

2.3.5 Deaggregation of ground motion prediction models

The deaggregation of GMPMs is similar in concept to the deaggregation of magnitude, distance, and epsilon. It tells us the probability that the exceedance of a given Sa level is predicted by a specific GMPM, $P(GMPM_k|Sa > y)$, and can be found as follows, similar to Equation 2.3:

$$\begin{aligned} & P(GMPM_k|Sa > y) \\ &= \frac{1}{v(Sa > y)} \sum_j v_j \iiint f_{M,R,E}(m, r, \epsilon) P(Sa > y|m, r, \epsilon, GMPM_k) dm dr d\epsilon P(GMPM_k) \end{aligned} \quad (2.11)$$

This conditional probability is not necessarily equal to the weight assigned to the GMPM at the beginning of analysis. The initially assigned weight to the k^{th} GMPM, $P(GMPM_k)$, is analogous to a prior probability, while the deaggregated weight, $P(GMPM_k|Sa > y)$, is analogous to a posterior probability in decision analysis (Benjamin and Cornell, 1970). Note that all of the terms required in Equation 2.11 are already computed as part of the standard PSHA calculation of Equation 2.2, so obtaining this probability is merely a matter of outputting additional information and does not require complex calculations.

2.3.6 Deaggregation of GMPM-specific parameters

To match the contribution of each GMPM to its associated ground motion parameters, we also need to obtain the joint conditional distribution of magnitudes (and of distances and of epsilons) and the specified GMPM that causes $Sa > y$, as follows:

$$\begin{aligned} & f_{M,GMPM|Sa>y}(m, GMPM_k, y) \\ &= \frac{1}{v(Sa > y)} \sum_j v_j \iint f_{M,R,E}(m, r, \epsilon) P(Sa > y|m, r, \epsilon, GMPM_k) dr d\epsilon P(GMPM_k) \end{aligned} \quad (2.12)$$

Similarly to above, when the continuous variables are discretized, the corresponding conditional distribution is expressed as $P(M = m_j, GMPM_k | Sa > y)$ instead. It follows that the relative contribution of magnitude to $Sa > y$ given a GMPM is:

$$P(M = m_j | GMPM_k, Sa > y) = \frac{P(M = m_j, GMPM_k | Sa > y)}{P(GMPM_k | Sa > y)} \quad (2.13)$$

The resulting expected magnitude can be calculated as follows:

$$\bar{M}_k = E(M | GMPM_k, Sa > y) = \sum_j m_j P(M = m_j | GMPM_k, Sa > y) \quad (2.14)$$

where \bar{M}_k is used to denote the deaggregated (posterior) mean magnitude associated with $GMPM_k$. Deaggregation of GMPMs with their associated ground motion parameters enables the improved computation of the CS with probabilistic consistency as discussed in the next chapter.

2.4 Example application

To illustrate the use of the above equations, we now perform PSHA and deaggregation for an example site. First, we estimate the ground motion hazard at the example site using PSHA that incorporates multiple GMPMs. Next, we identify the relative contributions of the events (with associated properties) and GMPMs to the hazard prediction using the refined PSHA deaggregation.

2.4.1 Description of site and events

The example hypothetical site considered has two parallel faults, as shown in Figure 2.3. Fault A, produces earthquakes with magnitude, $M = 6$ and distance, $R = 10$ km from the site, and has an annual occurrence rate of $\nu = 0.01$; we denote this earthquake Event A. Fault B produces earthquakes with magnitude, $M = 8$ and distance, $R = 25$ km from the site, and has an annual occurrence rate of $\nu = 0.002$; we denote this earthquake Event B. Both events have strike slip mechanism. The site has mean shear wave velocity in the upper

30 m of $V_{S30} = 760$ m/s, corresponding to NEHRP Site Class B/C. Assuming a rupture that extends to the ground surface (a reasonable assumption for shallow crustal earthquakes in Coastal California), rupture distance, R_{RUP} , is the same as R_{JB} . The earthquake events are assumed to rupture the whole length of faults A and B, so the closest distance to the site for a given earthquake will be a known constant. We study the site for a structure with a period of vibration of interest, T^* , of 1 s.

2.4.2 PSHA computation

We use the three GMPMs discussed above with equal prior weights to evaluate the annual rates of exceeding a target Sa level for both events. The probability of exceeding a target Sa level given an event with its associated magnitude (m_j) and distance (r_j), $P(Sa > y | m_j, r_j, GMPM_k)$, is computed using logarithmic Sa mean ($\mu_{\ln Sa(T^*)}$) and standard deviation ($\sigma_{\ln Sa(T^*)}$) predictions from each GMPM. The annual rate of Sa exceedance, $v(Sa > y)$, is computed using Equation 2.2 for multiple values of y , and the resulting hazard curve is shown in Figure 2.4, along with individual hazard curves for Events A and B. We can find the target Sa values of interest from the hazard curve.

2.4.3 Deaggregation of events

In this simplified site, each event ($Event_j$) corresponds to a single magnitude (m_j) and distance (r_j). The conditional probability that each event causes $Sa > y$ is given by expressions such as Equation 2.3, and can be simplified for this site as follows:

$$P(Event_j | Sa > y) = \frac{v(Sa > y, Event_j)}{v(Sa > y)} \quad (2.15)$$

where

$$v(Sa > y, Event_j) = \sum_k P(Sa > y | Event_j, GMPM_k) v(Event_j) P(GMPM_k) \quad (2.16)$$

The probabilities obtained from Equation 17 are plotted in Figure 2.5. From Figure 2.5, we can see that the smaller but more frequent Event A is most likely to cause exceedance

of small Sa levels, whereas the larger and rarer Event B is most likely to cause exceedance of large Sa levels. This is because the annual hazard rate involves two competing factors: annual rate of occurrence for an earthquake, and probability of exceeding a Sa level given that earthquake. The results in Figure 2.5 are typical of PSHA analyses for more realistic sites.

2.4.4 Deaggregation of GMPMs

Following Equation 2.11, the deaggregation of GMPMs is performed, and the results of this deaggregation calculation are shown in Figure 2.6. The deaggregated GMPM contributions vary from 0.09 to 0.55, instead of having an equal weight of 0.33, as target Sa values vary. This is because the GMPMs are not equally likely to predict the exceedance of a given Sa level.

2.4.5 Deaggregation of ground motion parameters

The deaggregated mean magnitude associated with a specific GMPM can be found using Equation 2.14. The results are shown in Figure 2.7. In this figure, the thin lines indicate the mean magnitude, given $Sa > y$ and given that the associated GMPM is the model that predicts $Sa > y$. The heavy line provides a weighted average (composite) over all GMPMs, as computed using Equation 2.4.

The deaggregated mean distance and epsilon values can be obtained using similar procedures and are plotted in Figure 2.8 and Figure 2.9. The distance deaggregation results resemble the magnitude deaggregation results due to the one-to-one correspondence between magnitudes and distances in this simple example.

2.5 Availability of GMPM deaggregation

The USGS has recently begun providing GMPM deaggregation outputs in the 2008 Interactive Deaggregation website (USGS, 2012), as seen in the illustration of the tool shown in Figure 2.10. The deaggregation outputs now optionally include deaggregation of $M/R/\epsilon$ combinations for each GMPM as well as individual GMPM contribution to the overall

hazard in real sites. This will enable the assessment of the CMS or the CS computation incorporating aleatory and epistemic uncertainties, and benefit ground motion selection for real sites.

2.6 Conclusions

Probabilistic seismic hazard analysis (PSHA) deaggregation of ground motion prediction models (GMPMs) links the computation of a target spectrum to the total hazard prediction. PSHA is commonly used to compute the ground motion hazard for which geotechnical and structural systems are analyzed and designed. As a key step in defining the seismic load input to nonlinear dynamic analysis, ground motion selection often involves specification of a target spectrum, e.g., the Conditional Mean Spectrum (CMS) or the Conditional Spectrum (CS). Computation of such a target spectrum requires deaggregation to identify the causal ground motion parameters, along with the predictions from multiple GMPMs. Current ground motion selection incorporates the aleatory uncertainties from earthquake scenarios without considering the epistemic uncertainties from multiple GMPMs. Here we account for both aleatory and epistemic uncertainties in ground motion selection through PSHA deaggregation of GMPMs.

This GMPM deaggregation is consistent with the probabilistic treatment of the magnitude and distance random variables in traditional PSHA. The deaggregation of GMPMs provides additional insights into which GMPM contributes most to prediction of S_a values of interest. To match the contribution of each GMPM to its associated ground motion parameters, separate deaggregation of $M/R/\epsilon$ parameters for each GMPM is also performed. These calculations are illustrated through applications on an example site. First, we estimate the hazard using PSHA that incorporates multiple GMPMs. Next, we identify the relative contributions of events and GMPMs to the hazard prediction using the refined deaggregation procedures.

This GMPM deaggregation is now available at the USGS Interactive Deaggregation website. This tool facilitates assessments of real sites incorporating aleatory and epistemic uncertainties, and aids ground motion selection efforts through refined computation of a

PSHA-consistent target spectrum. The proposed methodology for deaggregation of prediction models can also be immediately applicable to other procedures that require multiple prediction models in an earlier stage of total prediction and a later stage of new target computation (Lin, 2012).

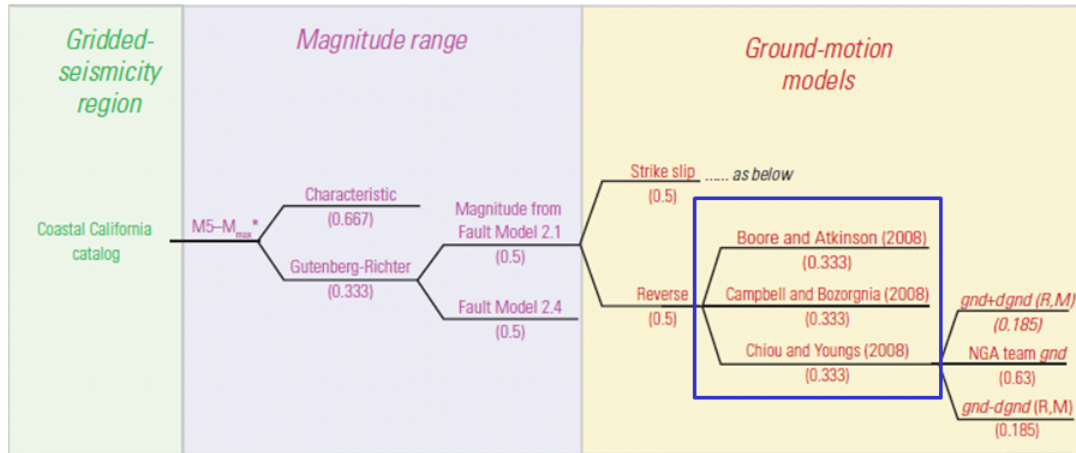


Figure 2.1: Uncertainties in USGS PSHA logic tree for Coastal California. (from Petersen et al., 2008)

Table 2.1: Parameters used for the Ground Motion Prediction Models considered in Coastal California

GMPM	Boore and Atkinson 2008	Campbell and Bozorgnia 2008	Chiou and Youngs 2008
Magnitude	M_W	M_W	M_W
Distance	R_{JB}	R_{JB}, R_{RUP}	R_{JB}, R_{RUP}, R_X
Fault Mechanism	Unspecified, strike slip, normal, thrust/reverse	Strike slip, normal/normal-oblique, reverse/reverse-oblique (dip and rake angles)	Strike slip/normal-oblique, normal, reverse/reverse-oblique (dip and rake angles)
Other Variables	V_{S30}	$V_{S30}, Z_{TOR}, Z_{2.5}$	$V_{S30}, Z_{TOR}, Z_{1.0}, AS$

M_W = Moment magnitude.

R_{JB} = Shortest distance from the recording site to the surface projection of the rupture.

R_{RUP} = Shortest distance from the recording site to the rupture.

R_X = Site coordinate measured perpendicular to the fault strike from the surface projection of the updip edge of the rupture, with the downdip direction being positive; used to determine hanging-wall flag.

V_{S30} = Shear wave velocity averaged over the top 30 m.

Z_{TOR} = Depth to the top of the rupture.

$Z_{1.0}$ = Depth to the 1.0 km/s shear-wave velocity horizon.

$Z_{2.5}$ = Depth to the 2.5 km/s shear-wave velocity horizon.

AS = Aftershock flag.

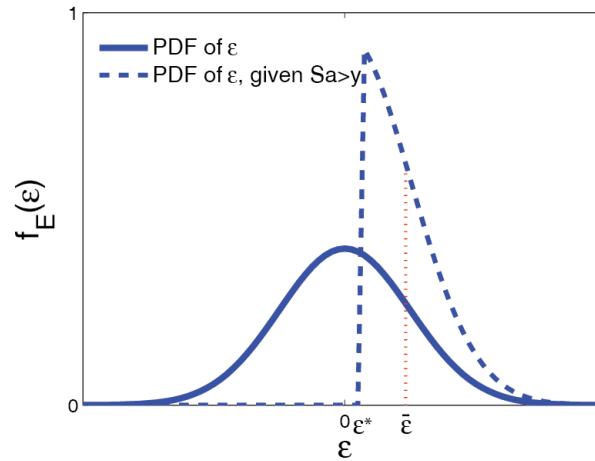


Figure 2.2: Probability density function of epsilons demonstrating the deaggregation difference between ϵ^* conditioned on $Sa = y$ in McGuire (1995) and $\bar{\epsilon}$ conditioned on $Sa > y$ in Bazzurro and Cornell (1999).

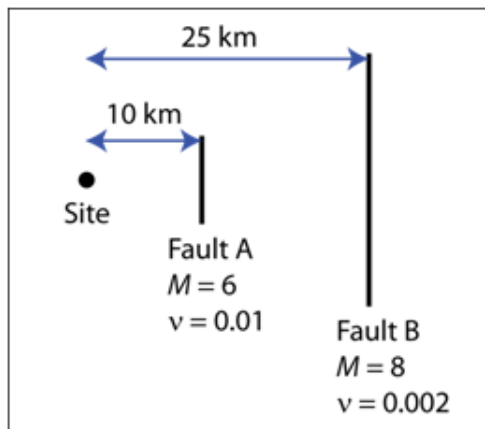


Figure 2.3: Layout of an example site dominated by two earthquake events A and B.

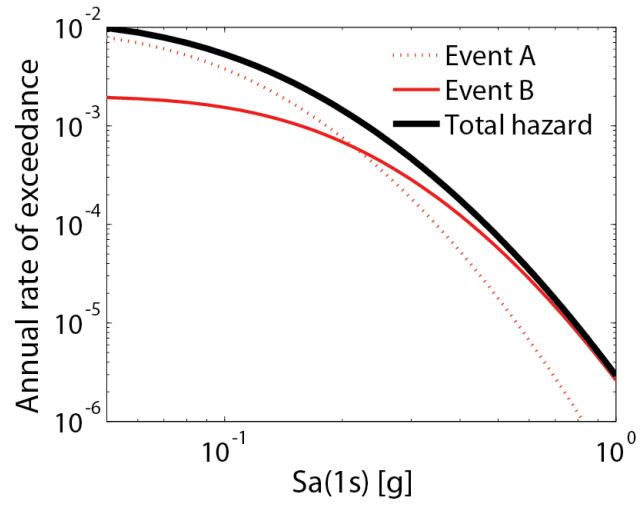


Figure 2.4: Hazard curves for the example site.

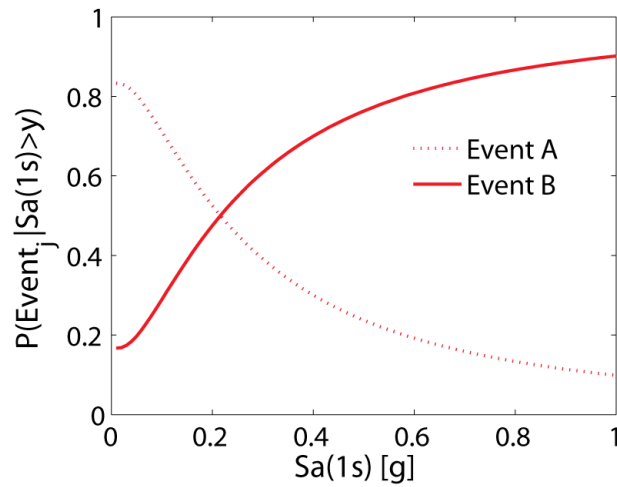


Figure 2.5: Deaggregation of events given $Sa(1s) > y$ for the example site.

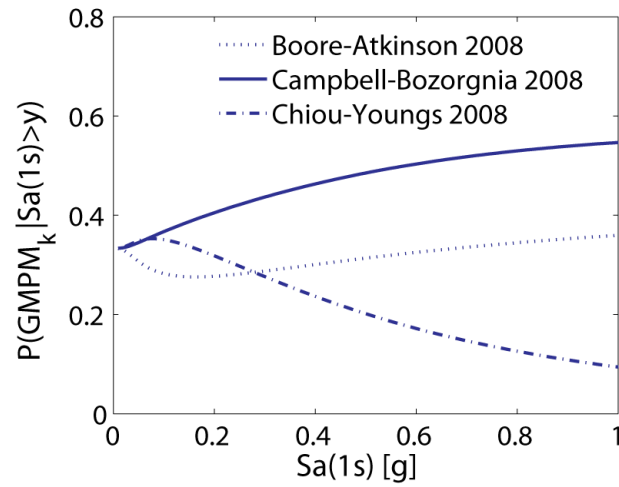


Figure 2.6: Deaggregation of GMPMs given $Sa(1s) > y$ for the example site.

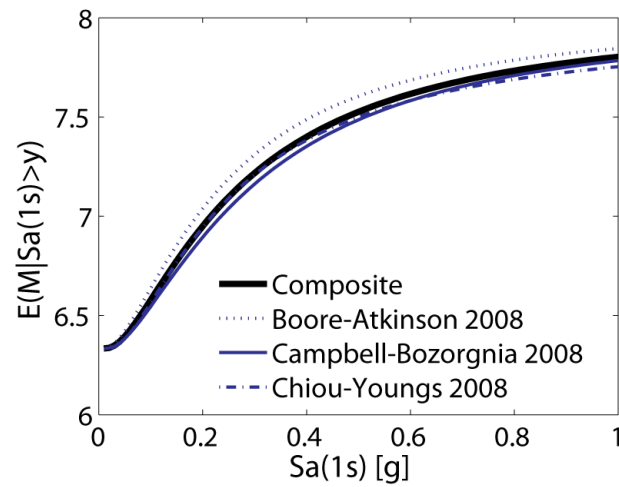


Figure 2.7: Deaggregation of magnitudes given $Sa(1s) > y$ for the example site.

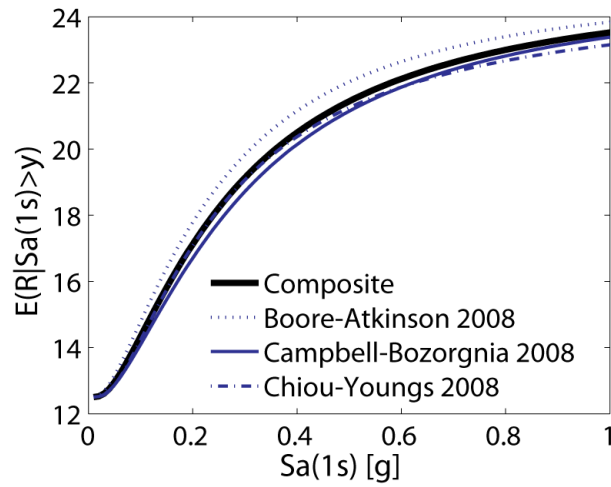


Figure 2.8: Deaggregation of distances given $Sa(1s) > y$ for the example site.

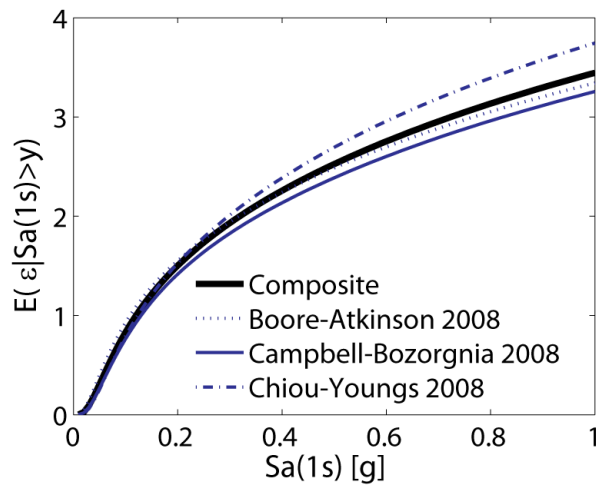
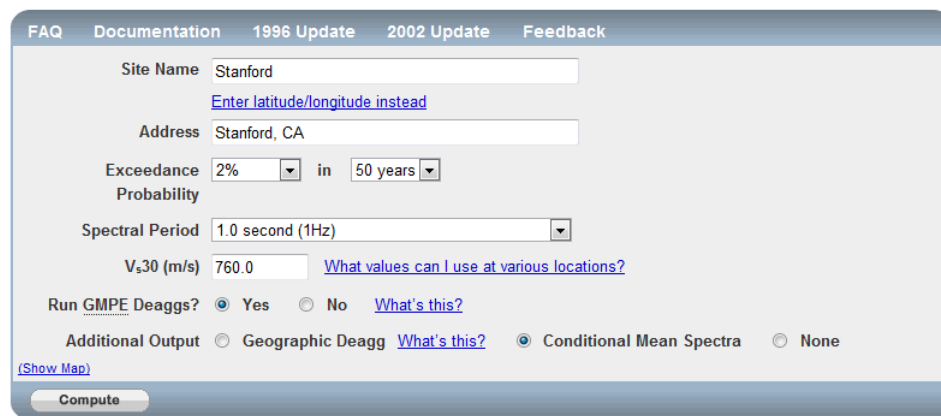


Figure 2.9: Deaggregation of epsilons given $Sa(1s) > y$ for the example site.



The screenshot shows a web interface for GMPM deaggregation. At the top, there are navigation links: [FAQ](#), [Documentation](#), [1996 Update](#), [2002 Update](#), and [Feedback](#). The main form contains the following fields and options:

- Site Name:** A text input field containing "Stanford". Below it is a blue link: [Enter latitude/longitude instead](#).
- Address:** A text input field containing "Stanford, CA".
- Exceedance Probability:** A dropdown menu set to "2%" followed by the text "in" and another dropdown menu set to "50 years".
- Spectral Period:** A dropdown menu set to "1.0 second (1Hz)".
- V_{s,30} (m/s):** A text input field containing "760.0". To its right is a blue link: [What values can I use at various locations?](#)
- Run GMPE Deaggs?:** Radio buttons for "Yes" (selected), "No", and a blue link: [What's this?](#)
- Additional Output:** Radio buttons for "Geographic Deagg" (with a blue link: [What's this?](#)), "Conditional Mean Spectra" (selected), and "None".

At the bottom left, there is a blue link: [\(Show Map\)](#). At the bottom center, there is a "Compute" button.

Figure 2.10: USGS implementation of GMPM deaggregation. (from USGS, 2012)

Chapter 3

Conditional Spectrum computation incorporating multiple causal earthquakes and ground motion prediction models

Lin, T., S. C. Harmsen, J. W. Baker, and N. Luco (2012). Conditional Spectrum computation incorporating multiple causal earthquakes and ground motion prediction models. *Bulletin of the Seismological Society of America* (in press).

3.1 Abstract

The Conditional Spectrum (CS) is a target spectrum (with conditional mean and conditional standard deviation) that links seismic hazard information with ground motion selection for nonlinear dynamic analysis. Probabilistic seismic hazard analysis (PSHA) estimates the ground motion hazard by incorporating the aleatory uncertainties in all earthquake scenarios and resulting ground motions as well as the epistemic uncertainties in ground motion prediction models (GMPMs) and seismic source models. Typical CS calculations to date are produced for a single earthquake scenario using a single GMPM, but more precise use requires consideration of at least multiple causal earthquakes and multiple GMPMs that

are often considered in a PSHA computation. This chapter presents the mathematics underlying these more precise CS calculations. Despite requiring more effort to compute than approximate calculations using a single causal earthquake and GMPM, the proposed approach produces an exact output that has a theoretical basis. To demonstrate the results of this approach and compare the exact and approximate calculations, several example calculations are performed for real sites in the western U.S. (WUS). The results also provide some insights regarding the circumstances under which approximate results are likely to closely match more exact results. To facilitate these more precise calculations for real applications, the exact CS calculations can now be performed for real sites in the U.S. using new deaggregation features in the U.S. Geological Survey hazard mapping tools. Details regarding this implementation are discussed in this chapter.

3.2 Introduction

Ground motion selection for structural and geotechnical system analysis is often associated with a target response spectrum that is derived from probabilistic seismic hazard analysis (PSHA) results. The Conditional Spectrum (CS) is one such target spectrum that estimates the distribution (with mean and standard deviation) of the response spectrum, conditioned on the occurrence of a target spectral acceleration value at the period of interest. As this CS concept is considered for practical use, several common approximations need to be further explored. Typical CS calculations to date are produced for a single earthquake ground motion scenario (i.e., magnitude, distance, and ground motion intensity of interest), and computed using a single ground motion prediction model (GMPM). The scenario is generally determined from PSHA deaggregation, but PSHA deaggregation calculations for real sites often show that multiple earthquake scenarios contribute to occurrence of a given ground motion intensity. Additionally, modern PSHA calculations are performed with multiple GMPMs using a logic tree that also includes seismic source models. Incorporating those features is thus necessary to compute a CS that is fully consistent with the PSHA calculations upon which it is based.

This chapter presents the methodology for performing refined CS computations that

precisely incorporate the aleatory uncertainties (which are inherently random) in earthquake events with all possible magnitudes and distances, as well as the epistemic uncertainties (which are due to limited knowledge) from multiple GMPMs and seismic source models. Three approximate calculation approaches and the exact calculation approach are presented, with increasing levels of complexity and accuracy. To demonstrate, several example calculations are performed for representative sites with different surrounding seismic sources: Stanford in northern California, Bissell in southern California, and Seattle in the Pacific Northwest. The results evaluate the exact and approximate calculations, and analyze factors that contribute to the differences in accuracy. Note that while the exact approach is more cumbersome, it does not need to be computed by the user, since these exact CS calculations have been implemented in the U.S. Geological Survey (USGS) seismic hazard mapping tools, and could be incorporated into other PSHA software as well. Details regarding this new tool, and issues related to implementation of these concepts, are provided below.

3.2.1 Basic Conditional Spectrum computation

A wide variety of techniques have been developed in the past to select ground motion inputs for nonlinear dynamic analysis (e.g., Haselton et al., 2009; Katsanos et al., 2010). One common approach involves selecting ground motions whose response spectra match the target spectrum (e.g., Watson-Lamprey and Abrahamson, 2006; Beyer and Bommer, 2007; ASCE, 2010; ATC, 2011). The Conditional Mean Spectrum (CMS) is one such spectrum that incorporates correlation across periods (Baker and Cornell, 2006a; Baker and Jayaram, 2008; Somerville and Hamburger, 2009; Abrahamson and Al Atik, 2010; Gulerce and Abrahamson, 2011; Somerville and Thio, 2011) to estimate the expected Sa values at all periods T_i ($Sa(T_i)$) given the target Sa value at the period of interest T^* ($Sa(T^*)$).

The basic CMS computation procedure is as follows. First, obtain the target spectral acceleration at period T^* , $Sa(T^*)$, from PSHA, and its associated mean causal earthquake magnitude (M), distance (R), and other parameters (θ), from deaggregation. Next, use a GMPM to obtain the logarithmic mean and standard deviation of Sa at all periods T_i , denoted as $\mu_{\ln Sa}(M, R, \theta, T_i)$ and $\sigma_{\ln Sa}(M, \theta, T_i)$. For any $Sa(T_i)$ value, compute the $\varepsilon(T_i)$, the

number of standard deviations by which $\ln Sa(T_i)$ differs from the mean spectral ordinate predicted by a given GMPM, $\mu_{\ln Sa}(M, R, \theta, T_i)$, at T_i

$$\varepsilon(T_i) = \frac{\ln Sa(T_i) - \mu_{\ln Sa}(M, R, \theta, T_i)}{\sigma_{\ln Sa}(M, \theta, T_i)} \quad (3.1)$$

The target $\varepsilon(T^*)$ (for the target $Sa(T^*)$ value) can also be computed using Equation 3.1. We can then compute the conditional mean spectral acceleration at other periods T_i , $\mu_{\ln Sa(T_i)|\ln Sa(T^*)}$, using the correlation coefficient between pairs of ε values at two periods, $\rho(\varepsilon(T_i), \varepsilon(T^*))$ (hereinafter referred to as $\rho(T_i, T^*)$) (from e.g., Baker and Jayaram, 2008)

$$\mu_{\ln Sa(T_i)|\ln Sa(T^*)} = \mu_{\ln Sa}(M, R, \theta, T_i) + \rho(T_i, T^*) \sigma_{\ln Sa}(M, \theta, T_i) \varepsilon(T^*) \quad (3.2)$$

The spectrum defined by $\mu_{\ln Sa(T_i)|\ln Sa(T^*)}$ in Equation 3.2 has been termed the ‘‘CMS’’, as it specifies the mean values of $\ln Sa(T_i)$, the exponentials of which are equivalent to the median values of $Sa(T_i)$ if it is lognormally distributed, conditional on the value of $\ln Sa(T^*)$ (e.g., Baker, 2011).

Similarly, we can compute $\sigma_{\ln Sa(T_i)|\ln Sa(T^*)}$, the conditional standard deviation of spectral acceleration at period T_i , conditioned on the value of Sa at T^*

$$\sigma_{\ln Sa(T_i)|\ln Sa(T^*)} = \sigma_{\ln Sa}(M, \theta, T_i) \sqrt{1 - \rho^2(T_i, T^*)} \quad (3.3)$$

The conditional standard deviation $\sigma_{\ln Sa(T_i)|\ln Sa(T^*)}$ from Equation 3.3, when combined with the conditional mean value $\mu_{\ln Sa(T_i)|\ln Sa(T^*)}$ from Equation 3.2, specifies a complete distribution of logarithmic spectral acceleration values at all periods (where the distribution at a given period is Gaussian, as justified by Jayaram and Baker (2008)). We term the resulting spectrum distribution as a ‘‘CS’’, to be distinguished from the ‘‘CMS’’ that does not consider the variability specified by Equation 3.3. It is noteworthy that as an extension of the CMS approach, Bradley (2010a) proposed a generalized conditional intensity measure (GCIM) approach that considers the complete distribution of conditional intensity measures other than Sa .

The input earthquake parameters required for the CS calculations above are those required by the GMPM, and can include magnitude (M), distance (R), and other parameters

such as rupture mechanism and site conditions (θ). In this chapter, we will sometimes use M/R in the text as an abbreviation for $M/R/\theta$ (although θ will be included in equations where appropriate). To implement the CS in practice, we need to determine which M/R and GMPM to use. Common approximations to compute the CS include using the mean magnitude and distance from deaggregation, along with a single GMPM (Baker, 2011). As explained more in the next section, these approximations need to be evaluated for the practical implementation of CS as a target spectrum for selecting ground motions.

3.2.2 Deaggregation

Computing CS at real sites requires us to consider the following two factors: First, deaggregation will produce multiple causal earthquake magnitude and distance values for a given $Sa(T^*)$ amplitude, as illustrated in the USGS deaggregation plots in Figure 3.1, where the height of each column represents the percentage contribution from each M/R combination. Second, PSHA calculations use multiple GMPMs and seismic source models to compute seismic hazard at a site through a logic tree (e.g., Kramer, 1996; McGuire, 2004; Scherbaum et al., 2005; Bommer and Scherbaum, 2008; Petersen et al., 2008). A refined CS computation, therefore, needs to consider multiple causal earthquakes and GMPMs, if not multiple seismic source models.

PSHA (e.g., Kramer, 1996; McGuire, 2004) accounts for the aleatory uncertainties in earthquake events, by combining the frequencies of occurrence of all earthquake scenarios with different magnitudes and distances with predictions of resulting ground motion intensity, in order to compute seismic hazard at a site. PSHA also incorporates the epistemic uncertainties in the seismic source models and ground motion predictions, by considering multiple models in a logic tree. For instance, the USGS utilizes three GMPMs (Boore and Atkinson, 2008; Campbell and Bozorgnia, 2008; Chiou and Youngs, 2008) for crustal seismic sources in the WUS (Petersen et al., 2008). Traditional PSHA deaggregation (McGuire, 1995; Bazzurro and Cornell, 1999; Harmsen, 2001), however, only reports distributions of causal $M/R/\epsilon$ values given an Sa amplitude. The McGuire (1995) deaggregation is conditional on Sa that equals a target value, termed “ Sa occurrence”, while the Bazzurro and Cornell (1999) deaggregation is conditional on Sa that exceeds a target

value, termed “ Sa exceedance”. Depending on the Sa values of interest, either deaggregation approach can be used. Such deaggregation can be extended to include distributions of the logic tree branches, such as GMPMs, that contribute to predictions of Sa occurrence (or exceedance).

Just as the deaggregation of magnitude and distance identifies the relative contribution of each earthquake scenario to Sa occurrence (or exceedance), the deaggregation of GMPMs tells us the probability that the occurrence (or exceedance) of that Sa level is predicted by a specific GMPM. Note that the GMPM deaggregation weights differ from the logic-tree weights; in decision analysis (e.g., Benjamin and Cornell, 1970), the logic-tree weights are equivalent to prior weights, whereas the deaggregation weights may be interpreted as posterior weights given the occurrence (or exceedance) of the ground motion amplitude of interest. Additional details on GMPM deaggregation are provided in Lin and Baker (2011). For the purpose of response spectrum predictions, the key elements are the GMPMs and their input earthquake parameters (e.g., M , R , ϵ). Hence, the focus of deaggregation here will be on these two. The other portions of the logic tree (e.g., recurrence type, rates, maximum magnitude) do not influence spectrum predictions and so can be grouped for the purpose of these calculations. The USGS has recently begun providing GMPM deaggregation outputs. These outputs facilitate the exact calculations of CS described below.

3.3 Conditional Spectrum calculation approaches

We now consider several options for computing CS that incorporate consideration of multiple causal earthquake scenarios and multiple GMPMs, as well as multiple seismic source models and their logic-tree branches. We introduce several approximate calculation approaches with increasing complexity but also with increasing accuracy, followed by the exact calculation. Differences between the approaches are highlighted, and these approaches are evaluated later to determine the accuracy of the approximate approaches.

3.3.1 Method 1: Approximate CS using mean M/R and a single GMPM

The most basic method for computing an approximate CS is to utilize a single earthquake scenario and single GMPM, so that Equations 3.2 and 3.3 can be used directly. In current practice, this is done by taking the mean value of the causal magnitudes and distances from deaggregation, denoted here as \bar{M} and \bar{R} (Baker, 2011). Similarly, the mean value of other causal parameters ($\bar{\theta}$) can be obtained or inferred from deaggregation. These mean values can then be used with a single GMPM (even though the underlying hazard analysis utilized several GMPMs). The resulting CS calculations are given below, utilizing subscript k 's to denote that the calculations are based on a single GMPM indexed by k . The equations are also denoted as being approximately equal to the true CS values, given the simplifications made here.

$$\mu_{\ln Sa, k(T_i)|\ln Sa(T^*)} \approx \mu_{\ln Sa, k}(\bar{M}, \bar{R}, \bar{\theta}, T_i) + \rho(T_i, T^*) \sigma_{\ln Sa, k}(\bar{M}, \bar{\theta}, T_i) \bar{\epsilon}(T^*) \quad (3.4)$$

$$\sigma_{\ln Sa, k(T_i)|\ln Sa(T^*)} \approx \sigma_{\ln Sa, k}(\bar{M}, \bar{\theta}, T_i) \sqrt{1 - \rho^2(T_i, T^*)} \quad (3.5)$$

where the mean and standard deviation predicted by GMPM k are denoted $\mu_{\ln Sa, k}$ and $\sigma_{\ln Sa, k}$, and the CS computed for GMPM k is denoted $\mu_{\ln Sa, k(T_i)|\ln Sa(T^*)}$ and $\sigma_{\ln Sa, k(T_i)|\ln Sa(T^*)}$. Note that the correlation coefficient, ρ , is assumed to be constant for each GMPM – this could be revised if desired.

3.3.2 Method 2: Approximate CS using mean M/R and GMPMs with logic-tree weights

We can refine Method 1 above by considering all GMPMs used in the PSHA computation. The PSHA logic tree weights each model (these weights can be equal or unequal), and here we denote the weight for model k as p_k^l where the superscript l refers to logic-tree. To obtain an approximate CS using all of these GMPMs, we repeat the single-GMPM calculation (Equations 3.4 and 3.5) to obtain $\mu_{\ln Sa, k(T_i)|\ln Sa(T^*)}$ and $\sigma_{\ln Sa, k(T_i)|\ln Sa(T^*)}$ for each GMPM. We then sum up the resulting mean spectra ($\mu_{\ln Sa(T_i)|\ln Sa(T^*)}$), weighted by

the logic-tree weights, to get a mean spectrum

$$\mu_{\ln Sa(T_i)|\ln Sa(T^*)} \approx \sum_k p_k^l \mu_{\ln Sa,k(T_i)|\ln Sa(T^*)} \quad (3.6)$$

The computation of conditional standard deviations is slightly more complicated, as it not only accounts for the mean of the standard deviations from the GMPMs, but also includes the additional uncertainty introduced by the variation in mean predictions among the GMPMs. Formal probabilistic modeling (e.g., Ditlevsen, 1981) can be used to show that the resulting conditional standard deviation is

$$\sigma_{\ln Sa(T_i)|\ln Sa(T^*)} \approx \sqrt{\sum_k p_k^l (\sigma_{\ln Sa,k(T_i)|\ln Sa(T^*)}^2 + (\mu_{\ln Sa,k(T_i)|\ln Sa(T^*)} - \mu_{\ln Sa(T_i)|\ln Sa(T^*)})^2)} \quad (3.7)$$

In Equations 3.6 and 3.7, we no longer have a subscript k on the resulting $\mu_{\ln Sa(T_i)|\ln Sa(T^*)}$ and $\sigma_{\ln Sa(T_i)|\ln Sa(T^*)}$, since the results are no longer specific to a single GMPM but incorporate multiple GMPMs.

While the use of logic-tree weights is not rigorously correct, we introduce it here as a convenient approximation because these equations do not require GMPM deaggregation outputs, which are not currently available from many PSHA software tools.

3.3.3 Method 3: Approximate CS using GMPM-specific mean M/R and GMPMs with deaggregation weights

In this section, we further refine the CS calculations by taking advantage of GMPM deaggregation if it is available (e.g., as it is from the new USGS tools). First, GMPM deaggregation will provide separate M/R deaggregation for each prediction model. Here we will use the mean M and R values for each model, denoted as \bar{M}_k and \bar{R}_k for GMPM k . Using these values, means and standard deviations of the CS can be computed for GMPM k as follows

$$\mu_{\ln Sa,k(T_i)|\ln Sa(T^*)} \approx \mu_{\ln Sa,k}(\bar{M}_k, \bar{R}_k, \bar{\theta}_k, T_i) + \rho(T_i, T^*) \sigma_{\ln Sa,k}(\bar{M}_k, \bar{\theta}_k, T_i) \bar{\epsilon}_k(T^*) \quad (3.8)$$

$$\sigma_{\ln Sa, k(T_i)|\ln Sa(T^*)} \approx \sigma_{\ln Sa, k}(\bar{M}_k, \bar{\theta}_k, T_i) \sqrt{1 - \rho^2(T_i, T^*)} \quad (3.9)$$

Note that the GMPM-specific \bar{M}_k and \bar{R}_k (in Equations 3.8 and 3.9) are different from the \bar{M} and \bar{R} with respect to all GMPMs (in Equations 3.4 and 3.5). As an intermediate step (between e.g., \bar{R} and \bar{R}_k), the concept of conditional deaggregation given GMPM can also be extended to compute $\bar{M}_k, \bar{R}_k|\bar{M}_k$, and $\bar{\epsilon}_k|\bar{M}_k, \bar{R}_k$ in a cascading or Rosenblatt-distribution manner.

The second GMPM deaggregation output used in this method is the probability that GMPM k predicted occurrence (or exceedance) of the Sa . These deaggregation probabilities are denoted as p_k^d where the superscript d refers to deaggregation, and they are generally not equal to the PSHA logic-tree weights that have been denoted as p_k^l . Utilizing these weights, along with the GMPM-specific $\mu_{\ln Sa, k(T_i)|\ln Sa(T^*)}$ and $\sigma_{\ln Sa, k(T_i)|\ln Sa(T^*)}$ from Equations 3.8 and 3.9, a composite CS can be computed

$$\mu_{\ln Sa(T_i)|\ln Sa(T^*)} \approx \sum_k p_k^d \mu_{\ln Sa, k(T_i)|\ln Sa(T^*)} \quad (3.10)$$

$$\sigma_{\ln Sa(T_i)|\ln Sa(T^*)} \approx \sqrt{\sum_k p_k^d (\sigma_{\ln Sa, k(T_i)|\ln Sa(T^*)}^2 + (\mu_{\ln Sa, k(T_i)|\ln Sa(T^*)} - \mu_{\ln Sa(T_i)|\ln Sa(T^*)})^2)} \quad (3.11)$$

As with Method 2, the mean spectrum is the mean (over GMPMs) of the GMPM-specific means, except that here we have utilized the more appropriate deaggregation weights p_k^d . The standard deviation of the spectrum again contains contributions from the individual GMPM conditional standard deviations, plus the uncertainty from the variations in mean spectra across GMPMs. While this method incorporates more exact information than Methods 1 or 2, it is still approximate in that it utilizes only the mean earthquake scenario for a given GMPM. Method 4 will resolve that final approximation.

3.3.4 Method 4: “Exact” CS using multiple causal earthquake M/R and GMPMs with deaggregation weights

With this final method we now account exactly for, when we compute the CS, the contribution that each earthquake magnitude/distance and each GMPM makes to the seismic

hazard. For each causal earthquake combination M_j/R_j and GMPM k , we can obtain a corresponding mean and standard deviation of the CS (denoted $\mu_{\ln Sa, j, k(T_i)|\ln Sa(T^*)}$ and $\sigma_{\ln Sa, j, k(T_i)|\ln Sa(T^*)}$) as follows

$$\mu_{\ln Sa, j, k(T_i)|\ln Sa(T^*)} = \mu_{\ln Sa, k}(M_j, R_j, \theta_j, T_i) + \rho(T^*, T_i) \varepsilon_j(T^*) \sigma_{\ln Sa, k}(M_j, \theta_j, T_i) \quad (3.12)$$

$$\sigma_{\ln Sa, j, k(T_i)|\ln Sa(T^*)} = \sigma_{\ln Sa, k}(M_j, \theta_j, T_i) \sqrt{1 - \rho^2(T_i, T^*)} \quad (3.13)$$

A PSHA deaggregation that includes GMPM deaggregation will provide the weights, $p_{j,k}^d$, that indicate the contribution of each M_j/R_j and $GMPM_k$ to occurrence (or exceedance) of the Sa of interest. Note that here we are considering the contributions of individual M_j/R_j rather than approximating all contributing earthquake scenarios by simply a mean M and R , as we did in Equations 3.8 and 3.9. The exact CS incorporating multiple M/R and GMPMs can then be evaluated by combining these individual $\mu_{\ln Sa, j, k(T_i)|\ln Sa(T^*)}$ and $\sigma_{\ln Sa, j, k(T_i)|\ln Sa(T^*)}$ with their corresponding weights, $p_{j,k}^d$

$$\mu_{\ln Sa(T_i)|\ln Sa(T^*)} = \sum_k \sum_j p_{j,k}^d \mu_{\ln Sa, j, k(T_i)|\ln Sa(T^*)} \quad (3.14)$$

$$\sigma_{\ln Sa(T_i)|\ln Sa(T^*)} = \sqrt{\sum_k \sum_j p_{j,k}^d (\sigma_{\ln Sa, j, k(T_i)|\ln Sa(T^*)}^2 + (\mu_{\ln Sa, j, k(T_i)|\ln Sa(T^*)} - \mu_{\ln Sa(T_i)|\ln Sa(T^*)})^2)} \quad (3.15)$$

The above equations are similar to those in Method 3, except that there is now a second set of summations in the equations to account for the effect of multiple M_j/R_j values instead of the single mean values \bar{M}_k and \bar{R}_k from Method 3. These equations provide an exact answer to the question, what is the mean and standard deviation of the response spectra associated with ground motions having a target $Sa(T^*)$, when that $Sa(T^*)$ could potentially result from multiple earthquake scenarios, and the Sa predictions come from a logic tree with multiple GMPMs? It requires more effort to compute than the approximate approaches commonly used today, and requires detailed deaggregation information including hazard contributions of GMPMs and other parameters, θ , that may not be available.

Alternatively, an exact CS can be computed directly from the earthquake parameters and GMPMs that were used in PSHA computation to aggregate the hazard, as described

in the next section. Although treatments of aleatory and epistemic uncertainties are often separated in PSHA, a single seismic hazard curve is typically derived with the consideration of aleatory uncertainties from multiple causal earthquakes and epistemic uncertainties from multiple GMPMs and seismic source models (e.g., Petersen et al., 2008). Here we take a similar approach to compute a single CS that combines these aleatory and epistemic uncertainties.

3.3.5 Aggregation approach to Method 4 (exact CS)

While the GMPM deaggregations used in Methods 3 and 4 are now available from the USGS, it would be impractical to provide deaggregations with respect to all of the other branches of the PSHA logic tree (e.g., for alternative moment-area equations in California and for body wave to moment magnitude equations in the central and eastern U.S. (CEUS)). Likewise it would be cumbersome to provide deaggregations with respect to all of the other GMPM input parameters besides M and R (e.g., rupture mechanism and hanging/foot-wall indicators), which are denoted above as θ . To account for these other branches and parameters in Method 4 without additional deaggregation results, during the PSHA computation a CS can be calculated (using Equations 3.12 and 3.13) for each and every earthquake source and logic-tree branch. These numerous CS results can then be combined using Equations 3.14 and 3.15, but now with j representing all the earthquake sources and k representing all the logic-tree branches. In this case, the deaggregation weights in the equations are simply taken from the PSHA contribution (mean annual exceedance frequency) for each earthquake source and logic-tree branch, normalized by the total aggregated hazard.

An advantage of this aggregation approach to Method 4 is that the other GMPM input parameters θ no longer need to be inferred in calculating a CS. This is because, as explained above, we can first calculate a CS for each and every earthquake source (not to mention logic tree branch) using the same corresponding GMPM input parameters used in the PSHA computation. Based on the examples for three sites presented below, any numerical differences between the aggregation approach and Method 4 are not expected to be significant for the CMS (or mean CS) at a site. Also based on the examples, however, the standard deviation of a CS (via Equation 3.15) using the results for every earthquake

source and logic-tree branch would be expected to yield differences although the practical significance of the differences is not known. The standard deviation from the aggregation approach would capture all of the uncertainties considered in the PSHA computation.

An implementation of this aggregation approach to calculating an exact CS is now provided as part of USGS online hazard tools. Details and limitations of this implementation are discussed in the final section on “Conditional Spectrum calculation tools from USGS”.

3.4 Example calculations for three sites

To demonstrate the numerical results that are now available using the above equations and USGS online hazard tools, this section provides a set of example calculations to determine whether using the “exact” Method 4 provides results that have practical differences from those obtained using the simpler approximate Methods 1 to 3.

To evaluate the accuracy of the approximate methods, CS for three locations are computed using the methods described above. Target spectral accelerations are obtained for $Sa(0.2s)$ with 10% probability of exceedance in 50 years (i.e., a return period of 475 years), and for $Sa(1s)$ with 2% probability of exceedance in 50 years (i.e., a return period of 2475 years).

3.4.1 Description of example sites and GMPMs

We consider three locations in the WUS with relatively high hazard but differing surrounding seismic sources: Stanford, Bissell, and Seattle. Deaggregation results for these three sites are shown in Figure 3.1. Ground motion hazard at Stanford, located in northern California, is dominated by a single shallow crustal earthquake source, the San Andreas fault zone. Ground motion hazard at Bissell, located in southern California, has contributions from multiple earthquake sources but they are all shallow crustal sources. Ground motion hazard at Seattle has contributions from multiple earthquake sources of different types – shallow crustal, and subduction zone interface and intraplate (each of which has its own set of GMPMs). All three sites are assumed to have a time-averaged shear-wave velocity in the top 30 meters of the soil (V_{S30}) of 760 m/s.

The hazard calculations and deaggregation results all come from the USGS models and hazard mapping tools. The USGS model (Petersen et al., 2008) assigns equal logic-tree weights to GMPMs near Stanford and Bissell, but unequal logic-tree weights to GMPMs near Seattle. The USGS model uses three GMPMs for the crustal sources near Stanford, Bissell, and Seattle (Boore and Atkinson, 2008; Campbell and Bozorgnia, 2008; Chiou and Youngs, 2008), three GMPMs for the subduction zone interface sources (Youngs et al., 1997; Atkinson and Boore, 2003; Zhao et al., 2006), and three GMPMs for the intraplate sources near Seattle (Youngs et al., 1997; Atkinson and Boore, 2003, which provides models that can be used in both Global and Cascadia regions). The Youngs et al. (1997), Atkinson and Boore (2003), and Zhao et al. (2006) models are developed for both subduction zone interface and intraplate sources. The GMPMs vary in their required input variables. The mean $\ln Sa$ predictions depend on M , R , and other source and site characteristics (θ) such as depth to top of rupture, faulting mechanism, and hanging wall effect. Some of the GMPMs predict standard deviations of $\ln Sa$ that depend only on the period of interest (e.g., Boore and Atkinson, 2008), while others are magnitude-dependent (e.g., Chiou and Youngs, 2008).

3.4.2 Deaggregation information

The target $Sa(0.2s)$ with 10% probability of exceedance in 50 years and $Sa(1s)$ with 2% probability of exceedance in 50 years are obtained from PSHA for the three example sites considered. The associated causal earthquake magnitudes and distances are obtained from USGS deaggregation and their deaggregation plots are shown in Figure 3.1. Other parameters, θ , that are associated with each causal earthquake M/R combination can be obtained directly from the parameters that were used for PSHA computation (i.e., via the aggregation approach to Method 4), from deaggregation outputs if available, or inferred from the characteristics of contributing earthquake sources. With the target $Sa(T^*)$ and $\mu_{\ln Sa}(M, R, \theta, T^*)$ and $\sigma_{\ln Sa}(M, \theta, T^*)$ predictions for each causal $M/R/\theta$, we can then back-calculate $\varepsilon(T^*)$ using Equation 3.1. The logic-tree weights for each GMPM (p_k^l) are obtained from the USGS documentation (Petersen et al., 2008), and the deaggregation weights (p_k^d and $p_{j,k}^d$) are obtained from the USGS deaggregation tools.

3.4.3 Conditional Spectra results

CS can be computed for each example case using the approximate or exact methods described above. Depending on the level of approximation, the CS for a GMPM k can be computed using Method 1 (Equations 3.4 and 3.5) for approximate CS with mean M/R (\bar{M} and \bar{R}), Method 3 (Equations 3.8 and 3.9) for approximate CS with GMPM-specific mean M/R (\bar{M}_k and \bar{R}_k), or Method 4 (Equations 3.12 and 3.13) for all contributing CS with GMPM-specific causal earthquake M/R (M_j and R_j). The composite CS can then be computed with the corresponding weights, using Method 2 (Equations 3.6 and 3.7) for approximate CS with GMPM logic-tree weights (p_k^l), Method 3 (Equations 3.10 and 3.11) for approximate CS with GMPM deaggregation weights (p_k^d), or Method 4 (Equations 3.14 and 3.15) for exact CS with deaggregation weights associated with each causal earthquake and GMPM ($p_{j,k}^d$). The resulting CS obtained from these four Methods are plotted in Figure 3.2. Also plotted in the figure are the CMS (but not conditional standard deviations) resulting from the aggregation approach to Method 4, which are nearly identical to the Method 4 results despite the inclusion of additional logic-tree branches and earthquake sources. These CMS are obtained from the USGS calculation tools described below in the final section.

We can make several observations from the results of Figure 3.2. For the Stanford and Bissell sites, CS computed using Method 1 are very similar to results from Methods 2 and 3, but they differ more for Seattle. This is because the GMPMs used in Seattle, some of which are for subduction zone events, result in more varied predictions; using a mean \bar{M}/\bar{R} that represents a variety of earthquake sources with a GMPM appropriate for a single source type could be anticipated to produce these varied predictions. For Seattle, Methods 2 and 3, which more carefully address the contributions of multiple GMPMs, do a better job of approximating the exact results from Method 4.

For all three sites, the approximate Methods 2 and 3 work better for conditional mean estimation than for conditional standard deviation estimation compared to the exact Method 4, as Method 4 produces higher conditional standard deviations in every case. A closer examination of Equation 3.15 reveals two components of contribution to the exact conditional standard deviations: first, a contribution from σ_{lnSa} , that is, variance in $lnSa$ for a

given M_j/R_j & $GMPM_k$; second, a contribution from μ_{lnSa} , due to variation in M_j/R_j & $GMPM_k$. In other words, the total variance comes from the expectation of the variance, which is the first term, and the variance of the expectation, which is the second term (e.g., Ditlevsen, 1981). The individual contributions from these two terms are plotted in Figure 3.3a-c. Methods 2 and 3 very closely approximate the contribution from σ_{lnSa} for the Stanford and Bissell sites, although the match is not as good for Seattle. Method 4 also includes the contribution from μ_{lnSa} , which is, however, not well captured by Methods 2 and 3. Figure 3.3d-f show the μ_{lnSa} predicted for each M_j/R_j & $GMPM_k$, and it is the weighted variance of these spectra that creates the contribution to the overall standard deviation from μ_{lnSa} . We thus see that this “variance of expectations” contribution may not be negligible, and the approximate methods do not capture this well because they consider only mean M/R values and thus cannot identify the contribution to uncertainty from multiple M/R contributions to ground motion hazard. Similarly, we anticipate that the deaggregation approach to the exact Method 4 underestimates the conditional standard deviation, relative to the aggregation approach that accounts for every logic tree branch and earthquake source used in the PSHA computation. We do not yet know whether this underestimation is practically significant.

Figure 3.4 shows the target CS computed using Methods 2 and 4 for all three sites and both target Sa values: $Sa(0.2s)$ with 10% probability of exceedance in 50 years and $Sa(1s)$ with 2% probability of exceedance in 50 years. Method 2 is chosen as the reference approximate method here because it has an appealing combination of incorporating multiple GMPMs but not requiring any GMPM deaggregation information. For all three sites, the approximate and exact methods’ mean estimates are in close agreement, while the approximate standard deviations underestimate the exact result – this effect is most pronounced at periods far from the conditioning period (i.e., 0.2s or 1s).

The Method 2 approximation appears to work best for sites with a single earthquake source (e.g., Stanford), followed by sites with multiple earthquakes sources of the same type (e.g., Bissell) and sites with multiple differing earthquake source types (e.g., Seattle). This is because there are several contributing factors to the accuracy of the approximation: (1) the input causal earthquake parameters; (2) the GMPMs used; (3) the GMPM deaggregation weights.

First, the importance of considering multiple causal M/R values depends upon how many M/R values contribute significantly to the hazard. In cases where all contributions to hazard come from a narrow range of magnitudes and distances (e.g., Stanford), the mean M/R is representative of the most important individual contributing M/R , so computations based only on the mean M/R are very precise. However, in cases where hazard contributions come from a broader range of magnitudes and distances (especially in the case of Seattle), the mean M/R deviates from any individual contributing M/R , so computations based on the mean M/R only may result in a slight shift in conditional mean estimates in addition to reduced conditional standard deviations. Similarly, for the common situation of low- or moderate-seismicity sites in the CEUS, e.g., those that are located several hundred kilometers from the New Madrid seismic region where the low-frequency deaggregation can be strongly bimodal, computations based on the mean M/R only may not be precise. Furthermore, variation in other parameters besides M and R , such as depth to the top of rupture for different source types, can also affect the accuracy of the approximation since they contribute to the S_a prediction.

Second, the similarity of the GMPMs affects approximations in their treatment. For cases where the ground motion predictions for a given M/R vary significantly between models (e.g., Seattle, where the subduction zone and crustal prediction models vary significantly), approximate treatment of GMPMs is less effective and so a CS using a single GMPM (or using approximate weights on multiple models) may produce inaccurate results. Similar inaccuracies can be expected in the CEUS. On the other hand, the three GMPMs used at Stanford and Bissell all tend to produce similar predictions, so for those cases the choice of the GMPM used to compute CS may not be as critical.

Third, as the GMPM deaggregation weights differ more from the GMPM logic-tree weights, approximate treatment of those weights works less effectively. For instance, in the (not too uncommon) case where one GMPM strongly dominates the deaggregation, the approximation that assumes GMPM logic-tree weights is expected to deviate more substantially from the computation that utilizes GMPM deaggregation weights. The GMPM deaggregation weights vary with the period of interest (T^*), the target $S_a(T^*)$ amplitude of interest, and the location, so it is difficult to develop simple rules for when the approximations work well. But if the GMPM predictions are similar to each other for the M/R values

contributing significantly to hazard, then the deaggregation weights are often similar to the logic-tree weights and the predictions are also in good agreement (as noted in the previous paragraph), so the approximations are generally good in those cases.

3.5 Impact of approximations on ground motion selection

The importance of approximations in the CS computations will depend upon how the results affect any engineering decisions that may be made. The most common use for a CS is as a target response spectrum for ground motion selection and scaling (Baker, 2011; Baker and Cornell, 2006a). Approximations to the CS might have an influence on ground motions selected from a database (because the selected ground motions match the target response spectrum), and that could affect nonlinear dynamic analysis results. On the other hand, the finite size of recorded ground motion databases means that minor changes in the spectrum target may not result in substantially different ground motions being selected, and in that case the approximations would not have an appreciable impact on structural analysis results.

To illustrate, the target CS mean and variance are computed using both the exact (Method 4) and approximate (Method 2) approaches, at the Bissell site for the $Sa(0.2s)$ amplitude with 10% probability of exceedance in 50 years. Ground motions can be selected to match these target spectrum mean and variance using the procedure of Jayaram et al. (2011), which assumes a Gaussian distribution. In general the conditional logarithmic Sa distribution is not Gaussian when multiple causal earthquakes and/or multiple GMPMs are considered, and hence the mean and variance alone may not describe the entire distribution; they still provide useful insights, however. Alternatively, Bradley (2010a) considers multiple causal earthquake sources and the complete distribution of the conditional ground motion intensity measure. The target response spectra and corresponding ground motions selected via Jayaram et al. (2011) are shown in Figures 3.4b and 3.5. The means of the CS using both methods are in close agreement, but the standard deviation of the CS using Method 4 is higher than that using Method 2, especially at periods further away from the conditioning period of 0.2s. Consequently, the spectra of the ground motions selected using Method 4 are expected to show a similar mean but a higher standard deviation than those

using Method 2. The larger exact CS standard deviation results in selecting a few more ground motions with high spectra at periods other than 0.2s, and this can result in a slightly increased probability of observing large structural responses or collapses (as seen in, e.g., Jayaram et al., 2011). Note that the spectra of the selected ground motion sets, however, do not differ substantially in Figure 3.5, relative to variations between ground motion spectra within a set. Structural analyses to date suggest that in cases such as this, the exact method results in similar median but increased dispersion in structural response estimates.

The difference in structural response can be larger, however, if Methods 2 and 4 result in substantial differences in both the mean and the variance of the CS, such as those illustrated in Figure 3.4c and f for the Seattle site. In such cases, in addition to a slight increase in structural response dispersion, the median of the structural response may shift as well. To reflect contributions from different earthquake sources, individual CS can be constructed for each earthquake source, and separate sets of ground motions selected to match both the target spectra as well as other characteristics of each source (Goda and Atkinson, 2011). These CS for different earthquake sources are available as intermediate steps to compute the exact CS described above, and are provided by the USGS as part of the CMS feature that is described in the next section. As the difference between approximate and exact spectra increases, more refined target spectra will have increasing benefits for ground motion selection and structural response assessment.

3.6 Conditional Spectrum calculation tools from USGS

The USGS National Seismic Hazard Mapping Project website (<http://earthquake.usgs.gov/hazards>) now provides an option for CMS, as part of the 2008 Interactive Deaggregations web tool (<http://geohazards.usgs.gov/deaggint/2008>). The spectra are consistent with the 2008 National Seismic Hazard Maps for the continental United States, and are computed via the section “Aggregation approach to Method 4 (exact CS)” described above. Described below are the inputs to and outputs from the tool, issues with the current implementation, and future features. One such future feature is providing the standard deviations of CS in addition to the means.

3.6.1 Description of calculation tool

As shown in Figure 3.6, the USGS 2008 Interactive Deaggregation web tool provides CMS for a user-specified

- location (address or latitude and longitude) anywhere in the continental United States;
- mean exceedance probabilities of 1%, 2%, 5%, 10%, 20%, or 50% in 30, 50, 75, 100 or 200 years;
- spectral acceleration period of 0s (corresponding to peak ground acceleration), 0.1s, 0.2s, 0.3s, 0.5s, 1s, or 2s, or additionally 3s, 4s, or 5s for locations in the WUS (west of -115 degrees longitude);
- V_{S30} of soil between 180 to 1300 m/s for locations in the WUS, of 760 or 2000 m/s in the CEUS (east of -100 degrees longitude), or of 760 m/s for locations in between.

As output, the tool currently provides graphs, tables, and text files for four different types of CMS, all calculated according to the section “Aggregation approach to Method 4 (exact CS)” described above. The four different types are:

- an overall CMS that accounts for all of the earthquake sources and logic tree branches considered in the USGS PSHA computation (with a few exceptions described in the next section below);
- a CMS for each GMPM that accounts for all of the earthquake sources and logic tree branches related to the particular GMPM;
- a CMS for each of several (currently seven) $M/R/\epsilon$ bins that contribute most to the total aggregated hazard, accounting for all of the earthquake sources and logic tree branches within that bin;
- a CMS for each $M/R/\epsilon$ bin and GMPM (currently only in text output), accounting for all of the earthquake sources and logic tree branches within the bin that are related to the particular GMPM.

The CMS for each GMPM demonstrates the effect of using only a single GMPM. As mentioned above, this effect can be particularly significant in cases when more than one earthquake source type (e.g., subduction zone, shallow crustal) contributes significantly to the total aggregated hazard. In such cases, the CMS for two or more $M/R/\epsilon$ bins and/or GMPMs, each corresponding to a different source type, may be more useful than a single overall CMS.

3.6.2 Current implementation issues

While the web tool implementation described above accounts for practically all of the earthquake sources and logic-tree branches considered in computing the USGS 2008 National Seismic Hazard Maps, there are some exceptions. The least significant of these is that CMS calculations are not carried out for earthquake sources that do not contribute appreciably to the total aggregated hazard (i.e., those with mean annual exceedance frequency less than 10^{-6}). Also for the sake of limiting computation time, CMS are not calculated for the two USGS logic-tree branches that quantify additional epistemic uncertainty amongst the GMPMs for shallow crustal earthquakes in the WUS (see Petersen et al. (2008) for details). The logic tree branches corresponding to the GMPMs themselves are fully accounted for, however. In the CEUS, the USGS logic tree branch for temporal clustering of New Madrid Seismic Zone earthquakes is not yet incorporated into the 2008 Interactive Deaggregations web tool, and hence is not accounted for in the CMS calculations. The numerical impacts of these exceptions on the calculated CMS have not yet been quantified, but they are anticipated to be relatively insignificant.

In being consistent with the 2008 National Seismic Hazard Maps, the USGS web tool utilizes several different GMPMs for shallow crustal, subduction zone, and stable continental earthquake sources. However, for the correlation coefficients needed to calculate CS, the tool currently only uses the Baker and Jayaram (2008) model, which was developed with ground motion data exclusively from shallow crustal earthquakes. A recent study of subduction zone ground motions from Japan suggests that this correlation model is also a reasonable representation for subduction zone earthquake sources (Jayaram et al., 2011). For stable continental earthquake sources, there is little data to either confirm or contradict

this model. In general, studies of correlation models have shown them to be relatively insensitive to the particular GMPM, earthquake magnitude, distance, and rupture mechanism (e.g., Baker, 2005; Jayaram et al., 2011). Thus, the numerical impact of using the single correlation model is anticipated to be relatively insignificant. Additional and/or updated correlation models corresponding to different earthquake sources and/or GMPMs could be incorporated into the web tool as they become available.

3.6.3 Future features

As mentioned above, in the future the USGS web tool will provide CS, not just CMS. The conditional standard deviations will likewise be calculated according to the aggregation approach to computing an exact CS. Whereas the current implementation for the conditional means has been seen to match results from the deaggregation approach of Method 4, the standard deviations of a CS calculated by the web tool are anticipated to be higher and more inclusive of all the uncertainties accounted for in the USGS National Seismic Hazard Maps.

Lastly, the current web tool calculates CMS with weights that are for exceedance of the S_a value specified by a user (via a selected mean exceedance probability). A future tool will provide weights for occurrence of an S_a value. In order to do so, the tool will optionally allow a user to specify an S_a value of interest, e.g., a Risk-Targeted Maximum Considered Earthquake (MCE_R) ground motion value from ASCE (2010).

3.7 Conclusions

Approximate and exact computations of CS were proposed and used for example calculations for Stanford, Bissell and Seattle. Exact CS mean and standard deviation calculations can incorporate multiple GMPMs and causal earthquake $M/R/\theta$ combinations, as well as multiple seismic source models and their logic-tree branches. Varying levels of approximations were also considered, that replaced multiple M/R combinations with simply the mean M/R from deaggregation, and either considered only a single GMPM or performed an approximate weighting of several GMPMs. These approximations are potentially appealing

because of their ease of computation and because they do not require deaggregation of GMPM weights – a result that is not yet widely available in conventional PSHA software.

The approximate CS calculations appear to be more accurate for conditional mean estimation than for conditional standard deviation estimation. The exact conditional standard deviation is always higher than approximate results because of the additional contribution from the variance in mean logarithmic spectral accelerations due to variation in causal earthquakes and GMPMs. The input causal earthquake parameters and the GMPMs used along with the corresponding weights affect the accuracy of the approximation in CS computation. Exact calculation methods may be needed for locations with hazard contributions from multiple earthquake sources, where errors from approximations are higher as a result of multiple contributing earthquake magnitudes and distances, and variation in predictions from the input GMPMs.

The exact CS calculations require extension of traditional PSHA deaggregation, which considers only magnitude, distance and ϵ , to deaggregation of GMPMs. This additional deaggregation output is now available as part of the hazard results provided by the USGS. Further, the USGS now provides CMS results using the exact calculation aggregation approach described here. These new calculation tools should be useful in facilitating hazard-consistent ground motion selection for nonlinear dynamic analysis, and will allow for exact spectra to be computed without requiring cumbersome calculations by users.

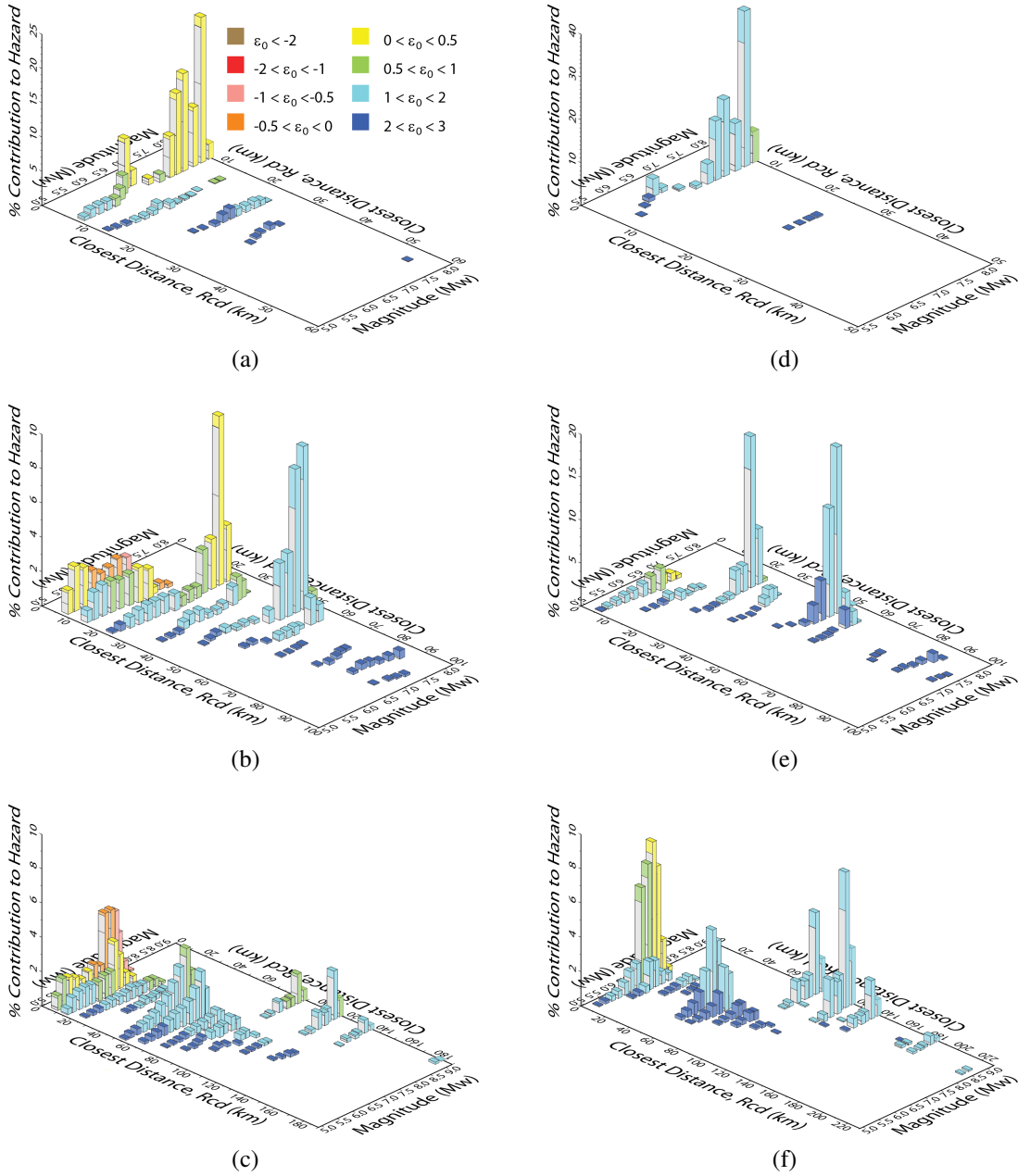


Figure 3.1: Deaggregation for $Sa(0.2s)$ with 10% probability of exceedance in 50 years at Stanford, Bissell, and Seattle (a, b, and c respectively) and for $Sa(1s)$ with 2% probability of exceedance in 50 years at Stanford, Bissell, and Seattle (d, e, and f respectively) (adapted from USGS, 2012).

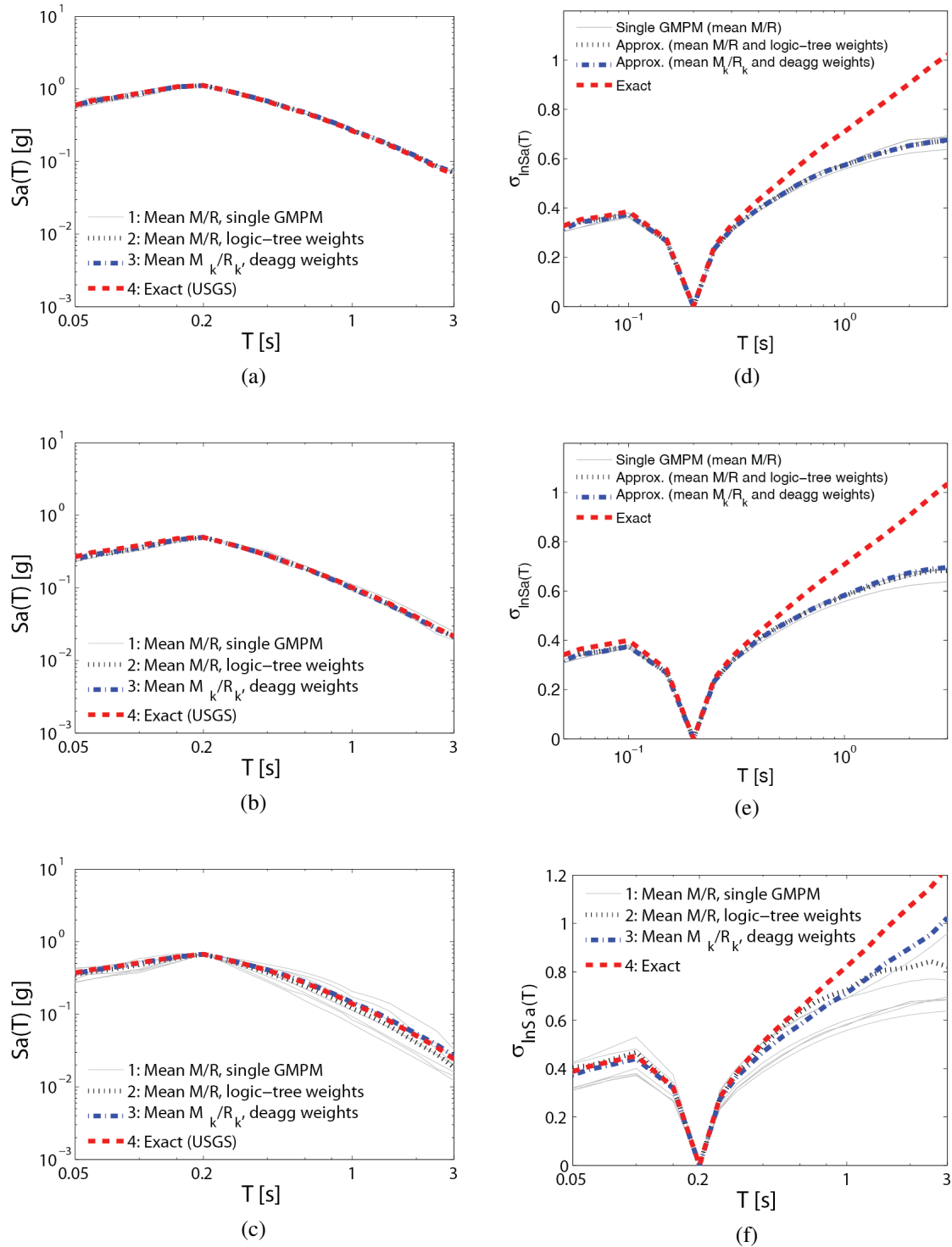


Figure 3.2: CMS at Stanford, Bissell and Seattle (a, b, and c respectively) and conditional standard deviation spectra at Stanford, Bissell, and Seattle (d, e, and f respectively) using Methods 1 to 4, for $Sa(0.2s)$ with 10% probability of exceedance in 50 years.

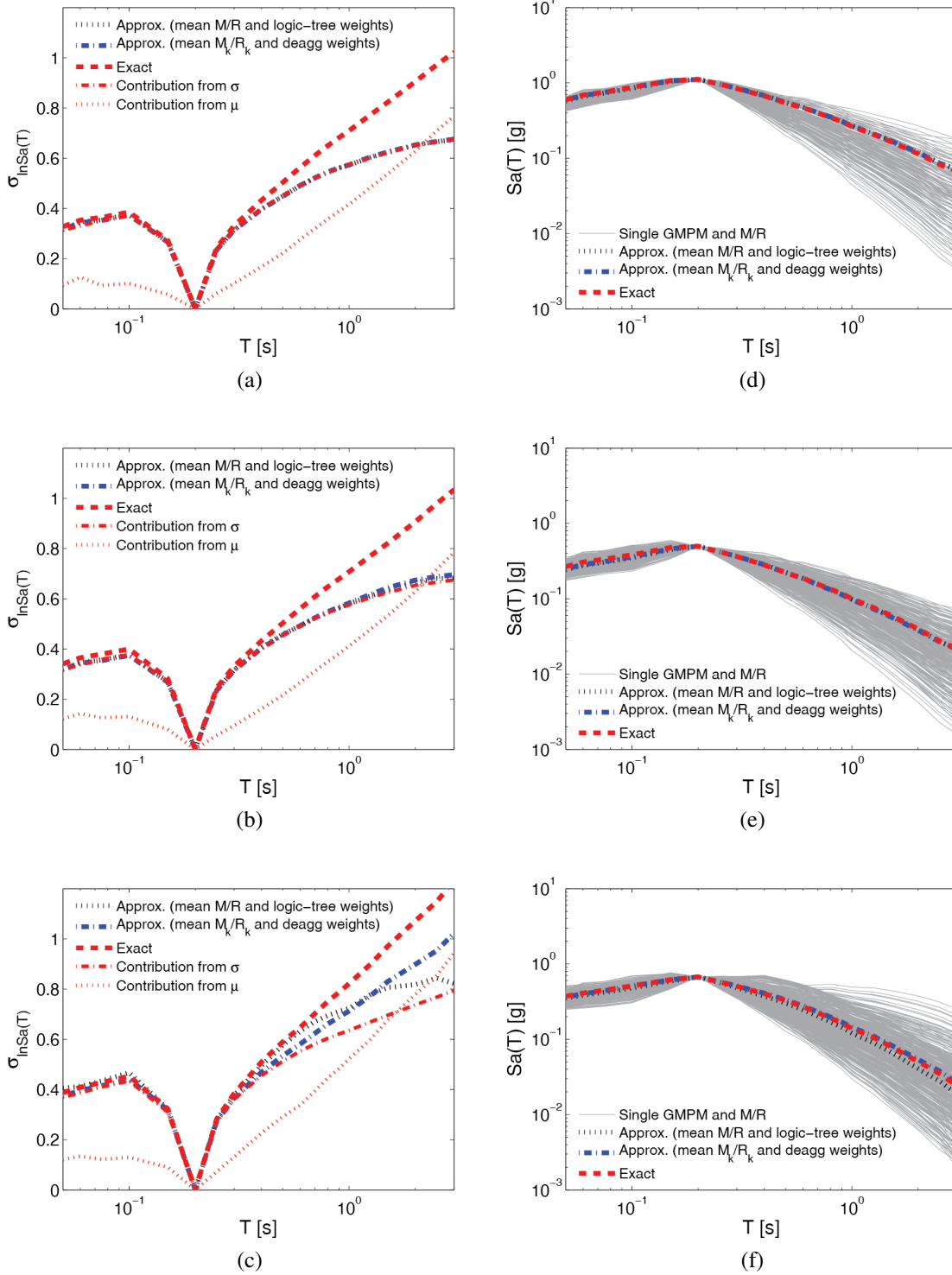


Figure 3.3: Conditional standard deviation spectra with contribution from $\sigma_{\ln Sa}$ (variance in $\ln Sa$ for a given M_j/R_j & $GMPM_k$) and $\mu_{\ln Sa}$ (due to variation in M_j/R_j & $GMPM_k$) at Stanford, Bissell, and Seattle (a, b, and c respectively) and CMS for each considered M_j/R_j & $GMPM_k$ at Stanford, Bissell, and Seattle (d, e, and f respectively) using Methods 2 to 4, for $Sa(0.2s)$ with 10% probability of exceedance in 50 years.

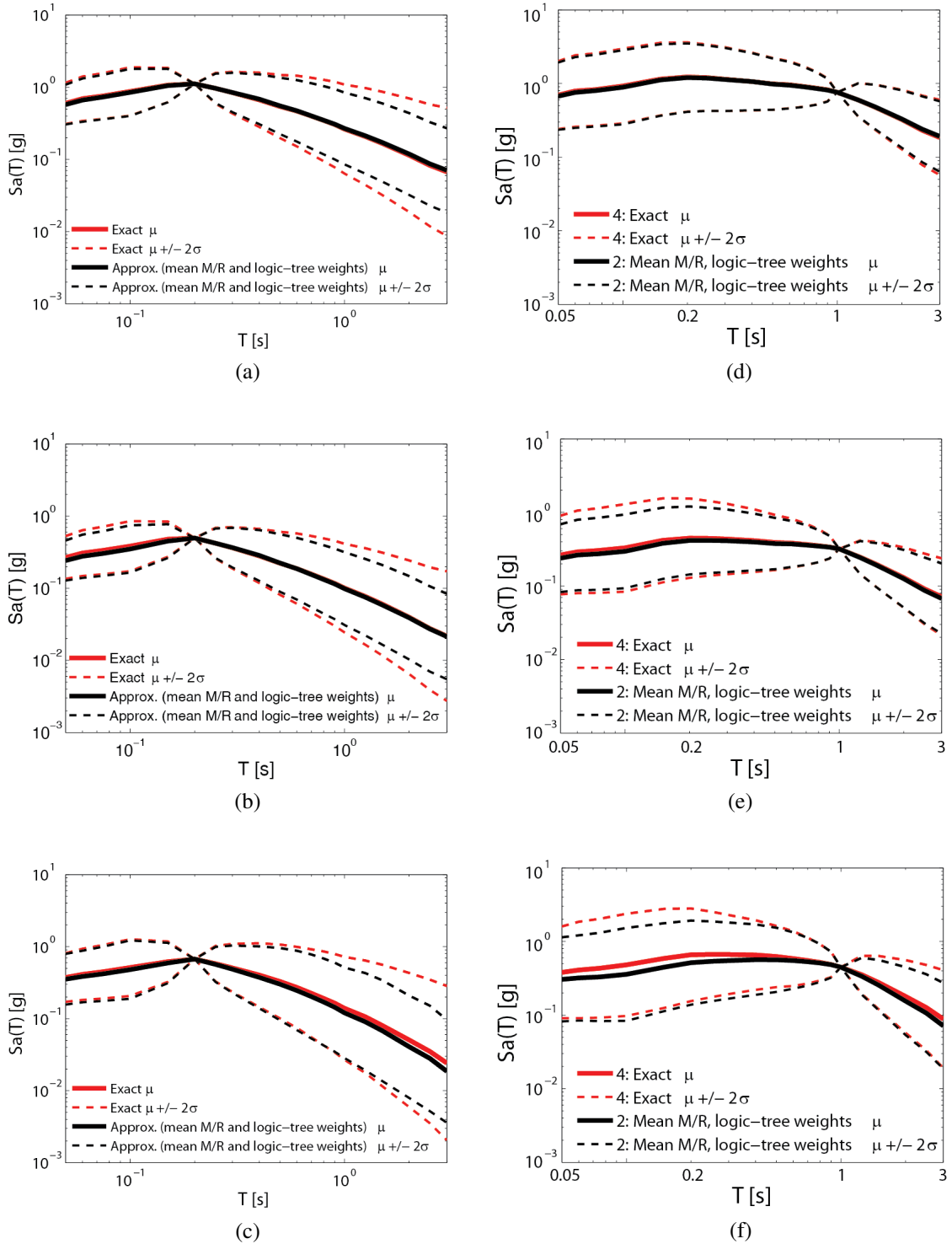


Figure 3.4: CS computed using Methods 2 and 4, for $Sa(0.2s)$ with 10% probability of exceedance in 50 years at Stanford, Bissell, and Seattle (a, b, and c respectively) and $Sa(1s)$ with 2% probability of exceedance in 50 years at Stanford, Bissell, and Seattle (d, e, and f respectively).

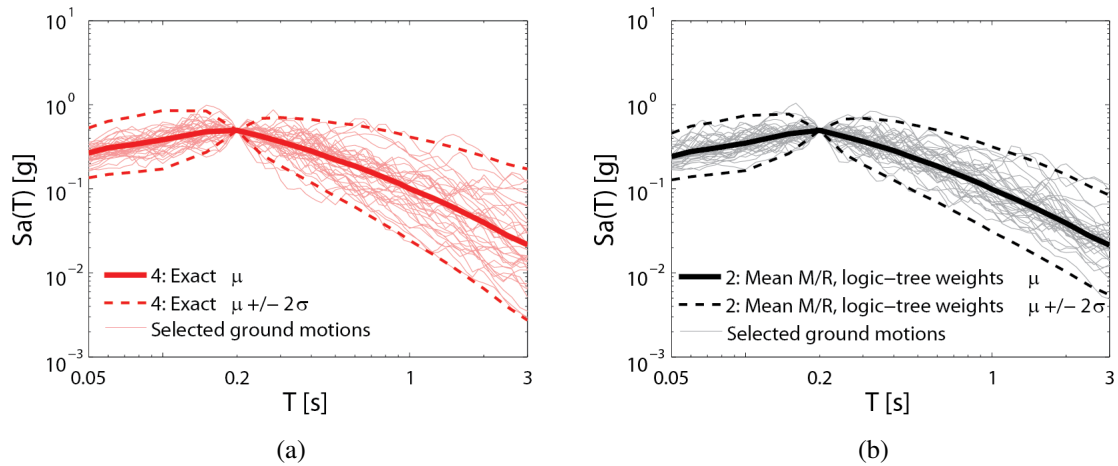


Figure 3.5: Response spectra of ground motions selected match CS obtained using (a) Method 4 and (b) Method 2 at Bissell site for $S_a(0.2s)$ with 10% probability of exceedance in 50 years.

Figure 3.6 shows a web interface for USGS online interactive deaggregations. The interface includes a navigation bar with links for 'FAQ', 'Documentation', '1996 Update', '2002 Update', and 'Feedback'. The main form contains the following fields and options:

- Site Name:** Stanford (with a link to 'Enter latitude/longitude instead')
- Address:** Stanford, CA
- Exceedance Probability:** 2% in 50 years
- Spectral Period:** 1.0 second (1Hz)
- V_{s30} (m/s):** 760.0 (with a link to 'What values can I use at various locations?')
- Run GMPE Deaggs?:** Yes (selected), No, What's this?
- Additional Output:** Geographic Deagg, Conditional Mean Spectra (selected), None
- [\(Show Map\)](#)
- Compute** button

Figure 3.6: Interface for USGS online interactive deaggregations, including options to request GMPM deaggregation and CMS computation (from USGS, 2012).

Chapter 4

Conditional-Spectrum-based ground motion selection: Hazard consistency for risk-based assessments

Lin, T., C. B. Haselton, and J. W. Baker (2012a). Conditional-Spectrum-based ground motion selection. Part I: Hazard consistency for risk-based assessments. *Earthquake Engineering & Structural Dynamics* (in review).

4.1 Abstract

The Conditional Spectrum (CS, with mean and variability) is a target response spectrum that links nonlinear dynamic analysis back to probabilistic seismic hazard analysis for ground motion selection. The CS is computed based on a specified conditioning period, whereas structures under consideration may be sensitive to response spectral amplitudes at multiple periods of excitation. Questions remain regarding the appropriate choice of conditioning period when utilizing the CS as the target spectrum. This paper focuses on risk-based assessments, which estimate the annual rate of exceeding a specified structural response amplitude. Seismic hazard analysis, ground motion selection, and nonlinear dynamic analysis are performed, using the Conditional Spectra with varying conditioning periods, to assess the performance of a 20-story reinforced concrete frame structure. It

is shown here that risk-based assessments are relatively insensitive to the choice of conditioning period when the ground motions are carefully selected to ensure hazard consistency. This observed insensitivity to the conditioning period comes from the fact that, when CS-based ground motion selection is used, the distributions of response spectra of the selected ground motions are consistent with the site ground motion hazard curves at all relevant periods; this consistency with the site hazard curves is independent of the conditioning period. The importance of an exact CS (which incorporates multiple causal earthquakes and ground motion prediction models) to achieve the appropriate spectral variability at periods away from the conditioning period is also highlighted. The findings of this paper are expected theoretically but have not been empirically demonstrated previously.

4.2 Introduction

Ground motion selection provides the necessary link between seismic hazard and structural response. It determines ground motion input for a structure at a specific site for nonlinear dynamic analysis. As nonlinear dynamic analysis becomes more common in research and practice, there is an increased need for clear guidance on appropriate ground motion selection methods. Ground motion selection has a significant impact on conclusions regarding structural safety, since ground motion uncertainty contributes significantly to uncertainty in structural analysis output. In order to select representative ground motions to effectively assess the future reliability of a structure at a given location, it is important to ensure hazard consistency of ground motion inputs and evaluate structural response using a risk-based approach.

Risk-based assessment of structural response estimates the mean annual rate of exceeding a specified structural response amplitude, or engineering demand parameter, *EDP*. This calculation is also often referred to as the first step of the “PEER Integral” (Cornell and Krawinkler, 2000), a “drift hazard” calculation (Krawinkler and Miranda, 2004), or a “time-based assessment” (ATC, 2011). It differs from intensity-based assessment, which only considers structural response amplitude at a given ground motion intensity level. It is obtained using full distributions of structural response for ground motions at each given intensity, and considers multiple intensity levels, along with their occurrence rates.

Ground motion selection is often associated with a target response spectrum. Recent work has illustrated that scaling up arbitrarily selected ground motions to a specified spectral acceleration (Sa) level at vibration period (or “period”, for brevity in lieu of “vibration period”) T can produce overly conservative structural responses, because a single extreme $Sa(T)$ level of interest for engineering analysis does not imply occurrence of equally extreme Sa levels at all periods (Baker and Cornell, 2006a). The “Conditional Mean Spectrum” (CMS) and “Conditional Spectrum” (CS) have been developed to describe the expected response spectrum associated with a ground motion having a specified $Sa(T)$ level (e.g., Baker and Cornell, 2006a; Baker, 2011; Lin et al., 2012). The CMS for a rare (i.e., large positive ε) $Sa(T)$ level has a relative peak at T and tapers back towards the median spectrum for the considered causal scenario event at other periods. The CS differs from the CMS only in that it also considers the variability in response spectra at periods other than the conditioning period (which by definition has no variability). The CS (with mean and variance) is a target spectrum that links ground motion hazard to structural response. A computationally efficient algorithm has been developed for selecting ground motions to match this target spectrum mean and variance (Jayaram et al., 2011). Alternatively, a generalized conditional intensity measure approach that considers intensity measures other than Sa can be used if non-spectral ground motion parameters are also deemed important for predicting the EDP of interest (Bradley, 2010a, 2012a,b).

The CS is computed based on a specified conditioning period (denoted here as T^*), whereas structures under consideration generally have responses that are sensitive to excitation at a range of periods, including both higher-mode periods and “lengthened periods” associated with nonlinear behavior (Haselton and Baker, 2006). A structure’s first-mode period (T_1) is often chosen as T^* to calculate Peak Story Drift Ratio ($PSDR$, i.e., maximum story drift ratio observed over all stories, over the duration of shaking) – this is done because $Sa(T_1)$ is often a “good” predictor of that EDP for low- or mid-rise buildings, so scaling ground motions based on $Sa(T_1)$ can lead to reduced scatter in resulting response predictions and thus minimizes the required number of nonlinear dynamic analyses (Shome et al., 1998). There are, however, circumstances under which the EDP of interest is not dominated by the first-mode period, e.g., Peak Floor Acceleration (PFA , i.e., maximum acceleration observed over all floors including the ground, over the duration of shaking).

Furthermore, when the structural design is not yet finalized, it is difficult to identify a single conditioning period. Questions remain regarding the appropriate choice of conditioning period when utilizing the CS as the target spectrum. This chapter investigates the effect of conditioning period on risk-based structural response assessments and the significance of hazard consistency in ground motion inputs. The methodology to perform ground motion selection and structural analysis is presented, and an illustrative example is used where appropriate.

Section 4.3 “Conditional-Spectrum-based ground motion selection” outlines the procedures for seismic hazard analysis and deaggregation, target spectrum computation, and ground motion selection to match target spectrum. Next, Section 4.4 “Hazard consistency of ground motion response spectra” compares distributions of selected ground motion response spectra with the target seismic hazard curves and shows how to make adjustments to the target spectra to ensure hazard consistency, when necessary. Last, structural analyses are carried out in Section 4.5 to perform a risk-based assessment for *PSDR*. Such nonlinear dynamic analyses are repeated using ground motions matching the CS at various conditioning periods, in order to examine the impact of conditioning period; ground motions are also reselected to examine the significance of hazard consistency. Analyses for additional *EDPs* are then conducted in Section 4.6 to illustrate and confirm the generality of the procedures and findings.

The primary illustrative structure considered is a 20-story reinforced concrete special moment frame located at Palo Alto, California, with the perimeter frame designed to resist lateral forces. This building was designed for the recent FEMA P695 project (ATC, 2009; Haselton and Deierlein, 2007), and is denoted Building 1020 in that study. It is a 2-D model in OpenSEES (2011), with strength deterioration (both cyclic and in-cycle) and stiffness deterioration. The first three elastic modal periods are 2.6s, 0.85s, and 0.45s. The building was designed per the IBC 2003 (ICC, 2003), for a site with a slightly lower design ground motion level than the site being utilized in this study (by approximately 20%). This structure is analyzed using ground motions selected to match the CS conditioned on various periods of interest. These conditioning periods include the first-mode period, T_1 , the higher-mode (second- and third-mode) periods, T_2 and T_3 , and a lengthened period due to nonlinearity, $2T_1$, which are used to illustrate the range of conditioning periods that

may be of interest (the specific conditioning period used can be any period), and show the sensitivity of structural response results (e.g., *PSDR* and *PFA*) with respect to this range of conditioning periods.

4.3 Conditional-Spectrum-based ground motion selection

Procedures for ground motion selection based on a target spectrum are presented as follows: first, seismic hazard analysis is performed for the site and period of interest, and deaggregation is performed to identify the ground motion characteristics (such as magnitude, distance and ϵ) that contributed to occurrence of a specified ground motion intensity level; next, a target spectrum is computed using the deaggregation information and relevant ground motion prediction models (GMPMs); finally, ground motions are selected from a ground motion database to match the specified target spectrum.

4.3.1 Seismic hazard analysis and deaggregation

Probabilistic seismic hazard analysis is used to estimate the seismic hazard rate at any site for a period of interest. Given a site location and associated soil condition, the annual rate of spectral acceleration (Sa) exceedance at a period of vibration (T^*), $Sa(T^*)$, can be obtained from PSHA computation software such as the United States Geological Survey (USGS) web tool at <https://geohazards.usgs.gov/deaggint/2008/>. The period of interest, T^* , often corresponds to a structure's first-mode period of vibration, T_1 , but can also be another period such as a higher-mode period, a lengthened period, or any other period. The annual rate of Sa exceedance can be expressed in terms of return period, and the Sa amplitude is often referred to as an "intensity level". For instance, an intensity level with 2% in 50 years exceedance rate corresponds to a Sa value with a return period of 2475 years under a Poissonian assumption of ground motion occurrence.

For a specified intensity level, deaggregation is used to identify the characteristics associated with occurrence of given ground motion intensity levels, such as magnitude (M), distance (R) and ϵ . This can be the full conditional distribution of M , R , and ϵ or their

mean values. Such deaggregation information can also be obtained from PSHA computation software such as the USGS web tool. In cases where results for the period of vibration (T^*) or exceedance rate of interest cannot be obtained directly from PSHA computation software, interpolation can be used for intermediate values of interest.

To illustrate, a seismic hazard curve and deaggregation are obtained for a site located in Palo Alto, California, with a shear wave velocity in the top 30 meters of the soil, V_{S30} , of 400 m/s. Assuming that a period of 2.6s (which corresponds to the first-mode period of vibration, T_1 , for the example 20-story structure) is of interest, the seismic hazard curve for Sa at this period, $Sa(2.6s)$, is plotted in Figure 4.1a. As the ground motion intensity, $Sa(2.6s)$, increases, the annual rate of exceedance decreases. The $Sa(2.6s)$ which is associated with 2% in 50 years probability of exceedance (an annual rate of 0.0004) can be identified through the hazard curve as $Sa(2.6s) = 0.45g$. Deaggregation can also be obtained to identify the causal M , R , ϵ values, as shown in Figure 4.1b, both as histograms and mean values. The tallest column in such figures corresponds to the range of the $M/R/\epsilon$ combination with the highest contribution to seismic hazard at the site.

4.3.2 Target spectrum computation

Based on the deaggregation information, a target spectrum can be computed using relevant GMPMs (in this case, Boore and Atkinson, 2008; Campbell and Bozorgnia, 2008; Chiou and Youngs, 2008). From the previous section, the target Sa at period T^* , $Sa(T^*)$, is obtained from PSHA, and its associated mean causal earthquake magnitude (M) and distance (R) are obtained from deaggregation. Now, a GMPM can be used to obtain the logarithmic mean and standard deviation of Sa at all periods T_i , denoted as $\mu_{lnSa}(M, R, T_i)$ and $\sigma_{lnSa}(M, T_i)$. For the target $Sa(T^*)$ value, compute the target $\epsilon(T^*)$, the number of standard deviations by which $lnSa(T^*)$ differs from the mean prediction $\mu_{lnSa}(M, R, T^*)$, at T^*

$$\epsilon(T^*) = \frac{lnSa(T^*) - \mu_{lnSa}(M, R, T^*)}{\sigma_{lnSa}(M, T^*)} \quad (4.1)$$

This $\epsilon(T^*)$ value can also be obtained directly from deaggregation.

For a Uniform Hazard Spectrum (UHS) associated with an annual rate of exceedance

(which is uniform across all periods), Sa values at various periods T_i can be obtained directly from PSHA hazard curves for periods T_i associated with the given annual rate of exceedance.

The CMS utilizes correlation across periods to estimate the expected Sa values at all periods T_i ($Sa(T_i)$) given the target Sa value at the period of interest T^* ($Sa(T^*)$) (e.g., Baker and Cornell, 2006a; Abrahamson and Al Atik, 2010; Baker, 2011; Gulerce and Abrahamson, 2011). For the CMS, $\varepsilon(T_i)$ is not the same as $\varepsilon(T^*)$. Additional information regarding the correlation coefficient between pairs of ε values at two periods, $\rho(\varepsilon(T_i), \varepsilon(T^*))$ (hereinafter referred to as $\rho(T_i, T^*)$) (e.g., from Baker and Jayaram, 2008) is needed to compute the conditional mean Sa at other periods T_i , $\mu_{\ln Sa(T_i)|\ln Sa(T^*)}$:

$$\mu_{\ln Sa(T_i)|\ln Sa(T^*)} = \mu_{\ln Sa}(M, R, T_i) + \rho(T_i, T^*)\varepsilon(T^*)\sigma_{\ln Sa}(M, T_i) \quad (4.2)$$

Similarly, the conditional standard deviation of Sa at period T_i , $\sigma_{\ln Sa(T_i)|\ln Sa(T^*)}$, can be computed as

$$\sigma_{\ln Sa(T_i)|\ln Sa(T^*)} = \sigma_{\ln Sa}(M, T_i)\sqrt{1 - \rho^2(T_i, T^*)} \quad (4.3)$$

The conditional standard deviation $\sigma_{\ln Sa(T_i)|\ln Sa(T^*)}$ from Equation 4.3, when combined with the conditional mean value $\mu_{\ln Sa(T_i)|\ln Sa(T^*)}$ from Equation 4.2, specifies a distribution of Sa values at all periods (where the distribution at a given period is Gaussian, as justified by Jayaram and Baker (2008)). We term the resulting spectrum distribution as a ‘‘Conditional Spectrum’’ (CS), to be distinguished from the ‘‘Conditional Mean Spectrum (CMS)’’ that does not consider the variability specified by Equation 4.3.

Mean values of M , R , ε from deaggregation and a single GMPM can be used to compute an approximate CS. Probabilistic Seismic Hazard Analysis, however, utilizes multiple GMPMs to come up with the hazard estimates, while deaggregation shows that a range of M , R , ε contributed to any given $Sa(T^*)$. An exact computation of the CS mean and standard deviation that incorporates multiple causal earthquakes and multiple GMPMs is documented in Lin et al. (2012). For practical use to select ground motions, the exact mean and standard deviation can be combined with a lognormal distribution assumption. The exact CMS can also be obtained from the USGS web tool. Alternatively, Bradley (2010a) extends the concept of the CMS to develop the Generalized Conditional Intensity Measures

and computes the exact distribution (Equation 8, Bradley, 2010a), which has implications for ground motion selection as elaborated upon by Bradley (2012a), though that approach does not yet allow for consideration of multiple GMPMs in hazard analysis. The exact CS does not change the conditional mean significantly but increases the conditional standard deviation, especially for periods away from the conditioning period (Lin et al., 2012), as will be discussed further below.

In the illustrative example, the CS, which includes both mean and variability, is computed for ten intensity levels at four periods of interest, using Equations 4.2 and 4.3. The ten intensity levels of $Sa(T^*)$ were chosen to correspond to specified probabilities of exceedance ranging from 50% in 20 years to 1% in 200 years (the range that is provided by USGS), and the periods of interest, T^* , correspond to the first three modal periods (2.6s, 0.85s, and 0.45s) of the structure and a lengthened period (5s) that is associated with non-linear behavior. To obtain an approximate CS, mean deaggregation values of magnitude, M , and distance, R , given each $Sa(T^*)$ are obtained from the USGS deaggregation web tool, and used as inputs to Equations 4.2 and 4.3. Other relevant parameters, such as the depth to the top of rupture, are inferred for the rupture that dominates the hazard at the site considered here. A single GMPM (in this case, Campbell and Bozorgnia, 2008) is used to obtain the logarithmic mean and standard deviation, $\mu_{lnSa}(M, R, T_i)$ and $\sigma_{lnSa}(M, T_i)$. The target $\varepsilon(T^*)$ is back-calculated using Equation 4.1. The correlation coefficient between pairs of ε values at two periods, $\rho(T_i, T^*)$, is obtained from Baker and Jayaram (2008). These inputs, are then used to compute the CS with Equations 4.2 and 4.3.

The Conditional Mean Spectra (using Equation 4.2 alone) for these intensity levels and periods of interest are shown in Figure 4.2a and b. As the intensity level increases, the deaggregated mean ε value increases, and the spectral shape of the CMS becomes more peaked at the conditioning period, as illustrated in Figure 4.2a. For a Sa amplitude associated with 2% in 50 years Sa exceedance, the UHS, superimposed on the CMS at various periods, is an envelope of all the CMS, as illustrated in Figure 4.2b. The Sa values of the CMS at their respective conditioning periods equal those of the UHS.

4.3.3 Ground motion selection to match target spectrum

With the target spectra identified and computed, ground motions can then be selected from a ground motion database to match each target spectrum. Suites of ground motions can be selected and scaled such that they collectively match the entire distribution of the CS, using a computationally efficient algorithm (Jayaram et al., 2011). With this publicly available software (http://www.stanford.edu/~bakerjw/gm_selection.html), the user provides a target spectrum or deaggregation information, along with any desired limitations on such parameters as magnitude, distance, site condition, and scale factor, and the software produces selected and scaled ground motions from the PEER NGA database (Chiou et al., 2008).

To illustrate, Figure 4.3 shows the response spectra of 40 ground motions selected and scaled to match the CS (mean and standard deviation) via Jayaram et al. (2011) with $S_a(2.6s)$ having 2% in 50 year probability of exceedance. Both linear and logarithmic scale plots are presented to orient the reader familiar with either format. The same procedure was repeated to select ground motions for all other intensity levels and periods described above.

4.4 Hazard consistency of ground motion response spectra

Once ground motions are selected for all intensity levels and periods, distributions of selected ground motion response spectra can be computed and compared with the target seismic hazard curves to check hazard consistency. Hazard consistency implies that the distributions of response spectra from the selected ground motions (through the CS as the target spectrum) are consistent with the site ground motion hazard curves at all relevant periods. In theory, use of the exact CS results in consistent rates of exceedance between selected ground motion response spectra and the target seismic hazard curves. If an approximate CS is used and the resulting ground motion response spectra do not match well with the target seismic hazard curve, adjustments in the logarithmic standard deviation of the target CS may need to be made and ground motions reselected prior to structural analysis.

4.4.1 Linking ground motion response spectra to seismic hazard

The ground motion selection procedure, as illustrated in Figure 4.3, is used for ten intensity levels (where the mean and standard deviation of the selected ground motions’ response spectra are consistent with those of the target CS at each intensity level), and the response spectra of the selected ground motions (with a total of four hundred ground motions) at each conditioning period can be plotted. In Figure 4.4a and 4.4b, we see the response spectra of the ground motions selected and scaled to match the specific values that the spectra are conditioned upon, $Sa(2.6s)$ and $Sa(0.85s)$; we see the “pinched” shapes of the spectra at 2.6s and 0.85s in Figure 4.4a and 4.4b, respectively, since only ten $Sa(T^*)$ amplitudes were used here. At other periods, the spectra are more varied, as the amplitudes at other periods have variability even when $Sa(T^*)$ is known with certainty. But these ground motions were selected to maintain proper conditional means and variances, ensuring that the distributions of spectra at all periods are still consistent with all known hazard information for the site being considered. It is difficult to evaluate this consistency by simply counting the number of ground motions exceeding a given spectral amplitude, because there are 40 ground motions at each Sa amplitude, while the real site will have many more low-amplitude ground motions than high-amplitude motions.

To make a quantitative evaluation of the “hazard consistency” of the selected ground motions’ response spectra at an arbitrary period T , the rate of exceedance of $Sa(T)$ implied by the ground motions selected conditional on $Sa(T^*)$ is computed using the following equation:

$$\lambda(Sa(T) > y) = \int_x P(Sa(T) > y | Sa(T^*) = x) |d\lambda(Sa(T^*) > x)| \quad (4.4)$$

where $P(Sa(T) > y | Sa(T^*) = x)$ is the probability that a ground motion selected and scaled to have $Sa(T^*) = x$ has an Sa at period T that is greater than y . Here this probability is estimated as simply the fraction of the 40 ground motions with $Sa(T^*) = x$ that have $Sa(T) > y$. The multiplication of these probabilities by the derivative of the hazard curve for $Sa(T^*)$ reweights the results according to the predicted rate of observing ground motions with $Sa(T^*) = x$.

Figure 4.4c shows the computed rate of ground motions with $Sa(2.6s) > y$ for each

set of selected motions (the two in Figure 4.4a and 4.4b plus the sets selected based on $T^* = 0.45s$ and $T^* = 5.0s$). Also shown for reference is the “direct hazard curve” for $Sa(2.6s)$ obtained from seismic hazard analysis. Ideally the selected ground motions would be consistent with this direct hazard curve. The ground motions selected using $T^* = 2.6s$ have a stepped plot in Figure 4.4c, due to the ten discrete $Sa(2.6s)$ amplitudes that were considered when selecting motions and the fact that $P(Sa(T) > y | Sa(T^*) = x)$, when $T = T^*$, is equal to either 0 when $y < x$ or 1 when $y > x$. The ground motions with other T^* values have smoother curves. All of the curves are in good general agreement, indicating that even though the other sets of ground motions did not scale ground motions to match $Sa(2.6s)$, they have the proper distribution of $Sa(2.6s)$ as specified by the hazard curve at that period. A similar plot is shown in Figure 4.4d for the rate of exceeding $Sa(5s)$; in this case the ground motions with $T^* = 5s$ have the stepped curve, and the other T^* cases are smooth. Again the curves are in relatively good agreement with the true ground motion hazard curve, except for the case of $T^* = 0.45s$ at high amplitudes.

As seen from Figures 4.4c and 4.4d, ground motions selected using the conditioning period, $T^* = 0.85s$, seem to be rather consistent with the direct hazard curves at 2.6s and 5s. It is important to ensure that response spectra of the selected ground motions match well with the target seismic hazard at the periods that are important to the structural response of interest. If the goal of the analysis is to assess *PSDR* or collapse, then ground motion hazard consistency at the longer periods (2.6s and 5s) may suffice if higher-mode responses do not contribute significantly to that response parameter. If the goal of the analysis involves structural responses that are sensitive to shorter periods (e.g., *PFA*), however, then ground motion hazard consistency needs to be enforced at the shorter periods as well. Let us revisit the $T^* = 0.85s$ case in the shorter period range in addition to the known good match in the longer period range. Spectra of ground motions selected using $T^* = 0.85s$ from Figure 4.4b are plotted with reference to four periods (0.45s, 0.85s, 2.6s, and 5s). The corresponding ground motion spectra distributions at these periods are plotted in Figure 4.4e. The dotted lines show the direct hazard curves, while the solid lines show the implied hazard curves from the selected ground motions. Note the stepped curve for the ground motions at 0.85s, due to the ten discrete $Sa(0.85s)$ amplitudes that were considered when selecting these motions. Figure 4.4e shows that ground motions selected using $T^* = 0.85s$ resulted in

response spectra that are relatively consistent with known seismic hazard information at all four periods of consideration (0.45s, 0.85s, 2.6s, and 5s). This set of ground motions using $T^* = 0.85s$ can thus perhaps be used to evaluate any structural responses, regardless of their corresponding periods of importance.

4.4.2 Comparison of approximate and exact Conditional Spectra

The quality of the match in response spectra between the selected ground motions and the target seismic hazard curve is good in some cases (e.g., $T^* = 0.85s$) but not others (e.g., $T^* = 0.45s$). The match quality would depend on (1) the accuracy of the computed target spectrum and (2) the consistency in the distribution between the selected ground motions and the target spectrum. Since the distribution of the selected ground motions matches well with the target spectrum, the major factor would then be the accuracy of the computed target spectrum, where multiple causal earthquakes and GMPMs would be important. When multiple magnitudes and distances (instead of a single earthquake scenario) associated with a given deaggregation are taken into consideration, the variability of the spectrum at periods other than T^* is increased relative to the approximate case using only a single mean magnitude and distance. A similar increase in variability also results from making predictions using multiple GMPMs (consistent with the use of multiple models in the hazard calculations) rather than just a single model (Lin et al., 2012).

The increased variability from these factors can be captured formally in the conditional standard deviation computation. The mean CS is in principle be affected by this approximation, but this does not appear to be as significant of a practical issue in many cases. Figure 4.5 shows approximate and exact CS results for the example site considered here, at a short and long conditioning period (Lin et al., 2012). Those results indicate that, for this particular site, the approximations that we are using here are very accurate for the 1s conditioning period, but that conditional standard deviations are underestimated by the approximation for the 0.2s conditioning period case. The accurate approximation for the 1s conditioning period (Figure 4.5b) explains why the response spectra of the selected ground motions using $T^* = 0.85s$ match the seismic hazard well at various periods (Figure 4.4e). As the underestimation of conditional standard deviation is most prominent at periods far

from the conditioning period (as seen prominently in Figure 4.5a and more generally in Lin et al. (2012)), it is perhaps not surprising that the conditional standard deviations at $Sa(5s)$ for the $T^* = 0.45s$ case is underestimated, resulting in a lack of high-amplitude $Sa(5s)$ values in those ground motions (Figure 4.5d). It is illustrated here that approximate CS may work well for some cases but not others. Ideally we would use the exact CS calculations for all results presented in this chapter, but those calculations are currently rather cumbersome for practical applications (although automated tools for such calculations are envisioned in the near future, and an alternative approach is developed by Bradley (2010b)).

4.4.3 Response spectra refinement

Given our current limitations with regard to computing exact CS, we approximately correct for the difference between the approximate and exact standard deviations (seen, for example, in Figure 4.5a) by inflating the approximate standard deviations by some constant. The value of that constant is determined by comparing the Sa distributions from the resulting selected ground motions to the numerical hazard curves at a range of periods. With an appropriate conditional standard deviation, the ground motions should match the corresponding target hazard curves as described above. No adjustment is made to the approximate mean spectra, as experience shows them to be similar to exact mean spectra in most cases Lin et al. (2012).

In the results above, the ground motions selected using $T^* = 0.85s$, $2.6s$ and $5s$ already showed good agreement with corresponding ground motion hazard curves at $2.6s$ and $5s$ (Figures 4.4c and 4.4d), so no adjustments were made in those cases. For the case of $T^* = 0.45s$, the conditional standard deviations were inflated by 10% and ground motions were reselected to match this new target. The spectra of the selected ground motions with $T^* = 0.45s$ are plotted at four periods versus the corresponding ground motion hazard curves in Figure 4.6. The spectra from the original ground motions are shown in Figure 4.6a, and the new motions with a 10% larger standard deviation are shown in Figure 4.6b.

Note again the stepped curve for the ground motions at $0.45s$, due to the ten discrete $Sa(0.45s)$ amplitudes that were considered when selecting these motions. The curves in Figure 4.6a are in relatively good agreement with the true ground motion hazard curve,

except for the case of $Sa(5s)$ at high amplitudes, and $Sa(2.6s)$ to a lesser extent. With a conditional standard deviation inflated by 10% for the Figure 4.6b motions, the curves at 5s and 2.6s are in better agreements, demonstrating improved consistency with the known hazard information.

4.5 Structural analysis

For each of the sets of ground motions selected at various intensity levels and conditioning periods, nonlinear dynamic analysis was performed to obtain structural response. The structural model used for the 20-story reinforced concrete perimeter frame accounts for strength deterioration (both cyclic and in-cycle) and stiffness deterioration. The objective of nonlinear dynamic analysis here is risk-based assessment which considers full distribution of structural response at multiple intensity levels along with their occurrence rates. To illustrate, we perform such a computation for Peak Story Drift Ratio (*PSDR*, i.e. maximum story drift ratio observed over all stories, over the duration of shaking). The structural analysis procedure will be presented for a single conditioning period followed by additional conditioning periods, and first for ground motion selected to match the approximate CS and next for ground motions with response spectra refinement to ensure hazard consistency.

4.5.1 Risk-based assessment procedure

The risk-based assessment procedure estimates the mean annual rate of structural response amplitude $> y$. It is obtained by integrating the probability of observing a structural response amplitude given a ground motion intensity level $= x$ with the rate of observing those ground motion intensities. The mean annual rate of *EDP* exceeding y , $\lambda(EDP > y)$ can be calculated as follows (Krawinkler and Miranda, 2004):

$$\lambda(EDP > y) = \int_x P(EDP > y | Sa(T^*) = x) |d\lambda(Sa(T^*) > x| \quad (4.5)$$

where $d\lambda(Sa(T^*) > x)$ is the derivative of the hazard curve for $Sa(T^*)$ multiplied by an increment of $dSa(T^*)$, and $P(EDP > y | Sa(T^*) = x)$ is the probability of *EDP* exceeding y given a ground motion with $Sa(T^*) = x$. For instance, if the *EDP* of interest is

$PSDR$, $P(EDP > y|Sa(T^*) = x)$, which is an input to Equation 4.5, would be $P(PSDR > y|Sa(T^*) = x)$, and the resulting risk-based assessment of $PSDR$, $\lambda(PSDR > y)$, can be termed “drift hazard”. The probability of $PSDR$ exceeding y given a ground motion with $Sa(T^*) = x$ can be computed below (Shome and Cornell, 1999):

$$P(PSDR > y|Sa(T^*) = x) = P(C) + (1 - P(C))(1 - \Phi(\frac{\ln y - \mu_{\ln PSDR}}{\sigma_{\ln PSDR}})) \quad (4.6)$$

where $P(C)$ is the probability of collapse given $Sa(T^*) = x$ estimated from the collapse fragility function and $\mu_{\ln PSDR}$ and $\sigma_{\ln PSDR}$ are the mean and standard deviation, respectively, of $\ln PSDR$ values given $Sa(T^*) = x$ and no collapse. One assumption here is that all collapse cases cause $PSDR > y$.

To illustrate, consider nonlinear dynamic analysis results of $PSDR$ given $Sa(2.6s)$ for ten intensity levels. As illustrated in Figure 4.7a, each “stripe” of nonlinear dynamic analysis results corresponds to $PSDR$ at one intensity level with its associated $Sa(2.6s)$ value. As the occurrence rate decreases (or return period increases), the associated $Sa(2.6s)$ value increases, resulting generally in higher structural response (except when a change in deformation mechanism of the system leads to a reduction in a particular response parameter, e.g., structural resurrection as presented in Vamvatsikos and Cornell (2002)). Structural response at each given ground motion intensity level is assumed to be lognormally distributed (e.g., Shome and Cornell, 1999; Song and Ellingwood, 1999; Shinozuka et al., 2000; Sasani and Kiureghian, 2001; Aslani and Miranda, 2005; Stoica et al., 2007). Since 40 ground motions are used for each intensity level, the uncertainty in the point-estimated distribution parameters (i.e., logarithmic mean and standard deviation) of structural response given intensity level are relatively small and therefore not explicitly considered. If a structural response threshold is specified (e.g., a $PSDR$ of 0.01), probabilities of structural response greater than the threshold value can be obtained as shaded in Figure 4.7a. The observed fractions of collapse can also be plotted for each intensity level, as shown in Figure 4.7b. A fragility function utilizing maximum likelihood (e.g., Shinozuka et al., 2000; Baker, 2005; Straub and Kiureghian, 2008) is used to fit the empirical collapse data. The $PSDR$ distribution and collapse fragility from Figures 4.7a and 4.7b can be combined with the corresponding seismic hazard curve from Figure 4.1a, to estimate the mean annual rate

of $PSDR > y$ in Figure 4.7c) for $T^* = 2.6s$ using Equation 4.5 (through Equation 4.6).

4.5.2 Varying conditioning periods

To evaluate the impact of conditioning period on risk-based assessment, structural analyses using ground motions selected to match the CS can be performed at various conditioning periods. Calculations similar to those for $T^* = 2.6s$ were repeated for the other three periods: $T^* = 0.45s$, $T^* = 0.85s$, and $T^* = 5s$. Collapse fragility functions obtained from the four sets of structural analyses are shown in Figure 4.7b and risk-based assessments of $PSDR$ in Figure 4.7c using the approximate CS. Risk-based assessments of $PSDR$ show fairly good agreements using the approximate CS at four conditioning periods except for 0.45s, which will be covered in the next section using the refined CS.

4.5.3 Significance of hazard consistency

Let us now look at what difference hazard-consistent refinement of target spectra would make on structural response. Recall that conditional standard deviation was inflated for 0.45s to approximately correct for the difference between the approximate and exact CS, so that the Sa distribution from the selected response spectra matches better with the target ground motion hazard curve.

The resulting collapse fragility functions are shown in Figure 4.8a. The inflated conditional standard deviation resolves the deficiency in high-amplitude Sa values especially for long periods (Figures 4.6b vs. 4.6a) which are important for collapse, and therefore results in a higher probability of collapse for a given $Sa(0.45s)$ amplitude.

Another potential reason that the 0.45s case did not work well compared to the other three conditioning periods (Figure 4.7c) is that the collapse fragility curve was not well constrained because of a lower fraction of observed collapses (only 40% even for the highest Sa amplitudes, as illustrated in Figure 4.7b). To test the sensitivity of the collapse results to the absence of higher-amplitude Sa levels, we performed additional ground motion selection and structural analyses for the 0.45s case at higher Sa amplitudes but found that the collapse fragility curves did not change much with more constraints from collapse observations at additional higher-amplitude Sa levels documented in Appendix A.3. There are

cases, however, when a poorly constrained collapse fragility curve may distort the result significantly, e.g., with the highest observed probability of collapse of less than 10%, as seen in some of the structures and period combinations in calculations of this type documented in Appendix A.

The risk-based assessment of *PSDR* was recomputed using these new motions with adjusted conditional standard deviation, and is compared to the original result for $T^* = 0.45s$ in Figure 4.8b. The horizontal portion of the *PSDR* risk-based assessment curve is dominated by collapse for higher *PSDR*, so the higher probability of collapse with the inflated conditional standard deviation would result in a higher annual rate of exceeding *PSDR* as well. The new risk-based assessment result is also compared to the previous risk-based assessment results using other conditional periods in Figure 4.9, and the agreement among these four curves is very good. This suggests that if we carefully select ground motions with appropriate conditional standard deviations to match the true hazard curves, risk-based assessments would be in good agreements regardless of the choice of conditioning periods.

Despite this refinement, we have still only considered spectral values here and not other ground motion properties that in some cases may be relevant to structural response (e.g. velocity pulses and duration). If non-spectral ground motion parameters are also deemed important for predicting the *EDP* of interest, the approach above can be generalized to account for those parameters and quantify the correlations between additional parameters of interest, as recently developed by Bradley (2012a).

4.6 Additional engineering demand parameters

Risk-based assessment of *PSDR* has been presented in the earlier sections. Story drift is often used in structural analysis as it is highly correlated with structural damage (e.g., ATC, 1982). However, depending on the focus of the structural analysis, the structural response parameter of interest may vary. To help illustrate the generality of the above results, we now consider Peak Floor Acceleration (*PFA*, i.e., maximum acceleration observed over all floors including the ground, over the duration of shaking) as well as Story Drift Ratio (*SDR*, i.e., maximum story drift ratio observed at a single story, over the duration of shaking) and Floor Acceleration (*FA*, i.e., maximum acceleration observed at a single floor, over the

duration of shaking). *PFA*s are often observed at upper stories of the example building and are sensitive to excitation of higher modes of the building, so they are not highly correlated with *PSDR*s (which are more closely related to first-mode response). Hazard consistency of ground motions should again be ensured at the periods of interest, i.e., at shorter periods (high-mode periods) for *PFA*s.

Some adjustments of conditional standard deviations were again needed in order to ensure hazard consistency of the short-period *Sa* when the conditioning period was first-mode or longer (because these short-period spectra are important for *PFA*). Figure 4.10 compares the *Sa* distributions from the ground motions selected with $T^* = 2.6s$ (Figure 4.10a and Figure 4.10b) and $T^* = 5s$ (Figure 4.10c and Figure 4.10d), to the numerical hazard curves at a range of periods (0.45s, 0.85s, 2.6s, 5s), without (Figure 4.10a and Figure 4.10c) and with (Figure 4.10b and Figure 4.10d) conditional standard deviation adjustments. Approximate CS (with a single causal earthquake $M/R/\epsilon$ and a single GMPM) were used in Figures 4.10a and 4.10c for $T^* = 2.6s$ and $T^* = 5s$ respectively. Note again the stepped curve for the ground motions at 2.6s (Figure 4.10a) and 5s (Figure 4.10c), due to the ten discrete $Sa(T^*)$ amplitudes that were considered when selecting these motions. The curves in Figures 4.10a and 4.10c using the selected ground motions match well with the true ground motion hazard curve at longer periods (2.6s and 5s), but not as well at shorter periods (especially 0.45s) which are important for *PFA*. By comparing the *Sa* distributions from the resulting selected ground motions (using approximate conditional standard deviation) to the true hazard curves, we approximately correct for the difference between the approximate and exact standard deviations by inflating the approximate standard deviations by some constant. For the case of $T^* = 2.6s$ and $T^* = 5s$, the conditional standard deviations were inflated by 30% and ground motions were reselected to match this new target. With a conditional standard deviation inflated by 30% for the Figures 4.10b and 4.10d motions, the curves at 0.45s are in better agreements, demonstrating improved consistency with the known hazard information.

The risk-based assessment procedure is similar to those for *PSDR* hazard calculations except the following: for *PFA*, collapse *PFA* is assumed to be the Peak Ground Acceleration (*PGA*) for the corresponding ground motion since *PFA* are close to *PGA* when the building experiences strong nonlinear behavior (except for collapse mechanisms that

cause partial collapse in the upper floors) (Aslani and Miranda, 2005). Hence, the logarithmic mean and standard deviation of PFA , $\mu_{\ln PFA}$ and $\sigma_{\ln PFA}$, can be evaluated directly including both collapse and non-collapse cases, slightly different from the $PSDR$ evaluations. The probability of PFA exceeding y given a ground motion with $Sa(T^*) = x$, $P(PFA > y|Sa(T^*) = x)$, can then be easily computed as

$$P(PFA > y|Sa(T^*) = x) = 1 - \Phi \left(\frac{\ln y - \mu_{\ln PFA}}{\sigma_{\ln PFA}} \right) \quad (4.7)$$

With the computed $P(PFA > y|Sa(T^*) = x)$, the mean annual rate of PFA s exceeding y , $\lambda(PFA > y)$ can be calculated according to Equation 4.5 where the EDP of interest is PFA .

Figure 4.11a shows the PFA risk-based assessment curves obtained with four choices of T^* using an approximate conditional standard deviation, whereas Figure 4.11b shows these curves using an inflated conditional standard deviation for the cases of $Sa(2.6s)$ and $Sa(5s)$. Once appropriate conditional standard deviations were determined for each conditioning period, the risk-based assessment results are more consistent, as illustrated through the improvements from Figure 4.11a to Figure 4.11b. This again shows the importance of hazard consistency on risk-based assessment results, and that once such hazard consistency is ensured, risk-based assessment results are relatively insensitive to the choice of conditioning period.

The results of Figures 4.9 and 4.11b are also presented in Table 4.1, to illustrate (1) the differences in the values of exceedance rate for a given EDP value using different conditional periods (in the top portion of the table), and (2) the differences in EDP for a given exceedance rate using different conditional periods (in the bottom portion of the table). Annual rates of $PSDR > 2\%$, annual rates of $PFA > 0.5g$, and annual rates of collapse as well as median $PSDR$ and median PFA corresponding to 10% in 50 year exceedance rates are shown for all four conditioning periods ($T^* = 0.45s, 0.85s, 2.6s, 5s$) considered here. While excluding the ground motions selected with an inflation in the logarithmic standard deviation of the CS, the differences in the values (1) range from 12% (for annual rates of $PFA > 0.5g$ with example values between 7.96×10^{-4} and 9.42×10^{-4}) to 20% (for annual rates of collapse with example values between 4.18×10^{-4} and 5.02×10^{-4}) and (2) are between 4% (for median PFA corresponding to 10% in 50 years exceedance rates

with example values between 0.509 and 0.529) and 9% (for median *PSDR* corresponding to 10% in 50 years exceedance rates with example values between 0.011 and 0.012). These differences are considered small for the range of conditioning periods investigated.

Similar results are shown in Figure 4.12 for story drift ratio and floor accelerations observed on the 15th story of the structure (rather than the maximum response across all stories). These parameters are used to illustrate prediction of single-story response parameters that are often of interest in loss assessment calculations. Figure 4.12 illustrates that these predictions are also consistent when differing conditioning periods are considered.

The results in this section again demonstrate the consistency of risk-based assessments across conditioning periods. They also indicate the importance of ensuring hazard consistency of the response spectra at periods related to the structural response parameter of interest (or more generally, hazard consistency of any ground motion intensity measure of interest). If an approximate CS is used as the target response spectrum, *EDP*-specific adjustments in conditional standard deviation may be needed to achieve better hazard consistency; this is because different *EDPs* are correlated with spectral amplitudes at different periods, and capturing the variability of spectra at periods (especially those associated with the *EDPs* of interest) away from the conditioning period is important. Although hazard consistency was improved for periods and *Sa* amplitudes of most interest given an *EDP*, uniformly inflating the conditional standard deviation of the target spectra (as was done in the approximate refinement cases) may result in over- or under-estimations at other periods or *Sa* amplitudes, since conditional standard deviations do not scale uniformly. Alternatively, if the exact CS is used as the target response spectrum, the same input ground motions can be used for structural analysis to obtain all *EDPs* of interest – this would be the most robust method for performance-based earthquake engineering that is interested in performance quantities which require characterization of the uncertainty in *EDP* estimates given ground motion intensity levels, e.g., loss estimation (as a result of damage to drift- and acceleration-sensitive components). The exact CS does not require *EDPs* to be known prior to ground motion selection; in other words, the *EDP*-specific spectra refinement to ensure hazard consistency is not needed for the exact CS.

4.7 Conclusions

This chapter has presented a study on the sensitivity of risk-based assessment (in the context of *EDP* hazard) results to the choice of conditioning period when using the CS as the target for ground motion selection and scaling. The study focused on risk-based assessments, with a specific emphasis on the rates of exceeding various levels of Peak Story Drift Ratio (i.e., drift hazard calculations) in the structure. Some additional *EDPs* were also considered, such as the Peak Floor Acceleration over the full building heights, a single-story Story Drift Ratio, and a single-story Floor Acceleration. The structure considered was a 20-story reinforced concrete frame structure assumed to be located in Palo Alto, California, using a structural model with strength and stiffness deterioration that is believed to reasonably capture the responses up to the point of collapse due to dynamic instability.

The risk-based assessments were performed based on ground motions selected and scaled to match the CS, where four conditioning periods, 0.45s, 0.85s, 2.6s, and 5s were used (i.e., the building's third-mode structural period up to approximately twice the first-mode period). These conditioning periods were chosen to illustrate how the assessment results varied across a wider range of periods, rather than because there is something special about these specific periods. For each case, the risk-based assessment results were found to be similar. The similarity of the results stems from the fact that the careful record selection ensures that the distributions of response spectra at all periods are nominally comparable, so the distribution of resulting structural responses should also be comparable (to the extent that response spectra describe the relationship between the ground motions and structural responses).

From these results, it is observed that if the analysis goal is to perform a risk-based assessment, then one should be able to obtain an accurate result using any conditioning period, provided that the ground motions are selected carefully to ensure proper representation of spectral values and other ground motion parameters of interest. Here "proper representation" refers to consistency with the site ground motion hazard curves at all relevant periods, and this is achieved by using the CS approach to determine target response spectra for the selected ground motions. The reproducibility of the risk-based assessment results, for varying conditioning periods, then results from the fact that the ground motion

intensity measure used to link the ground motion hazard and the structural response is not an inherent physical part of the seismic reliability problem considered; it is only a useful link to decouple the hazard and structural analysis. If this link is maintained carefully then one should obtain a consistent prediction (the correct answer) of the risk-based assessment in every case. The consistency in risk-based assessment that is demonstrated here is in contrast to some previous speculation on this topic, because this study utilizes the recently developed CS for ground motion selection, and uses the first available algorithm for selecting ground motions to match this CS target (which includes both mean and variability in the target spectra).

One practical challenge associated with these findings is that selecting ground motions that are truly consistent with ground motion hazard at all periods requires the use of an exact target CS (i.e., one that accounts for multiple causal magnitudes and distances associated with a given S_a amplitude, and for multiple GMPMs); practical computation of this CS target, however, typically considers only a single GMPM and only the mean magnitude and distance from deaggregation. The computation of the exact CS target is more difficult in practice. Here the approximate CS is used, and its conditional standard deviation is adjusted to achieve consistency of the selected ground motion spectra with corresponding ground motion hazard, at the periods important to the problem being studied. This adjustment is not needed in most cases, but in some cases it is necessary and greatly improves the robustness of the risk-based assessment results. In the future, exact CS targets can be more readily developed, and this adjustment will not be necessary.

This chapter has shown that the results of a risk-based assessment do not depend on conditioning period, T^* , provided that ground motions have been carefully selected using the Conditional-Spectrum-based selection process. The natural question is: Is the choice of conditioning period still important at all? Yes; the choice of a “good” conditioning period does still serve several useful purposes. Selecting a “good” conditioning period helps because the S_a at the conditioning period will be a good predictor of structural response; this leads to any inaccuracies in representing spectral values at other periods having a less severe impact on the resulting risk-based assessment predictions. Additionally, use of a good conditioning period reduces the variability in structural responses (effects of intensity

measure selection on structural response prediction and loss estimation are also investigated by Bradley et al. (2010a) and Bradley et al. (2010b)) and thus reduces the number of nonlinear dynamic analyses that are required to accurately estimate distributions of *EDP*. Luco and Cornell (2007) referred to these two properties as “sufficiency” and “efficiency”, respectively. Those concepts are taken further in this study, acknowledging that there is no intensity measure with perfect efficiency and sufficiency, and so careful ground motion selection is performed to compensate for shortcomings that are inherent in any intensity measure. Bradley (2012b) provides consistent and complementary results to those presented in this manuscript based on the use of the generalized conditional intensity measure.

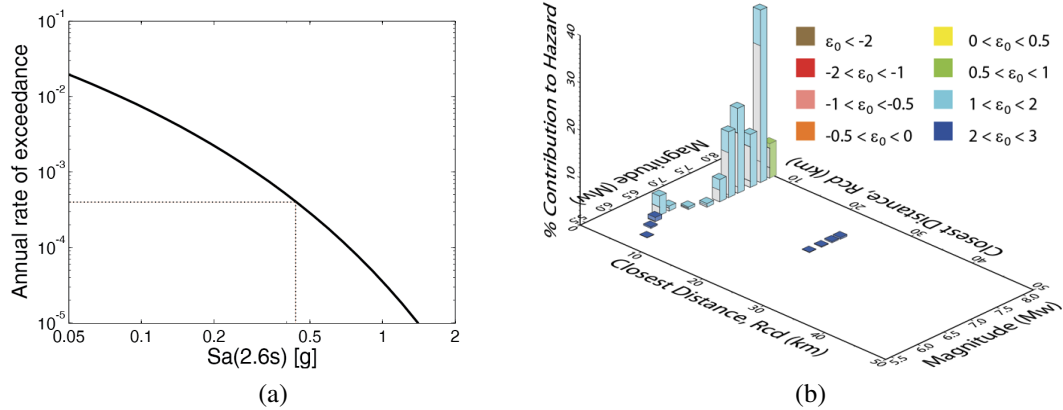


Figure 4.1: (a) Seismic hazard curve for $Sa(2.6s)$ and (b) deaggregation for $Sa(2.6s)$ amplitude with 2% in 50 years probability of exceedance.

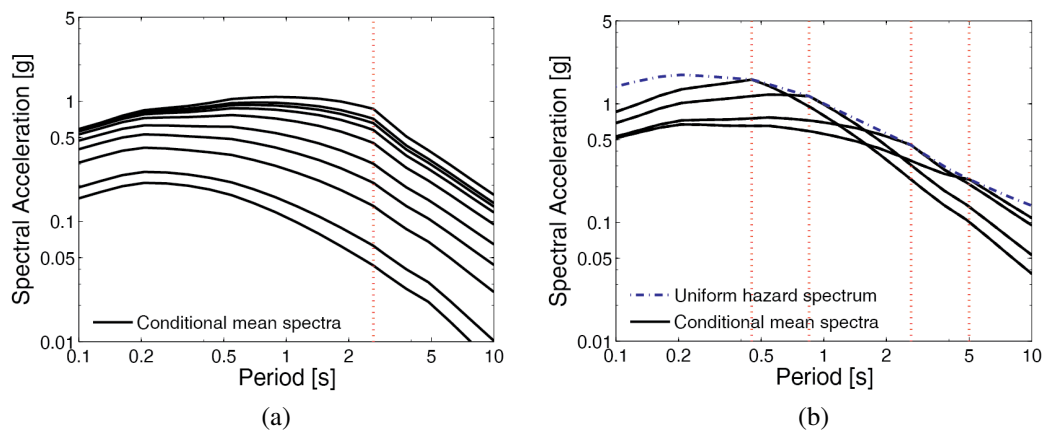


Figure 4.2: Target response spectra of (a) CMS at $T^* = 2.6s$ at multiple intensity levels (from 50% in 20 years to 1% in 200 years) and (b) CMS at multiple conditioning periods (0.45s, 0.85s, 2.6s, and 5s with UHS superimposed) at the 2% in 50 years intensity level.

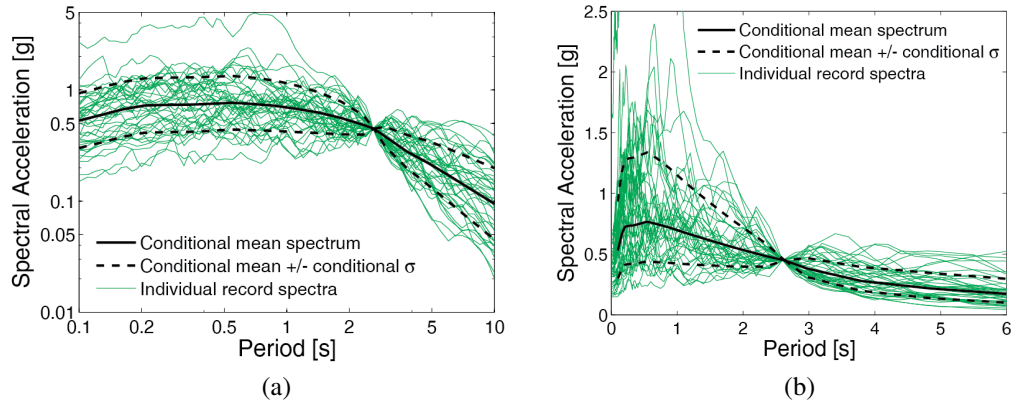


Figure 4.3: Response spectra of selected ground motions with CS as target spectra for $Sa(2.6s)$ associated with 2% in 50 years probability of exceedance (a) in log scale and (b) in linear scale.

Table 4.1: Summary of selected structural response results from risk-based assessments using ground motions selected to match the CS.

Risk-Based Performance Metrics		Conditioning Periods			
Type	Metric	0.45s	0.85s	2.6s	5s
Annual Rates	PSDR > 2%	6.46E-04	7.96E-04	9.42E-04	8.51E-04
	PFA > 0.5g	2.56E-03	2.28E-03	2.36E-03	2.12E-03
	Collapse	3.12E-04	4.66E-04	5.02E-04	4.18E-04
10% in 50 yrs EDPs	Median PSDR	0.011	0.012	0.012	0.011
	Median PFA	0.529	0.509	0.521	0.500

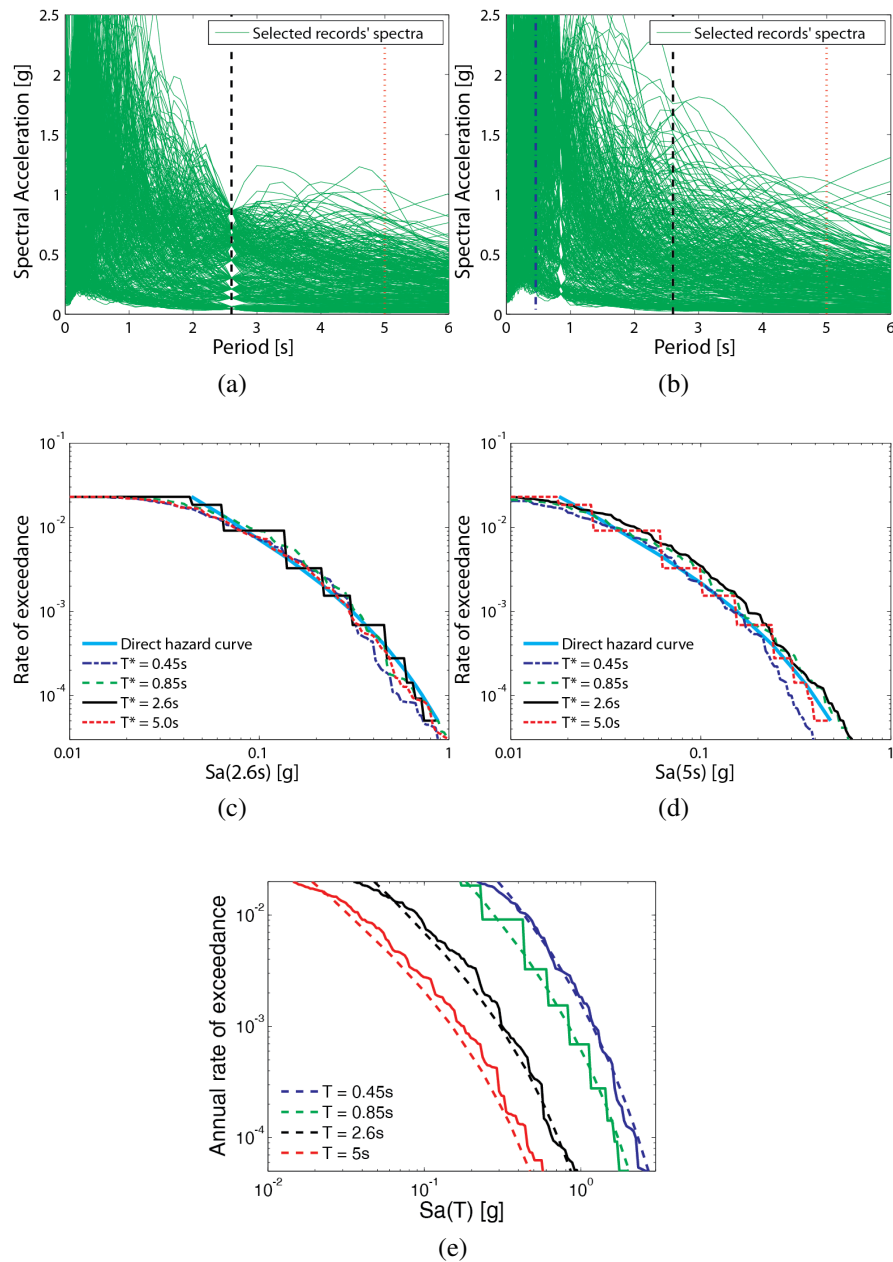


Figure 4.4: (a) Ground motion response spectra for ground motions selected at $T^* = 2.6s$, to match the CS μ and σ (at all intensity levels). (b) Ground motion response spectra for ground motions selected at $T^* = 0.85s$, to match the CS μ and σ (at all intensity levels). (c) Sa distribution at $Sa(2.6s)$ for ground motions selected at four conditioning periods, CS μ and σ . (d) Sa distribution at $Sa(5s)$ for ground motions selected at four conditioning periods, CS μ and σ . (e) Sa distribution at four periods for ground motions selected at $T^* = 0.85s$, CS μ and σ .

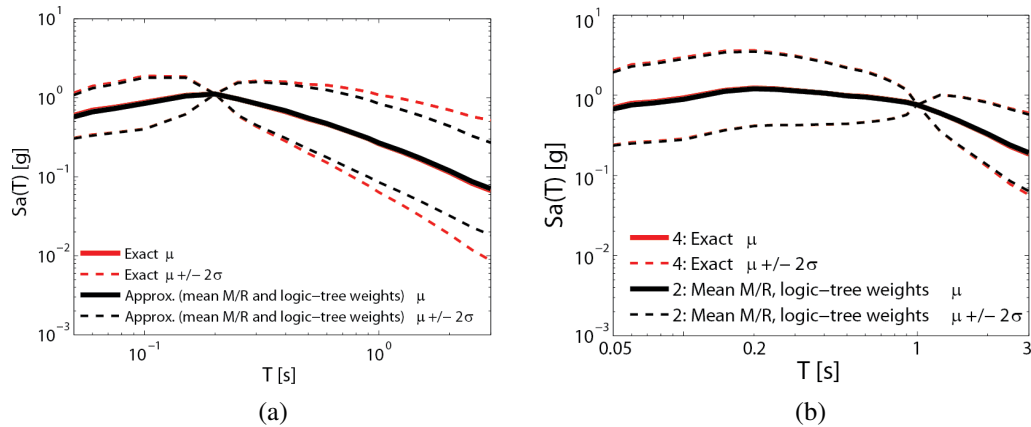


Figure 4.5: Exact and approximate CS, given $Sa(T^*)$ with 2% probability of exceedance in 50 years. Exact results are denoted “4: Exact” and approximate results are denoted “2: Mean M/R, logic tree weights” in the legend. (a) CS using $T^* = 0.2s$. (b) CS using $T^* = 1s$. Results from Lin et al. (2012).

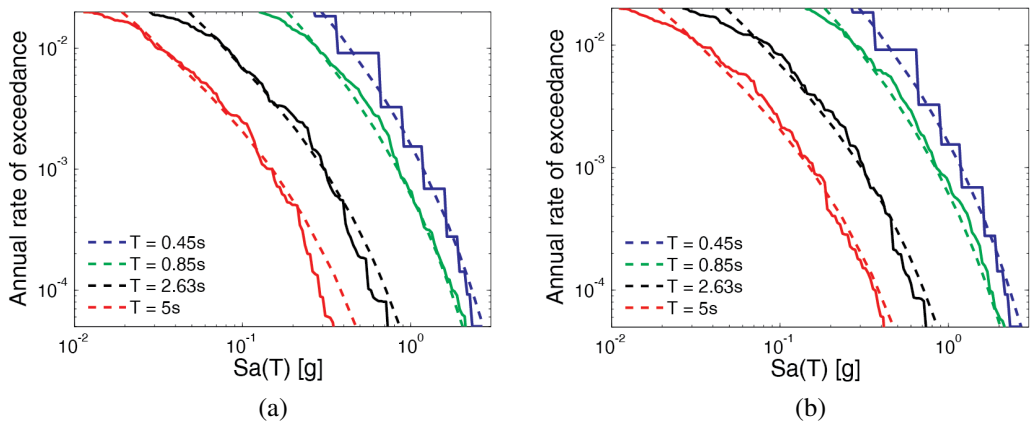


Figure 4.6: Comparison of selected ground motion spectra at 4 periods (in solid lines) versus corresponding ground motion hazard curves (in dashed lines) (a) Ground motions selected with $T^* = 0.45s$ and using basic approximate CS. (b) Ground motions selected with $T^* = 0.45s$ and using approximate CS with conditional standard deviations inflated by 10% (“1.1 σ ”).

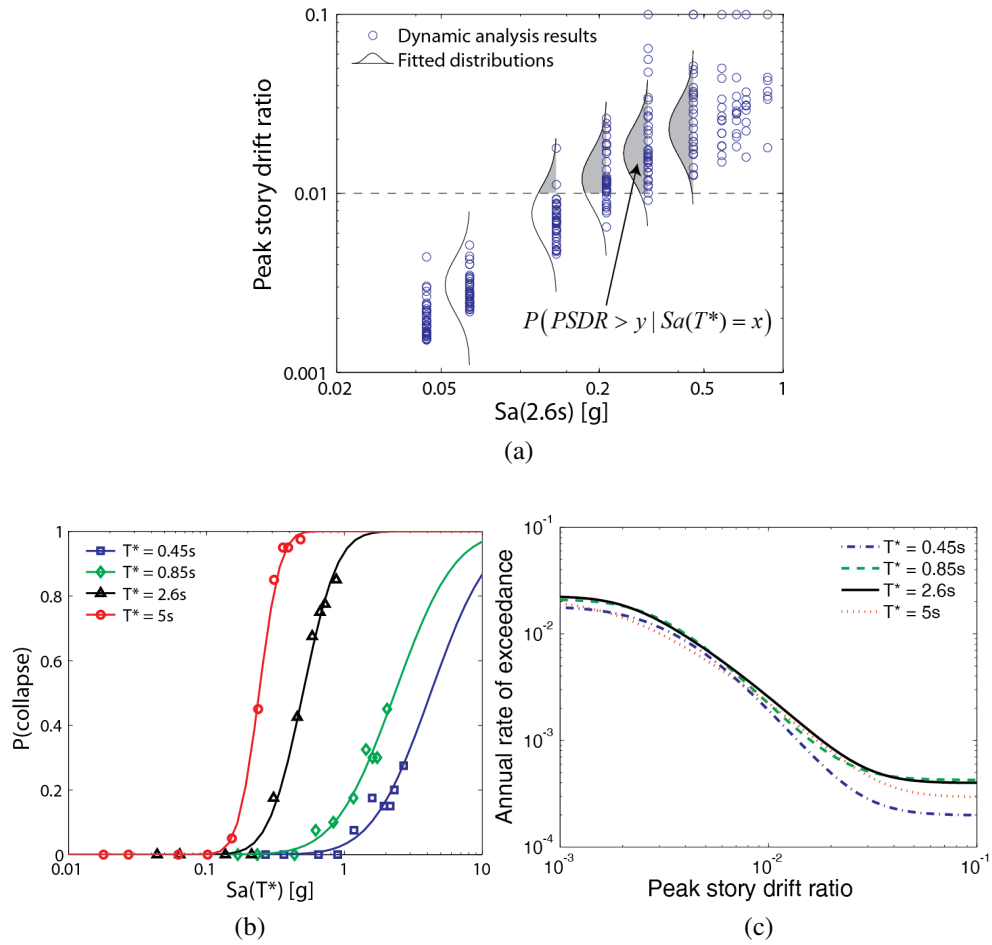


Figure 4.7: (a) $PSDR$ distribution for $Sa(2.6s)$. (b) Collapse fragility for Sa at four conditioning periods. (c) Risk-based assessments of $PSDR$ for Sa at four conditioning periods using approximate CS.

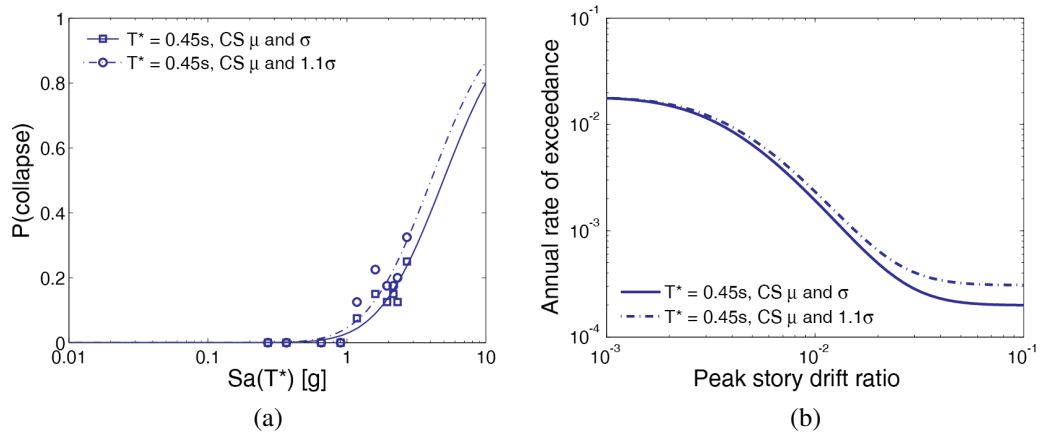


Figure 4.8: (a) Collapse fragility function and (b) risk-based assessments of *PSDR* obtained from ground motions with an approximate conditional standard deviation and inflated conditional standard deviations for the case of $Sa(0.45s)$.

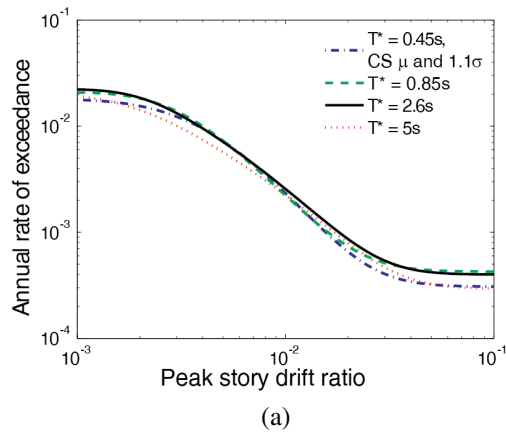


Figure 4.9: Risk-based assessments of *PSDR* obtained with four choices of T^* using an inflated conditional standard deviation for the case of $Sa(0.45s)$.

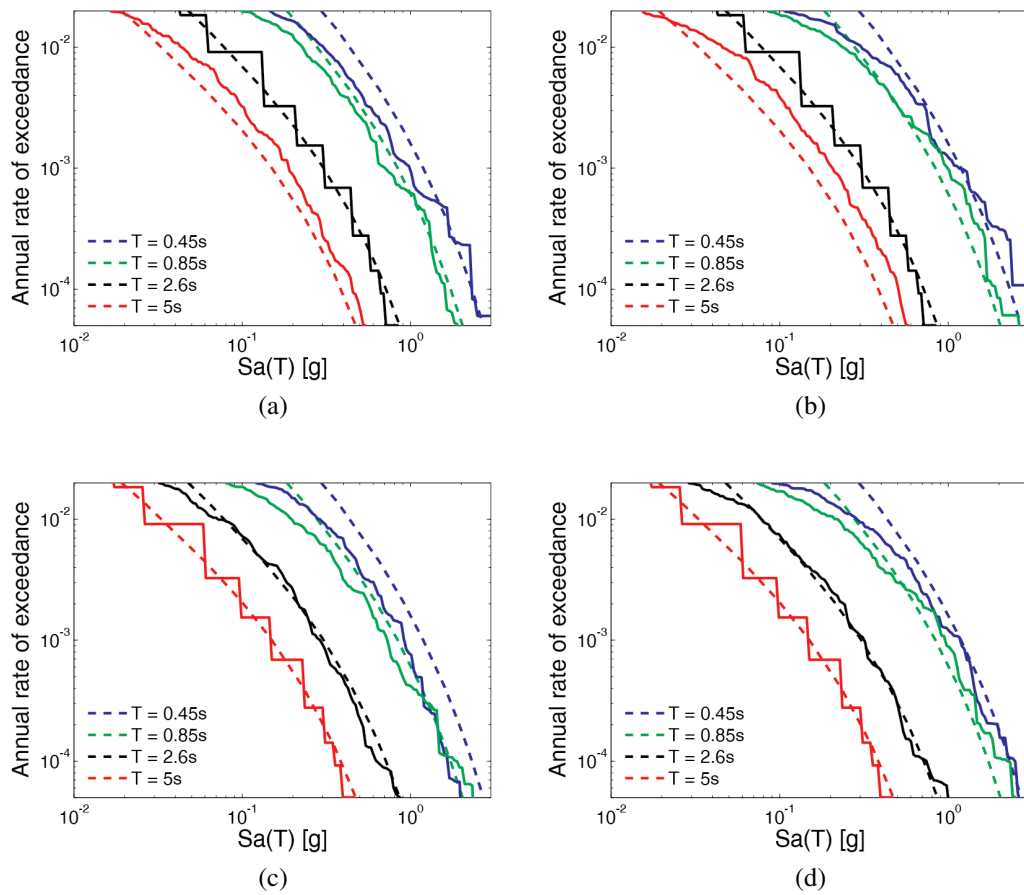


Figure 4.10: S_a distribution at four periods for ground motions selected at (a) $T^* = 2.6s$, CS μ and σ , (b) $T^* = 2.6s$, CS μ and 1.3σ , (c) $T^* = 5s$, CS μ and σ , and (d) $T^* = 5s$, CS μ and 1.3σ .

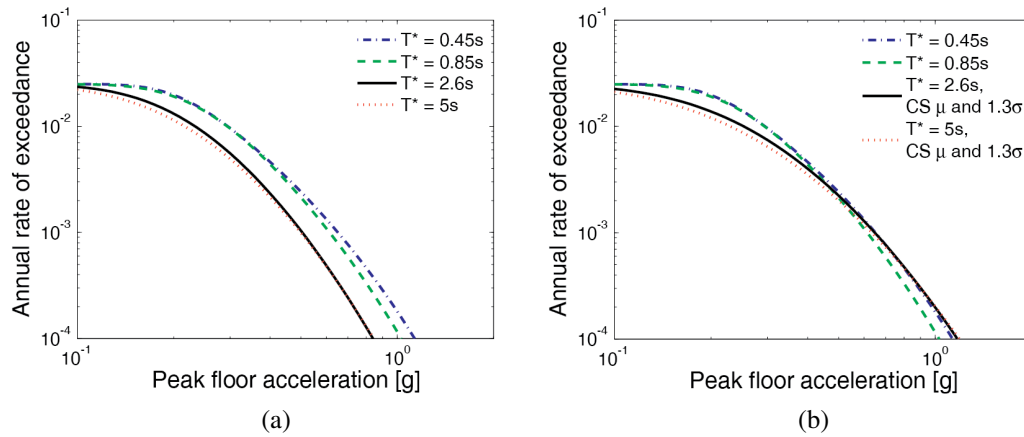


Figure 4.11: Risk-based assessments of PFA obtained with four choices of T^* using (a) an approximate conditional standard deviation and (b) an inflated conditional standard deviation for the cases of $Sa(2.6s)$ and $Sa(5s)$.

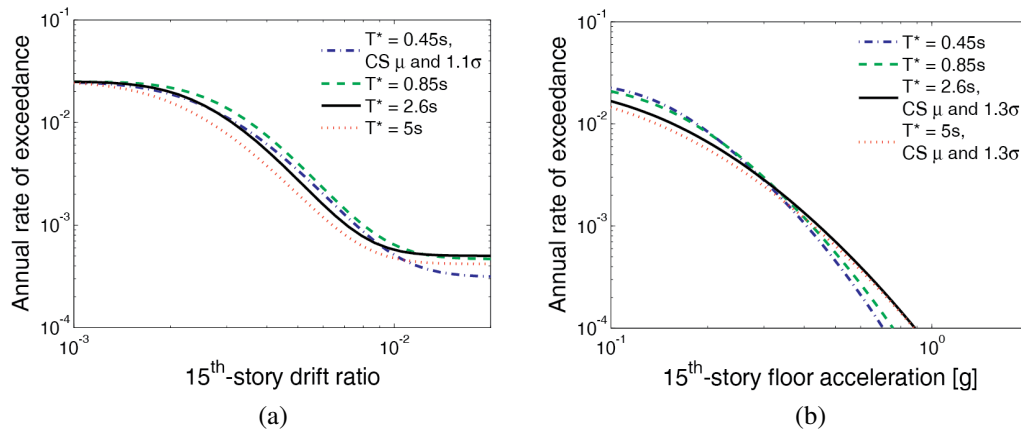


Figure 4.12: Rates of exceedance of drift ratios and floor accelerations on the 15th story of the building.

Chapter 5

Conditional-Spectrum-based ground motion selection: Intensity-based assessments and evaluation of alternative target spectra

Lin, T., C. B. Haselton, and J. W. Baker (2012b). Conditional-Spectrum-based ground motion selection. Part II: Intensity-based assessments and evaluation of alternative target spectra. *Earthquake Engineering & Structural Dynamics* (in review).

5.1 Abstract

In the previous chapter, an overview and problem definition was presented for ground motion selection based on the Conditional Spectrum (CS), to perform risk-based assessments (which estimate the annual rate of exceeding a specified structural response amplitude) for a 20-story reinforced concrete frame structure. Here the methodology is repeated for intensity-based assessments (which estimate structural response for ground motions with a specified intensity level) to determine the effect of conditioning period. Additionally, intensity-based and risk-based assessments are evaluated for two other possible target spectra, specifically the Uniform Hazard Spectrum (UHS) and the Conditional Mean Spectrum

(CMS, without variability). It is demonstrated for the structure considered that the choice of conditioning period in the CS can substantially impact structural response estimates in an intensity-based assessment. When used for intensity-based assessments, the UHS typically results in equal or higher median estimates of structural response than the CS; the CMS results in similar median estimates of structural response compared with the CS, but exhibits lower dispersion because of the omission of variability. The choice of target spectrum is then evaluated for risk-based assessments, showing that the UHS results in overestimation of structural response hazard, while the CMS results in underestimation. Additional analyses are completed for other structures to confirm the generality of the conclusions here. These findings have potentially important implications both for the intensity-based seismic assessments using the CS in future building codes and the risk-based seismic assessments typically used in Performance-Based Earthquake Engineering applications.

5.2 Introduction

Ground motion selection provides important seismic input to nonlinear dynamic analysis that is used to predict structural performance typically based on structural response parameters that are of most interest. The uncertainty in ground motion input typically accounts for a significant portion of the uncertainty in structural response output. To determine what ground motions would be appropriate for nonlinear dynamic analysis, we need to be clear about the structural analysis objective as well as the target response spectrum for which ground motions are selected and scaled to match. Nonlinear dynamic analysis can be carried out with the objectives of intensity-based (which estimates structural response given ground motions with a specified intensity level) (ATC, 2011) and risk-based (which estimates the mean annual rate of exceeding a specified structural response amplitude) assessments on the structural response of interest (which may include Peak Story Drift Ratio (*PSDR*), Peak Floor Acceleration (*PFA*), single-story engineering demand parameter (*EDP*), member forces, or any other *EDP* of interest). Target response spectra may include most commonly the Uniform Hazard Spectrum (UHS) that corresponds to spectral accelerations (S_a) with equal probabilities of exceedance at all periods, and more recently the Conditional Mean Spectrum (CMS) or the Conditional Spectrum (CS) that accounts for the

correlations between S_a values across periods. Depending on the structural analysis objective and the target response spectrum, conclusions regarding structural performance may differ, and it is important to investigate such impacts to provide ground motion selection insights for future nonlinear dynamic analysis.

The previous chapter outlines the ground motion selection procedures for risk-based assessments using the CS with a range of conditioning periods, and highlights the importance of hazard consistency in the selected ground motions. While risk-based assessments of structural response directly account for the uncertainty in ground motion hazard by considering different intensity levels and their corresponding occurrence rates, intensity-based assessments are used in practice as a simpler option to fulfill building code requirements (e.g., ICC, 2003; ASCE, 2010) which are mainly concerned with structural response at a specified intensity level, e.g., S_a associated with 2% in 50 years or 10% in 50 years probabilities of exceedance. In this chapter, we focus on the structural analysis objective of intensity-based assessments, with ground motions selected using the CS at various conditioning periods, to examine the impact of conditioning period on intensity-based assessments.

The CS was used as the target response spectrum for which ground motions were selected and scaled to match in the previous chapter. The CS accounts for both the mean and the variability of the ground motion spectra, and is proposed as an appropriate target for risk-based assessments (Baker, 2011; NIST, 2011). In practice, the UHS is more commonly used, especially through building codes (e.g., ICC, 2003; CEN, 2005; ASCE, 2010). However, shortcomings of the UHS include a lack of hazard consistency as it assumes the occurrence of high spectral values at all periods (e.g., Reiter, 1990; McGuire, 1995; Naeim and Lew, 1995; Bommer et al., 2000; Baker and Cornell, 2006a). Alternatively, the CMS is used to better capture the hazard information (e.g., Baker and Cornell, 2006a; Somerville and Hamburger, 2009; Abrahamson and Al Atik, 2010; Gulerce and Abrahamson, 2011; Somerville and Thio, 2011). However, the CMS does not account for the variability of the ground motion spectra. In this chapter, the UHS and CMS are used as target spectra to select ground motions, and their corresponding structural analysis results are compared to those using the CS, to examine the impact of target spectrum on structural response estimates.

The same 20-story reinforced concrete perimeter frame structure (ATC, 2009; Haselton and Deierlein, 2007) located in Palo Alto, California as used in the previous chapter is used for illustration. In Section 5.3, structural analyses are carried out with the objectives of intensity-based in addition to risk-based assessments on the structural response of interest (which include *PSDR* and *PFA*). Such nonlinear dynamic analyses are repeated for the CS at various conditioning periods to examine the impact of conditioning period, and additionally for the UHS and the CMS to examine the impact of target spectrum in Section 5.5. To verify the observations above more generally, one additional 4-story structure was analyzed using the same procedure with ground motions selected to match CS in Section 5.6.

5.3 Analysis objectives

Ground motions represent an important source of uncertainty in nonlinear dynamic analysis. Before analyzing structural response results or even selecting ground motions, it is important to ask the question: “What is the objective of the structural analysis?” Changing the question we ask (intensity-based or risk-based assessments) would essentially change the ground motion inputs we need and the structural response answers we get.

5.3.1 Risk-based assessments

Risk-based assessments using CS as a target spectrum with varying conditioning periods were introduced in the previous chapter. Detailed procedures and results were presented for risk-based assessments based on *PSDR* as an *EDP*, followed by brief illustrations with alternative *EDPs* that include *PFA*, single-story Story Drift Ratio, and single-story Floor Acceleration. If an exact CS (which incorporates multiple earthquake sources and multiple ground motion prediction models) is used, the choice of conditioning period does not matter for the purpose of risk-based assessments, and the same set of ground motions can be used to assess any structural response of interest. In practice, however, if we use an approximate CS we may need to adjust the target spectrum to account for spectral variability further away from the conditioning period to ensure the correct distribution for the period most important to each *EDP*. This is because an exact CS already correctly accounts for the

spectral variability at all periods of interest and thereby covers *EDPs* of interest without any further adjustments.

When the structural analysis objective is changed to an intensity-based assessment, which is only concerned with structural response at a given ground motion intensity level without consideration of ground motion occurrence rates, the choice of conditioning period in the CS may matter as we essentially change the question being asked. Here, the focus is on the intensity-based assessment and its difference from the risk-based assessment is highlighted, together with how it is impacted by the choice of conditioning period through ground motions selected and scaled using the CS at various conditioning periods.

5.3.2 Intensity-based assessments

An intensity-based assessment differs from a risk-based assessment in its analysis goal, and its procedures are in fact covered by the risk-based assessment. An intensity-based assessment is basically the first part of a risk-based assessment that looks at structural response at a given intensity level, without integration with seismic hazard curves. From structural analysis at a given intensity level, structural response parameters of interest (e.g., *PSDR* or *PFA*) are obtained, and their logarithmic mean, $\mu_{\ln EDP}$, and logarithmic standard deviation (also referred to as dispersion), $\sigma_{\ln EDP}$, are estimated, along with probability of collapse, $P(C)$. A lognormal distribution can be used to fit the structural response parameters at each intensity level (e.g., Shome and Cornell, 1999; Song and Ellingwood, 1999; Shinozuka et al., 2000; Sasani and Kiureghian, 2001; Aslani and Miranda, 2005; Stoica et al., 2007). The empirical probability of collapse at each intensity level can be computed by counting the number of collapses and dividing by the total number of analyses.

Here is another way to look at the difference based on the output. A risk-based assessment yields one number regarding the “risk” for each *EDP* level, i.e., the rate of exceedance, $\lambda(EDP > y)$ (by considering various intensity levels and *EDP* distribution at each intensity level). The results from risk-based assessments are found to be insensitive to the choice of conditioning period. Conversely, an intensity-based assessment yields information about *EDP* estimates (e.g., median and dispersion of *EDP*) at each intensity level (without considerations of multiple intensity levels and their occurrence rates). The results

from intensity-based assessments will be presented below in Section 5.4.

The target spectrum in building codes (e.g., ICC, 2003; CEN, 2005; ASCE, 2010) is often based on the UHS at one intensity level over a range of periods, e.g., $0.2 - 1.5T_1$, that covers the first-mode period of the structure as well as higher modes and lengthened periods due to nonlinear behavior. The UHS assumes equal probability of exceedance of Sa at all periods. This differs from the CS that accounts for correlations between Sa pairs at different periods, and essentially represents the distribution of Sa at all periods given Sa at one period, i.e., the conditioning period. If the CS is used instead of the UHS, it is not obvious which period to choose as the conditioning period if structural response is examined at only one intensity level. To examine the effect of conditioning period on intensity-based assessments, a range of conditioning periods are used at multiple intensity levels.

5.4 Impact of conditioning period on intensity-based assessments using the Conditional Spectrum

To illustrate, sets of forty ground motions are selected for the 20-story perimeter frame at ten intensity levels, using the CS at four conditioning periods. The conditioning periods, T^* , cover the structure's first three modal periods ($T_1 = 2.6s$, $T_2 = 0.85s$, and $T_3 = 0.45s$) and up to approximately twice the first-mode period ($2T_1 = 5s$). Each set of 40 ground motions correspond to one intensity level and one conditioning period. In the previous chapter, Figures 4.7a and 4.7b show the distribution of $PSDR$ and probability of collapse respectively at ten intensity levels for the conditioning period $T^* = 2.6s$. Based on fitting a lognormal distribution to the empirical $PSDR$ results, the logarithmic mean and standard deviation of $PSDR$ are shown as a function of $Sa(T^*)$ in Figure 4.7a. Alternatively, the logarithmic mean and standard deviation of $EDPs$ can be plotted as a function of ground motion intensity level for various conditioning periods, in order to investigate the effect of different conditioning periods on intensity-based assessments. Figure 4.7b shows the observed fractions of collapse at each $Sa(T^*)$ level, and a lognormal collapse fragility obtained based on the maximum-likelihood method (e.g., Shinozuka et al., 2000; Baker,

2005; Straub and Kiureghian, 2008). Similarly, probability of collapse can be plotted as a function of intensity level when multiple conditioning periods are considered.

Intensity-based calculations for *PSDR*, *PFA*, and probability of collapse given ten spectral amplitudes (corresponding to ten specified exceedance rates) for ground motions selected to match the CS at various conditioning periods are shown in Figure 5.1 and Table 5.1. As S_a associated with each exceedance rate vary among conditioning periods, all structural response results are plotted against return period, which is fixed for each intensity level regardless of its corresponding S_a . Figures 5.1a and 5.1b show the median *PSDR* and logarithmic standard deviation of non-collapse *PSDR* until the exceedance rate corresponding to an $S_a(T^*)$ level resulting in 50% collapse. Here, the solid line ($T^* = 2.6s$) in Figure 5.1a is equivalent to connecting the median values of *PSDR* at various intensity levels in Figure 4.7a in the previous chapter, except that the x-axis is return period in years instead of $S_a(T^*)$ in g. Also shown in Figure 5.1a are median *PSDR* results from analyses using CS with three other conditioning periods for comparison. Similarly, the solid line ($T^* = 2.6s$) in Figure 5.1b is equivalent to connecting the logarithmic standard deviation values of non-collapse *PSDR* at various intensity levels (up to 50% collapse) in Figure 4.7a in the previous chapter, superimposed with results from three other conditioning periods. At the $S_a(T^*)$ levels corresponding to greater than 50% probability of collapse, the median *PSDR* is governed by the collapse *PSDR*, and therefore is not illustrated here. Similarly, the logarithmic standard deviation of non-collapse *PSDR* is not informative at high probability of collapse, and therefore is cut off when 50% or more of the analyses cause collapse. Figures 5.1c and 5.1d show the median and logarithmic standard deviation of *PFA*. In the case of collapse (except for collapse mechanisms that cause partial collapse in the upper floors), *PFA* is substituted by the Peak Ground Acceleration (*PGA*) of individual ground motion (corresponding to the ground floor acceleration) (Aslani and Miranda, 2005). Figure 5.1e shows the probabilities of collapse obtained from these analyses.

As is evident from Figure 5.1 and Table 5.1, the structural responses at each intensity level are generally different among various conditioning periods, with differences of a factor of four or more being observed between results from varying conditioning periods. For instance, at shorter return periods (lower spectral amplitudes), the median *PSDR* does not differ much among the conditioning periods (e.g., about 50% difference between

0.008 and 0.012 for $Sa(T^*)$ associated with 10% in 50 years probability of exceedance); at longer return periods (higher spectral amplitudes), the discrepancy becomes larger, with results corresponding to $T^* = T_1$ and $2T_1$ showing higher median $PSDR$ than T_2 and T_3 (e.g., about 400% difference between 0.048 and 0.012 for $Sa(T^*)$ associated with 2% in 50 years probability of exceedance, see Figure 5.1a). At shorter return periods, the median PFA shows a slight discrepancy among all the conditioning periods; at longer return periods, the discrepancy becomes larger, with $2T_1$ and T_1 showing lower median PFA than T_2 and T_3 (e.g., 0.404 vs. 0.731 for $Sa(T^*)$ associated with 2% in 50 years probability of exceedance, see Figure 5.1c). The probability of collapse also differs more at longer return periods, with $2T_1$ and T_1 showing much higher probability of collapse than T_2 and T_3 (e.g., 0.4 vs. 0.15 for $Sa(T^*)$ associated with 2% in 50 years probability of exceedance, see Figure 5.1e). Similar collapse probability results as a function of return period are shown in Figure 5 of Bradley et al. (2010b). As illustrated in Figure 4.2a in the previous chapter, the spectral shape of the CMS becomes more peaked at higher intensity levels (longer return periods). In addition, as illustrated in Figure 4.2b in the previous chapter, the spectral shape of the CMS peaks at the respective conditioning period for a given intensity level. Since an ε value of 0 will result in the same spectral shape for the CMS at all conditioning periods but ε values increase as intensity levels increase, it is expected that the spectral shapes of the CMS for various conditioning periods differ more at higher intensity levels, driving a larger discrepancy among structural response obtained using the CS at various conditioning periods.

Over the range of return periods, T_1 gives the highest median $PSDR$ (see Figure 5.1a) and the lowest logarithmic standard deviation of $PSDR$ (see Figure 5.1b), while T_3 seems to give the highest median PFA (see Figure 5.1c) and the lowest logarithmic standard deviation of PFA (see Figure 5.1d). If we compare the $PSDR$ response (Figure 5.1a) with the target CS at the 2% in 50 years intensity level (or a return period of 2475 years) from Figure 4.2b in the previous chapter, it is apparent that the analysis using the CS with $T^* = 2.6s$ produces the largest responses, followed by those using the CS with $T^* = 5s$, $T^* = 0.85s$, and $T^* = 0.45s$, which is comparable to the order of the spectral values with the CS near 2.6s (highest spectral values for 2.6s followed by 5s, 0.85s, and 0.45s). Similarly, if we compare the PFA response with the target CS at the 2% in 50 years intensity level (Figure

4.2b in the previous chapter), the highest responses are produced by the $T^* = 0.45s$ spectrum followed by the spectra with T^* of 0.85s, 2.6s, and 5s, which is comparable to the order of the spectral values with the CS near 0.45s. The logarithmic standard deviations for *PFA* (Figure 5.1d) follow the reverse order (compared to median *PFA* responses) of 5s, 2.6s, 0.85s, and 0.45s. For this structure, $Sa(0.45s)$ seems to be most highly correlated with *PFA* responses and thus a relatively good predictor of *PFA*. Taghavi and Miranda (2003) show that *PFA* is strongly dominated by higher modes and that in many cases *PGA* was strongly correlated with *PFA*. On the contrary, *PSDR* responses seem to be most correlated with Sa at periods near 2.6s (between 2.6s and 5s). The order of structural response values with respect to various conditioning periods is reversed for *PSDR* and *PFA*, illustrating different important periods for different *EDPs*. For probability of collapse predictions (Figure 5.1e), results conditioned on $T^* = 5s$ show the lowest dispersion in the collapse fragility curve, followed by 2.6s, 0.85s, and 0.45s, demonstrating that $Sa(5s)$ is most correlated with collapse prediction. This is consistent with previous observations (e.g., Taghavi and Miranda, 2003; Haselton and Baker, 2006; Bradley et al., 2010a) that collapse is most closely related to a lengthened period for long return-period ground motions that induce nonlinear behavior in the structure, whereas *PSDR* is often correlated with first-mode response even when the response is nonlinear.

As seen from the results of the median and logarithmic standard deviation of *PSDR* and *PFA* and the probability of collapse, intensity-based assessments depend on the choice of the conditioning period for a given return period. Longer periods can be important for *PSDR* and collapse, while higher-mode periods can be important for *PFA*.

5.5 Alternative target spectra

To determine what ground motions would be appropriate for structural analysis, we first need to specify the target response spectrum in the context of this work. In this section, in addition to the previously considered CS, we consider the UHS that is defined as having Sa with an equal probability of exceedance at all periods, and the CMS. Depending on the choice of target spectrum, ground motions would be selected and scaled differently, therefore impacting conclusions regarding structural performance.

5.5.1 Uniform Hazard Spectrum and Conditional Mean Spectrum

The UHS can be obtained directly from seismic hazard curves at various periods, whereas the computation of the CMS involves computing the mean of the CS (without the variance) as presented in Equation 4.2 of the previous chapter. With the target spectrum identified and computed, ground motions can then be selected from a ground motion database and scaled to match the target spectrum. Individual ground motions are selected via Jayaram et al. (2011) such that the sum of squared errors between their response spectra and the target spectrum mean and variance (while setting the variance of the target spectrum to be zero) is minimized.

To illustrate, let us revisit the 2% in 50 year intensity level associated with $S_a(2.6s)$. Sets of forty ground motions are selected to match the UHS, the CMS and the CS in Figures 5.2a, 5.2b, and 5.2c respectively. The ground motions selected to match the UHS generally result in higher spectral values on average as the UHS is an envelope of CMS at multiple conditioning periods. The ground motions in Figures 5.2a and 5.2b show a lower standard deviation than those in Figure 5.2c where the distribution of the target spectrum (both mean and variance) is matched. The same procedure is repeated to select ground motions for other intensity levels and periods.

5.5.2 Impact of target spectra on intensity-based assessments

To evaluate the impact of target spectra on intensity-based and risk-based assessments, additional structural analyses can be performed using ground motions selected to match the UHS and CMS. Intensity-based calculations for $PSDR$, PFA , and probability of collapse performed using the CS in the previous section are now repeated here for the other two target spectra, and results are shown in Figure 5.3. Figures 5.3a and 5.3b show the median $PSDR$ and logarithmic standard deviation of non-collapse $PSDR$ for cases with less than 50% collapse respectively; Figures 5.3c and 5.3d show the median and logarithmic standard deviation of PFA respectively; Figure 5.3e shows the probability of collapse. Several observations can be made from Figure 5.3 and Table 5.2. First, as expected, the UHS-matched ground motions almost always produce larger median responses than the CS- and CMS-matched ground motions with an equivalent return period. The differences

are sometimes not large relative to the CMS ground motions at a specific conditioning period. Second, however, the CMS conditioning period associated with the largest median response is not constant over all cases considered. For the *PSDR* results in Figure 5.3a, conditioning on Sa at the first-mode period produces the largest medians at a given return period, consistent with intuition that *PSDR* would be dominated by first-mode elastic response and thus a spectrum that has the largest Sa amplitude at the first-mode period would produce the largest *PSDR*. For the *PFA* results in Figure 5.3c, the conditioning periods associated with large responses are much shorter. The third-mode elastic period produces the highest median values, with the second-mode period producing nearly as large of values and the longer periods producing much lower values; this is consistent with *PFA* being a higher-mode driven response parameter.

As seen from these results, intensity-based assessments depend on the choice of the conditioning period for the CS and the CMS. For all intensity levels at various conditioning periods, the CMS produce median *PSDR* and *PFA* that are similar to the CS while the UHS produces median *PSDR* and *PFA* that are higher than the CS; both the CMS and the UHS result in lower logarithmic standard deviation of *PSDR* and *PFA* than the CS. This is explained by the fact that the CMS and the CS share the same median (logarithmic mean) Sa , and that ground motions selected to match the CS additionally account for the spectral variability unlike those selected to match the UHS and CMS (see Figure 5.2).

5.5.3 Impact of target spectra on risk-based assessments

For comparison with the Conditional-Spectrum-based results presented in the previous chapter, the risk-based assessment procedure is repeated using additional sets of ground motions selected to match the CMS and the UHS (UHS) at each $Sa(T^*)$ level. For both of these target spectra, ground motions were selected to match the target spectra at each amplitude, nonlinear dynamic analyses were performed, and the results were used to compute $P(PSDR > y | Sa(T^*) = x)$ and repeat the risk-based calculation to obtain $\lambda(PSDR > y)$ (via Equations 4.6 and 4.5 in the previous chapter).

Risk-based assessment results from the UHS and CMS ground motions, using $T^* =$

2.6s are shown in Figure 5.4a, in comparison with the CS results from the previous chapter. In this case, the rate of exceeding large *PSDR* levels is overestimated when ground motions are selected to match UHS; this finding is consistent with previous observations (e.g., Naeim and Lew, 1995; Bommer et al., 2000) that use of the UHS as a target spectrum leads to conservative estimates of structural response. The CMS ground motions produce comparable estimates to the CS motions in this case.

Figures 5.5a and 5.5c show the distributions of response spectra from these two sets of ground motions. The CMS spectra at short periods (seen in Figure 5.5c) are deficient at high amplitudes relative to the target hazard curves, since variability in the spectra are omitted here. The UHS spectra in Figure 5.5a are relatively higher than the CMS results at all periods, and especially at 5s, which explains the high predicted rates of collapse in Figure 5.3e; they are still slightly low at short periods, because the ground motions have little spectral variability and this somewhat offsets the high mean values of the UHS at those periods.

For a second set of comparisons, Figure 5.4b shows CMS and UHS risk-based assessment results, but this time using a conditioning period of $T^* = 0.45s$. The UHS results are still high relative to CS results, and are comparable to the Figure 5.4a results, since the UHS target is not affected by conditioning period and thus the selected ground motions are similar regardless of conditioning period. The CMS results, however, are very low relative to the other results. The reason for this is apparent in Figures 5.5b and 5.5d, which show the distribution of response spectra from these two sets of ground motions. The ground motions selected based on the CMS spectra are extremely deficient in high-amplitude *S_a* at $T = 2.6s$ and $5s$, meaning that there are few ground motions in the selected set that are capable of causing collapse of this structure.

To examine the combined effects of conditioning periods and target spectra, risk-based assessments of *PSDR* for the CMS are repeated for the other two conditioning periods (in addition to the two conditioning periods demonstrated above), and are shown together with the results from the CS and the UHS in Figure 5.6a and Table 5.3. While the ground motions selected based on the CS at all four conditioning periods show similar *PSDR* hazard results (e.g., CS results in an annual rate of *PSDR* > 2% in the range of 6.46×10^{-4}

to 9.42×10^{-4}), the ground motions selected based on the CMS at the four conditioning periods show differing *PSDR* hazard results, with the results based on $T^* = 2.6s$ showing the highest values (e.g., CMS based on $T^* = 2.6s$ results in an annual rate of $PSDR > 2\% = 8.55 \times 10^{-4}$, which is within 10% of CS results based on $T^* = 2.6s$) and the results based on $T^* = 5s$ showing the second highest values but the results based on $T^* = 0.85s$ and $T^* = 0.45s$ showing values that are much lower than those from the CS (e.g., CMS based on $T^* = 0.45s$ results in an annual rate of $PSDR > 2\% = 2.35 \times 10^{-4}$, which is 301% lower than that of CS results based on $T^* = 2.6s$). This illustrates the difference between the CS results and the CMS results, and shows that the CMS results will deviate most from the CS results while using a conditioning period that is not a good predictor for the structural response of interest. The ground motions selected based on the UHS, however, results in higher *PSDR* hazard (e.g., UHS results in an annual rate of $PSDR > 2\% = 1.29 \times 10^{-3}$, which is 37% higher than that of CS results based on $T^* = 2.6s$) than those from the CS and the CMS.

Similarly, risk-based assessments of *PFA* for the CS in the previous chapter are now repeated for the CMS and the UHS, and are shown in Figure 5.6b and Table 5.3. Again, while the ground motions selected based on the CS at all four conditioning periods show similar *PFA* hazard results, the ground motions selected based on the CMS at the four conditioning periods show differing *PFA* hazard results, with the results based on $T^* = 0.45s$ showing the highest values (which are comparable to CS results) and the results based on $T^* = 0.85s$ showing the second highest values but the results based on $T^* = 2.6s$ and $T^* = 5s$ showing values that are much lower than those from the CS. The ground motions selected based on the UHS results in higher *PFA* hazard than those from the CS and the CMS.

As seen from the *PSDR* hazard and *PFA* hazard calculations, risk-based assessments are relatively insensitive to the choice of the conditioning period for the CS, but sensitive to the choice of the conditioning period for the CMS. Compared to the CS, the CMS typically underestimate structural response hazard (although the unconservatism may not be significant if Sa at the conditioning period is a good predictor of the *EDP* of interest) while the UHS overestimates structural response hazard for both *PSDR* and *PFA* hazards. The underestimation in the CMS results is a result of omission of spectral variability at periods

away from the conditioning period. The overestimation in the UHS results is due to the higher spectral values in the UHS at periods other than the conditioning period.

5.6 Additional structures

To verify the observations above more generally, eleven additional structures were analyzed using the same procedure with ground motions selected to match CS. Perimeter frame and space frame structures with heights from 1 to 20 stories, all originally designed as part of the FEMA P695 project (ATC, 2009), were considered. *PSDR* and *PFA* predictions were considered, for both risk-based and intensity-based assessments in all structures. Alternative target spectra were also considered for one of the additional structures, a 4-story perimeter frame. All structures were located at the same Palo Alto site used above, and *Sa* with the same exceedance probabilities were considered.

Conditioning periods for CS were T_1 , T_2 , T_3 and $2T_1$ (except in the case of the very short structures, where T_2 and T_3 were not considered in some cases). For each conditioning period and spectral amplitude, forty recorded ground motions were selected and scaled such that their spectra matched target CS. Additional sets of ground motions were selected in some cases to match a CS with an inflated conditional standard deviation, as was done with the $T^* = 0.45s$ (higher modes) case for *PSDR* and with the $T^* = 2.6s, 5s$ (longer periods) cases for *PFA* in the 20-story perimeter frame structure illustrated in the previous chapter.

Let us look at another example structure, a 4-story perimeter frame, denoted Building 1008 in the recent FEMA P695 project (ATC, 2009). The first three elastic modal periods are 0.91s, 0.29s and 0.17s. Results related to ground motions selected using CS are shown in Figures 5.7 and 5.8 for this structure. Conditional standard deviation inflation significantly improved the agreements for the *PSDR* hazard among all four conditioning periods (Figures 5.7b versus 5.7a). This again demonstrates the relative insensitivity of risk-based assessments to the choice of conditioning period when ground motions are carefully selected to ensure hazard consistency. However, the choice of conditioning period, again, can substantially impact structural response estimates, as illustrated in Figure 5.8. For the 4-story perimeter frame, *PFA* seems to be most dominated by the second-mode period, T_2

(compared to the third-mode period, T_3 for the 20-story perimeter frame and other 8- and 12-story frames not presented here), as indicated in Figure 5.8c and 5.8d. The first-mode period, T_1 continues to be important for *PSDR* (see Figures 5.8a and 5.8b), and the lengthened period, $2T_1$, continues to be important for collapse (see Figure 5.8e). The difference in logarithmic standard deviation of *PSDR* is now quite significant between the shorter and longer periods (see Figure 5.8b).

In all analysis cases, consistency of risk-based assessment results across conditioning periods was again observed, while intensity-based assessment results varied as the conditioning period varied, for a given structure. These results thus provide further empirical confirmation of the findings described in detail above. The large set of results supporting these statements is omitted from this chapter for brevity, but is documented in Appendix A.

5.7 Conclusions

This chapter has presented a study on the sensitivity of intensity-based assessment (which estimates structural response given ground motions whose intensity measure amplitudes have a specific exceedance probability) results to the choice of conditioning period when the CS is used as a target for ground motion selection and scaling. This chapter has also presented a study of the sensitivity of both risk-based and intensity-based assessments to the choice of target spectrum, including evaluation of the UHS and the CMS. The primary structure studied is a 20-story concrete frame structure assumed to be located in Palo Alto, California, using a structural model with strength and stiffness deterioration that is believed to reasonably capture the responses up to the point of collapse due to dynamic instability.

The study showed that the choice of conditioning period for the CS can substantially impact structural response estimates for an intensity-based assessment, but that risk-based assessments are relatively insensitive to the choice of conditioning period in the CS (given that the ground motions are carefully selected to ensure hazard consistency). For intensity-based assessments, use of the CMS, instead of the CS, does not significantly affect the median response estimates but does decrease both the dispersion of the response and the probability of collapse distribution. For risk-based assessments, use of the CMS, instead of the CS, typically results in underestimation of structural response hazard due to the

omission of spectral variability in the selected ground motions, while use of the UHS results in overestimation in the structural response hazard. These findings have potentially important implications for seismic assessments using the CS in future building code and Performance-Based Earthquake Engineering applications, as discussed in the next section.

An important issue regarding conditioning period arises when an intensity-based assessment is being used and the purpose is to compute the mean or median response associated with an $Sa(T^*)$ having a specified probability of exceedance (e.g., for a building-code-type check). In this extremely common case, the response prediction will always change depending upon the choice of conditioning period. This comes from the fact that the choice of conditioning period is an inherent part of the problem statement, and so in this case changing the conditioning period changes the question that is being asked. For example, computing the median drift response for a building subjected to a 2% in 50 year exceedance $Sa(1s)$ is not the same as computing the median drift response for a building subjected to a 2% in to 50 year exceedance $Sa(2s)$; these are two different questions. Resolution of this issue is not obvious, but likely lies in identifying a conditioning period and performance check that, when passed, confirms satisfactory reliability of the structural system.

Additional evaluations were completed for eleven other structures. While not reported in this chapter, they are available in Appendix A; these additional analyses confirm the generality of the conclusions made in this chapter, and collectively provide a more complete picture of the relationship between careful ground motion selection and robust structural response results.

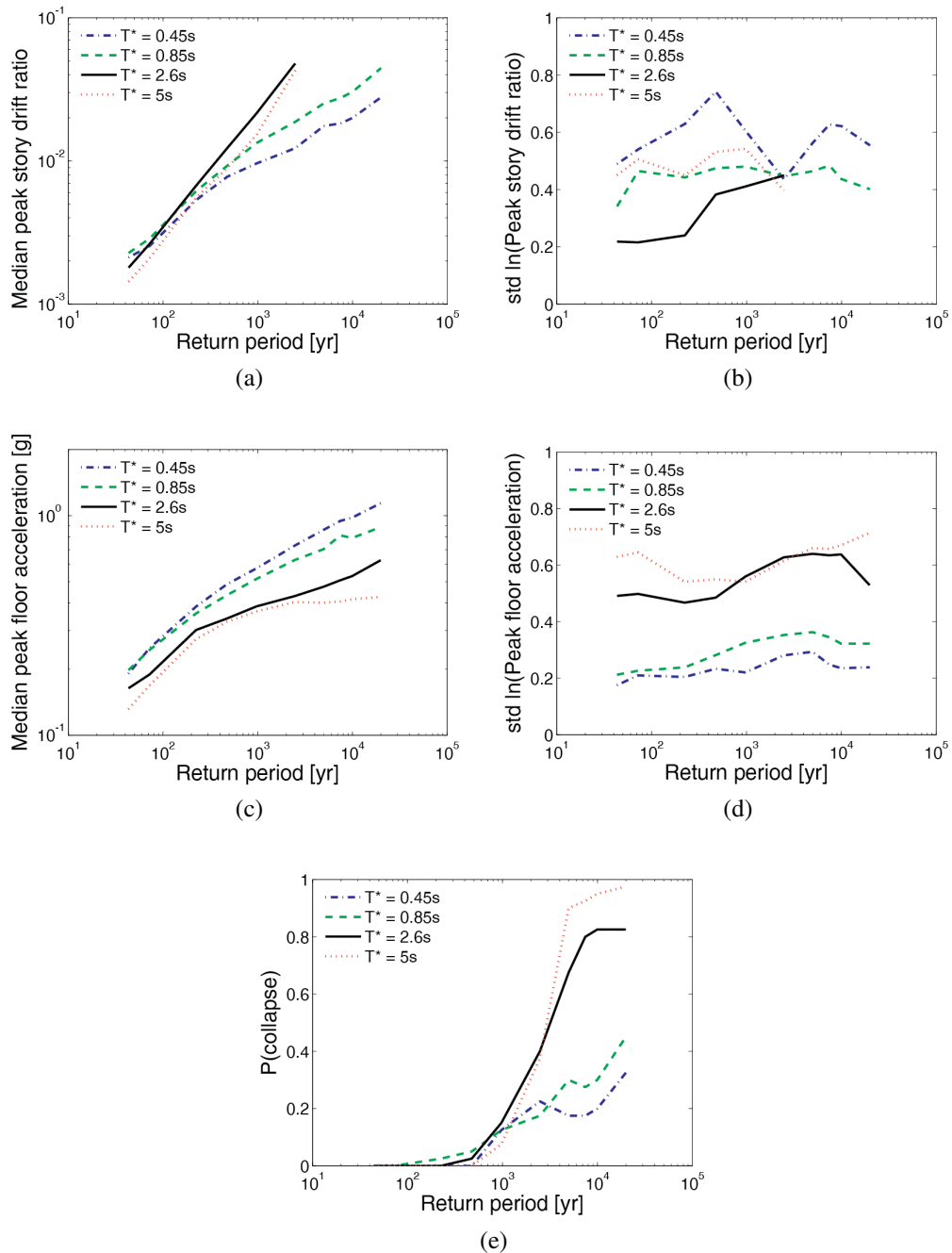


Figure 5.1: Statistics of structural responses from intensity-based assessments of the 20-story perimeter frame (Building No.1020) using the CS (a) median $PSDR$, (b) logarithmic standard deviation of $PSDR$, (c) median PFA , (d) logarithmic standard deviation of PFA , and (e) probability of collapse.

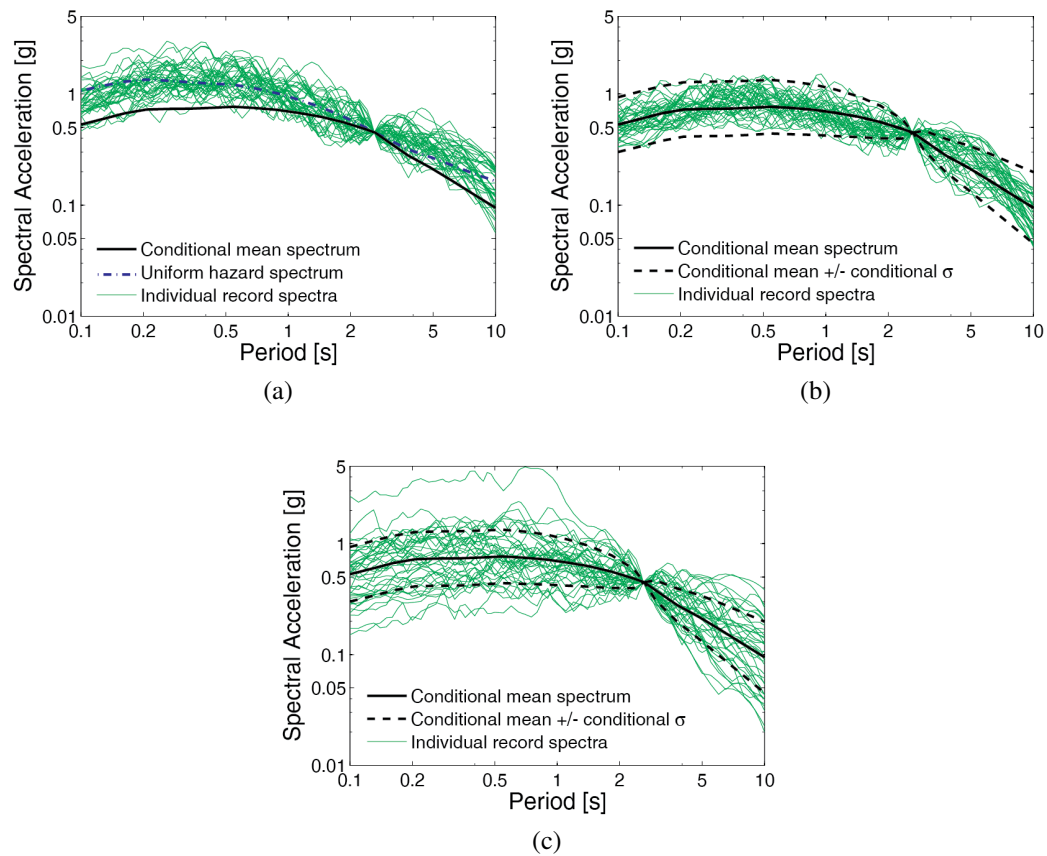


Figure 5.2: Response spectra of selected ground motions with (a) UHS, (b) CMS and (c) CS as target spectra for $Sa(2.6s)$ associated with 2% in 50 years probability of exceedance for the 20-story perimeter frame (Building No.1020).

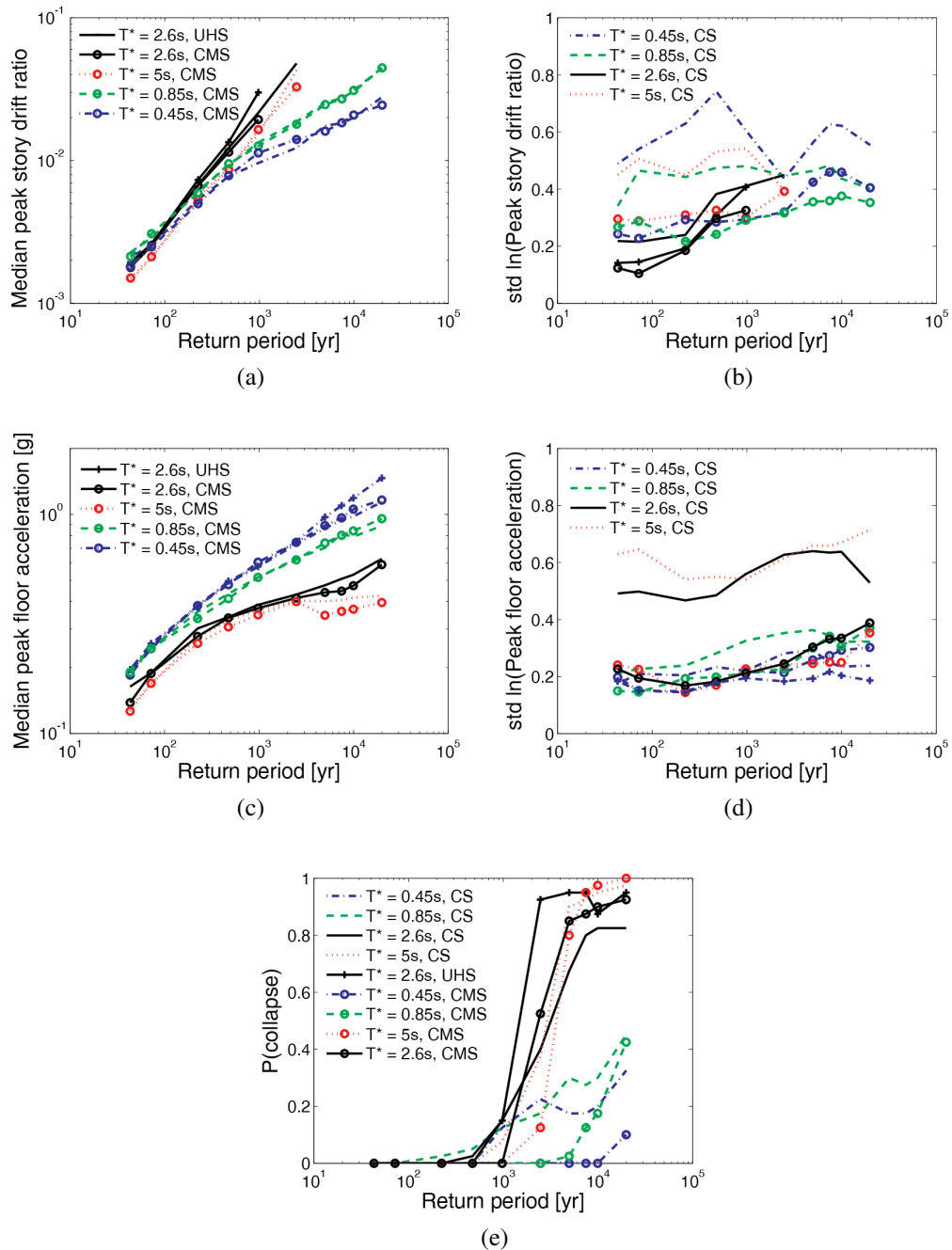


Figure 5.3: Statistics of structural responses from intensity-based assessments of the 20-story perimeter frame (Building No.1020) (a) median *PSDR*, (b) logarithmic standard deviation of *PSDR*, (c) median *PFA*, (d) logarithmic standard deviation of *PFA*, and (e) probability of collapse.

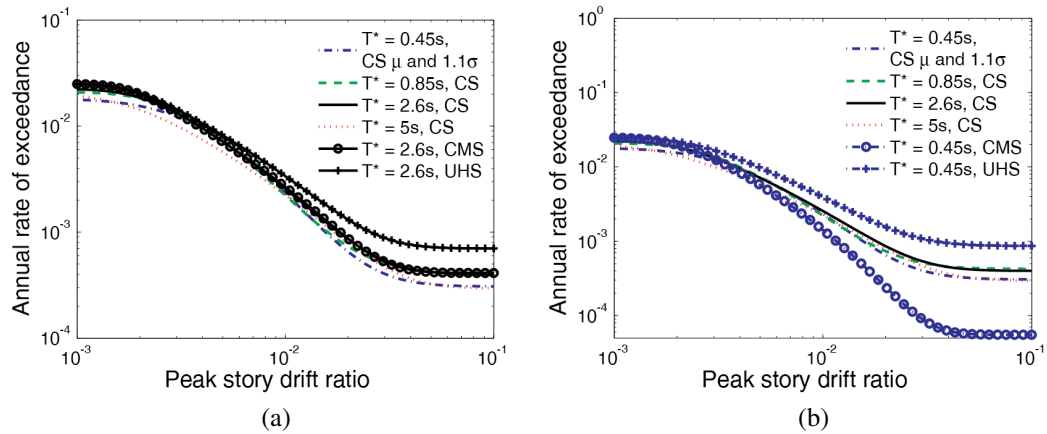


Figure 5.4: Risk-based assessments of *PSDR* of the 20-story perimeter frame (Building No.1020) obtained from ground motions selected to match the CS (all four conditioning periods) as well as the CMS and the UHS for (a) $T^* = 2.6s$ and (b) $T^* = 0.45s$.

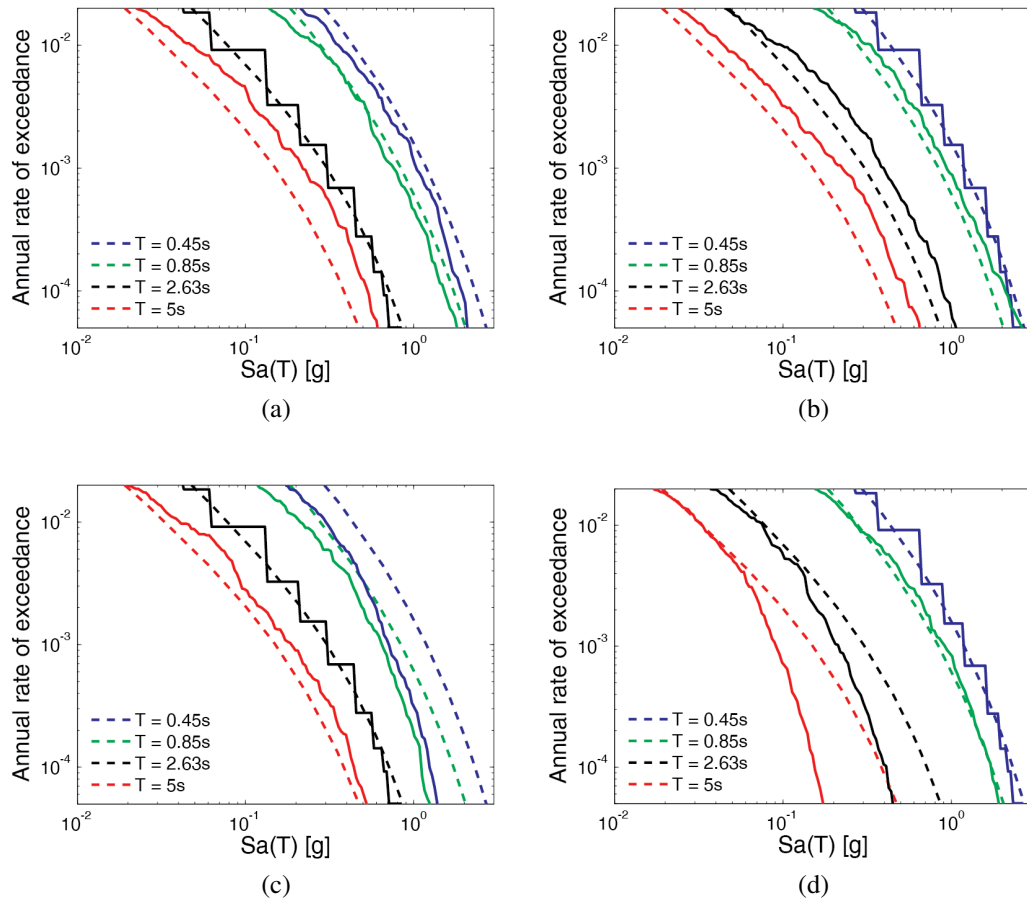


Figure 5.5: S_a distribution at four periods for ground motions selected at (a) $T^* = 2.6s$, UHS; (b) $T^* = 0.45s$, UHS; (c) $T^* = 2.6s$, CMS; and (d) $T^* = 0.45s$, CMS.

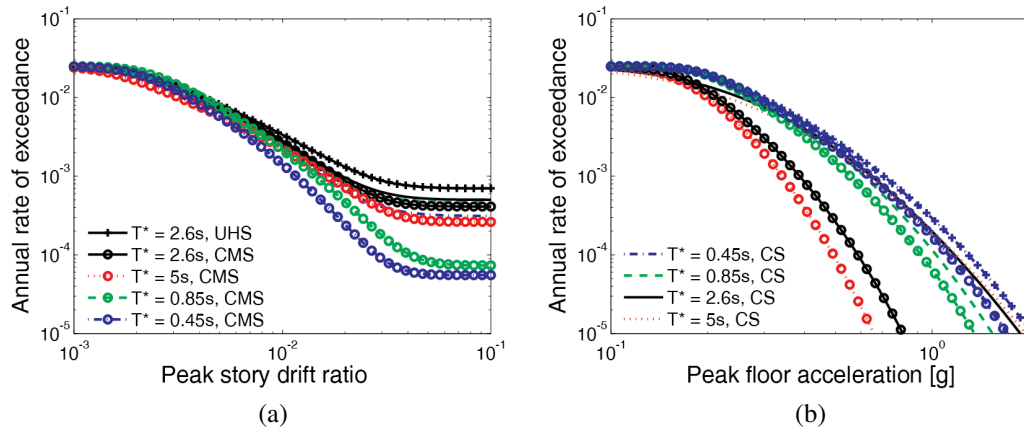


Figure 5.6: Risk-based assessments of (a) *PSDR* and (b) *PFA* of the 20-story perimeter frame (Building No.1020) obtained from ground motions selected to match the CS, the CMS, and the UHS.

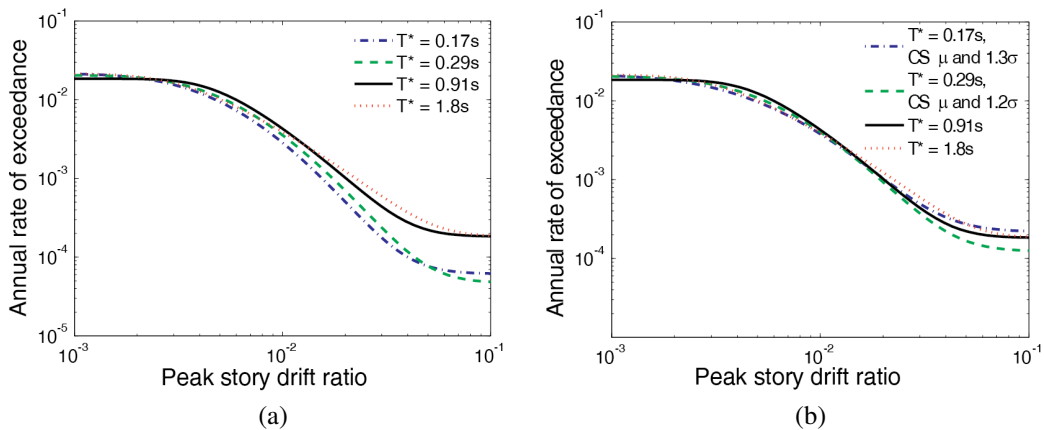


Figure 5.7: Risk-based assessments of *PSDR* of the 4-story perimeter frame (Building No.1008) obtained from ground motions with (a) approximate CS with approximate conditional standard deviations and (b) refined CS with inflated conditional standard deviations.

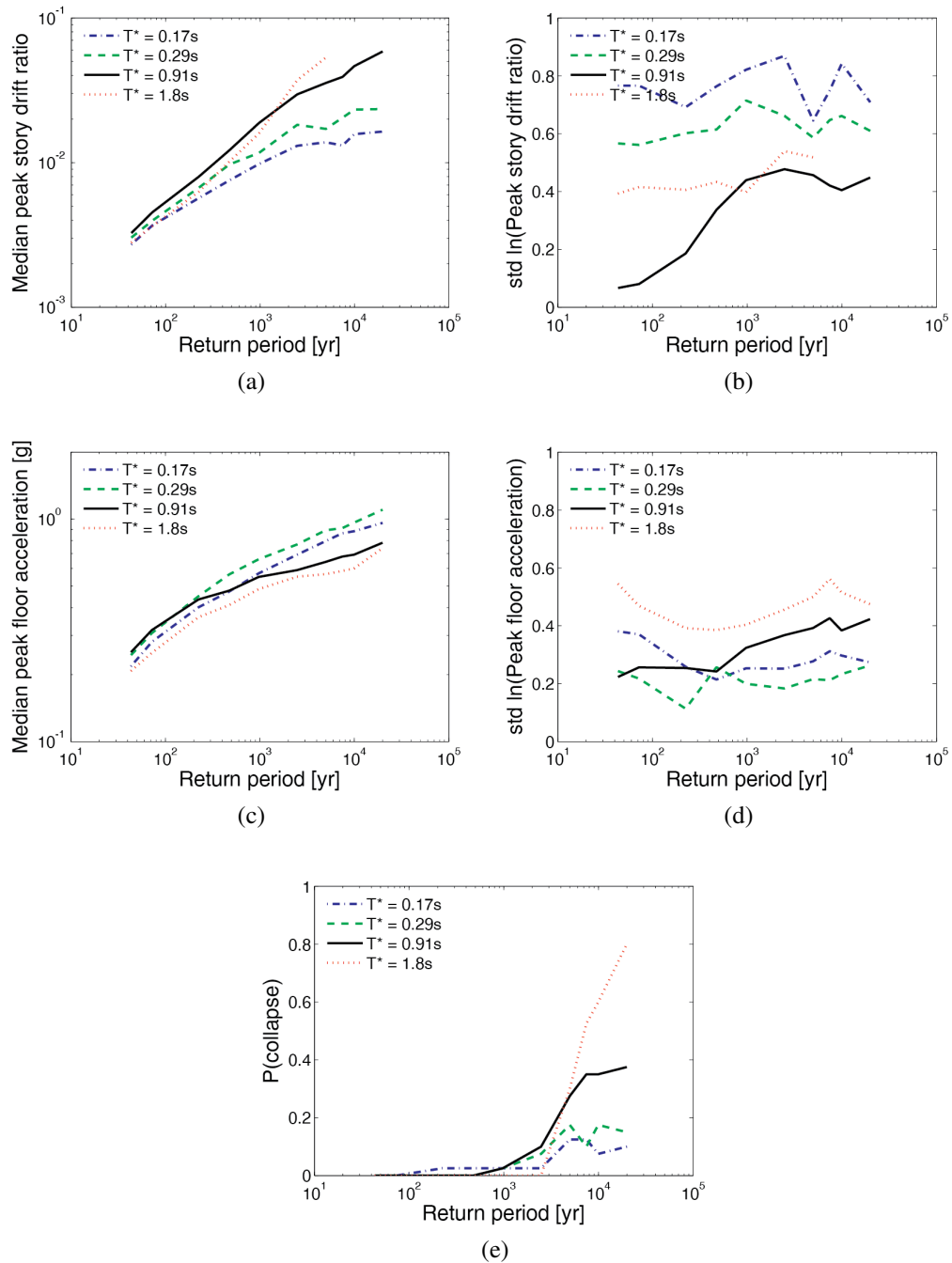


Figure 5.8: Statistics of structural responses from intensity-based assessments of the 4-story perimeter frame (Building No.1008) using the CS (a) median *PSDR*, (b) logarithmic standard deviation of *PSDR*, (c) median *PFA*, (d) logarithmic standard deviation of *PFA*, and (e) probability of collapse.

Table 5.1: Summary of selected structural response results from intensity-based assessments using ground motions selected to match the CS.

Intensity Levels	Median PSDR				Median PFA				Probability of Collapse			
	0.45s	0.85s	2.6s	5s	0.45s	0.85s	2.6s	5s	0.45s	0.85s	2.6s	5s
50% in 30 yrs	0.002	0.002	0.002	0.001	0.191	0.198	0.164	0.132	0	0	0	0
10% in 50 yrs	0.008	0.009	0.012	0.009	0.487	0.434	0.340	0.328	0	0.05	0.025	0
2% in 50 yrs	0.012	0.019	0.048	0.043	0.731	0.629	0.430	0.404	0.15	0.175	0.4	0.375

Table 5.2: Summary of selected structural response results from intensity-based assessments using ground motions selected to match the CS, the CMS, and the UHS.

Intensity level	Median PSDR					Median PFA					Probability of Collapse				
	2.6s		0.45s		UHS	2.6s		0.45s		UHS	2.6s		0.45s		UHS
	CS	CMS	CS	CMS		CS	CMS	CS	CMS		CS	CMS			
50% in 30 yrs	0.002	0.002	0.002	0.002	0.002	0.164	0.138	0.191	0.185	0.196	0	0	0	0	0
10% in 50 yrs	0.012	0.011	0.008	0.008	0.013	0.340	0.337	0.487	0.477	0.496	0.025	0	0	0	0
2% in 50 yrs	0.048	NaN	0.012	0.014	NaN	0.430	0.415	0.731	0.746	0.753	0.4	0.525	0.225	0	0.925

Table 5.3: Summary of selected structural response results from risk-based assessments using ground motions selected to match the CS, the CMS, and the UHS.

Risk-Based Performance Metrics		Conditioning Periods and Target Spectra				
		2.6s		0.45s		UHS
Type	Metric	CS	CMS	CS	CMS	
Annual Rates	PSDR > 2%	9.42E-04	8.55E-04	6.46E-04	2.35E-04	1.29E-03
	PFA > 0.5g	2.36E-03	2.94E-04	2.56E-03	2.38E-03	2.95E-03
	Collapse	5.02E-04	4.12E-04	3.12E-04	5.54E-05	8.68E-04
10% in 50 yrs EDPs	Median PSDR	0.012	0.012	0.011	0.009	0.015
	Median PFA	0.521	0.333	0.529	0.521	0.566

Chapter 6

Summary, implications, and future work

Constructed on the framework of performance-based earthquake engineering, this dissertation focuses on advancement of a hazard-consistent ground motion selection methodology that links structural response to seismic hazard. The Conditional Spectrum is proposed as an appropriate target response spectrum that is consistent with Probabilistic Seismic Hazard Analysis for ground motion selection. Contributions have been made to (1) the refined computation of the Conditional Spectrum by incorporating the aleatory uncertainties from multiple causal earthquakes and the epistemic uncertainties from ground motion prediction models, as well as (2) the use of the Conditional Spectrum in ground motion selection for various conditioning periods, spectral acceleration levels, and structural analysis objectives, with comparisons to alternative target spectra. The following sections highlight the important findings, limitations and future work related to this dissertation.

6.1 Summary and conclusions

Hazard-consistent ground motion selection requires careful consideration of aleatory and epistemic uncertainties, refined computation of an appropriate target response spectrum, and the use of this spectrum with a clear structural analysis objective. This study carefully accounts for ground motion uncertainty for structural response assessments, through the Conditional Spectrum (CS) that builds upon the Conditional Mean Spectrum (CMS) (e.g., Baker, 2011) and additionally includes variability. The CS explicitly accounts for the

changes in spectral shape with intensity levels and conditioning periods. Its refined computation captures uncertainties from ground motion prediction models (GMPMs) in addition to causal earthquakes. It is demonstrated that with such a rigorous target spectrum, the resulting selected and scaled ground motions show spectral acceleration (Sa) distributions that are consistent with the seismic hazard curves at all periods of interest, and therefore can be used to assess structural response of drift- and acceleration-sensitive components.

6.1.1 Deaggregation of ground motion prediction models

Probabilistic seismic hazard analysis (PSHA) deaggregation of GMPMs links the computation of a target spectrum to the total hazard prediction. PSHA is commonly used to compute the ground motion hazard for which structural and geotechnical systems are analyzed and designed. As a key step in defining the seismic input to nonlinear dynamic analysis, ground motion selection often involves specification of a target spectrum, e.g., the CMS or the CS. Computation of such a target spectrum requires deaggregation to identify the causal ground motion parameters, along with the predictions from multiple GMPMs. Current ground motion selection incorporates the aleatory uncertainties from earthquake scenarios without considering the epistemic uncertainties from multiple GMPMs. Here we account for both aleatory and epistemic uncertainties in ground motion selection through PSHA deaggregation of GMPMs.

This GMPM deaggregation is consistent with the probabilistic treatment of the magnitude and distance random variables in traditional PSHA. The deaggregation of GMPMs provides additional insights into which GMPM contributes most to prediction of Sa values of interest. To match the contribution of each GMPM to its associated ground motion parameters, separate deaggregation of $M/R/\epsilon$ parameters for each GMPM is also performed. These calculations are illustrated through applications on an example site. First, we estimate the hazard using PSHA that incorporates multiple GMPMs. Next, we identify the relative contributions of events and GMPMs to the hazard prediction using the refined deaggregation procedures.

The deaggregation of GMPMs is performed as an intermediate step to develop a refined mean and, more importantly, a refined standard deviation of the CS. This can also be used

to develop, in general, any new target response spectrum that is consistent with PSHA. The side product of this computation is the posterior weights of GMPMs. The proposed methodology for deaggregation of prediction models can also be immediately applicable to other procedures which require multiple prediction models in an earlier stage of total prediction and a later stage of new target computation.

6.1.2 Refined computation of Conditional Spectrum

Approximate and exact implementations of CS computations are proposed and used for example calculations in Stanford, Bissell and Seattle. Exact CS mean and standard deviation calculations can incorporate multiple GMPMs and causal earthquake M/R combinations. Varying levels of approximations are also considered, that replace multiple M/R combinations with the mean M/R from deaggregation, and either consider only a single GMPM or perform an approximate weighting of several GMPMs. These approximations are potentially appealing because of their ease of computation and because they do not require deaggregation of GMPM weights—a result that is not yet widely available in conventional PSHA software.

The approximate CS calculations appear to be more accurate for conditional mean estimation than for conditional standard deviation estimation. The exact conditional standard deviation is always higher than approximate results because of the additional contribution from the variance in mean logarithmic spectral accelerations due to variation in causal earthquakes and GMPMs.

The approximation appears to work best for sites with a single earthquake source (e.g., Stanford), followed by sites with multiple earthquake sources of the same type (e.g., Bissell) and sites with multiple differing earthquake source types (e.g., Seattle). This is because there are several contributing factors to the accuracy of the approximation: (1) the input causal earthquake parameters; (2) the GMPMs used; (3) the GMPM deaggregation weights. Hence, exact calculation methods may be needed for locations with hazard contributions from multiple earthquake sources especially with multiple source types, and/or for sites with larger variation in predictions from various GMPMs.

6.1.3 Hazard consistency in risk-based assessments

The CS can be used as the target response spectrum for ground motion selection and scaling. The sensitivity of risk-based assessment results to the choice of conditioning period is investigated. The study focuses on risk-based assessments, with a specific emphasis on the rates of exceeding various levels of Peak Story Drift Ratio (i.e., drift hazard calculations) in the structure. Some additional engineering demand parameters (*EDPs*) are also considered, such as the Peak Floor Acceleration over the full building heights, a single-story Story Drift Ratio, and a single-story Floor Acceleration. The primary structure considered is a 20-story reinforced concrete frame structure assumed to be located in Palo Alto, California, using a structural model with strength and stiffness deterioration that is believed to reasonably capture the responses up to the point of collapse due to dynamic instability.

The risk-based assessments are performed several times, using ground motions selected and scaled to match Conditional Spectra, where the conditioning period used for these calculations is varied from 0.45s to 5.0s (i.e., the building's third-mode structural period up to approximately twice the first-mode period). For each case, the risk-based assessment results are found to be similar. The similarity of the results stems from the fact that the careful record selection ensures that the distributions of response spectra at all periods are nominally comparable, so the distribution of resulting structural responses should also be comparable (to the extent that response spectra describe the relationship between the ground motions and structural responses).

From these results, it is observed that if the analysis goal is to perform a risk-based assessment obtaining the mean annual frequency of exceeding an *EDP*, then one should be able to obtain an accurate result using any conditioning period, provided that the ground motions are selected carefully to ensure proper representation of spectral values and other ground motion parameters of interest. Here "proper representation" refers to consistency with the site ground motion hazard curves at all relevant periods, and this is achieved by using the CS approach to determine target response spectra for the selected ground motions. The reproducibility of the risk-based assessment results, for varying conditioning periods, then results from the fact that the ground motion intensity measure used to link the ground motion hazard and the structural response is not an inherent physical part of the seismic

reliability problem considered; it is only a useful link to decouple the hazard and structural analysis. If this link is maintained carefully then one should obtain a consistent prediction (the correct answer) of the risk-based assessment in every case. The consistency in risk-based assessment that is demonstrated here is in contrast to some previous speculation on this topic, because this study utilizes the recently developed CS for ground motion selection, and uses the first available algorithm for selecting ground motions to match this CS target (which includes both mean and variability in the target spectra).

6.1.4 Intensity-based assessments and evaluation of alternative target spectra

This work presents a study on the sensitivity of intensity-based assessment results to the choice of conditioning period when the CS is used as a target for ground motion selection and scaling. It also presents a study of the sensitivity of both risk-based and intensity-based assessments to the choice of target spectrum, including evaluation of the Uniform Hazard Spectrum (UHS) and the Conditional Mean Spectrum (CMS).

The study shows the different effects of conditioning periods on intensity-based and risk-based assessments. In contrast to risk-based assessments, which are relatively insensitive to the choice of conditioning period in the CS, the choice of conditioning period for the CS can substantially impact structural response estimates for an intensity-based assessment. It is therefore critical to specify the structural analysis objective clearly.

The study also demonstrates the importance of target spectrum. For intensity-based assessments, use of the CMS, instead of the CS, does not significantly affect the median response estimates but does decrease both the dispersion of the response and the probability of collapse, while use of the UHS typically results in higher median response. For risk-based assessments, use of the CMS, instead of the CS, results in underestimation of structural response hazard due to the omission of spectral variability, while use of the UHS results in overestimation in the structural response hazard.

An important issue regarding conditioning period arises when an intensity-based assessment is being used and the purpose is to compute the mean or median response associated with an $Sa(T^*)$ having a specified probability of exceedance (e.g., for a building-code-type

check). In this extremely common case, the response prediction will always change depending upon the choice of conditioning period. This comes from the fact that the choice of conditioning period is an inherent part of the problem statement, and so in this case changing the conditioning period changes the question that is being asked. For example, computing the median drift response for a building subjected to a 2% in 50 year exceedance $Sa(1s)$ is not the same as computing the median drift response for a building subjected to a 2% in to 50 year exceedance $Sa(2s)$; these are two different questions. Resolution of this issue is not obvious, but likely lies in identifying a conditioning period and performance check that, when passed, confirms satisfactory reliability of the structural system.

6.2 Implications for buildings codes and performance-based earthquake engineering

The proposed GMPM deaggregation and exact CMS computation are now available as optional outputs in the U.S. Geological Survey hazard mapping tools, and could also be incorporated into other PSHA software. These additional features provide insights regarding individual GMPM contribution to the overall hazard in real sites, and generate automated output of a site-specific hazard-consistent target response spectrum, the CMS (or the CS that additionally includes variability). Such implementations, coupled with the availability of a computationally efficient algorithm to match the target spectrum mean and variability, facilitate the practical use of the CS as a potential target spectrum for ground motion selection. Implications of the choice of conditioning period and target spectrum for building-code-type check and performance-based earthquake engineering are discussed below.

6.2.1 Risk-based assessments

For risk-based assessments (typically used in performance-based earthquake engineering), the CS (including variability) is a recommended target spectrum. Results are relatively insensitive to the choice of conditioning period, T^* , but the choice of an efficient T^* (closely related to the structural response of interest) may reduce the number of required structural analyses. If the CMS is used, the structural response hazard is typically underestimated,

especially for conditioning periods that are further away from the period closely related to the structural response of interest. In contrast, if the UHS is used, the structural response hazard estimate is usually conservative.

6.2.2 Intensity-based assessments

For intensity-based building-code-type checks, the CMS and the CS are both defensible target spectra. The choice of CS or CMS depends on the goal of the analyses. If the median structural response is of interest, either spectrum can be used – the CMS can be an efficient choice for this purpose. If the full distribution of structural response is of interest, the CS should be used to capture the variability in structural response. Results will fully depend on the conditioning period, T^* , because different T^* implies a different question being asked. If the conditioning period, T^* , most closely relates to the structural response parameter of interest is known, that T^* alone may be sufficient to evaluate the specified structural response. Such conditioning period is often associated with the lowest dispersion estimate and the highest median estimate of structural response.

6.2.3 Selection of target spectrum

In the absence of more complete guidance on “what the right question is”, a tentative recommendation for building-code-type checks is to use a conditioning period, T^* , that results in the highest response. Multiple T^* and Conditional Spectra or Conditional Mean spectra may be needed if multiple responses are of interest. For instance, if the objective is to limit first-mode sensitive response parameters (e.g., Peak Story Drift Ratio), a single spectrum conditioned at T_1 may be sufficient; if the goal is to additionally ensure that higher-mode-sensitive response parameters (e.g., Peak Floor Acceleration or member forces) are limited, a second higher-mode spectrum may be needed.

Unless conservatism is intentional, use of the UHS is not recommended, because ground motions associated with a UHS are typically not consistent with the ground motion hazard for which they are selected. If future building codes allow use of Conditional Spectra or Conditional Mean Spectra in place of a UHS, the average values of responses computed in those checks may be reduced even if the target return period of the ground motion

is unchanged due to the eliminated conservatism of the UHS target. The level of reduction depends upon the extent to which the response parameter of interest is associated with spectral values at multiple periods; structures that behave like elastic single-degree-of-freedom oscillators are sensitive only to S_a at a single period and thus the responses from CS-matched or UHS-matched motions conditioned on that period will be identical. Conversely, structural response parameters sensitive to multiple modes of excitation or to significant nonlinearity (such as collapse, where the structure's effective period lengthens) may experience reduced responses from CS-matched motions relative to UHS-matched motions with the same intensity at the conditioning period.

6.3 Limitations and future work

This work has investigated the computation and use of the CS as the target response spectrum for ground motion selection and scaling. Several limitations and future work are presented below.

6.3.1 Automation of exact Conditional Spectrum computation

The exact computation of the Conditional Spectrum is presented with mathematical formulations, and illustrated through three examples sites. This exact computation allows the consideration of uncertainties from multiple causal earthquakes and GMPMs in both mean and standard deviation estimations. It is demonstrated, both theoretically and empirically, that the incorporation of these uncertainties is particularly important for the conditional standard deviation estimation.

Progress has been made to implement the exact calculation of the CMS (i.e., the mean of the CS) in the U.S. Geological Survey hazard mapping tools. This new feature automates the complex computation of the exact CMS for any site in the continental U.S., and allows practitioners to download the site-specific response spectrum directly. Current implementation, however, is limited to the exact CMS (rather than the CS). Future efforts can be directed towards the automated computation of the exact CS, with the conditional standard deviation implementation in addition to the recent conditional mean implementation. With

this automation of exact CS computation, adjustments of CS computation, such as those presented in Chapter 4, are no longer needed. This will facilitate use of the exact CS for practical applications, without additional computational efforts from the user.

In addition, the refined CS computation in this study is based on the currently available GMPMs and the Baker and Jayaram (2008) correlation model. As more GMPMs and correlation models are developed and integrated, this computation can be updated with different inputs using the same mathematical formulations. The CS computation remains consistent with the PSHA upon which it is based.

6.3.2 Linking performance goals and design checks

Both risk-based and intensity-based assessments are investigated in this work. Risk-based assessments are often used in performance-based earthquake engineering, while intensity-based assessments often resemble those from the building-code type design checks. There is a recent shift in building codes towards risk-based assessments (e.g., the collapse risk performance goal in ASCE/SEI 7-10 (ASCE, 2010)) but the design checks are still intensity-based (i.e., assessing structural response at a single intensity level). In the case of ASCE/SEI 7-10, the stated objective of the design requirements is to achieve building designs that have less than a 1% probability of collapse in 50 years, and the intensity-based assessment (and corresponding acceptance criteria) is implicitly intended to measure whether this objective is being achieved.

The findings from this study imply a missing link between the implicit performance goals and the explicit design checks that needs to be reconciled. A detailed study to determine whether the current intensity-based design checks are optimal for and consistent with the risk-based performance goals would be valuable. The implied intensity for design checks from the risk-based performance goal can be obtained through inverse FORM that calculates environmental contours (e.g., Winterstein et al., 1993), and more recently through ongoing research by Loth and Baker. Such a study is needed in order to better determine the appropriate intensity-based question that ASCE 7 should be asking (to be consistent with its fundamental goal of acceptable collapse risk).

6.3.3 Refinements for bidirectional ground motion inputs

Only 2D structural models are used in this study, with a single ground motion component as seismic inputs. In the future, 3D structural models with multiple ground motion components can be investigated, to achieve a more realistic representation. An arbitrary component is used as ground motion input in this study; future work may consider using other definitions of ground motion components, e.g., geometric mean and maximum component. Only horizontal components are used in this study; future work may consider vertical components and potentially use the CS with vertical components. In general, the CS can be developed for all definitions of ground motion components as long as consistency is carefully maintained with PSHA.

The findings in this study provide some reassurance that risk-based assessments can be robustly performed for 3D structural models as long as hazard-consistent ground motions are used for the analysis. For the 3D case, hazard consistency requires that ground motions have S_a distributions consistent with hazard curves at all periods and orientations of interest. This should be the case regardless of the choice of response spectra definition (i.e., arbitrary component, geometric mean or maximum component). This hypothesis follows from the results in this study showing consistent risk-based results if ground motions have hazard consistent spectra at multiple periods, and extending it to spectra at multiple orientations. This thinking is also consistent with earlier research on this topic (Baker and Cornell, 2006b). Further work to empirically verify this hypothesis, and to develop appropriate intensity-based assessment rules, would be valuable.

6.3.4 Engineering demand parameters, structures, and systems

This study examines several Engineering Demand Parameters, including Peak Story Drift Ratio, Peak Floor Acceleration, single-story Story Drift Ratio, and single-story Floor Acceleration. This is an expansion beyond previous related studies which typically have examined Peak Story Drift Ratio (e.g., Baker, 2005; Haselton et al., 2009; Jayaram et al., 2011). However, more *EDPs* can be studied in the future. Of specific interest would be the member forces that are often used in design, such as shear force demands in shear walls. Another example *EDP* would be residual drift, which in excess, can cause structures

beyond repair and lead to losses due to demolition.

The structural models used here are considered to be representative of actual designed buildings in practice. They vary in heights (from one to twenty stories, with fundamental period of vibration ranging from 0.42s to 2.6s) and configurations, and include both perimeter and space frames. The strength and stiffness deterioration in these structural models is believed to reasonably capture the responses up to the point of collapse due to dynamic instability. However, all structural models are reinforced concrete frames. In the future, other structural materials and systems should be considered, e.g., steel frames and concrete walls. Further study of reinforced concrete walls is of particular interest due to the need for assessing shear force demands for design. The structures considered can also have irregularities and incorporate more complex features that are representative of the range of existing or new buildings. Structures that have fundamental periods of vibration outside the current range of study (e.g., super-tall buildings with an extremely long period) can be examined as well to further investigate the generality of the methodology presented in this study.

Although the focus of this study is on the structural response of buildings to earthquake ground motions, ground motion selection is not limited to buildings. Such study can be extended to nonlinear dynamic analyses of other structural systems (e.g., bridges). Also of interest may be facilities (e.g., nuclear power plants) where extremely rare ground motions are of concern. The structural counterpart, geotechnical systems (e.g., dams), can also be investigated using similar methods; these systems may be sensitive to ground motion properties other than elastic spectra, so care is needed to match conditional distributions of other properties (Bradley, 2010a, 2012a,b). More complex models can incorporate soil-structure interactions. It would be valuable to test the robustness of the CS as a potential candidate target spectrum for nonlinear dynamic analyses of other systems.

6.3.5 Sources of ground motion inputs

The ground motion inputs considered are from recorded ground motions, in particular, the NGA database (Chiou et al., 2008). The candidate ground motions used in this study are

limited to the availability of records in the particular ground motion database. To supplement this database, other ground motion databases (e.g., Aoi et al., 2011) can also be used with updated recordings from recent events. Other sources of seismic inputs that are not presented here may include ground motions through simulations (either physics-based, stochastic, or hybrid) and spectral matching. In the future, these alternative ground motion inputs can be considered while using the CS as the target response spectrum.

Great potential exists in the collaborative research between earth science and engineering. One such recent effort is the coordination between the Ground Motion Selection and Modification (GMSM) group from the Pacific Earthquake Engineering Research (PEER) Center and the Ground Motion Simulation and Validation (GMSV) group from the Southern California Earthquake Center (SCEC). While earthquake engineers are investigating structural response to seismic input from a stochastic perspective, earthquake scientists are modeling earthquake phenomenon based on physical principles. The future of ground motion study may lie in the interface between the two, as physics-based PSHA (Graves et al., 2011) advances.

6.3.6 Integration of ground motion hazard and structural modeling uncertainties

Extensive efforts of this study are devoted towards characterization of ground motion uncertainty through refined computation of the CS and explicit consideration of spectral shape variations with intensity levels and conditioning periods in ground motion selection. However, the issue of structural modeling uncertainty is not included in this study, but is examined elsewhere (e.g., Esteva and Ruiz, 1989; Porter et al., 2002; Ibarra and Krawinkler, 2005; Aslani and Miranda, 2005; Krawinkler, 2005; Baker and Cornell, 2008; Dolsek, 2009; Liel et al., 2009). A more complete study would integrate structural modeling uncertainty with the ground motion uncertainty presented here. This can be performed using a single structural model with multiple ground motions, multiple structural models with a single ground motion, and eventually multiple structural models with multiple ground

motions, in a matrix-like fashion to cover the entire space of interest using sampling techniques. With the additional consideration of structural modeling uncertainty, the total uncertainty is directly accounted for and is expected to increase. The combined effect of modeling uncertainty and ground motion uncertainty can be examined for different conditioning periods, intensity levels, and structural analysis objectives.

6.3.7 Sites

The hypothetical site considered in the GMPM deaggregation computation is highly simplified to illustrate the underlying mathematics. The three real sites considered in the refined CS computation include Stanford from Northern California, Bissell from Southern California, and Seattle from Pacific Northwest. These sites are representative of active seismic regions in the Western U.S. (WUS) with various contributing seismic sources. However, only one site, Palo Alto, California, is considered in the study of the Conditional-Spectrum-based ground motion selection. To extend investigations similar to those in this dissertation, more sites can be explored. For instance, a more complex site such as Seattle can be used in the study of the Conditional-Spectrum-based ground motion selection. Moreover, other regions with low- to mid-seismicity can be studied, for both the computation and the use of the CS—representative regions in the U.S. can be Central and Eastern U.S. (CEUS). This study can also be conducted in other regions outside the U.S. (e.g., Japan, Chile, New Zealand, Italy, Turkey, Iran, China, Mexico, and Haiti), and updated with field observations and laboratory testing that complement computer simulations. Extension of this study to international regions is potentially valuable for the development of the Global Earthquake Model (GEM, 2012).

6.3.8 Other effects not captured in elastic response spectra

This study is based on elastic response spectra and ordinary ground motions. The underlying assumption of the use of elastic response spectra is that it sufficiently describes the structural behavior of interest. This implies that the limitations of this study include effects not captured in elastic response spectra that may be important for structural response predictions. In particular, this study does not cover near-fault rupture directivity, velocity

pulses, and fling step that are of specific interest to near-fault sites. Nor does it consider the effect of duration which is critical to structures with components that degrade under cyclic loading. These considerations of near-fault effects and duration are active areas of research by other researchers and would be important for assessments of *EDPs* such as residual drift. Other effects that are not considered here include basin effects and basin-edge effects that have limited recordings and are very site dependent. The considerations of the effects omitted in this study can be potentially integrated back in future studies to complement and supplement this dissertation. An example application of practical interest would be to implement the probabilistic near-fault directivity hazard computation from Shahi and Baker (2011) in ground motion selection, and to investigate its additional effect on structural response assessments for near-fault sites.

6.4 Concluding remarks

This work contributes to the advancement of hazard-consistent ground motion selection methodology through the refined computation and practical use of the Conditional Spectrum. The findings and conclusions drawn from this work should, however, be carefully evaluated with considerations of the limitations of the study. The promising results presented here demonstrate the feasibility of the Conditional Spectrum as a target response spectrum for ground motion selection, and warrant opportunities for future work to extend this study to more complex structures and sites with a wider range of ground motion inputs and considerations of modeling uncertainty and other effects that are important in practical implementations.

Appendix A

Conditional-Spectrum-based ground motion selection: Additional structures

To support the conclusions of Chapters 4 and 5, twelve structures (including the one in the demonstration analysis) were analyzed using the same procedure with ground motions selected to match Conditional Spectra conditioned on various periods of interest. These conditioning periods including the first-mode period, T_1 , the higher-mode periods, T_2 and T_3 , and the lengthened period due to nonlinearity, $2T_1$. The structures considered here include both perimeter frames and space frames, and have heights ranging from 1- to 20-story. Two to four conditioning periods were used for each structure based on structural heights, e.g., T_1 and $2 T_1$ for 1-story frames, T_2 , T_1 , and $2 T_1$ for 2-story frames, T_3 , T_2 , T_1 , and $2 T_1$ for 4-, 8-, 12-, and 20-story frames.

All structures being studied are assumed to be located at the same Palo Alto, California site used in Chapters 4 and 5. For spectral accelerations at various conditioning periods of interest, seismic hazard analysis was performed to obtain ground motion hazard curves and deaggregation information associated with a given amplitude exceedance rate. Ten rates of spectral amplitude exceedance were considered for each conditioning period, ranging from 0.023 to 0.00005 per year (i.e., 50% in 30 years to 1% in 200 years probability of exceedance).

For each conditioning period and spectral amplitude, forty recorded ground motions

were selected and scaled such that their spectra matched the target mean and standard deviations computed using Equations 4.2 and 4.3. Note that the target Conditional Spectrum (CS) here is an approximation using a single magnitude and distance with a single ground motion prediction model. To account for the underestimation of the conditional standard deviation using the approximate CS, sets of recorded ground motions were reselected such that their spectra matched the approximate CS mean and an inflated standard deviation. The amount of conditional standard deviation inflation to achieve hazard consistency is indicated where appropriate.

Nonlinear dynamic analyses of the twelve structures were performed. The Engineering Demand Parameters (*EDPs*) considered here include Peak Story Drift Ratio (*PSDR*) and Peak Floor Acceleration (*PFA*). Collapse fragility functions were developed. Both Performance-Based Earthquake Engineering (PBEE) and building-code-based approaches were evaluated.

Summary figures are shown in this appendix. The figures related to ground motions selected using Conditional Spectra are organized by structure. The structures are presented in two groups, A.1. Perimeter Frames and A.2. Space Frames, with structural heights descending from 20- to 1-story. Figures are also presented for additional spectral amplitudes to investigate their effect on collapse fragility in A.3. Ground motions selected using other target spectra (e.g., Conditional Mean Spectra and Uniform Hazard Spectra) are also illustrated in A.4.

A.1 Conditional Spectra for perimeter frames

Six perimeter frames with heights of 20-, 12-, 8-, 4-, 2-, and 1-story were analyzed. The corresponding figures are shown in Figures A.1 to A.30.

A.1.1 20-story perimeter frame

The first structure considered is also the structure chosen for the demonstration analysis in Chapters 4 and 5. It is a 20-story reinforced concrete special moment frame with the perimeter frame designed to resist lateral forces, in short, a 20-story perimeter frame. This

building was designed for the recent FEMA P695 project (ATC, 2009; Haselton and Deierlein, 2007), and is denoted Building 1020 in that study. It is modeled in OpenSEES (2011), with strength deterioration (both cyclic and in-cycle) and stiffness deterioration. The first three elastic modal periods are 2.6s, 0.85s and 0.45s. The building was designed per the ICC (2003), for a site with a slightly lower design ground motion level than the site being utilized in this study. Results related to ground motions selected using Conditional Spectra are shown in Figures A.1 to A.5 for this structure.

The Spectral acceleration (Sa) distributions at four periods for “basic” ground motions selected to match the approximate CS mean and standard deviation at $T^* = 0.45s, 0.85s, 2.6s,$ and $5s$ are shown in Figures A.1a, A.1c, A.1d, A.1e respectively. The spectra of the selected ground motions with each T^* (solid lines) are plotted at four periods versus the corresponding ground motion hazard curves (dotted lines). The ground motions selected using $T^* = 0.85s, 2.6s,$ and $5s$ already showed good agreement with corresponding ground motion hazard curves especially at longer period, so no adjustments were made in those cases. For the case of $T^* = 0.45s$, to improve hazard consistency, the conditional standard deviations were inflated by 10% and ground motions were re-selected to match this new target. The reselected ground motions that match the approximate CS mean and inflated standard deviation are denoted “improved” ground motions. The spectra from the “basic” ground motions are shown in Figure A.1a, and the “improved” motions with a 10% larger standard deviation are shown in Figure A.1b. The corresponding probability of collapse, Peak Story Drift Ratio ($PSDR$) hazard, Peak Floor Acceleration (PFA) hazard for these “basic” and “improved” ground motions are shown in Figure A.2.

The “improved” ground motions with an inflated conditional standard deviation at $T^* = 0.45s$ resulted in a better match at $Sa(5s)$ between the spectra of the selected ground motions and the true hazard compared to the “basic” ground motions, especially at high spectral amplitudes (Figure A.1a and b). The inflated conditional standard deviation resolved the deficiency in high-amplitude Sa values, and therefore resulted in a higher probability of collapse for a given $Sa(0.45s)$ amplitude (see Figure A.2b versus Figure A.2a). Compared to the “basic” ground motions, the “improved” ground motions showed a better agreement among various conditioning periods in $PSDR$ drift hazard (see Figure A.2d versus Figure

A.2c). This suggests that if we carefully select ground motions with appropriate conditional standard deviations to match the true hazard curves, the *PSDR* drift hazard would be in good agreements regardless of the choice of conditioning periods.

The structural dynamic analysis results for *PSDR* related to the Performance-Based Earthquake Engineering (PBEE) approach at various conditioning periods for the “improved” ground motions are shown in Figure A.3. Individual results of *PSDR* (along with the median and logarithmic standard deviation of *PSDR*) at $T^* = 0.45\text{s}$, 0.85s , 2.6s , and 5s for the non-collapse cases can be obtained from Figures A.3a, A.3b, A.3c, and A.3d respectively. The probability of collapse is shown in Figure A.2b. Combining the ground motion hazard curves (Figure A.1) with the median and logarithmic standard deviation of *PSDR* for the non-collapse cases (Figure A.3) and the probability of collapse (Figure A.2b), the *PSDR* hazard can be obtained using Equation 4.5 (through Equation 4.6), and is shown in Figure A.2d. We demonstrate that the *PSDR* hazard is relatively insensitive to the choice of the conditioning period (see Figure A.2d) given careful selection of hazard-consistent ground motions (see Figure A.1b).

Similarly, the structural dynamic analysis results for *PFA* at various conditioning periods for the “improved” ground motions are shown in Figure A.4. These can be used for computations of the type performed in Chapters 4 and 5.

Intensity-based calculations for *PSDR*, *PFA*, and probability of collapse given ten return periods (corresponding to ten spectral amplitude exceedance rates) at various conditioning periods for the “improved” ground motions are shown in Figure A.5. The median and logarithmic standard deviation of *PSDR* for the non-collapse cases are plotted versus return periods in Figures A.5a and A.5b. The median and logarithmic standard deviation of *PFA* for the non-collapse cases are plotted versus return periods in Figures A.5c and A.5d. The probability of collapse is plotted versus return periods in Figure A.5e. At shorter return periods, the median *PSDR* does not differ much among all the conditioning periods; at longer return periods, the discrepancy becomes larger, with $2T_1$ and T_1 showing higher median *PSDR* than T_2 and T_3 (see Figure A.5a). At shorter return periods, the median *PFA* does not differ much among all the conditioning periods, but differs more than that for the median *PSDR*; at longer return periods, the discrepancy becomes larger, with $2T_1$ and T_1 showing lower median *PFA* than T_2 and T_3 (see Figure A.5c). The probability of collapse

also differs more at longer return periods, with $2T_1$ and T_1 showing much higher probability of collapse than T_2 and T_3 (see Figure A.5e). Over the range of return periods, T_1 seems to give the highest median *PSDR* (see Figure A.5a) and the lowest logarithmic standard deviation of *PSDR* (see Figure A.5b), while T_3 seems to give the highest median *PFA* (see Figure A.5c) and the lowest logarithmic standard deviation of *PFA* (see Figure A.5d) for this structure. *Sa*(2.6s) appears to be a more efficient predictor of *PSDR* than *Sa*(0.45s), but *Sa*(0.45s) appears to be a more efficient predictor of *PFA* than *Sa*(2.6s). The order of structural response values with respect to various conditioning periods is reversed for *PSDR* and *PFA*, illustrating different important periods for different *EDPs*. We demonstrate that the median and logarithmic standard deviation of *PSDR* and *PFA* for the non-collapse cases and the probability of collapse depend on the choice of the conditioning period for a given return period.

The same figure formats for the 20-story perimeter frame are used for the rest of the structures.

A.1.2 12-story perimeter frame

The second structure considered is a 12-story perimeter frame, denoted Building 1013 in the recent FEMA P695 project (ATC, 2009; Haselton and Deierlein, 2007). The first three elastic modal periods are 2.0s, 0.68s and 0.39s. Results related to ground motions selected using Conditional Spectra are shown in Figures A.6 to A.10 for this structure.

The spectra of the “basic” selected ground motions compared well with the true hazard curves at $T^* = 0.68\text{s}$, 2s , and 3.9s (see Figures A.6c, A.6d, A.6e). With an “improved” conditional standard deviation inflation of 20% at $T^* = 0.39\text{s}$, the match to the true hazard curve was better (see Figure A.6b versus Figure A.6a), resulting in a higher probability of collapse at $T^* = 0.39\text{s}$ (see Figure A.7b versus Figure A.7a) and bringing the *PSDR* hazard curve at $T^* = 0.39\text{s}$ closer to those at the other conditioning periods (see Figure A.7d versus Figure A.7c). The improvement from the “basic” to “improved” ground motions in this structure is consistent with observations from the 20-story perimeter frame.

For almost any given return period, median *PSDR* values decrease from $T^* = 2T_1$, T_1 , T_2 , to T_3 ; logarithmic standard deviations of *PSDR* increase from $T^* = 2T_1$, T_1 , T_2 , to T_3 ;

median *PFA* values increase from $T^* = 2T_1, T_1, T_2$, to T_3 ; logarithmic standard deviations of *PSDR* decrease from $T^* = 2T_1, T_1, T_2$, to T_3 ; probabilities of collapse decrease from $T^* = 2T_1, T_1, T_2$, to T_3 . This again suggests that longer periods can be better predictors of *PSDR* and collapse, while higher-mode periods can be better predictors of *PFA*.

Again, the *PSDR* hazard is relatively insensitive to the choice of the conditioning period (see Figure A.7d) given careful selection of hazard-consistent ground motions (see Figure A.6b). On the other hand, the median and logarithmic standard deviation of *PSDR* and *PFA* for the non-collapse cases and the probability of collapse depend on the choice of the conditioning period for a given return period (Figure A.10).

The findings seem to be fairly consistent between the 12- and 20-story perimeter frames. For the following structures, only brief observations will be noted.

A.1.3 8-story perimeter frame

The third structure considered is a 8-story perimeter frame, denoted Building 1011 in the recent FEMA P695 project (ATC, 2009; Haselton and Deierlein, 2007). The first three elastic modal periods are 1.7s, 0.58s and 0.33s. Results related to ground motions selected using Conditional Spectra are shown in Figures A.11 to A.15 for this structure.

Conditional standard deviations were adjusted for both $T^* = 0.58\text{s}$ and 0.33s (see Figures A.11b and A.11d), resulting in very good agreements for the *PSDR* hazard among all four conditioning periods (see Figure A.12d). Again, T_1 seems to be important for *PSDR*, T_3 seems to be important for *PFA*, and $2T_1$ seems to be important for collapse.

A.1.4 4-story perimeter frame

The fourth structure considered is a 4-story perimeter frame, denoted Building 1008 in the recent FEMA P695 project (ATC, 2009; Haselton and Deierlein, 2007). The first three elastic modal periods are 0.91s, 0.29s and 0.17s. Results related to ground motions selected using Conditional Spectra are shown in Figures A.16 to A.20 for this structure.

Conditional standard deviation inflation again significantly improved the agreements for the *PSDR* hazard among all four conditioning periods (Figures A.16 and A.17). For the 4-story perimeter frame, *PFA* seems to be most dominated by T_2 (compared to T_3 for the 8-,

12-, and 20-story perimeter frames), as indicated in Figure A.20c and A.20d. T_1 continues to be important for *PSDR* (see Figures A.20a and A.20b), and $2T_1$ continues to be important for collapse (see Figure A.20e). The difference in logarithmic standard deviation of *PSDR* is now quite significant between the shorter and longer periods (see Figure A.20b).

A.1.5 2-story perimeter frame

The fifth structure considered is a 2-story perimeter frame, denoted Building 2064 in the recent FEMA P695 project (ATC, 2009; Haselton and Deierlein, 2007). The first two elastic modal periods are 0.63s and 0.18s. Results related to ground motions selected using Conditional Spectra are shown in Figures A.21 to A.25 for this structure.

Only three periods are plotted here because there is no third-mode period for the 2-story structure. Conditional standard deviation adjustments improved the agreements for the *PSDR* hazard among all three conditioning periods (Figures A.21 and A.22). T_1 seems to be important for *PSDR*, T_2 seems to be important for *PFA*, and $2T_1$ seems to be important for collapse. There is a distinct difference in logarithmic standard deviation of *PSDR* between T_1 (or $2T_1$) and T_2 (see Figure A.25b). There is, however, not much difference in logarithmic standard deviation of *PFA* among the three periods of interest.

A.1.6 1-story perimeter frame

The sixth structure considered is a 1-story perimeter frame, denoted Building 2069 in the recent FEMA P695 project (ATC, 2009; Haselton and Deierlein, 2007). The only first elastic modal period is 0.68s. Results related to ground motions selected using Conditional Spectra are shown in Figures A.26 to A.30 for this structure.

Only two periods are plotted here because there are no second- and third-mode periods for the 1-story structure. The spectra of the “basic” ground motions showed good agreement with the true hazard curves (Figure A.26a and A.26b), so no adjustments are needed for the target conditional standard deviation in this case. The resulting *PSDR* hazard curves are in reasonable agreements with each other (Figure A.27b). No much distinction exists between the only two conditioning periods in terms of their importance for *PSDR* or *PFA*, while $2T_1$ continues to be important for collapse (see Figure A.30e).

A.2 Conditional Spectra for space frames

Six perimeter frames with heights of 20-, 12-, 8-, 4-, 2-, and 1-story were analyzed. The corresponding figures are shown in A.31 to A.55.

A.2.1 20-story space frame

The seventh structure considered is a 20-story space frame, denoted Building 1021 in the recent FEMA P695 project (ATC, 2009; Haselton and Deierlein, 2007). The first three elastic modal periods are 2.5s, 0.92s and 0.54s. Results related to ground motions selected using Conditional Spectra are shown in Figures A.31 to A.35 for this structure. The observations are consistent with previous cases.

A.2.2 12-story space frame

The eighth structure considered is a 12-story space frame, denoted Building 1014 in the recent FEMA P695 project (ATC, 2009; Haselton and Deierlein, 2007). The first three elastic modal periods are 2.2s, 0.78s and 0.45s. Results related to ground motions selected using Conditional Spectra are shown in Figures A.36 to A.40 for this structure. The observations are consistent with previous cases.

A.2.3 8-story space frame

The ninth structure considered is an 8-story space frame, denoted Building 1012 in the recent FEMA P695 project (ATC, 2009; Haselton and Deierlein, 2007). The first three elastic modal periods are 1.8s, 0.64s and 0.36s. Results related to ground motions selected using Conditional Spectra are shown in Figures A.41 to A.45 for this structure. The observations are consistent with previous cases.

A.2.4 4-story space frame

The tenth structure considered is a 4-story space frame, denoted Building 1003 in the recent FEMA P695 project (ATC, 2009; Haselton and Deierlein, 2007). The first three elastic

modal periods are 1.1s, 0.33s and 0.17s. Results related to ground motions selected using Conditional Spectra are shown in Figures A.46 to A.50 for this structure. The observations are consistent with previous cases.

A.2.5 2-story space frame

The eleventh structure considered is a 2-story space frame, denoted Building 1001 in the recent FEMA P695 project (ATC, 2009; Haselton and Deierlein, 2007). The first two elastic modal periods are 0.60s and 0.17s. Results related to ground motions selected using Conditional Spectra are shown in Figures A.51 to A.55 for this structure.

Only three periods are plotted here because there is no third-mode period for the 2-story structure. The collapse fragility function in Figure A.52a for the $T^*=0.17s$ case was very poorly constrained, as even the highest considered $Sa(0.17s)$ amplitude produced only 1 collapse out of 40 analyses. In this extreme case, additional ground motions selected at higher spectral amplitudes would help with the collapse fragility. Alternatively, the inflation of the conditional standard deviation by 30% also made the collapse fragility fit more meaningful, as illustrated in Figure A.52b.

A.2.6 1-story space frame

The twelfth structure considered is a 1-story space frame, denoted Building 2061 in the recent FEMA P695 project (ATC, 2009; Haselton and Deierlein, 2007). The only first elastic modal period is 0.42s. Results related to ground motions selected using Conditional Spectra are shown in Figures A.56 to A.60 for this structure.

Only two periods are plotted here because there are no second- and third-mode periods for the 1-story structure. Again, the spectra of the “basic” ground motions showed good agreement with the true hazard curves (Figure A.56a and A.56b), resulting in no adjustments for the target conditional standard deviation.

A.3 Additional spectral amplitudes

For the 20-story perimeter frame, we first note that for the $T^*=0.45\text{s}$ case, the collapse fragility function in Figure 4.7 was relatively poorly constrained, as even the highest considered $Sa(0.45\text{s})$ amplitude produced only 11 collapses out of 40 analyses. Further structural analyses at higher $Sa(0.45\text{s})$ amplitudes were performed for this case, and are shown in Figure A.61. For the Conditional Spectrum with mean and one standard deviation, additional structural analyses with higher Intensity Measures (IMs), i.e., five higher $Sa(0.45\text{s})$ amplitudes associated with up to 2% in 10000 years probability of exceedance, produced up to 19 collapses out of 40 analyses, but only changed the collapse fragility function (see Figure A.61a) and consequently $PSDR$ drift hazard (see Figure A.61b) by a small amount compared to those with the “basic” ten $Sa(0.45\text{s})$ amplitudes. For the Conditional Spectrum with mean and a standard deviation inflated by 10%, however, the change in the collapse fragility function (see Figure A.61a) and consequently $PSDR$ drift hazard (see Figure A.61b) were more substantial.

This confirms that the relatively poorly constrained collapse fragility function noted in Figure 4.7 was not the source of the discrepancy in drift hazard. While adding higher $Sa(0.45\text{s})$ amplitudes corresponding to longer return periods would help with constraining the collapse fragility function better (especially for cases such as Figure A.52a where even fewer collapses were produced), the fundamental source of the problem was the lack of high-amplitude $Sa(0.45\text{s})$ values associated with the given return periods in ground motions selected to match the approximate Conditional Spectrum mean and standard deviation. This problem was alleviated by inflating the approximate conditional standard deviation to better match the known ground motion hazard information (see Figure A.1b versus Figure A.1a) that resulted in a better agreement for the $PSDR$ drift hazard among various conditioning periods (see Figure A.2d versus Figure A.2c).

A.4 Other target spectra

For comparison with the Conditional-Spectrum-based results presented above, the drift hazard calculation procedure is repeated using two additional sets of ground motions: one

selected with ground motions having spectra to match the Conditional Mean Spectrum only (not accounting for spectrum variability), and one selected to match Uniform Hazard Spectrum at each $Sa(T^*)$ level. Results using all conditioning periods for these two target spectra were obtained for the 20-story and 4-story perimeter frames, and are shown in Figures A.62 to A.81.

As shown in Figure 5.4a, the rate of exceeding large *PSDR* levels is comparable between ground motions matched to the CMS at $T^* = 2.6\text{s}$ and ground motions matched to the CS at various T^* 's; this result changes, however, when the conditioning period, T^* in the CMS is varied. Since the CMS does not account for spectrum variability, conditioning on one period changes the 4 distribution at other periods (see Figure A.62). For instance, for ground motions selected to match the CMS at $T^* = 0.45\text{s}$, its $Sa(2.6\text{s})$ and $Sa(5\text{s})$ distributions deviated quite substantially from the corresponding true ground motion hazard (see Figure A.62a). Similarly, for ground motions selected to match the CMS at $T^* = 5\text{s}$, its $Sa(0.45\text{s})$ and $Sa(0.85\text{s})$ distributions deviated quite substantially from the corresponding true ground motion hazard (see Figure A.62d). This in turn resulted in *PSDR* drift hazards that did not show good agreements among different conditioning periods (see Figure A.63b), implying the need for caution in choosing a conditioning period for the CMS to estimate *PSDR* drift hazard.

As shown in Figure 5.4a, the rate of exceeding large *PSDR* levels is over-estimated when ground motions are matched to the UHS; this finding is consistent with previous observations that use of the UHS as a target spectrum leads to conservative estimates of structural response. One exception is the UHS results using $T^* = 5\text{s}$ (see Figure A.68b), where the drift hazard results are comparable to the CS results; this may be because $Sa(5\text{s})$ is an effective predictor of nonlinear response and collapse in this structure, and so the inaccuracy of spectral values at other periods in this set of ground motions (see Figure A.67d) does not have a strong impact on resulting structural responses given $Sa(5\text{s})$.

The conclusions drawn in Chapters 4 and 5 appear to hold for the additional eleven structures and analyses considered here.

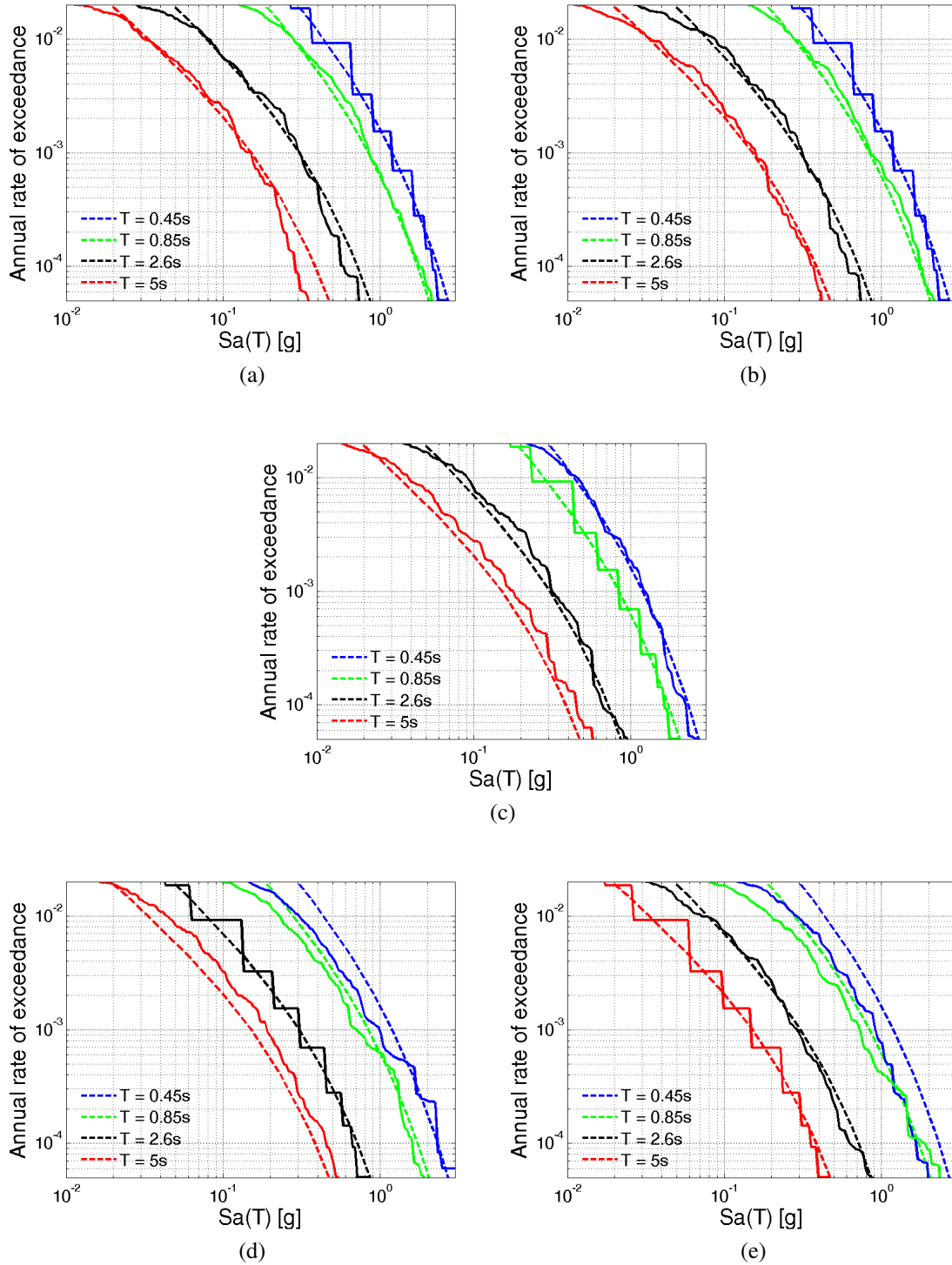


Figure A.1: 20-story perimeter frame (Building No.1020) S_a distribution at four periods for ground motions selected at (a) $T^* = T_3$, CS μ and σ , (b) $T^* = T_3$, CS μ and 1.1σ , (c) $T^* = T_2$, CS μ and σ , (d) $T^* = T_1$, CS μ and σ , and (e) $T^* = 2T_1$, CS μ and σ .

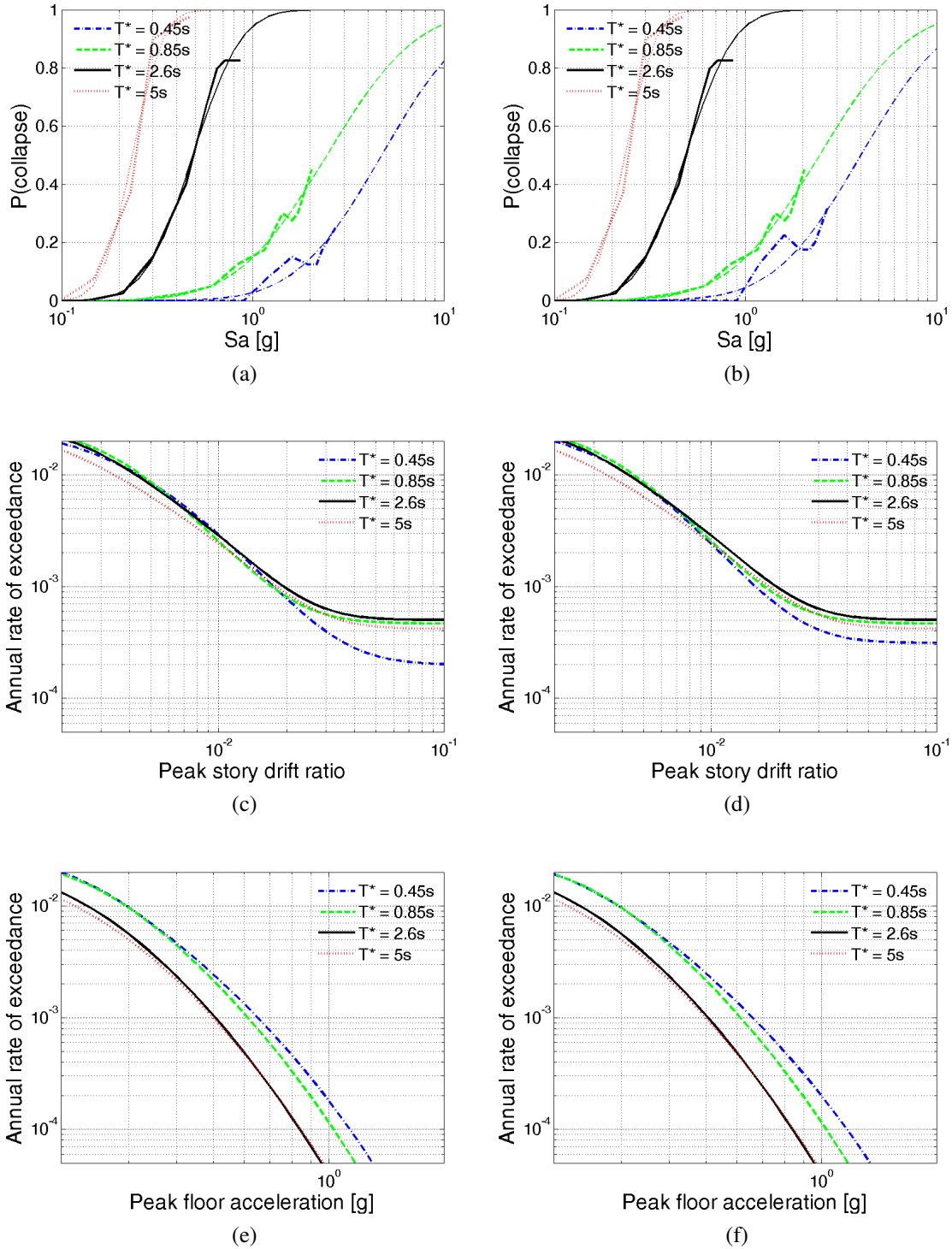


Figure A.2: 20-story perimeter frame (Building No.1020) (a-b) probability of collapse, (c-d) *PSDR* hazard, and (e-f) *PFA* hazard for “basic” ground motions selected to match CS μ and σ ($T_3, T_2, T_1, 2T_1$) at (a, c, e) and “improved” ground motions selected to match CS μ and σ ($T_2, T_1, 2T_1$) and CS μ and 1.1σ (T_3) at (b, d, f).

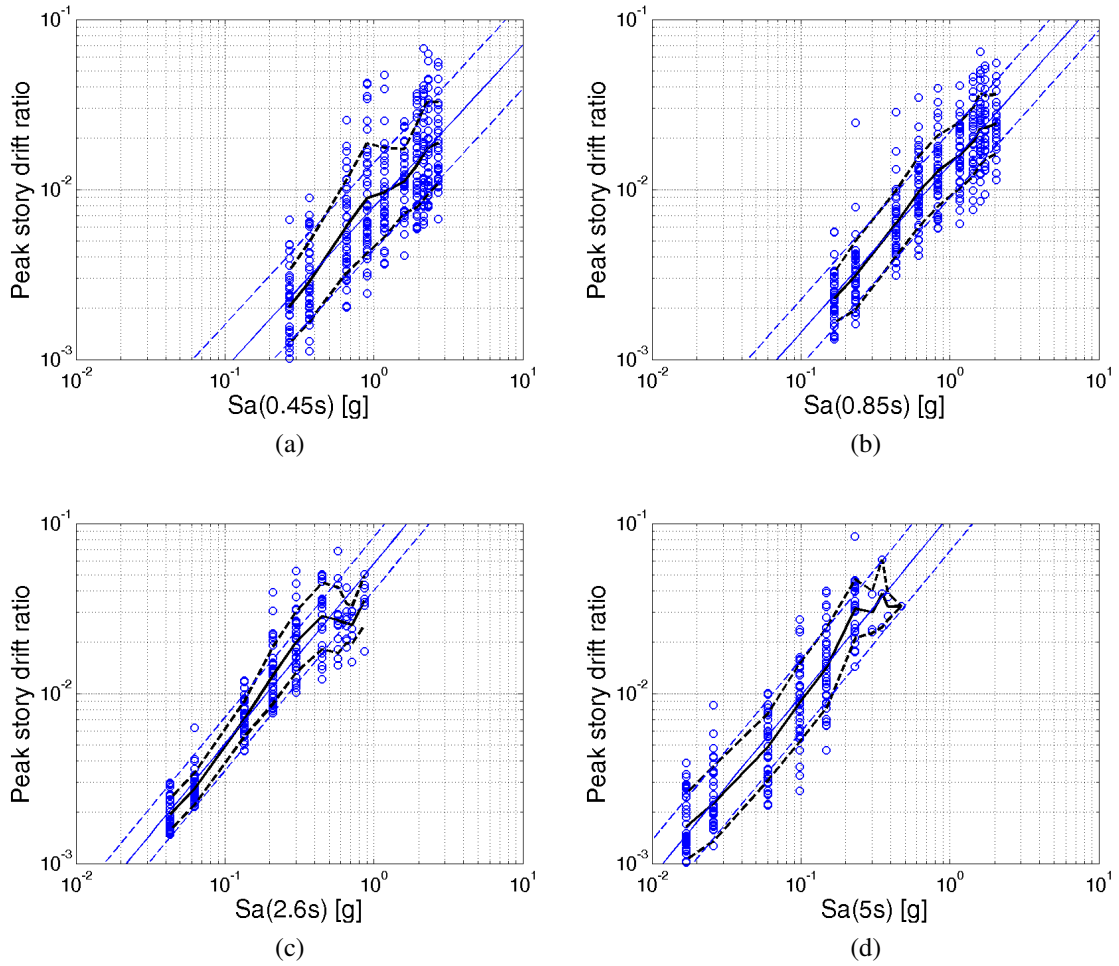


Figure A.3: 20-story perimeter frame (Building No.1020) *PSDR* at (a) $T^* = T_3$, (b) $T^* = T_2$, (c) $T^* = T_1$, and (d) $T^* = 2T_1$ for “improved” ground motions selected to match CS μ and σ ($T_2, T_1, 2T_1$) and CS μ and 1.1σ (T_3).

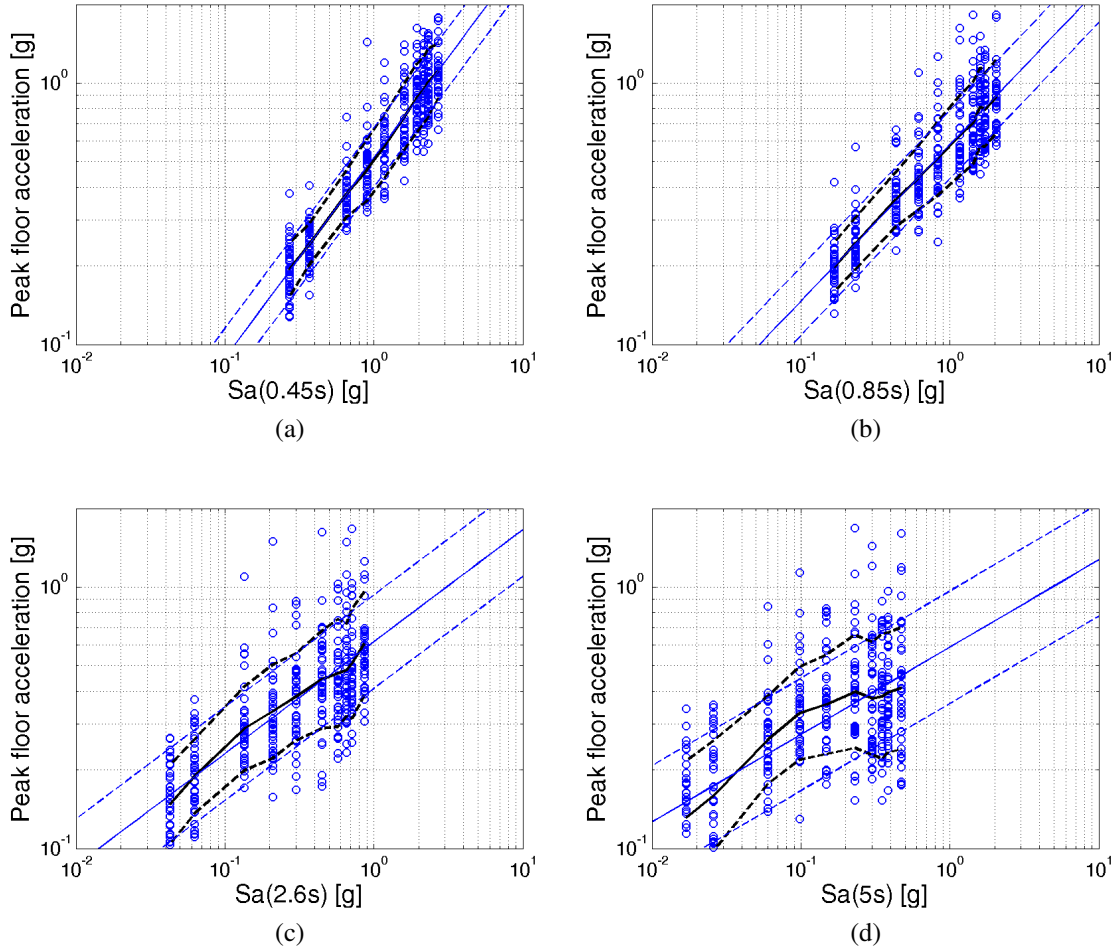


Figure A.4: 20-story perimeter frame (Building No.1020) PFA at (a) $T^* = T_3$, (b) $T^* = T_2$, (c) $T^* = T_1$, and (d) $T^* = 2T_1$ for “improved” ground motions selected to match CS μ and σ ($T_2, T_1, 2T_1$) and CS μ and 1.1σ (T_3).

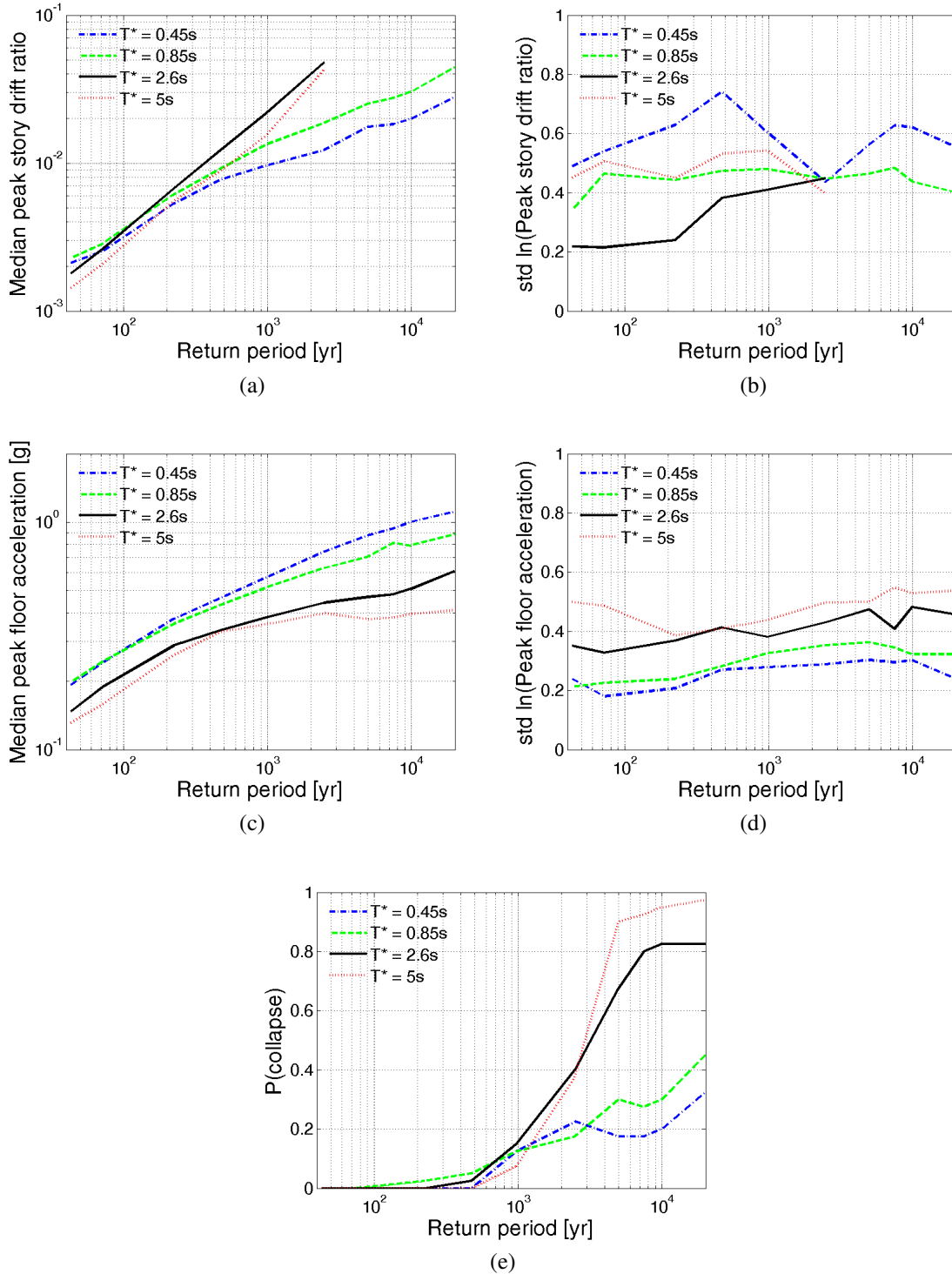


Figure A.5: 20-story perimeter frame (Building No.1020) (a) median $PSDR$, (b) logarithmic standard deviation of $PSDR$, (c) median PFA , (d) logarithmic standard deviation of PFA , and (e) probability of collapse given return period for “improved” ground motions selected to match CS μ and σ ($T_2, T_1, 2T_1$) and CS μ and 1.1σ (T_3).

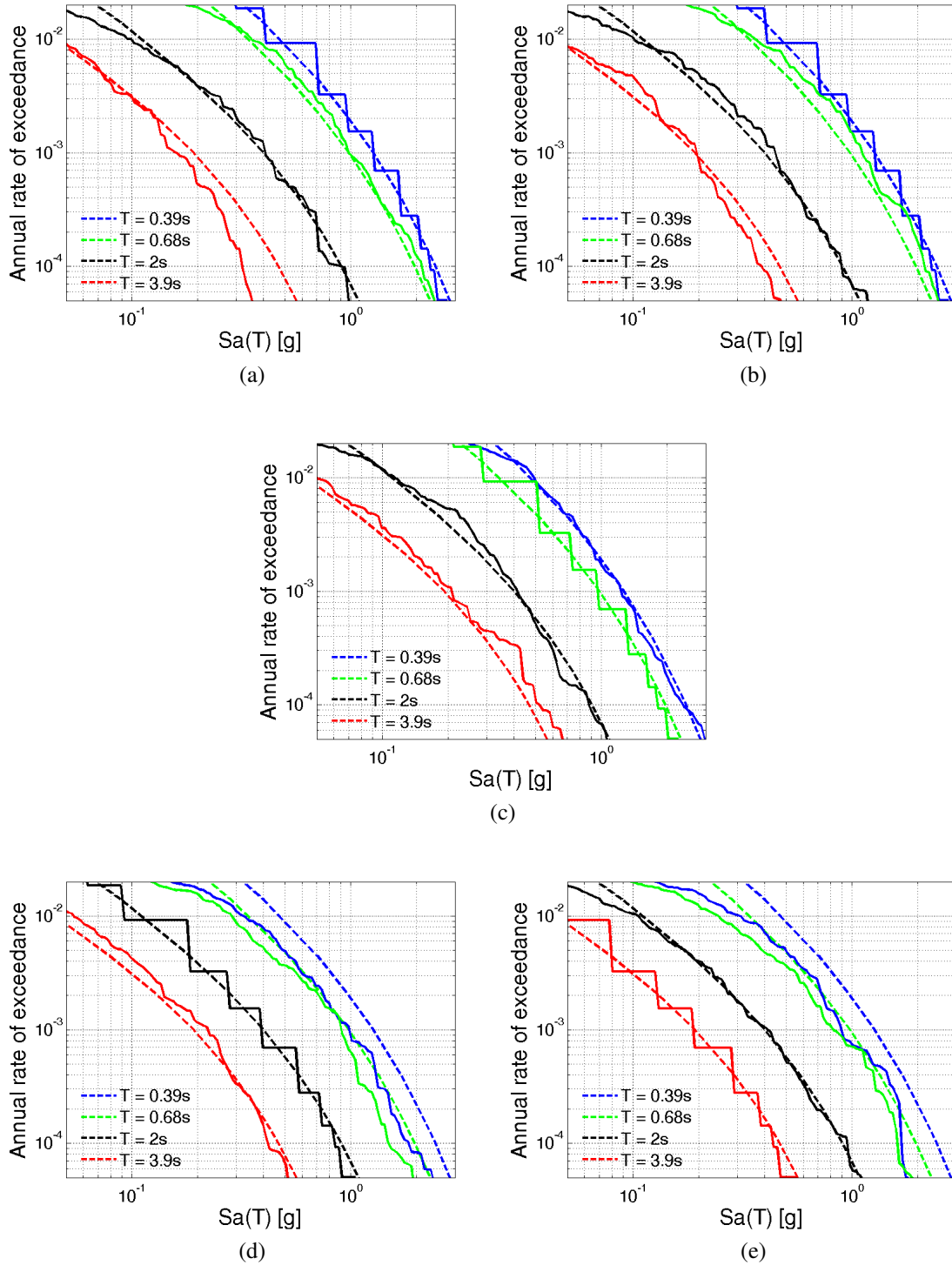


Figure A.6: 12-story perimeter frame (Building No.1013) Sa distribution at four periods for ground motions selected at (a) $T^* = T_3$, CS μ and σ , (b) $T^* = T_3$, CS μ and 1.2σ , (c) $T^* = T_2$, CS μ and σ , (d) $T^* = T_1$, CS μ and σ , and (e) $T^* = 2T_1$, CS μ and σ .

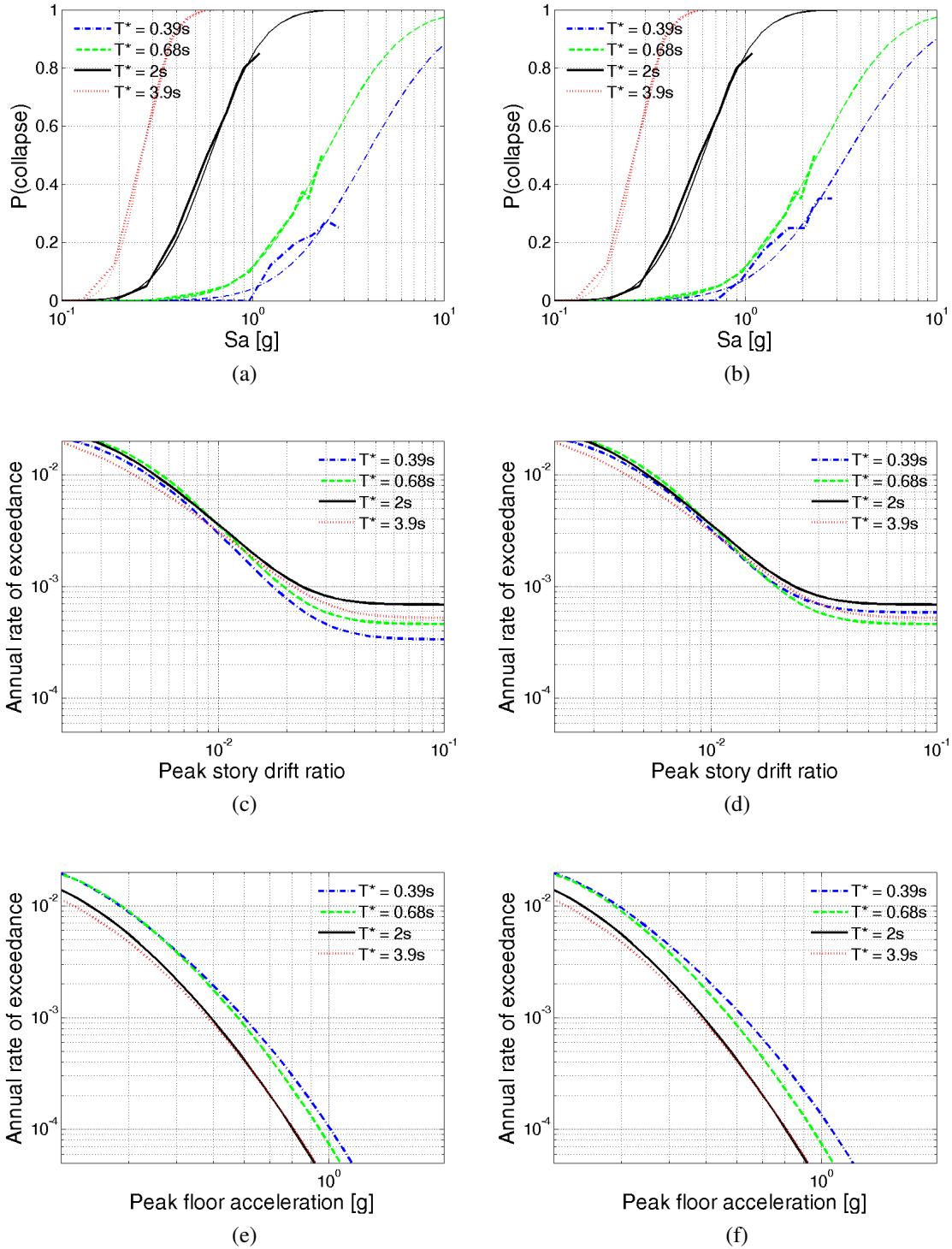


Figure A.7: 12-story perimeter frame (Building No.1013) (a-b) probability of collapse, (c-d) *PSDR* hazard, and (e-f) *PFA* hazard for “basic” ground motions selected to match CS μ and σ ($T_3, T_2, T_1, 2T_1$) at (a, c, e) and “improved” ground motions selected to match CS μ and σ ($T_2, T_1, 2T_1$) and CS μ and 1.2σ (T_3) at (b, d, f).

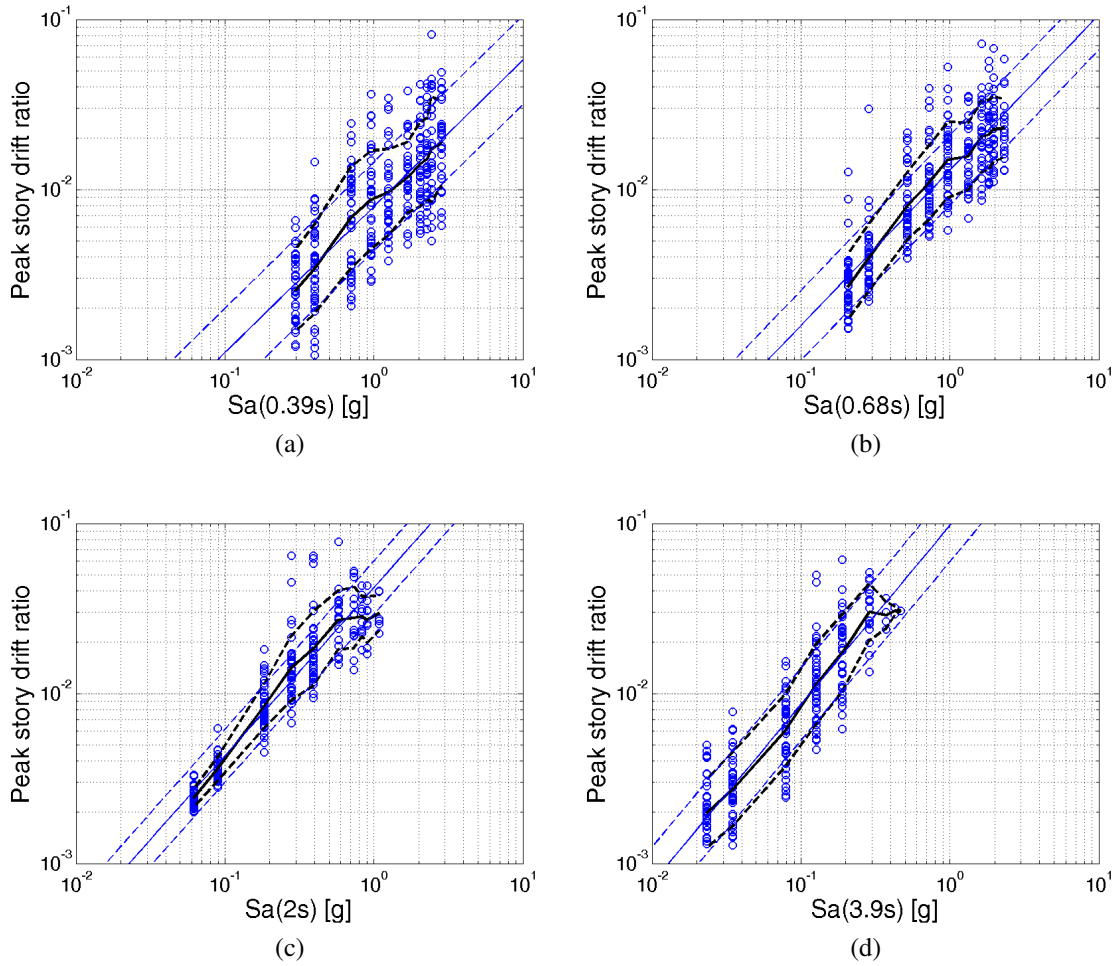


Figure A.8: 12-story perimeter frame (Building No.1013) *PSDR* at (a) $T^* = T_3$, (b) $T^* = T_2$, (c) $T^* = T_1$, and (d) $T^* = 2T_1$ for “improved” ground motions selected to match CS μ and σ ($T_2, T_1, 2T_1$) and CS μ and 1.2σ (T_3).

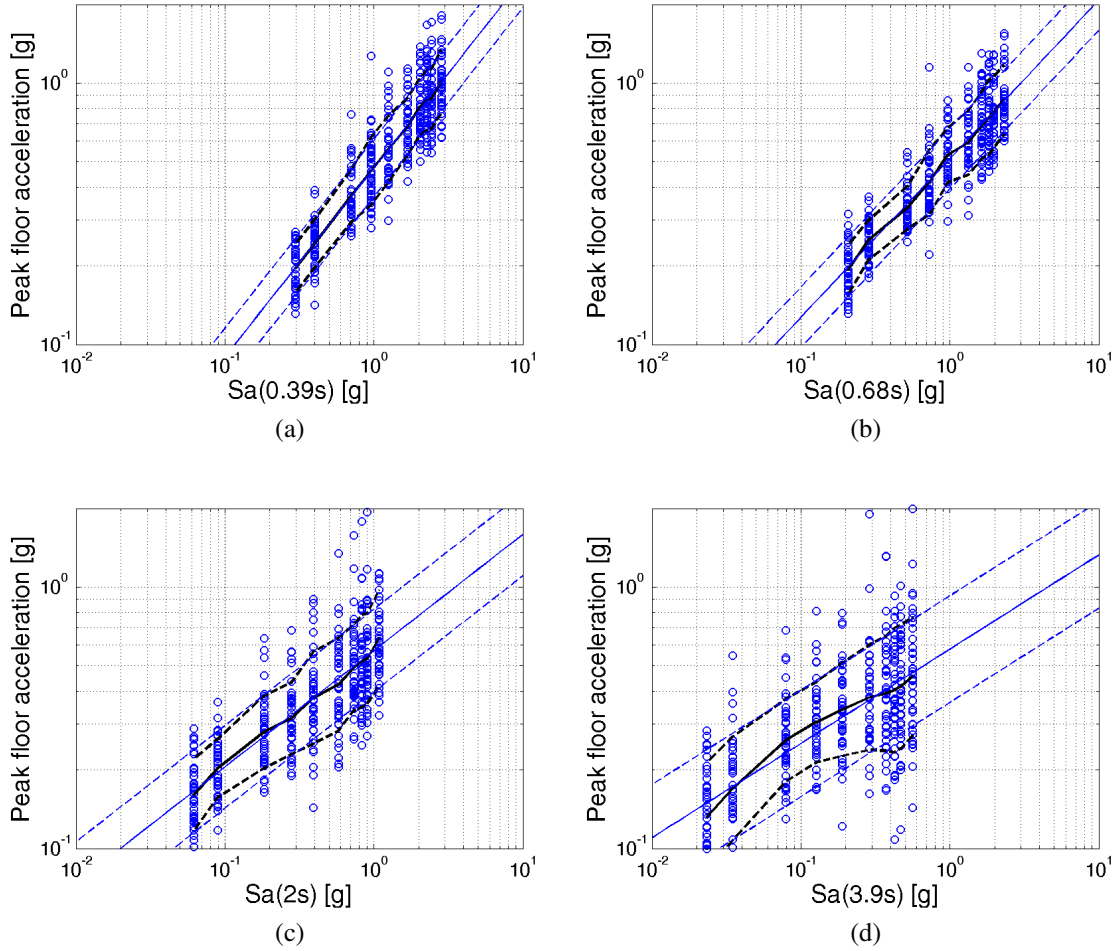


Figure A.9: 12-story perimeter frame (Building No.1013) PFA at (a) $T^* = T_3$, (b) $T^* = T_2$, (c) $T^* = T_1$, and (d) $T^* = 2T_1$ for “improved” ground motions selected to match CS μ and σ ($T_2, T_1, 2T_1$) and CS μ and 1.2σ (T_3).

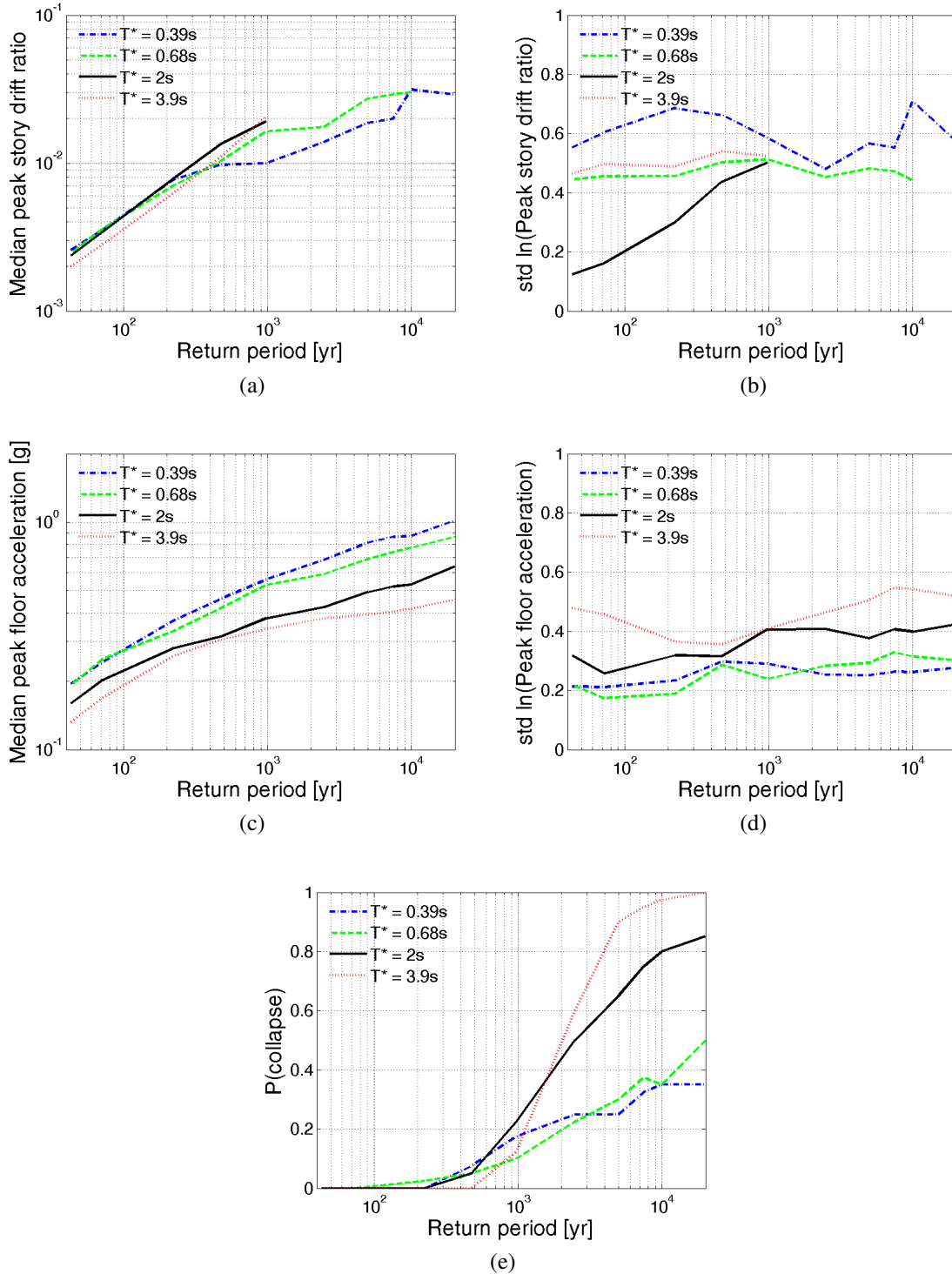


Figure A.10: 12-story perimeter frame (Building No.1013) (a) median $PSDR$, (b) logarithmic standard deviation of $PSDR$, (c) median PFA , (d) logarithmic standard deviation of PFA , and (e) probability of collapse given return period for “improved” ground motions selected to match CS μ and σ ($T_2, T_1, 2T_1$) and CS μ and 1.2σ (T_3).

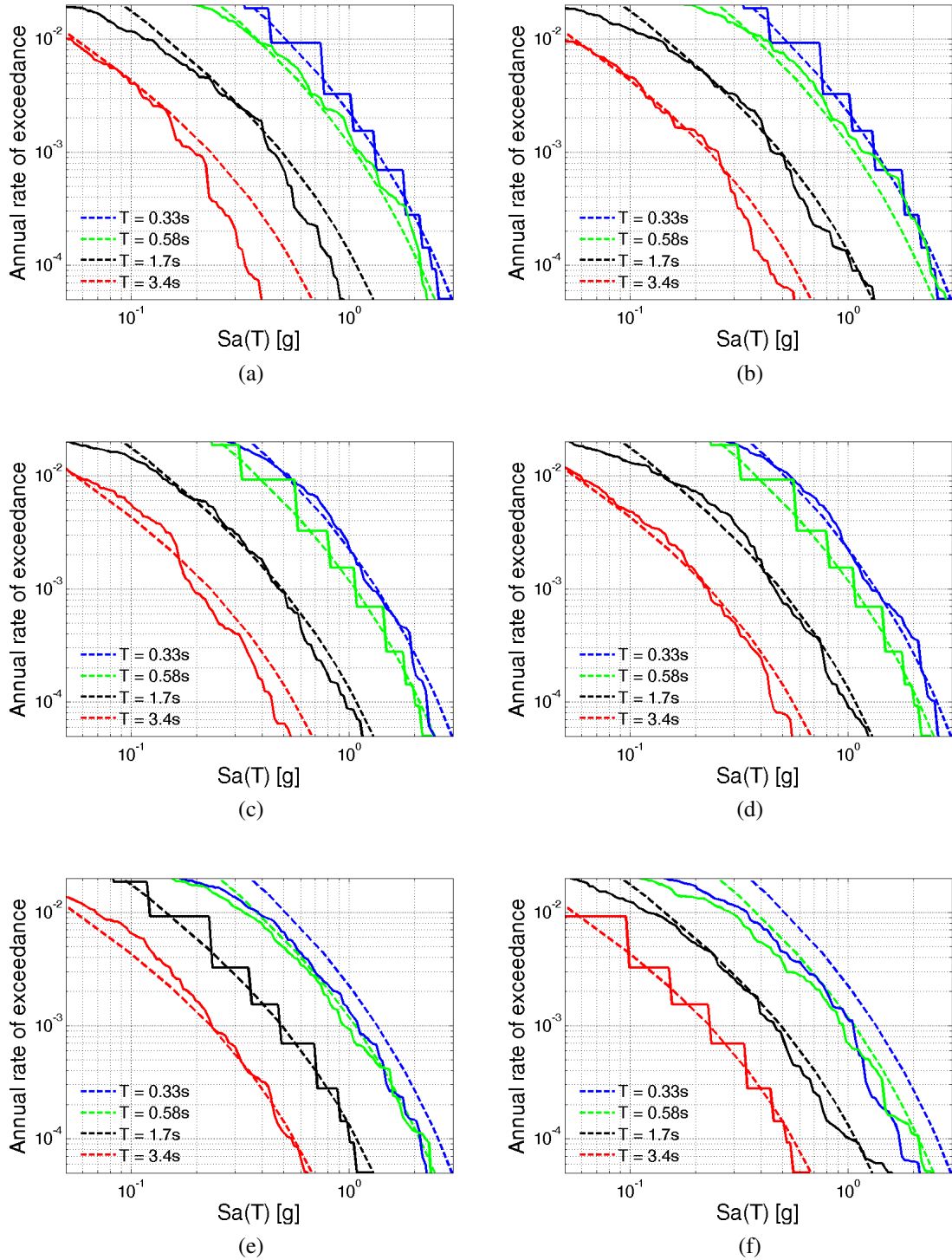


Figure A.11: 8-story perimeter frame (Building No.1011) Sa distribution at four periods for ground motions selected at (a) $T^* = T_3$, CS μ and σ , (b) $T^* = T_3$, CS μ and 1.2σ , (c) $T^* = T_2$, CS μ and σ , (d) $T^* = T_2$, CS μ and 1.1σ , (e) $T^* = T_1$, CS μ and σ , and (f) $T^* = 2T_1$, CS μ and σ .

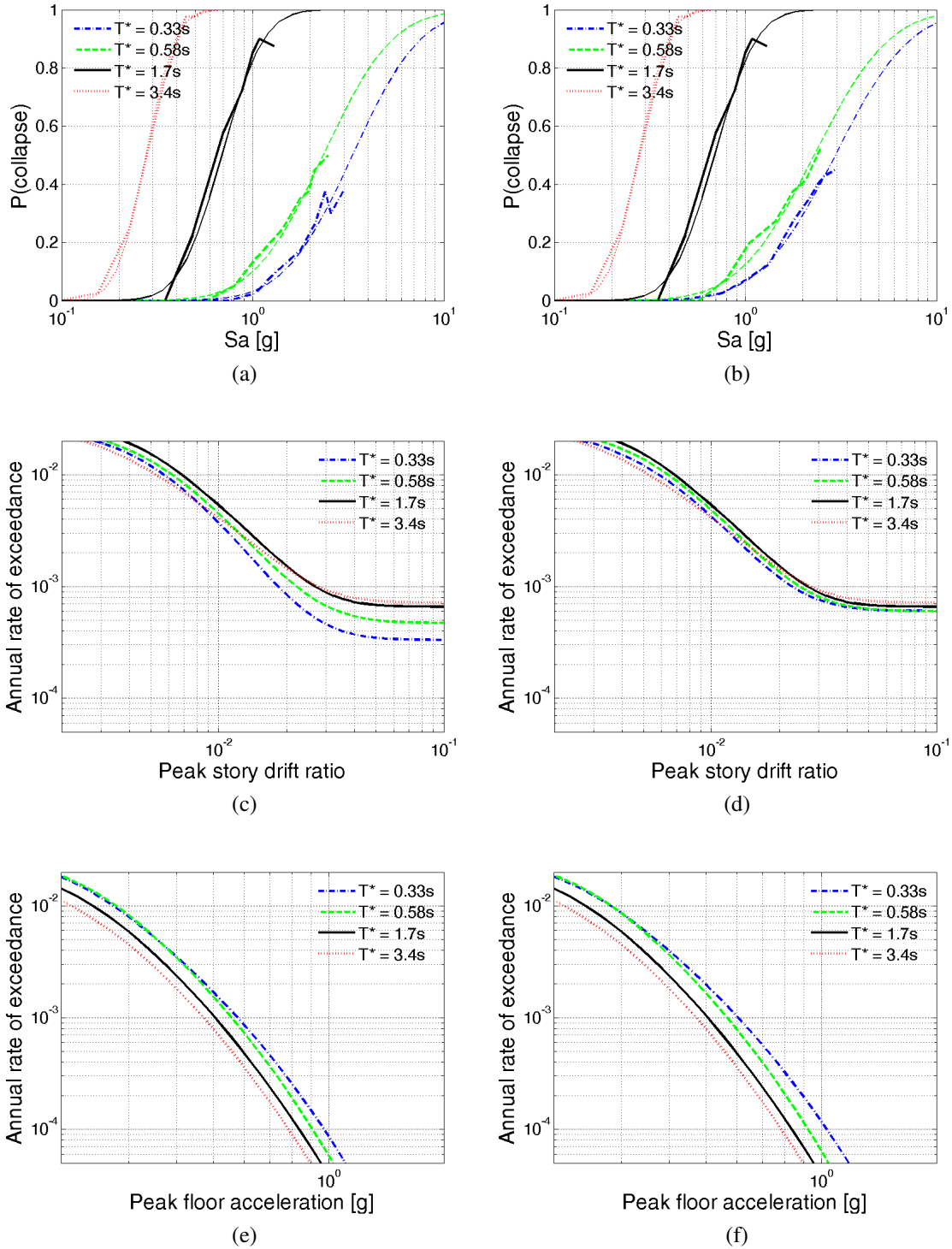


Figure A.12: 8-story perimeter frame (Building No.1011) (a-b) probability of collapse, (c-d) *PSDR* hazard, and (e-f) *PFA* hazard for “basic” ground motions selected to match CS μ and σ ($T_3, T_2, T_1, 2T_1$) at (a, c, e) and “improved” ground motions selected to match CS μ and σ ($T_1, 2T_1$), CS μ and 1.1σ (T_2), and CS μ and 1.2σ (T_3) at (b, d, f).

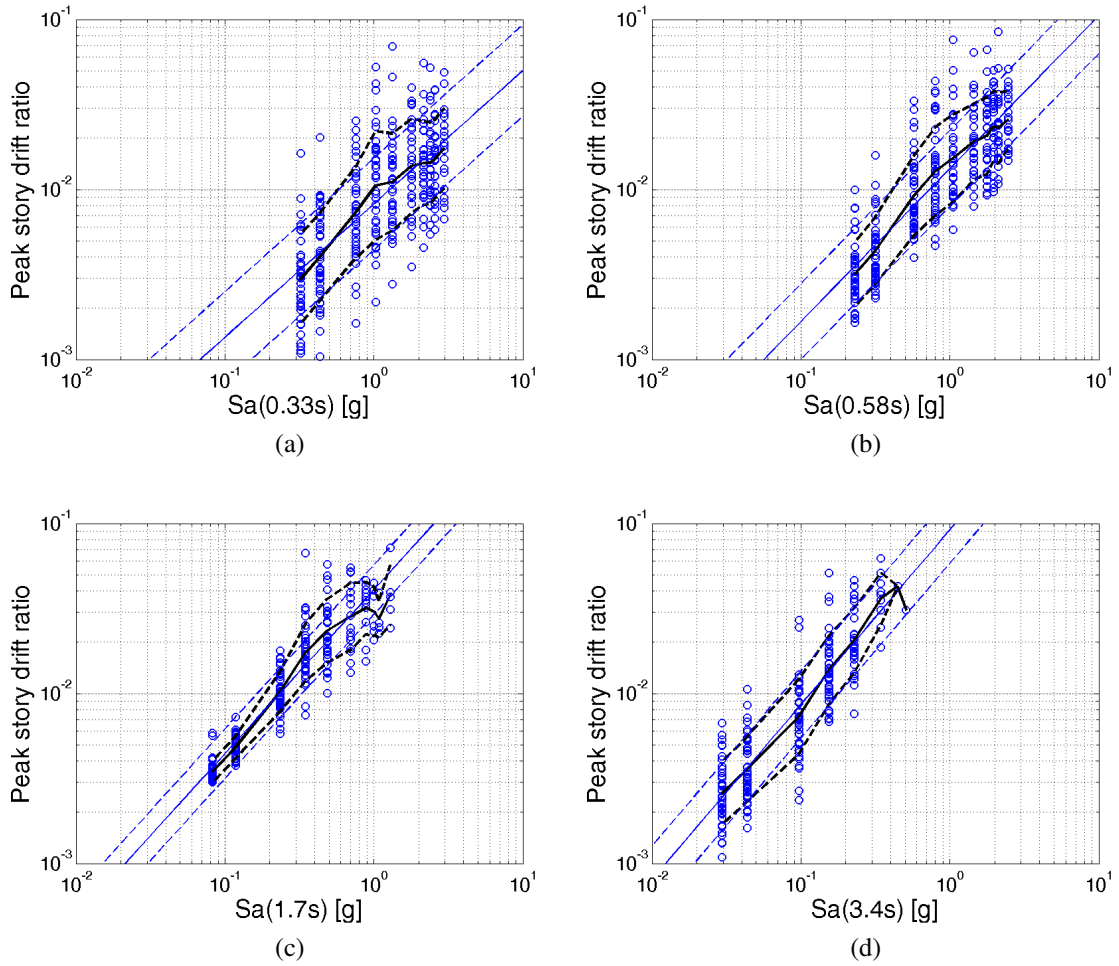


Figure A.13: 8-story perimeter frame (Building No.1011) *PSDR* at (a) $T^* = T_3$, (b) $T^* = T_2$, (c) $T^* = T_1$, and (d) $T^* = 2T_1$ for “improved” ground motions selected to match CS μ and σ ($T_1, 2T_1$), CS μ and 1.1σ (T_2), and CS μ and 1.2σ (T_3).

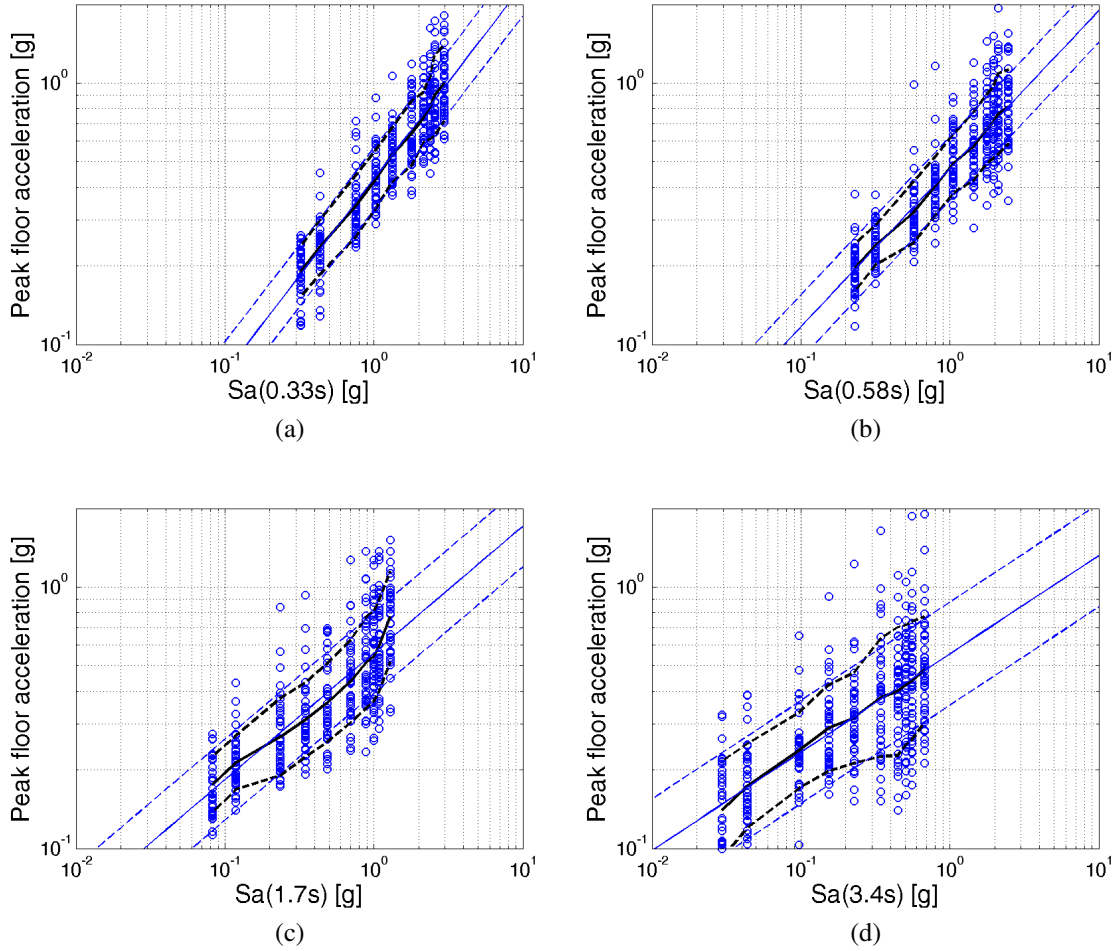


Figure A.14: 8-story perimeter frame (Building No.1011) PFA at (a) $T^* = T_3$, (b) $T^* = T_2$, (c) $T^* = T_1$, and (d) $T^* = 2T_1$ for “improved” ground motions selected to match CS μ and σ ($T_1, 2T_1$), CS μ and 1.1σ (T_2), and CS μ and 1.2σ (T_3).

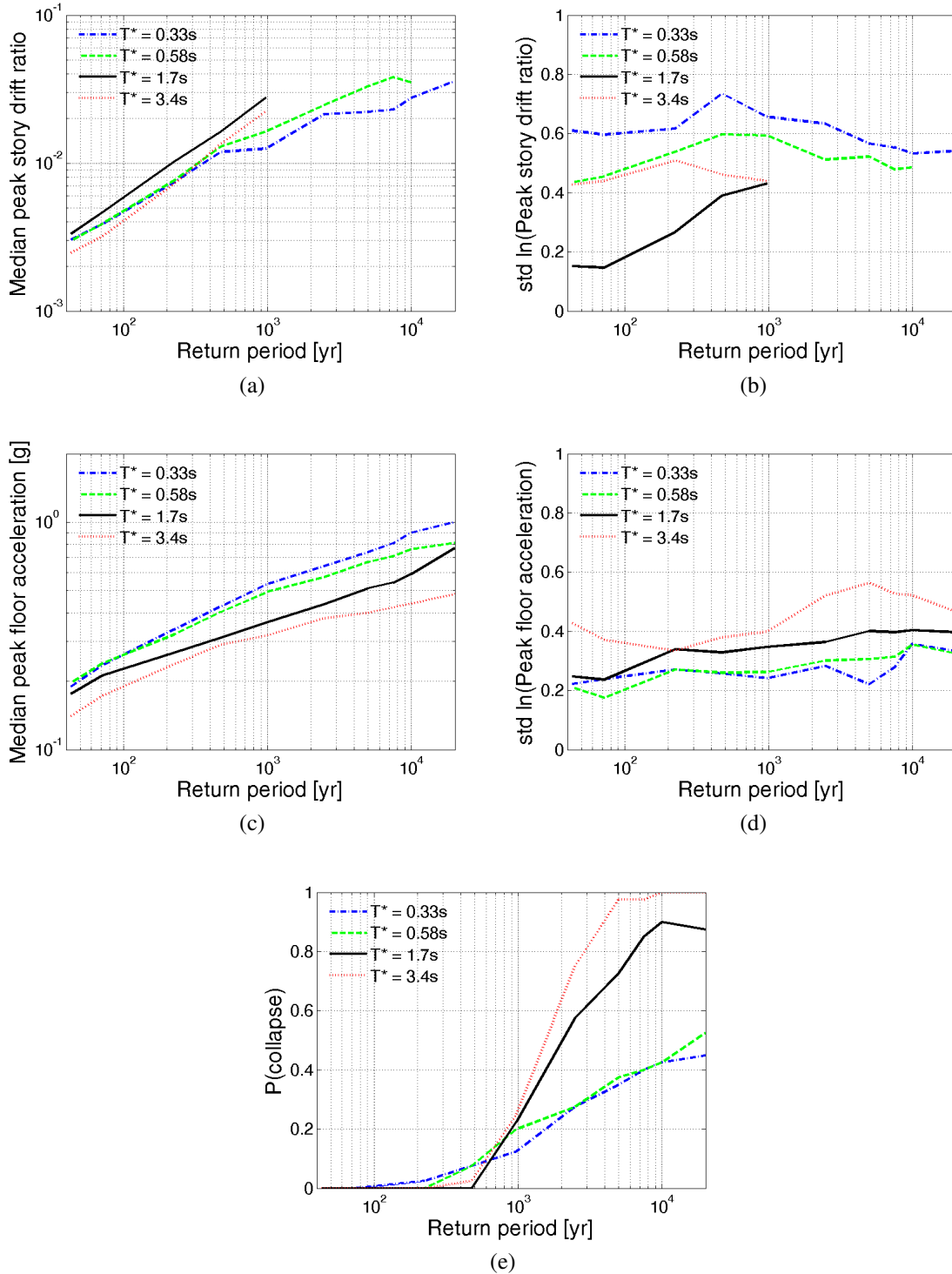


Figure A.15: 8-story perimeter frame (Building No.1011) (a) median $PSDR$, (b) logarithmic standard deviation of $PSDR$, (c) median PFA , (d) logarithmic standard deviation of PFA , and (e) probability of collapse given return period for “improved” ground motions selected to match CS μ and σ ($T_1, 2T_1$), CS μ and 1.1σ (T_2), and CS μ and 1.2σ (T_3).

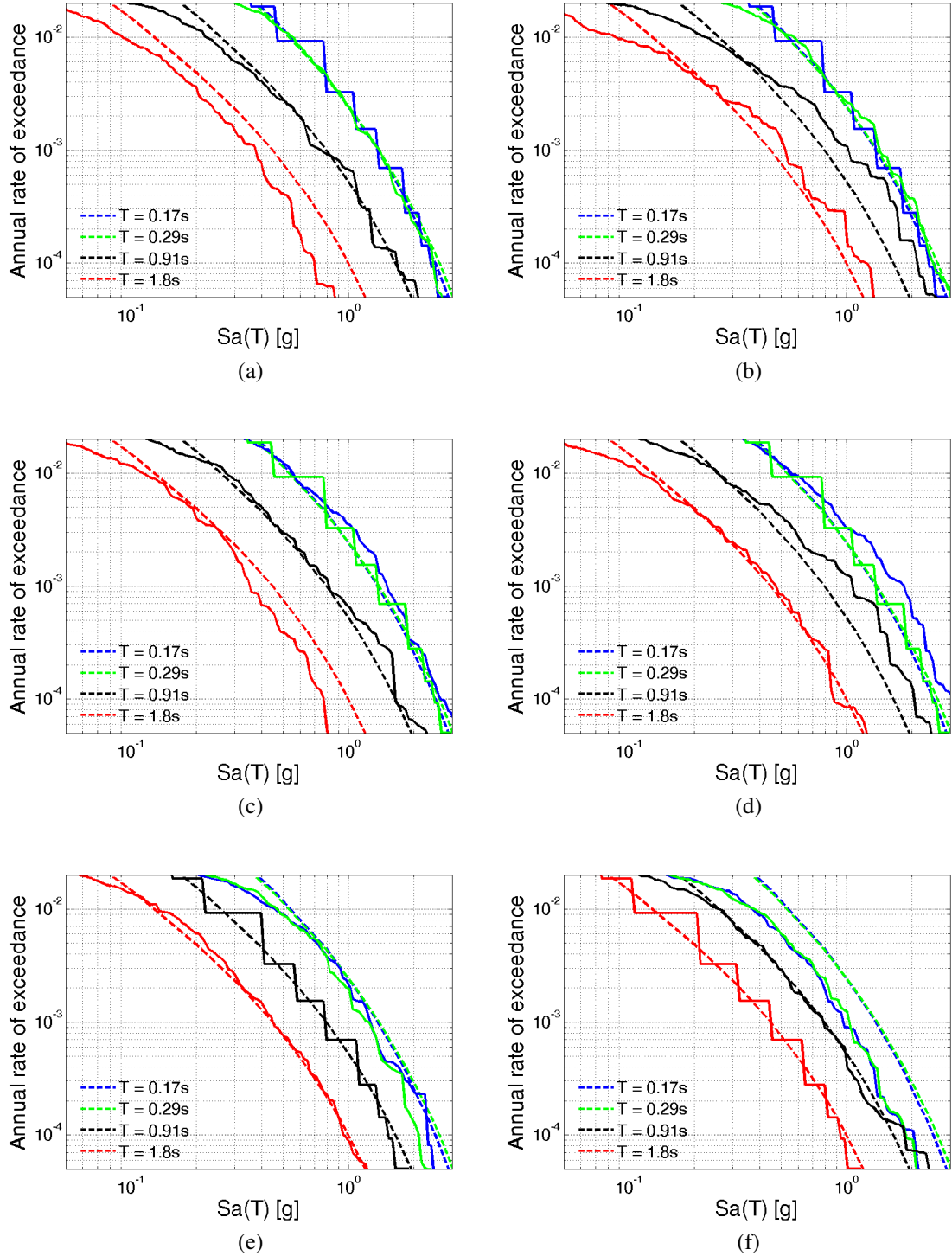


Figure A.16: 4-story perimeter frame (Building No.1008) Sa distribution at four periods for ground motions selected at (a) $T^* = T_3$, CS μ and σ , (b) $T^* = T_3$, CS μ and 1.3σ , (c) $T^* = T_2$, CS μ and σ , (d) $T^* = T_2$, CS μ and 1.2σ , (e) $T^* = T_1$, CS μ and σ , and (f) $T^* = 2T_1$, CS μ and σ .

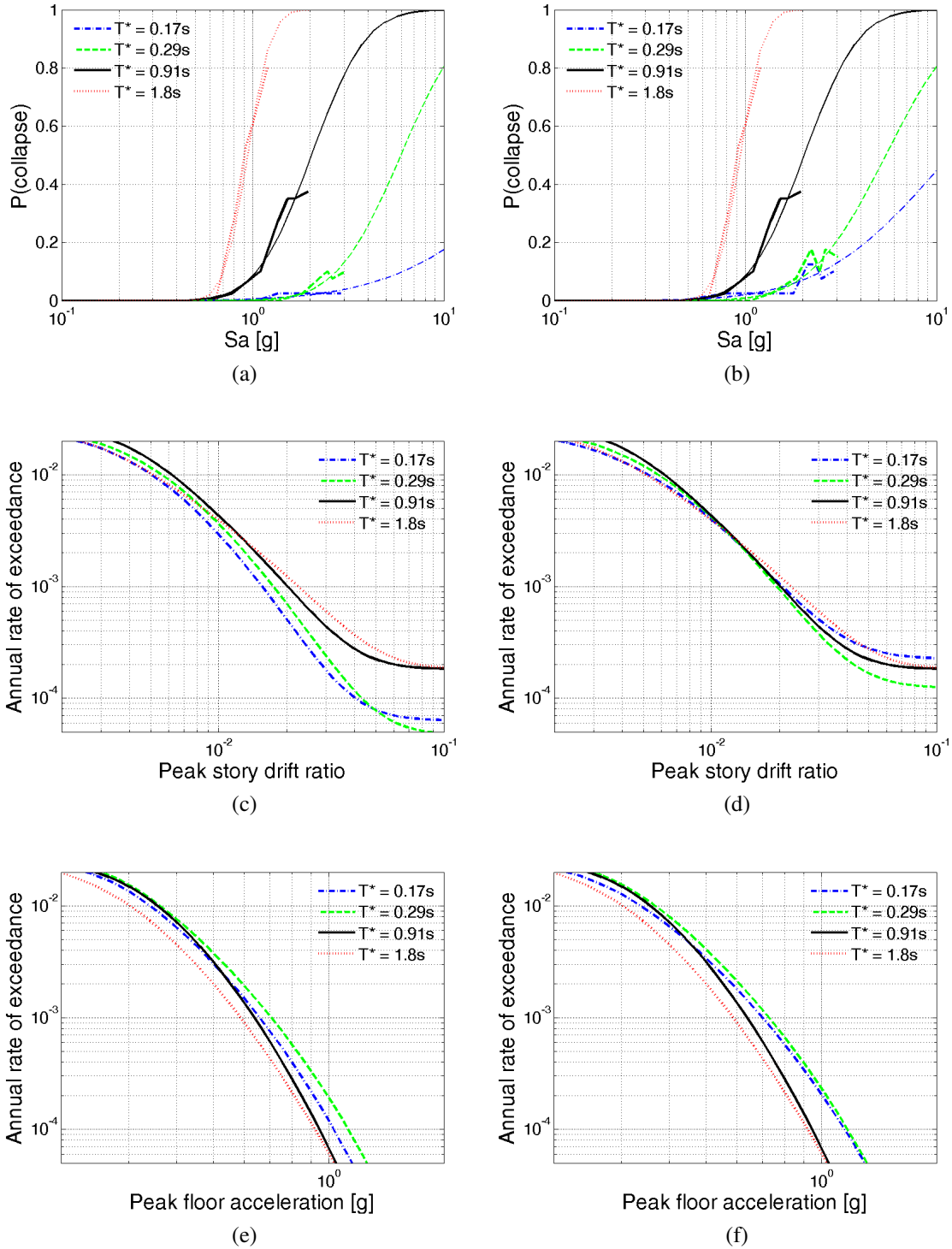


Figure A.17: 4-story perimeter frame (Building No.1008) (a-b) probability of collapse, (c-d) *PSDR* hazard, and (e-f) *PFA* hazard for “basic” ground motions selected to match CS μ and σ ($T_3, T_2, T_1, 2T_1$) at (a, c, e) and “improved” ground motions selected to match CS μ and σ ($T_1, 2T_1$), CS μ and 1.2σ (T_2), and CS μ and 1.3σ (T_3) at (b, d, f).

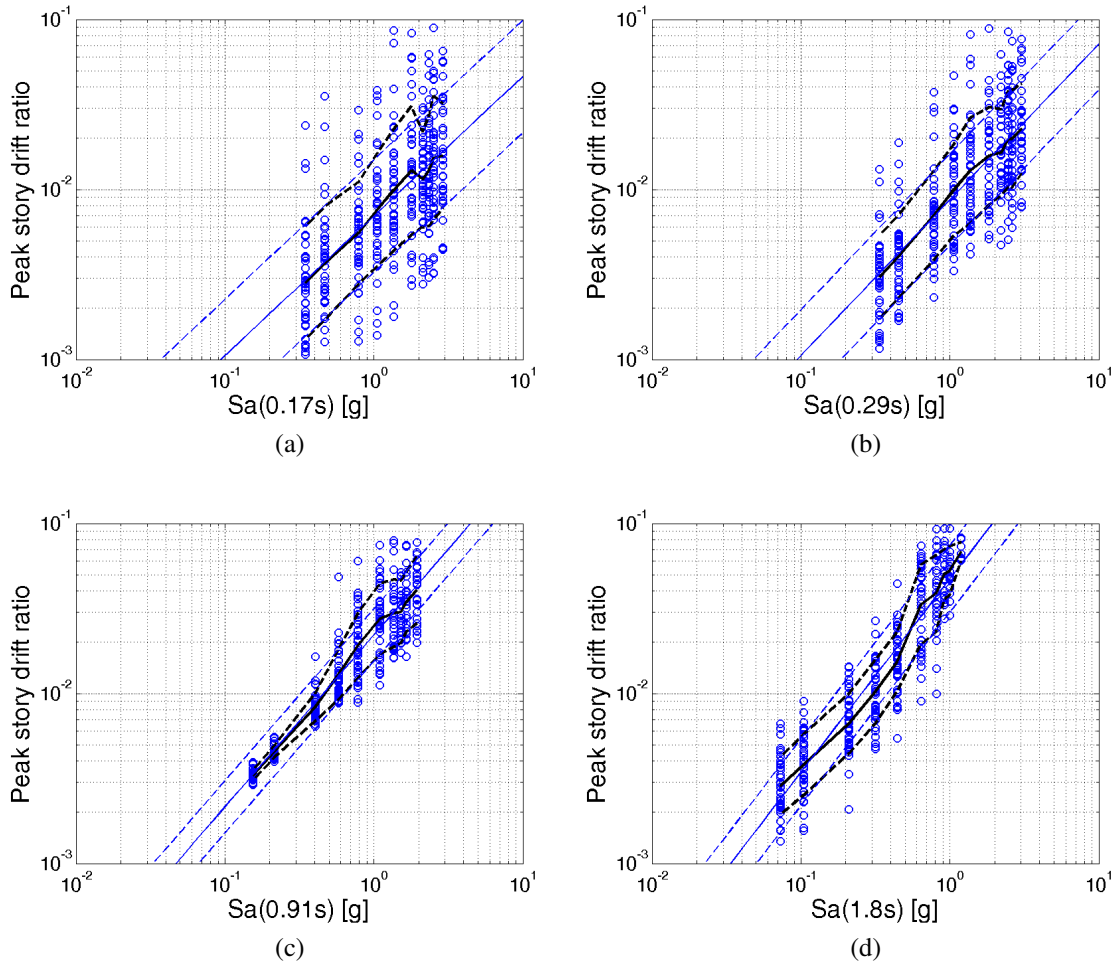


Figure A.18: 4-story perimeter frame (Building No.1008) *PSDR* at (a) $T^* = T_3$, (b) $T^* = T_2$, (c) $T^* = T_1$, and (d) $T^* = 2T_1$ for “improved” ground motions selected to match CS μ and σ ($T_1, 2T_1$), CS μ and 1.2σ (T_2), and CS μ and 1.3σ (T_3).

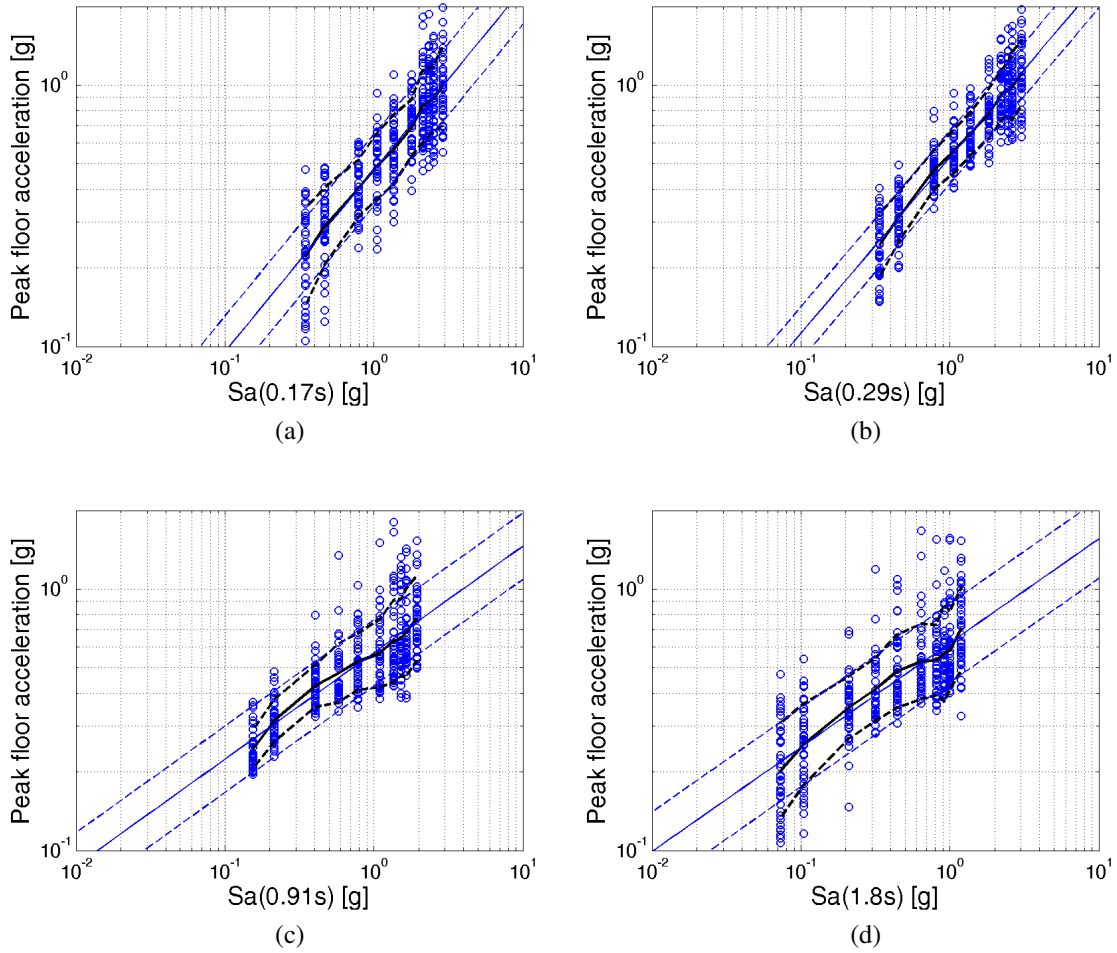


Figure A.19: 4-story perimeter frame (Building No.1008) PFA at (a) $T^* = T_3$, (b) $T^* = T_2$, (c) $T^* = T_1$, and (d) $T^* = 2T_1$ for “improved” ground motions selected to match CS μ and σ ($T_1, 2T_1$), CS μ and 1.2σ (T_2), and CS μ and 1.3σ (T_3).

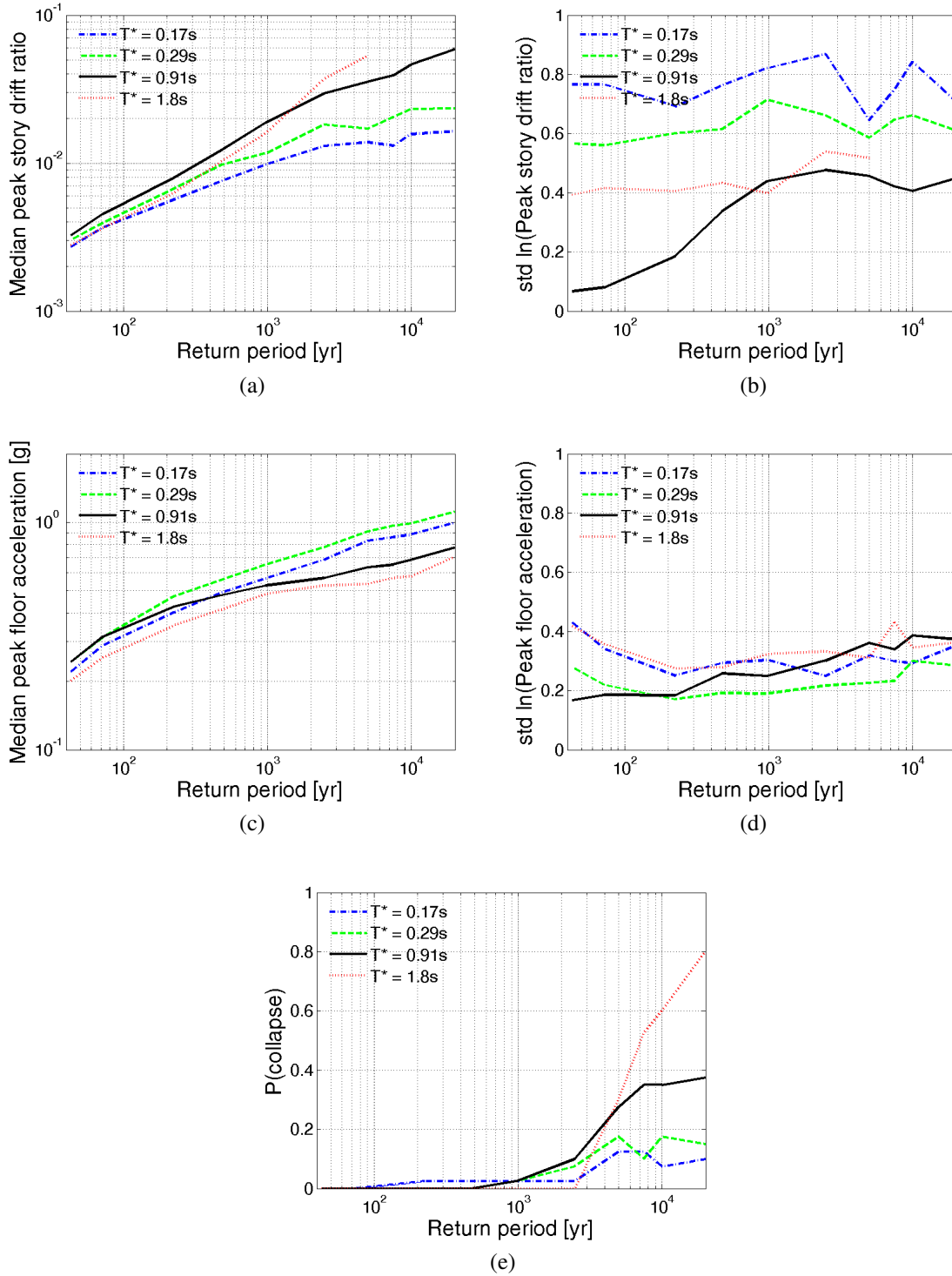


Figure A.20: 4-story perimeter frame (Building No.1008) (a) median *PSDR*, (b) logarithmic standard deviation of *PSDR*, (c) median *PFA*, (d) logarithmic standard deviation of *PFA*, and (e) probability of collapse given return period for “improved” ground motions selected to match CS μ and σ ($T_1, 2T_1$), CS μ and 1.2σ (T_2), and CS μ and 1.3σ (T_3).

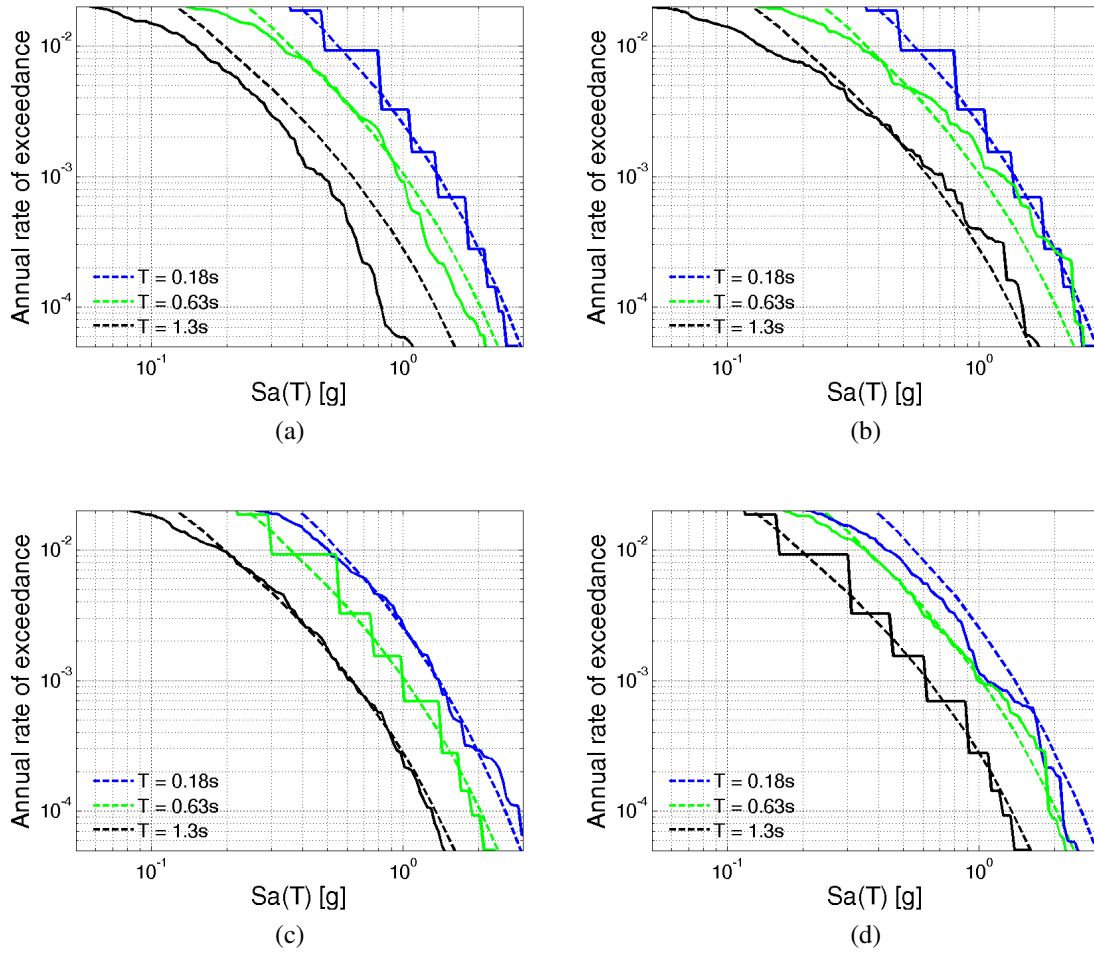


Figure A.21: 2-story perimeter frame (Building No.2064) S_a distribution at three periods for ground motions selected at (a) $T^* = T_2$, CS μ and σ , (b) $T^* = T_2$, CS μ and 1.3σ , (c) $T^* = T_1$, CS μ and σ , and (d) $T^* = 2T_1$, CS μ and σ .

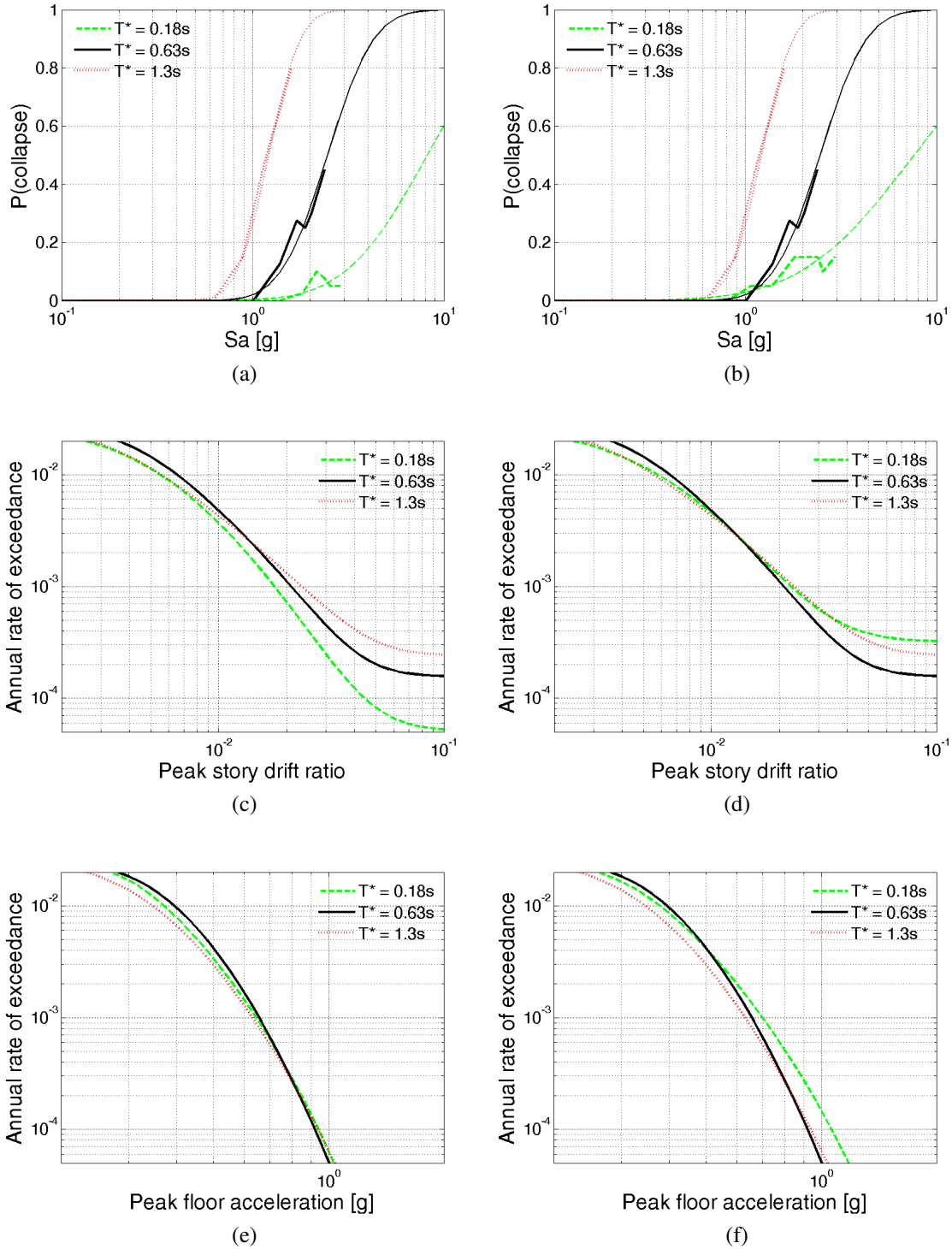


Figure A.22: 2-story perimeter frame (Building No.2064) (a-b) probability of collapse, (c-d) *PSDR* hazard, and (e-f) *PFA* hazard for “basic” ground motions selected to match CS μ and σ ($T_2, T_1, 2T_1$) at (a, c, e) and “improved” ground motions selected to match CS μ and σ ($T_1, 2T_1$) and CS μ and 1.3σ (T_2) at (b, d, f).

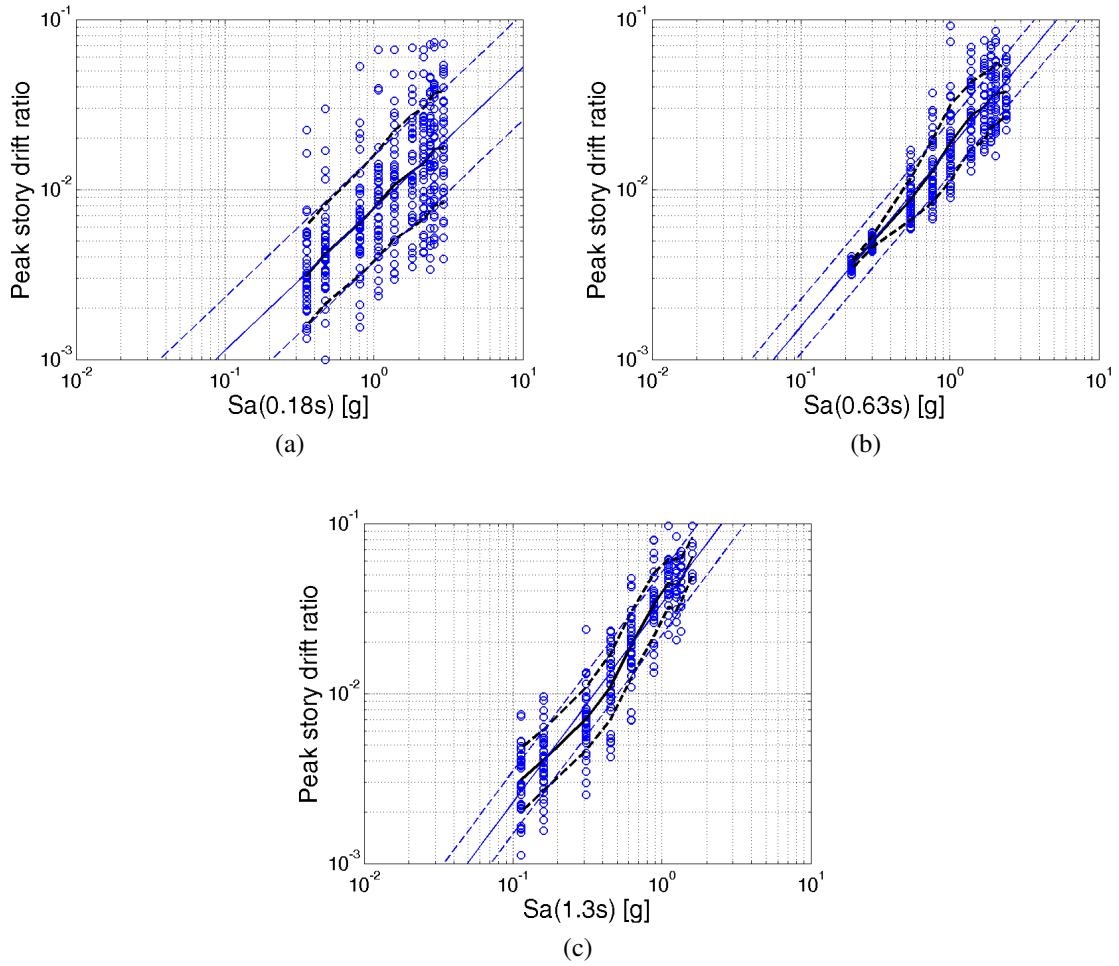


Figure A.23: 2-story perimeter frame (Building No.2064) *PSDR* at (a) $T^* = T_2$, (b) $T^* = T_1$, and (c) $T^* = 2T_1$ for “improved” ground motions selected to match CS μ and σ ($T_1, 2T_1$) and CS μ and 1.3σ (T_2).

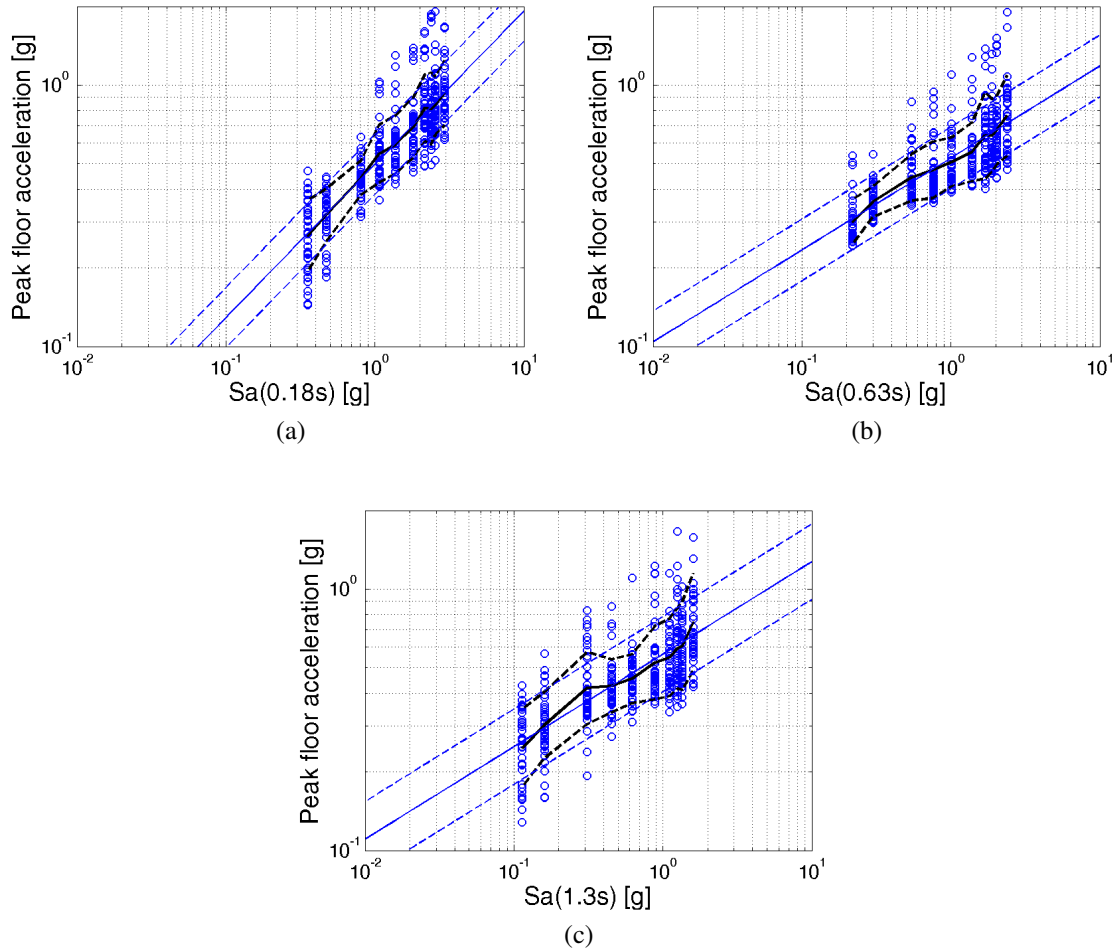


Figure A.24: 2-story perimeter frame (Building No.2064) PFA at (a) $T^* = T_2$, (b) $T^* = T_1$, and (c) $T^* = 2T_1$ for “improved” ground motions selected to match CS μ and σ ($T_1, 2T_1$) and CS μ and 1.3σ (T_2).

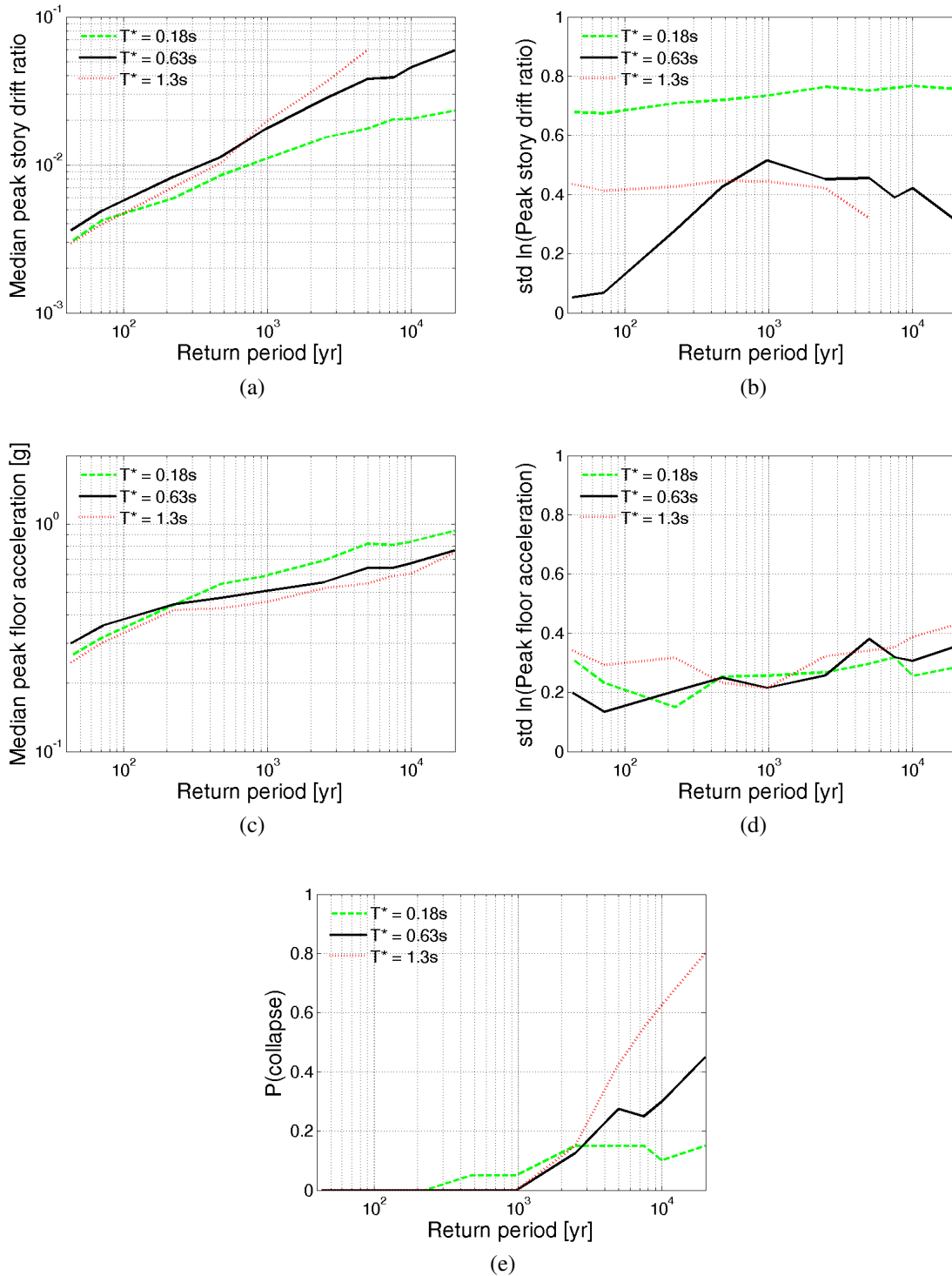
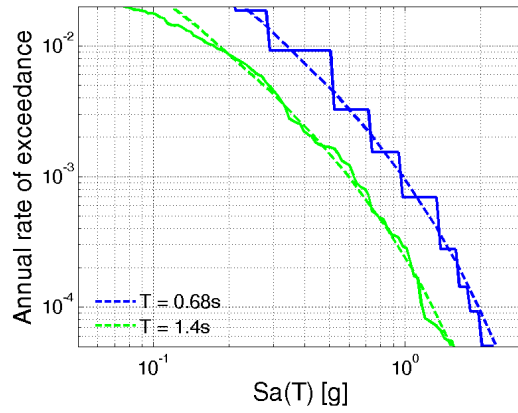
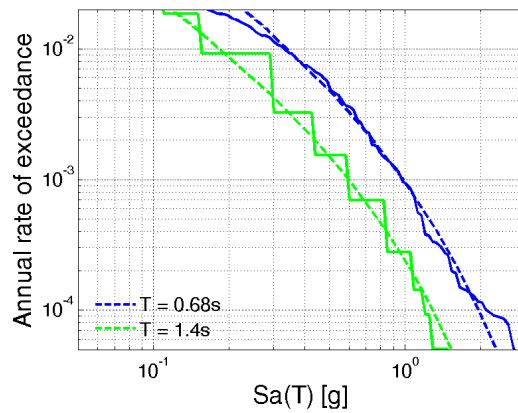


Figure A.25: 2-story perimeter frame (Building No.2064) (a) median $PSDR$, (b) logarithmic standard deviation of $PSDR$, (c) median PFA , (d) logarithmic standard deviation of PFA , and (e) probability of collapse given return period for “improved” ground motions selected to match $CS \mu$ and $\sigma (T_1, 2T_1)$ and $CS \mu$ and $1.3\sigma (T_2)$.



(a)



(b)

Figure A.26: 1-story perimeter frame (Building No.2069) Sa distribution at two periods for ground motions selected at (a) $T^* = T_1$, CS μ and σ and (b) $T^* = 2T_1$, CS μ and σ .

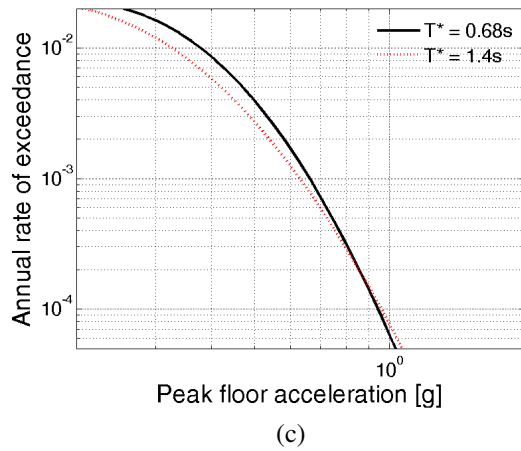
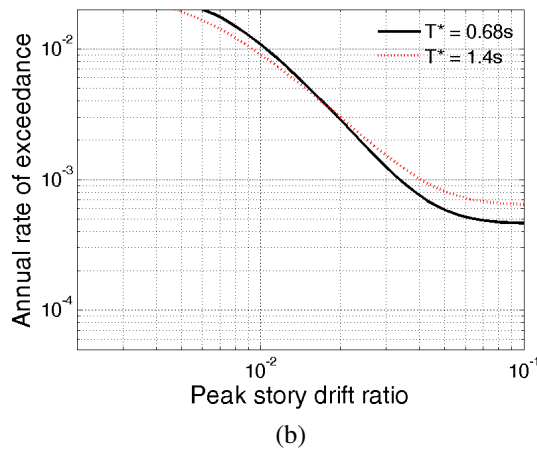
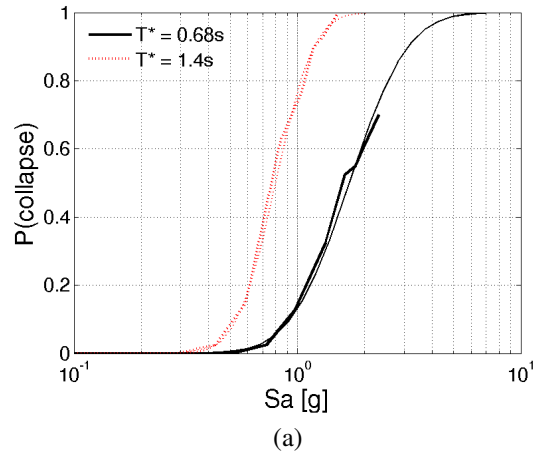


Figure A.27: 1-story perimeter frame (Building No.2069) (a) probability of collapse, (b) *PSDR* hazard, and (c) *PFA* hazard for “basic” ground motions selected to match CS μ and σ .

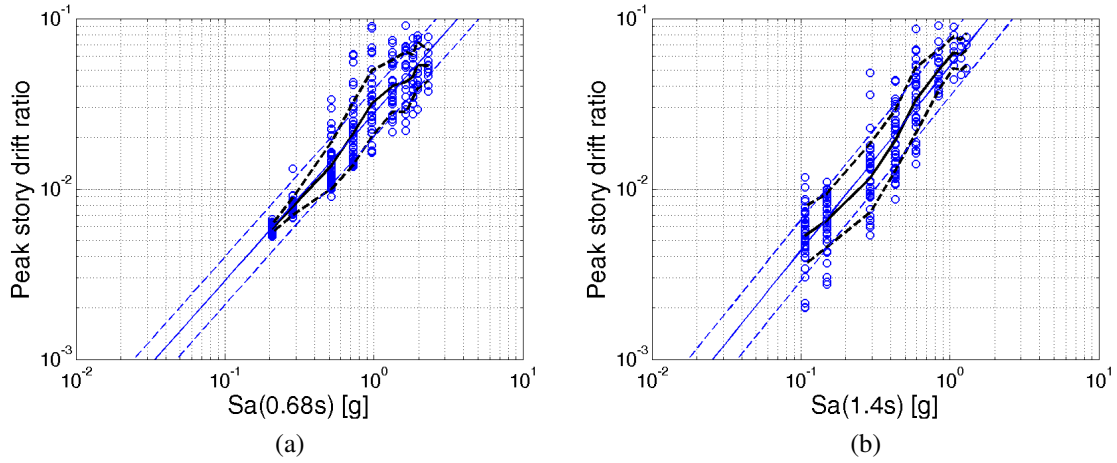


Figure A.28: 1-story perimeter frame (Building No.2069) *PSDR* at (a) $T^* = T_1$ and (b) $T^* = 2T_1$ for “basic” ground motions selected to match CS μ and σ .

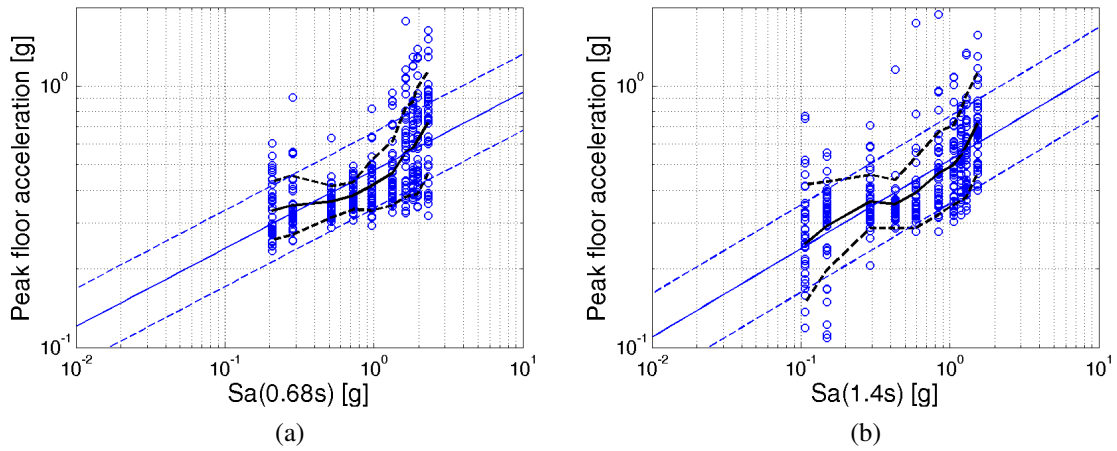


Figure A.29: 1-story perimeter frame (Building No.2069) *PFA* at (a) $T^* = T_1$ and (b) $T^* = 2T_1$ for “basic” ground motions selected to match CS μ and σ .

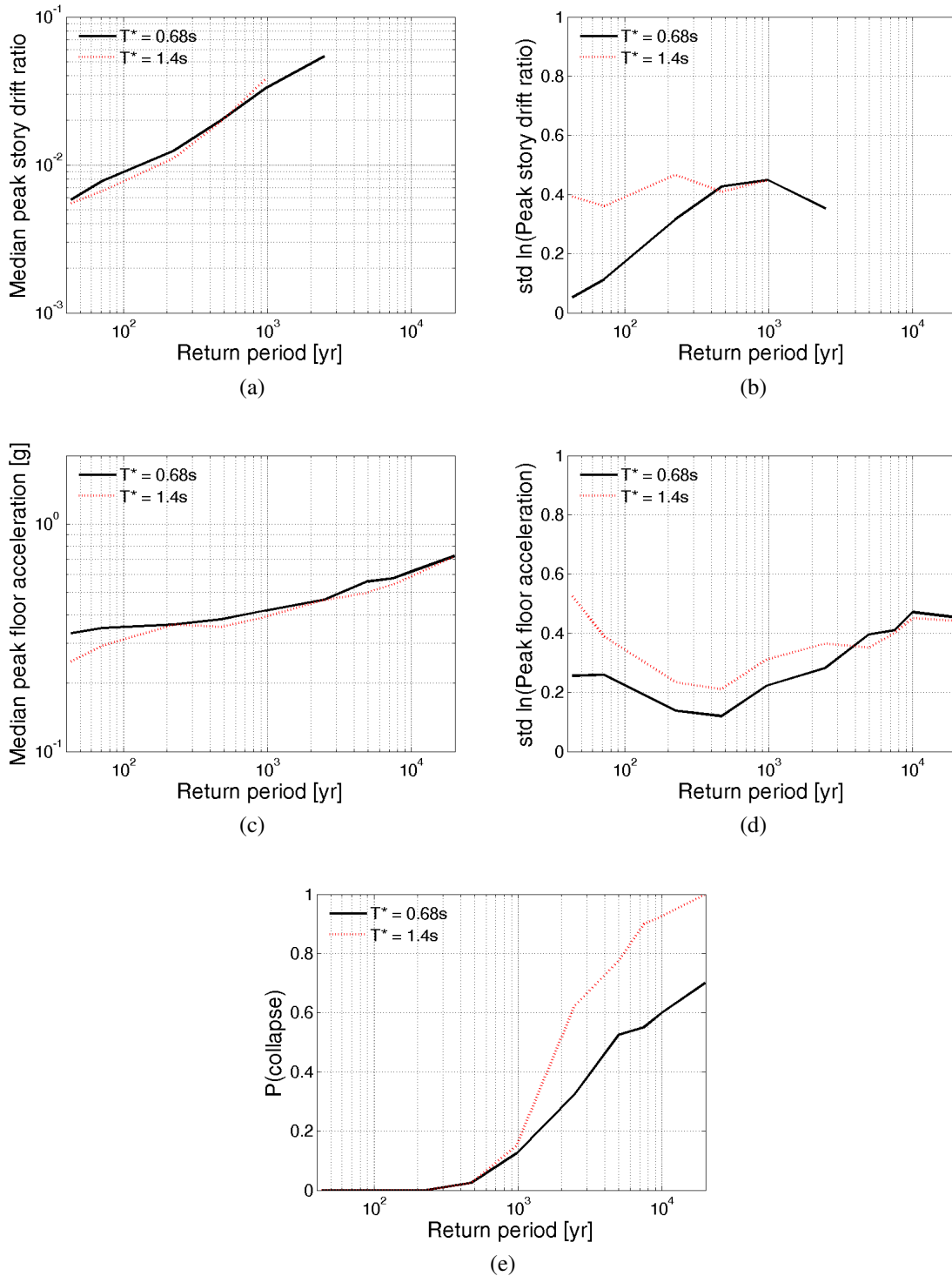


Figure A.30: 1-story perimeter frame (Building No.2069) (a) median *PSDR*, (b) logarithmic standard deviation of *PSDR*, (c) median *PFA*, (d) logarithmic standard deviation of *PFA*, and (e) probability of collapse given return period for “basic” ground motions selected to match CS μ and σ .

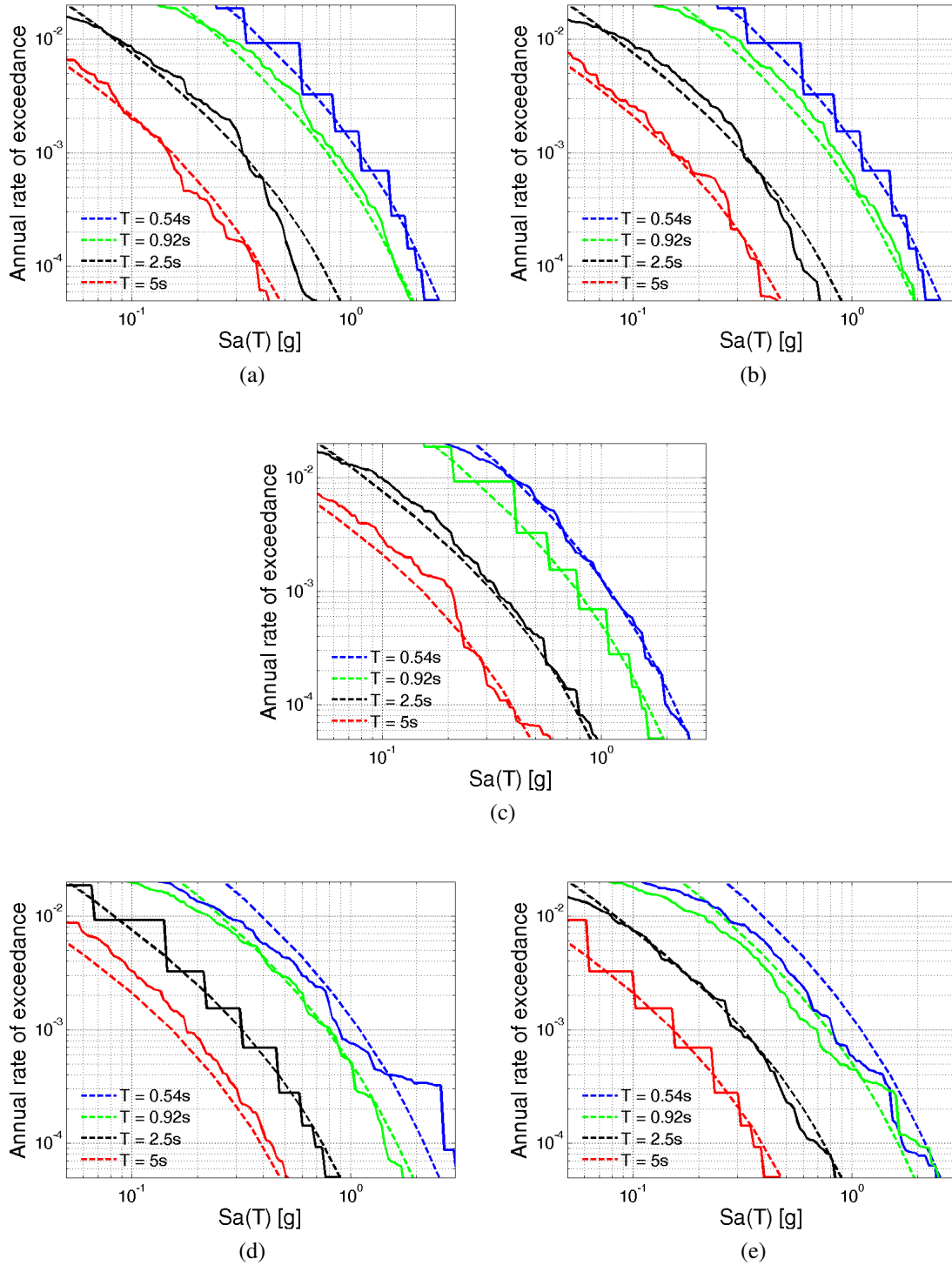


Figure A.31: 20-story space frame (Building No.1021) Sa distribution at four periods for ground motions selected at (a) $T^* = T_3$, CS μ and σ , (b) $T^* = T_3$, CS μ and 1.1σ , (c) $T^* = T_2$, CS μ and σ , (d) $T^* = T_1$, CS μ and σ , and (e) $T^* = 2T_1$, CS μ and σ .

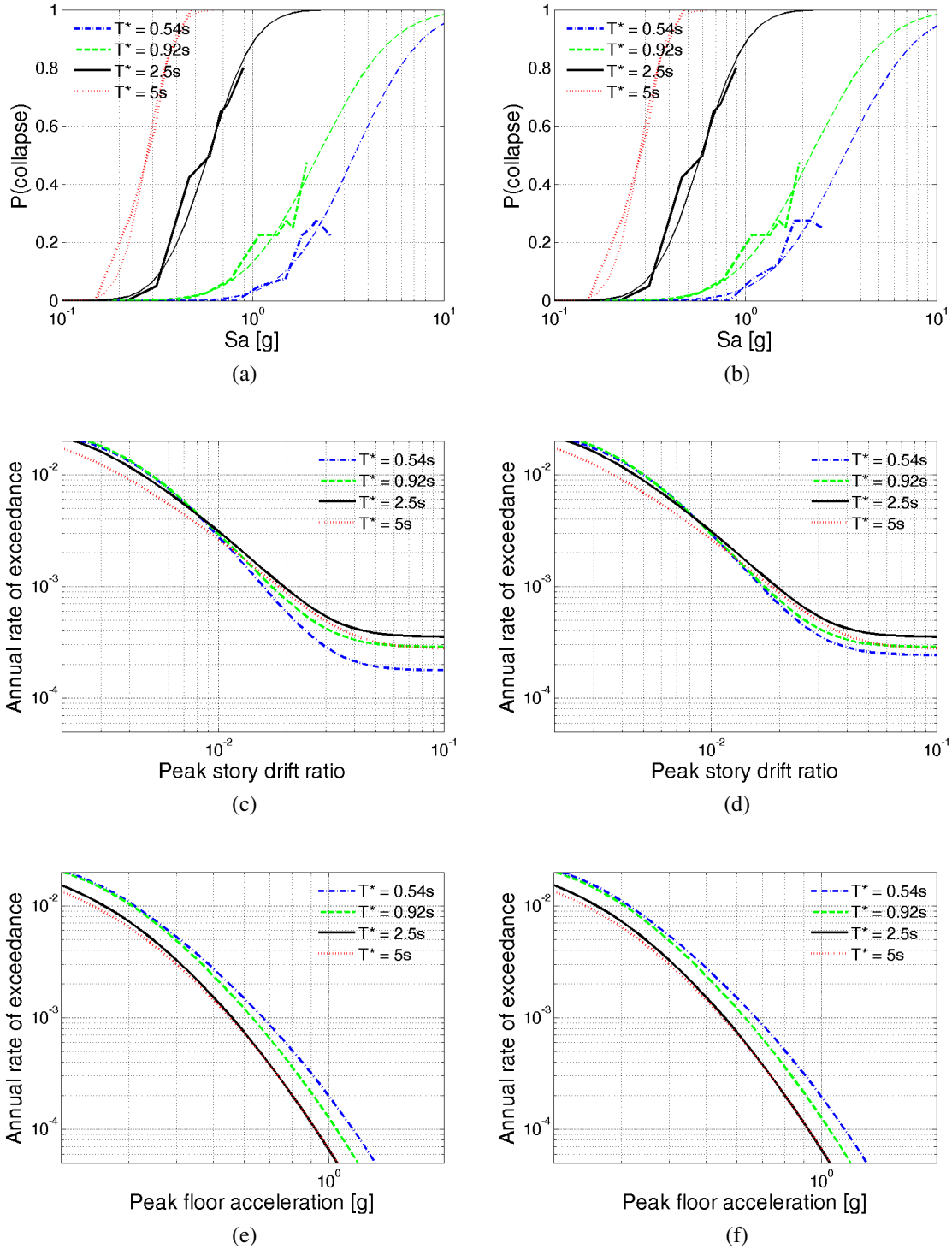


Figure A.32: 20-story space frame (Building No.1021) (a-b) probability of collapse, (c-d) *PSDR* hazard, and (e-f) *PFA* hazard for “basic” ground motions selected to match CS μ and σ ($T_3, T_2, T_1, 2T_1$) at (a, c, e) and “improved” ground motions selected to match CS μ and σ ($T_2, T_1, 2T_1$) and CS μ and 1.1σ (T_3) at (b, d, f).

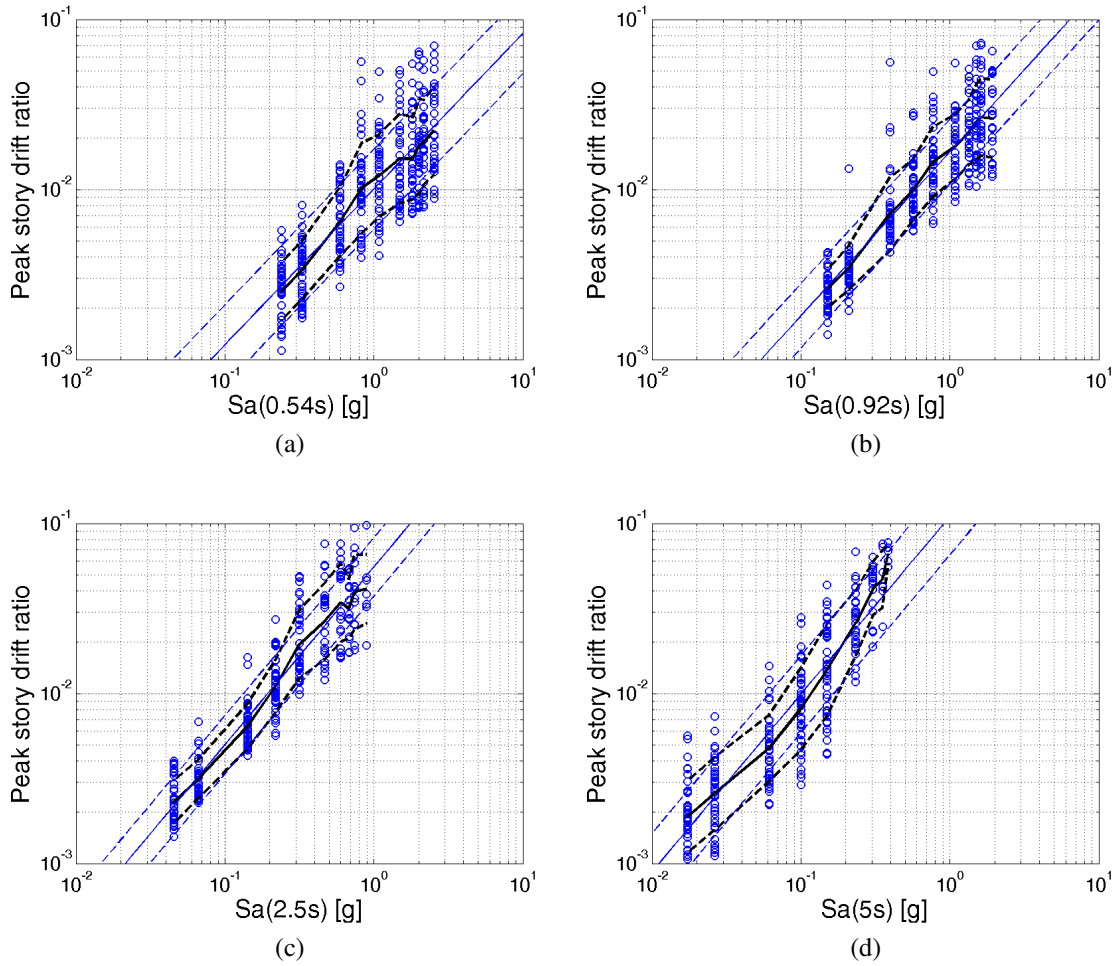


Figure A.33: 20-story space frame (Building No.1021) *PSDR* at (a) $T^* = T_3$, (b) $T^* = T_2$, (c) $T^* = T_1$, and (d) $T^* = 2T_1$ for “improved” ground motions selected to match CS μ and σ ($T_2, T_1, 2T_1$) and CS μ and 1.1σ (T_3).

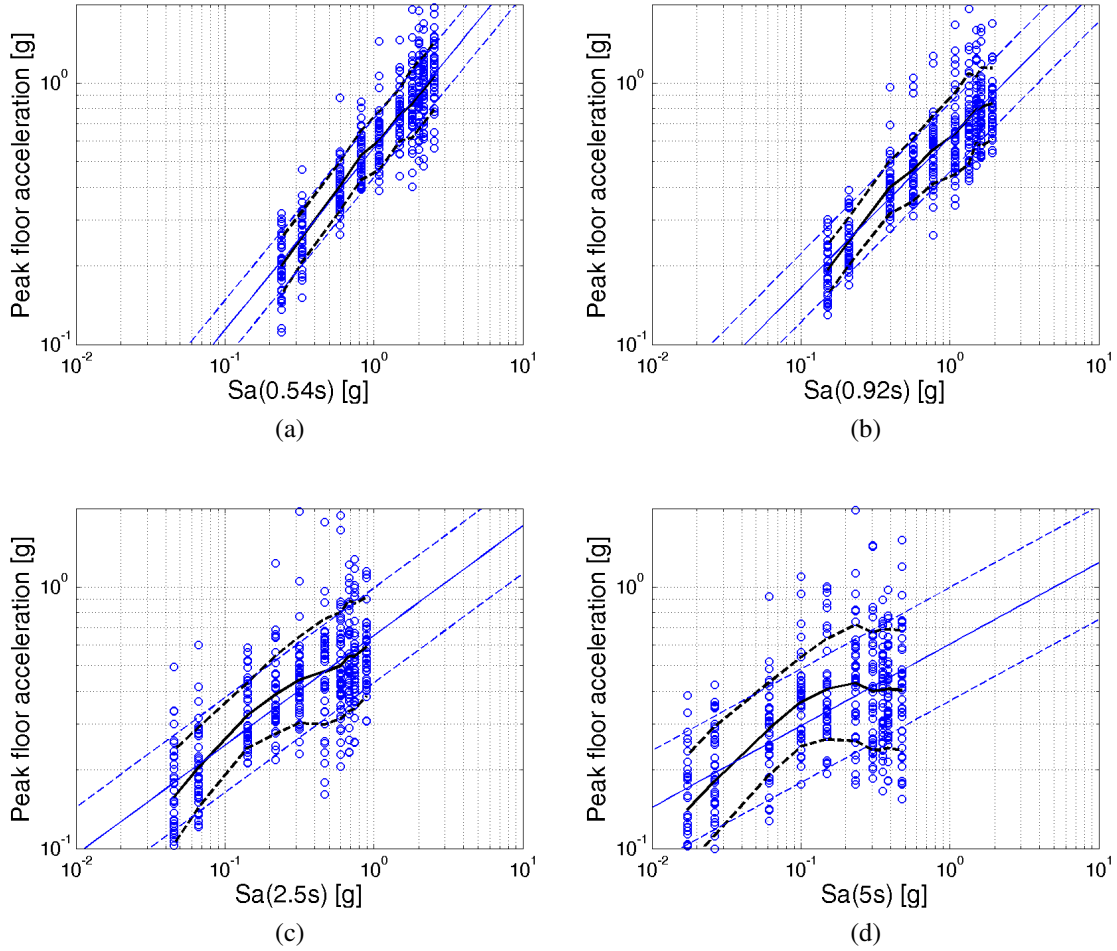


Figure A.34: 20-story space frame (Building No.1021) PFA at (a) $T^* = T_3$, (b) $T^* = T_2$, (c) $T^* = T_1$, and (d) $T^* = 2T_1$ for “improved” ground motions selected to match CS μ and σ ($T_2, T_1, 2T_1$) and CS μ and 1.1σ (T_3).

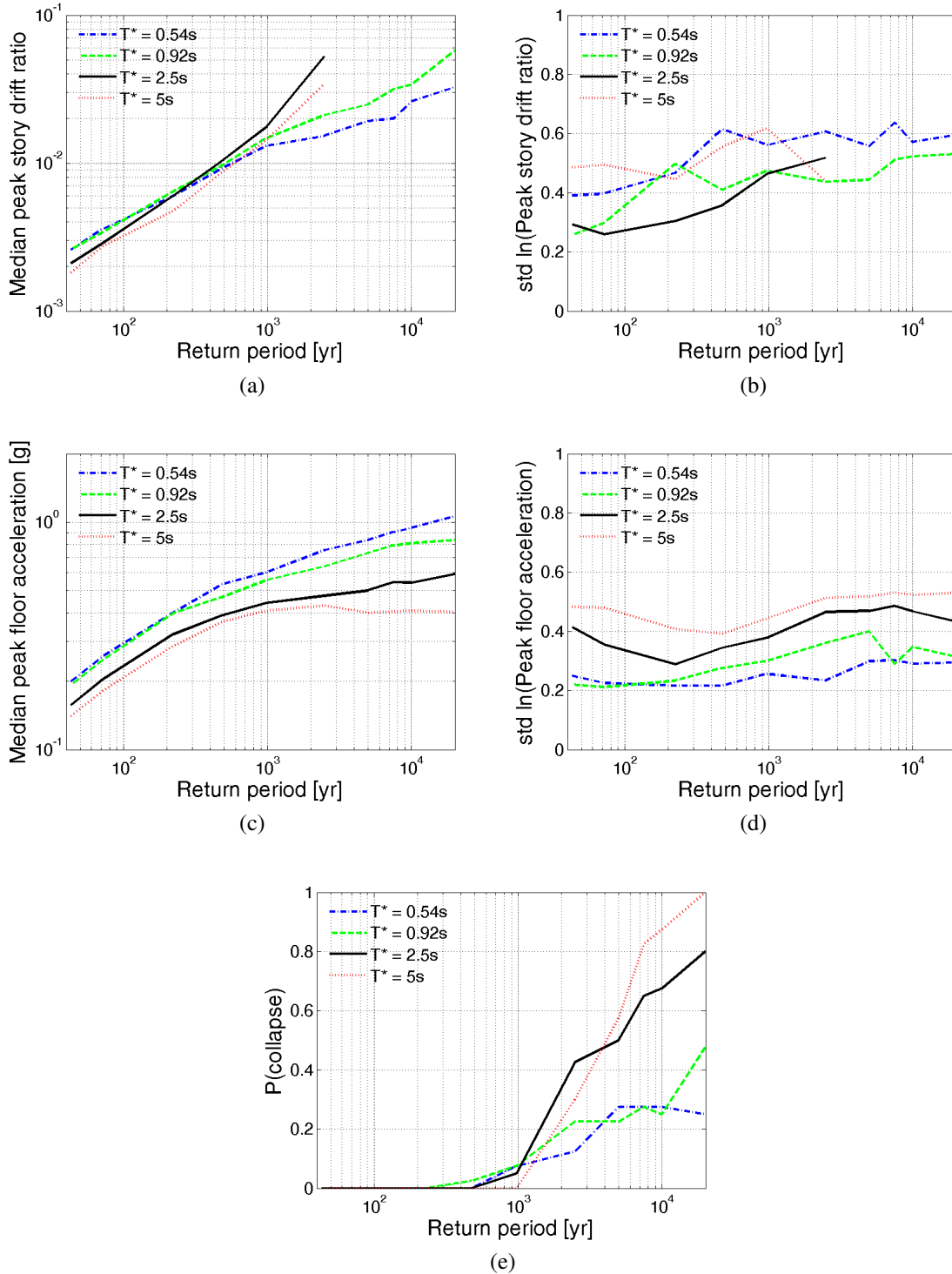


Figure A.35: 20-story space frame (Building No.1021) (a) median *PSDR*, (b) logarithmic standard deviation of *PSDR*, (c) median *PFA*, (d) logarithmic standard deviation of *PFA*, and (e) probability of collapse given “improved” return period for ground motions selected to match CS μ and σ ($T_2, T_1, 2T_1$) and CS μ and 1.1σ (T_3).

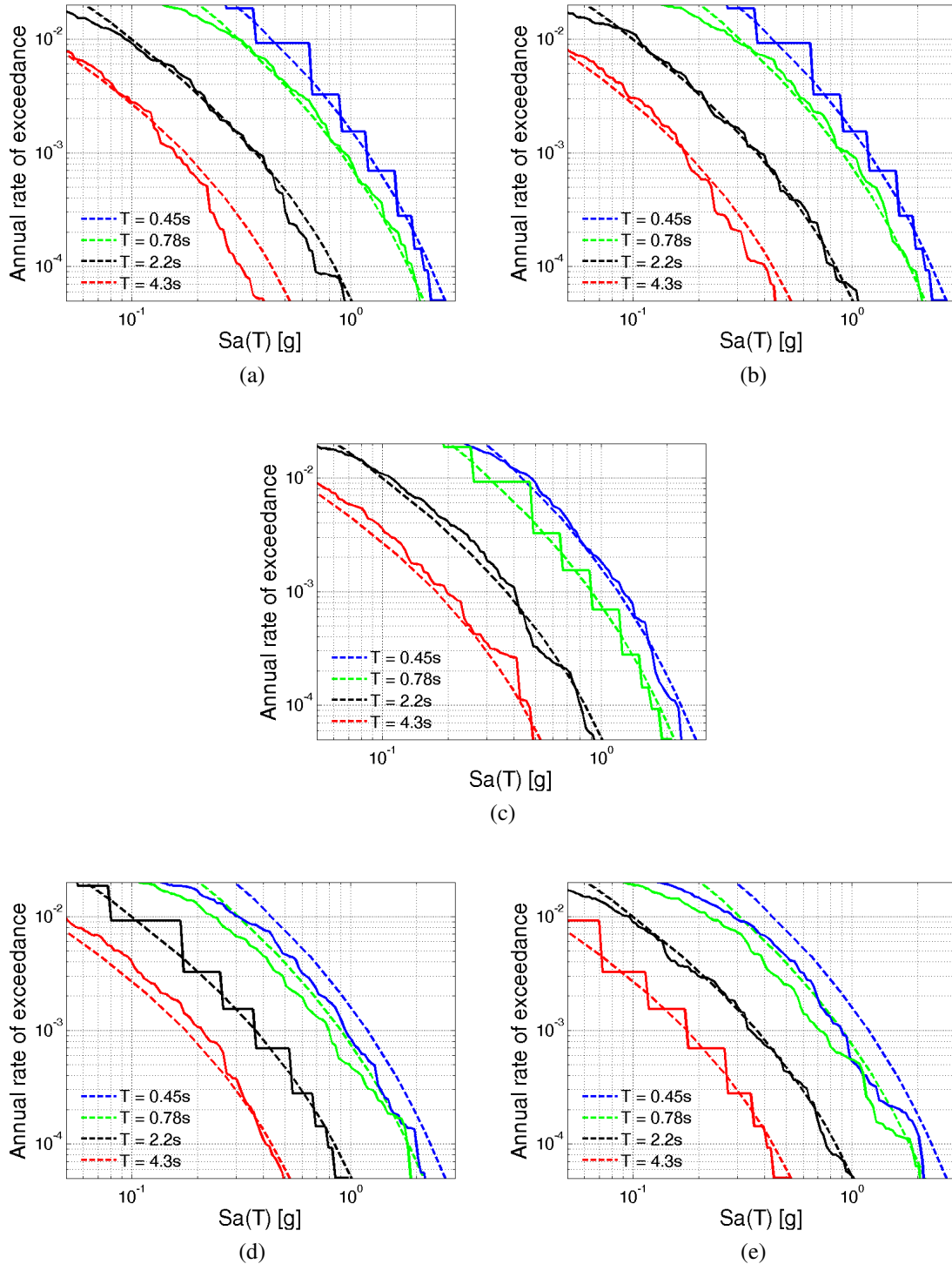


Figure A.36: 12-story space frame (Building No.1014) Sa distribution at four periods for ground motions selected at (a) $T^* = T_3$, CS μ and σ , (b) $T^* = T_3$, CS μ and 1.1σ , (c) $T^* = T_2$, CS μ and σ , (d) $T^* = T_1$, CS μ and σ , and (e) $T^* = 2T_1$, CS μ and σ .

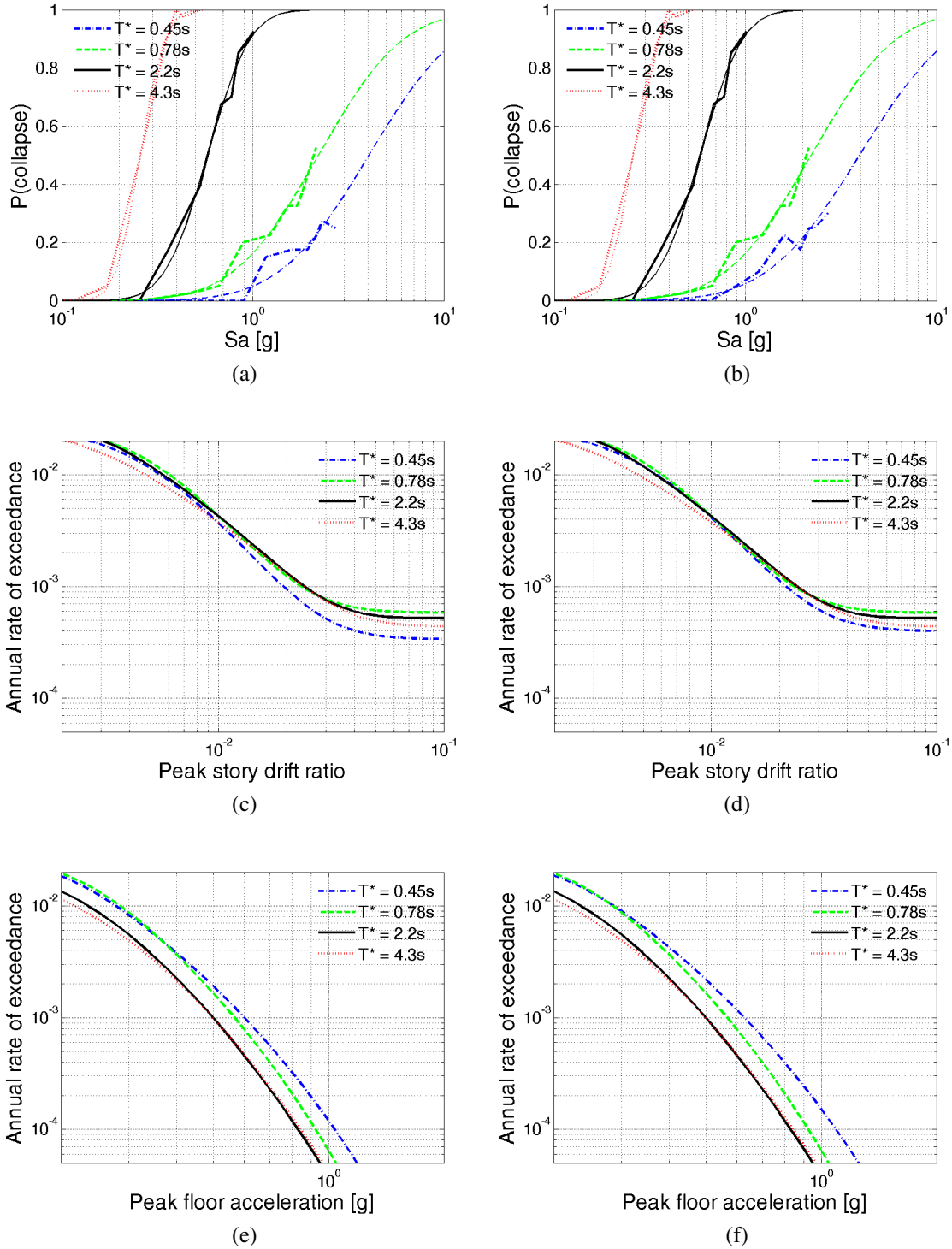


Figure A.37: 12-story space frame (Building No.1014) (a-b) probability of collapse, (c-d) *PSDR* hazard, and (e-f) *PFA* hazard for “basic” ground motions selected to match CS μ and σ ($T_3, T_2, T_1, 2T_1$) at (a, c, e) and “improved” ground motions selected to match CS μ and σ ($T_2, T_1, 2T_1$) and CS μ and 1.1σ (T_3) at (b, d, f).

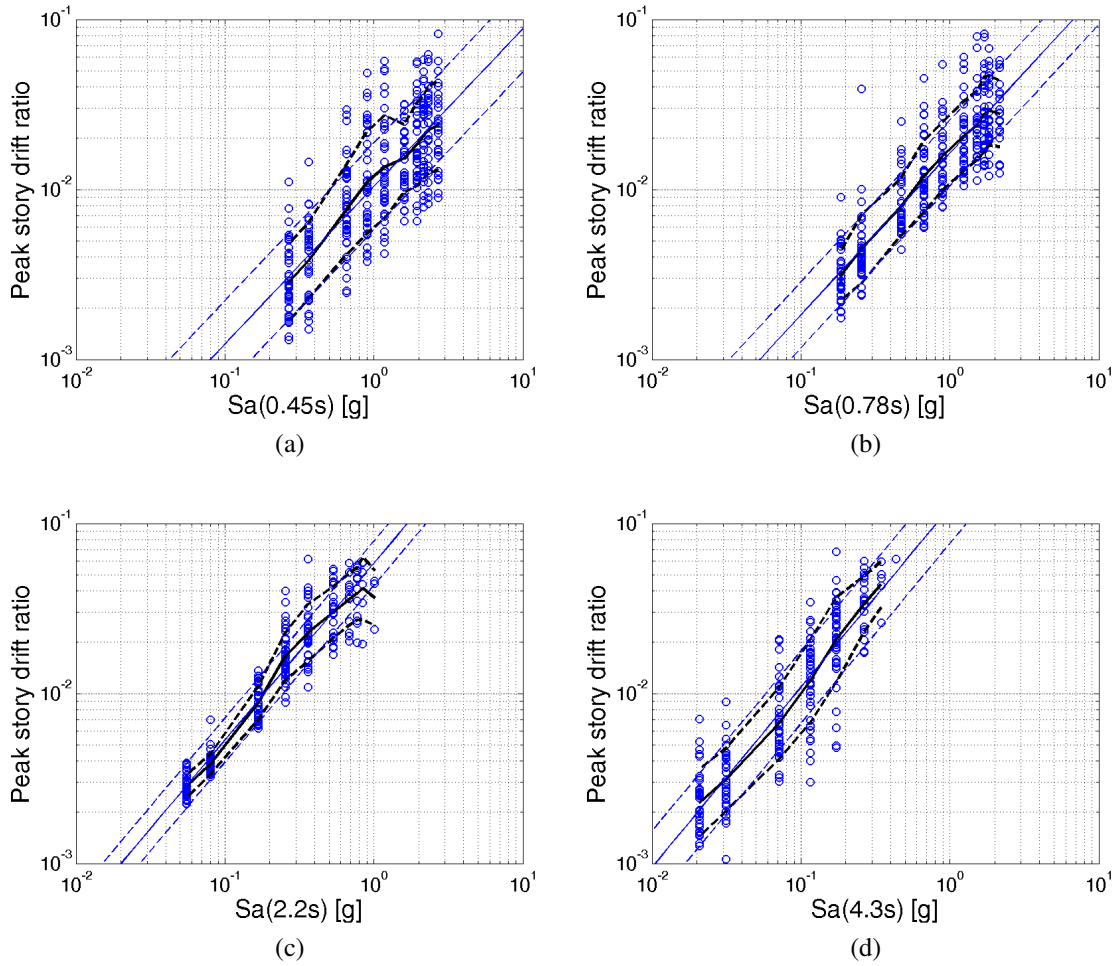


Figure A.38: 12-story space frame (Building No.1014) *PSDR* at (a) $T^* = T_3$, (b) $T^* = T_2$, (c) $T^* = T_1$, and (d) $T^* = 2T_1$ for “improved” ground motions selected to match CS μ and σ ($T_2, T_1, 2T_1$) and CS μ and 1.1σ (T_3).

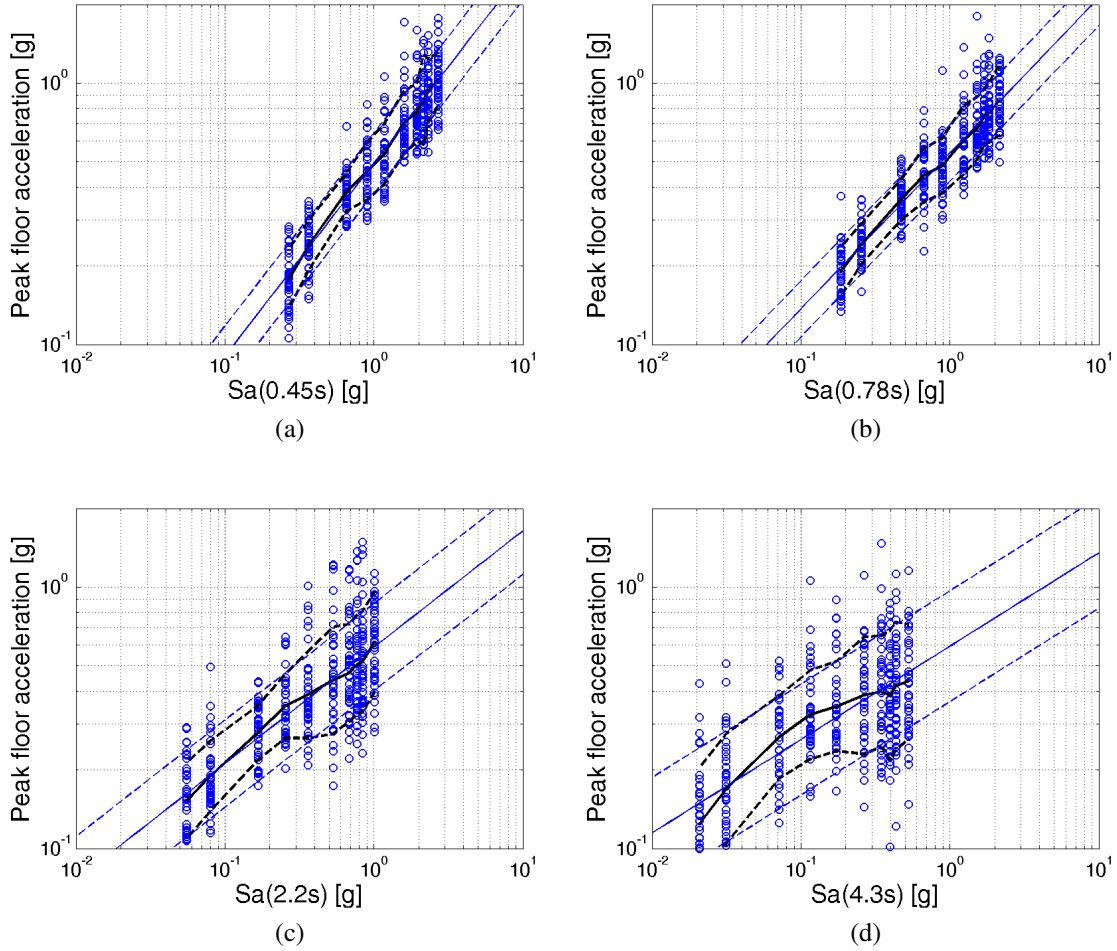


Figure A.39: 12-story space frame (Building No.1014) PFA at (a) $T^* = T_3$, (b) $T^* = T_2$, (c) $T^* = T_1$, and (d) $T^* = 2T_1$ for “improved” ground motions selected to match CS μ and σ ($T_2, T_1, 2T_1$) and CS μ and 1.1σ (T_3).

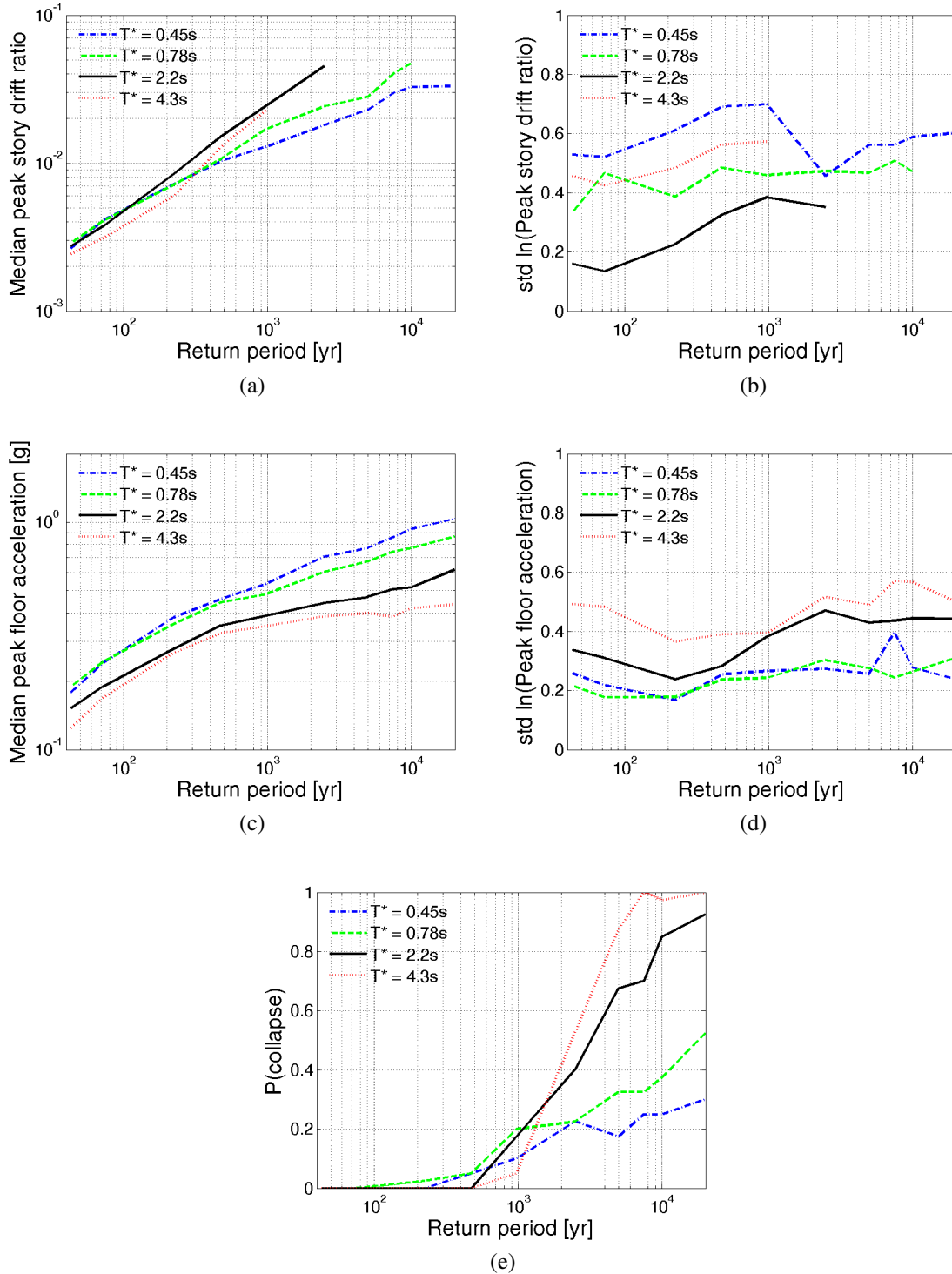


Figure A.40: 12-story space frame (Building No.1014) (a) median *PSDR*, (b) logarithmic standard deviation of *PSDR*, (c) median *PFA*, (d) logarithmic standard deviation of *PFA*, and (e) probability of collapse given return period for “improved” ground motions selected to match CS μ and σ ($T_2, T_1, 2T_1$) and CS μ and 1.1σ (T_3).

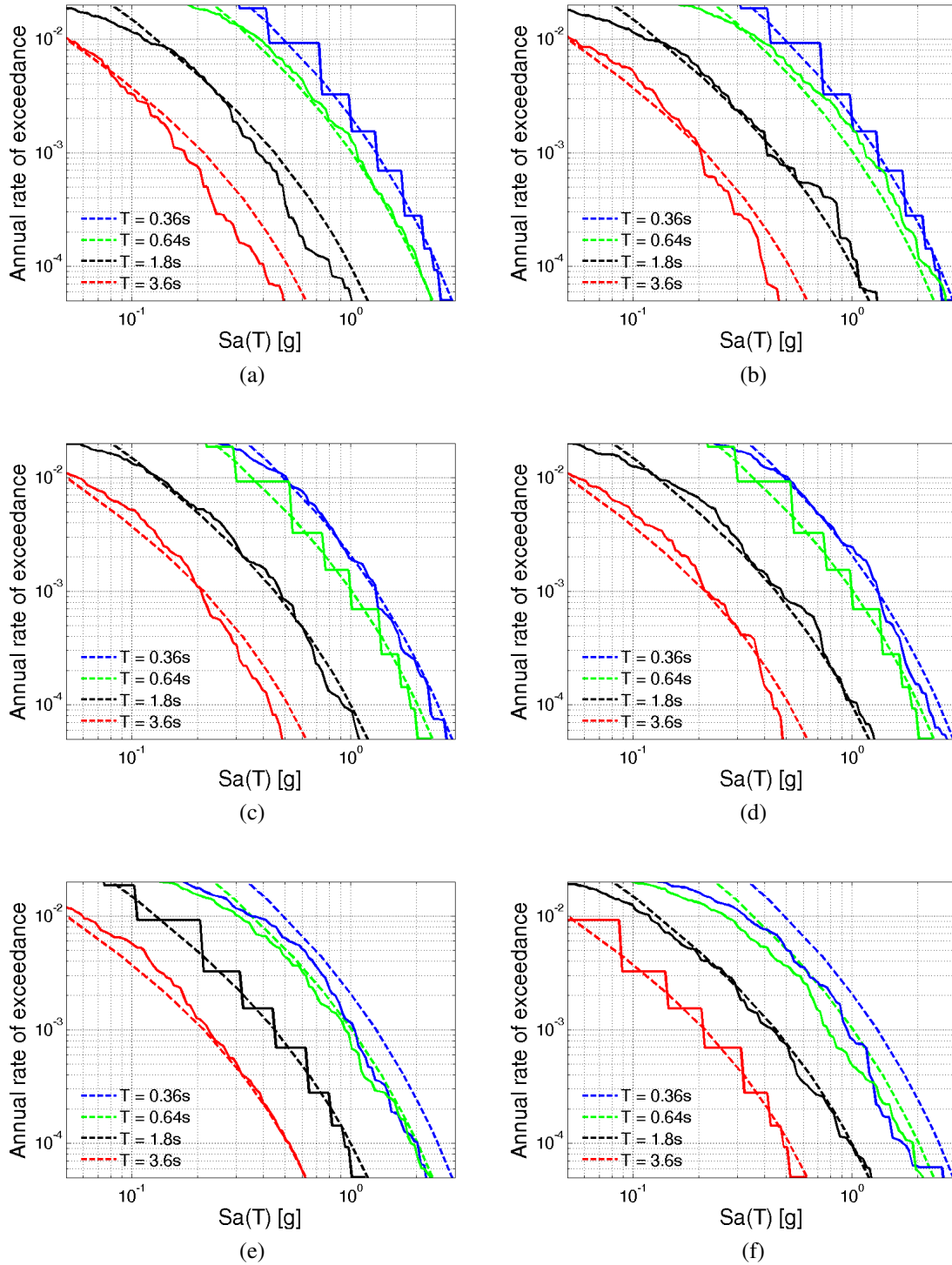


Figure A.41: 8-story space frame (Building No.1012) Sa distribution at four periods for ground motions selected at (a) $T^* = T_3$, CS μ and σ , (b) $T^* = T_3$, CS μ and 1.2σ , (c) $T^* = T_2$, CS μ and σ , (d) $T^* = T_2$, CS μ and 1.1σ , (e) $T^* = T_1$, CS μ and σ , and (f) $T^* = 2T_1$, CS μ and σ .

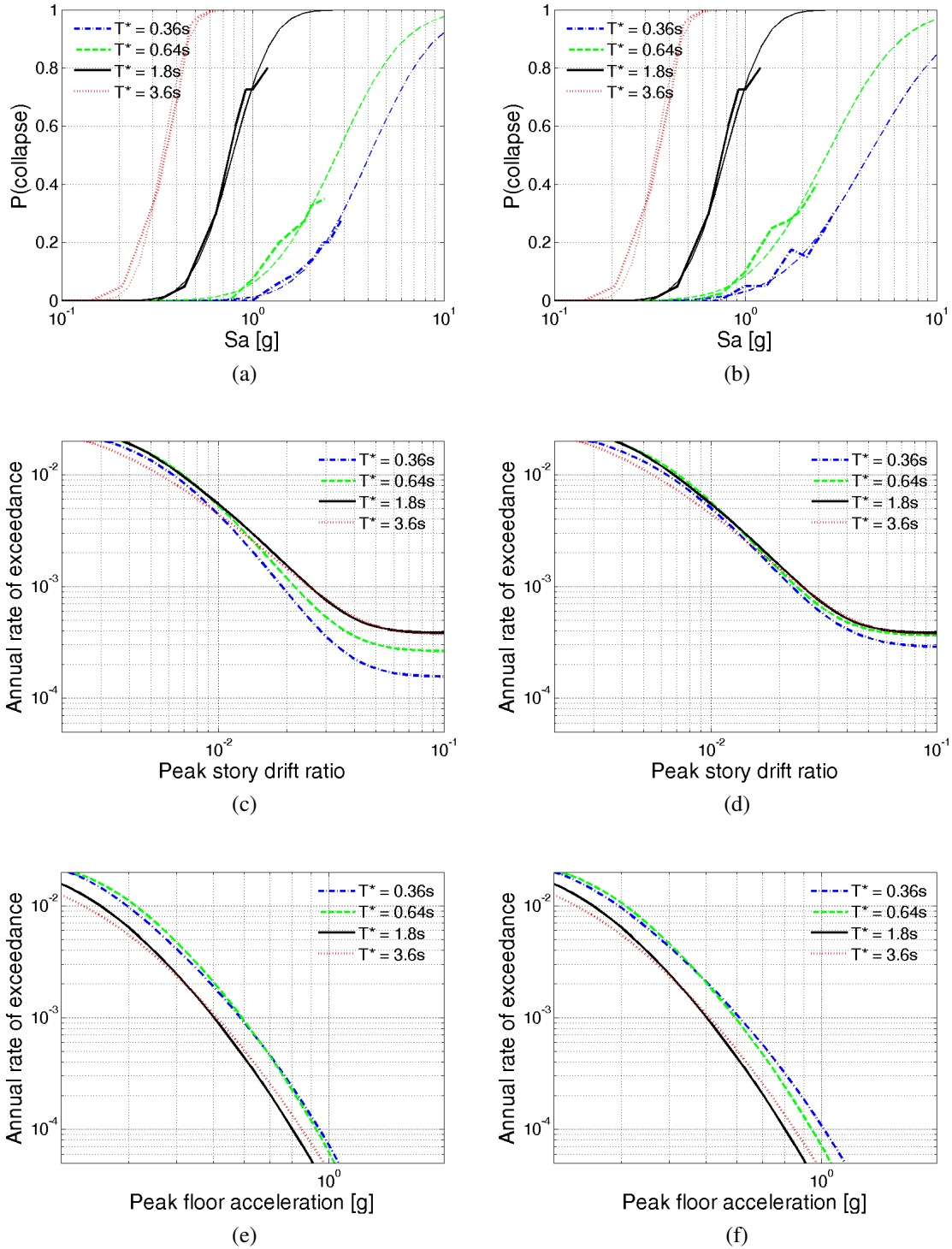


Figure A.42: 8-story space frame (Building No.1012) (a-b) probability of collapse, (c-d) *PSDR* hazard, and (e-f) *PFA* hazard for “basic” ground motions selected to match CS μ and σ ($T_3, T_2, T_1, 2T_1$) at (a, c, e) and “improved” ground motions selected to match CS μ and σ ($T_1, 2T_1$), CS μ and 1.1σ (T_2), and CS μ and 1.2σ (T_3) at (b, d, f).

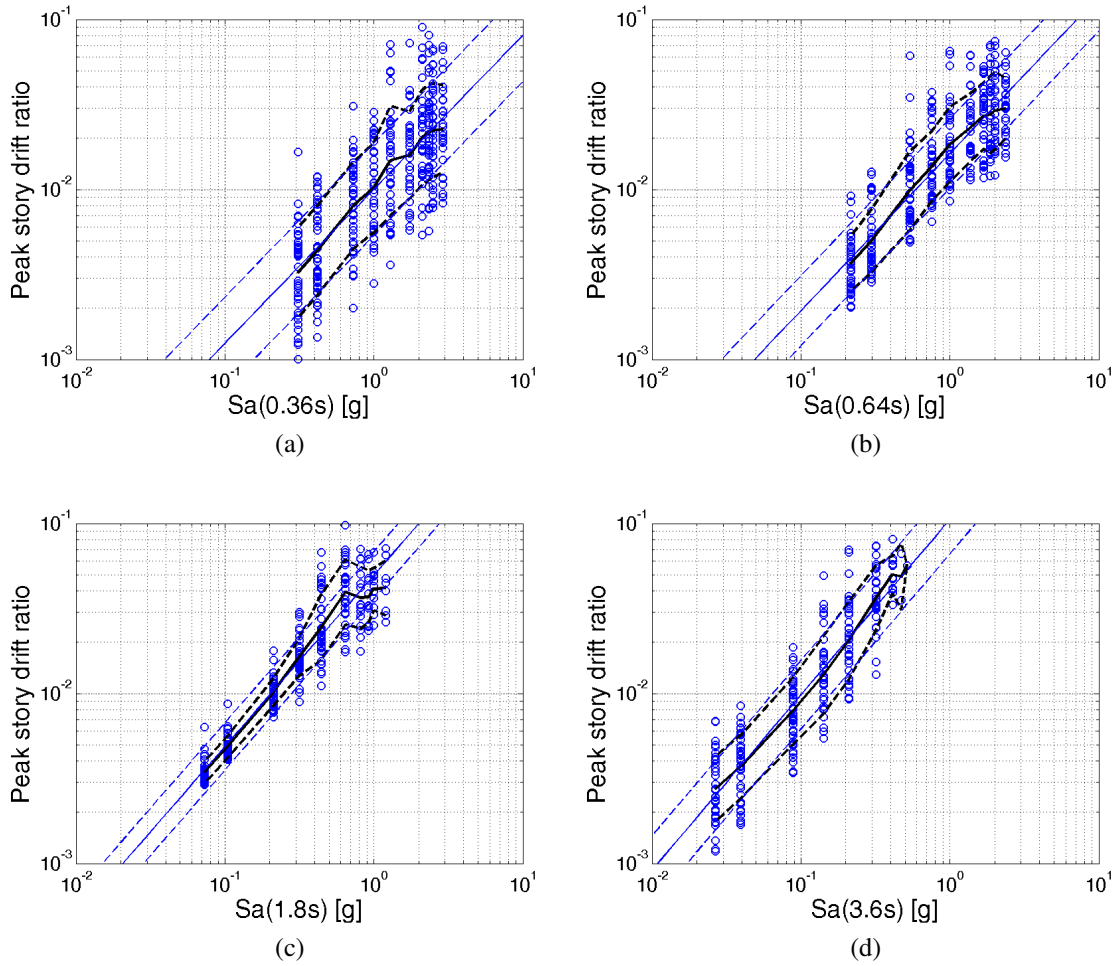


Figure A.43: 8-story space frame (Building No.1012) *PSDR* at (a) $T^* = T_3$, (b) $T^* = T_2$, (c) $T^* = T_1$, and (d) $T^* = 2T_1$ for “improved” ground motions selected to match CS μ and σ ($T_1, 2T_1$), CS μ and 1.1σ (T_2), and CS μ and 1.2σ (T_3).

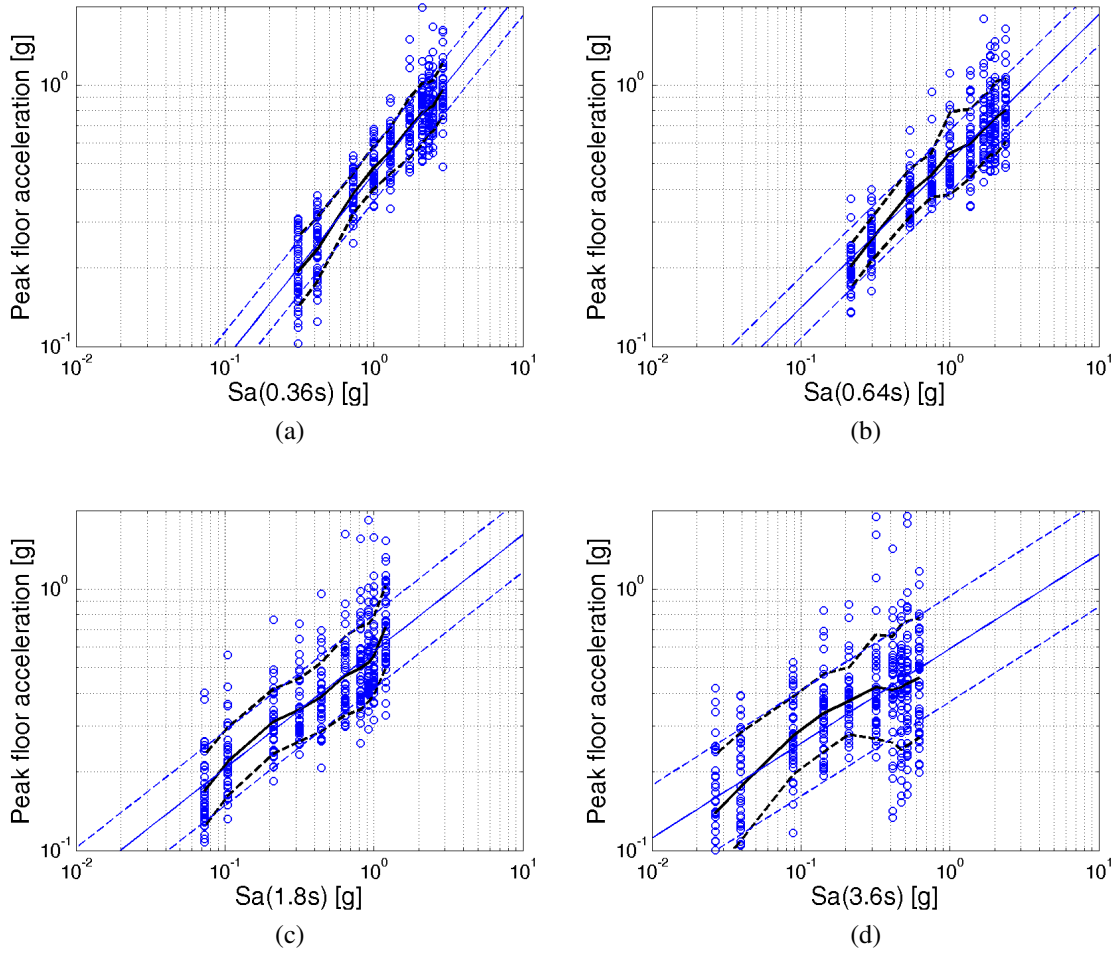


Figure A.44: 8-story space frame (Building No.1012) PFA at (a) $T^* = T_3$, (b) $T^* = T_2$, (c) $T^* = T_1$, and (d) $T^* = 2T_1$ for “improved” ground motions selected to match CS μ and σ ($T_1, 2T_1$), CS μ and 1.1σ (T_2), and CS μ and 1.2σ (T_3).

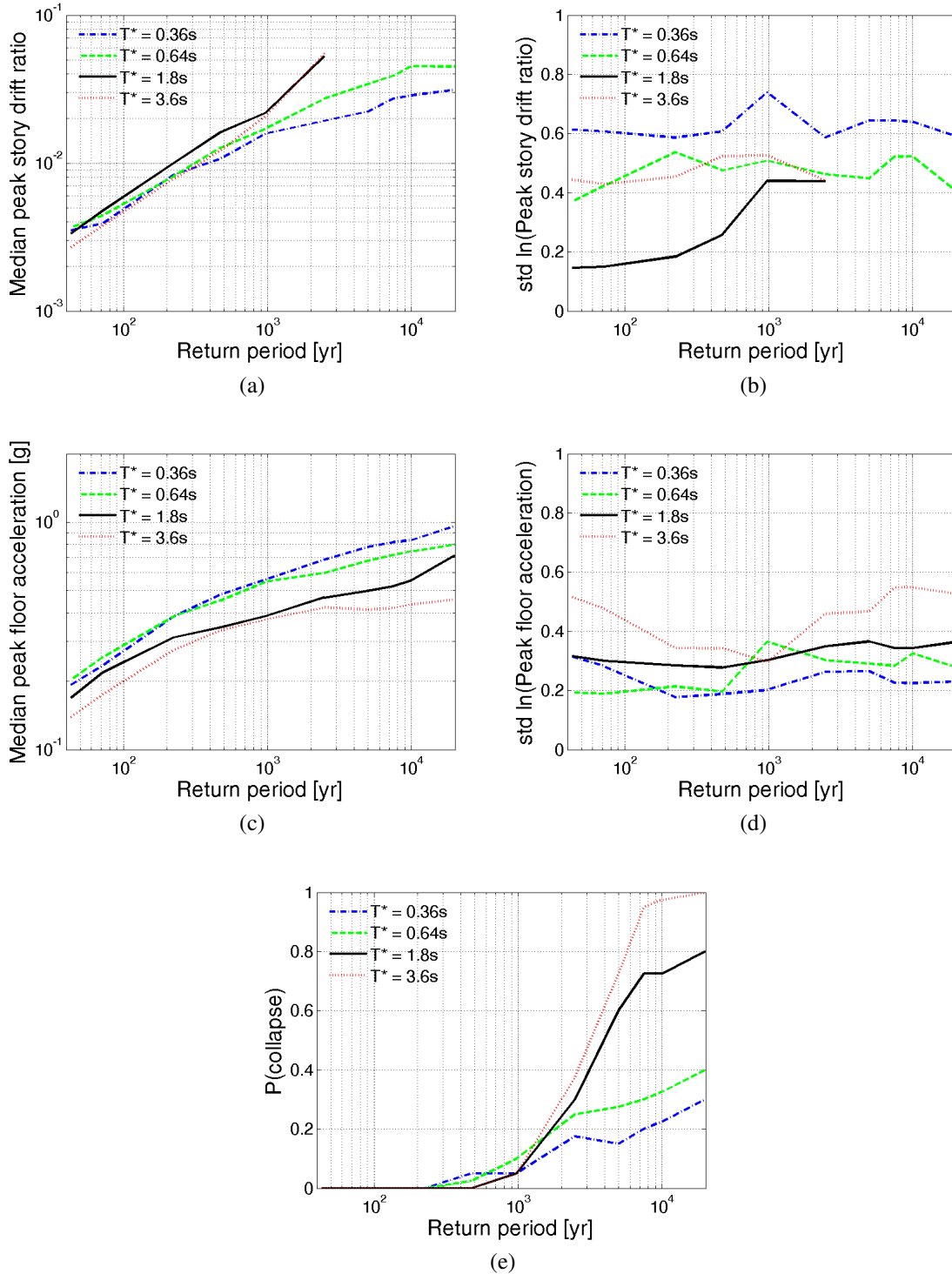


Figure A.45: 8-story space frame (Building No.1012) (a) median *PSDR*, (b) logarithmic standard deviation of *PSDR*, (c) median *PFA*, (d) logarithmic standard deviation of *PFA*, and (e) probability of collapse given return period for “improved” ground motions selected to match CS μ and σ ($T_1, 2T_1$), CS μ and 1.1σ (T_2), and CS μ and 1.2σ (T_3).

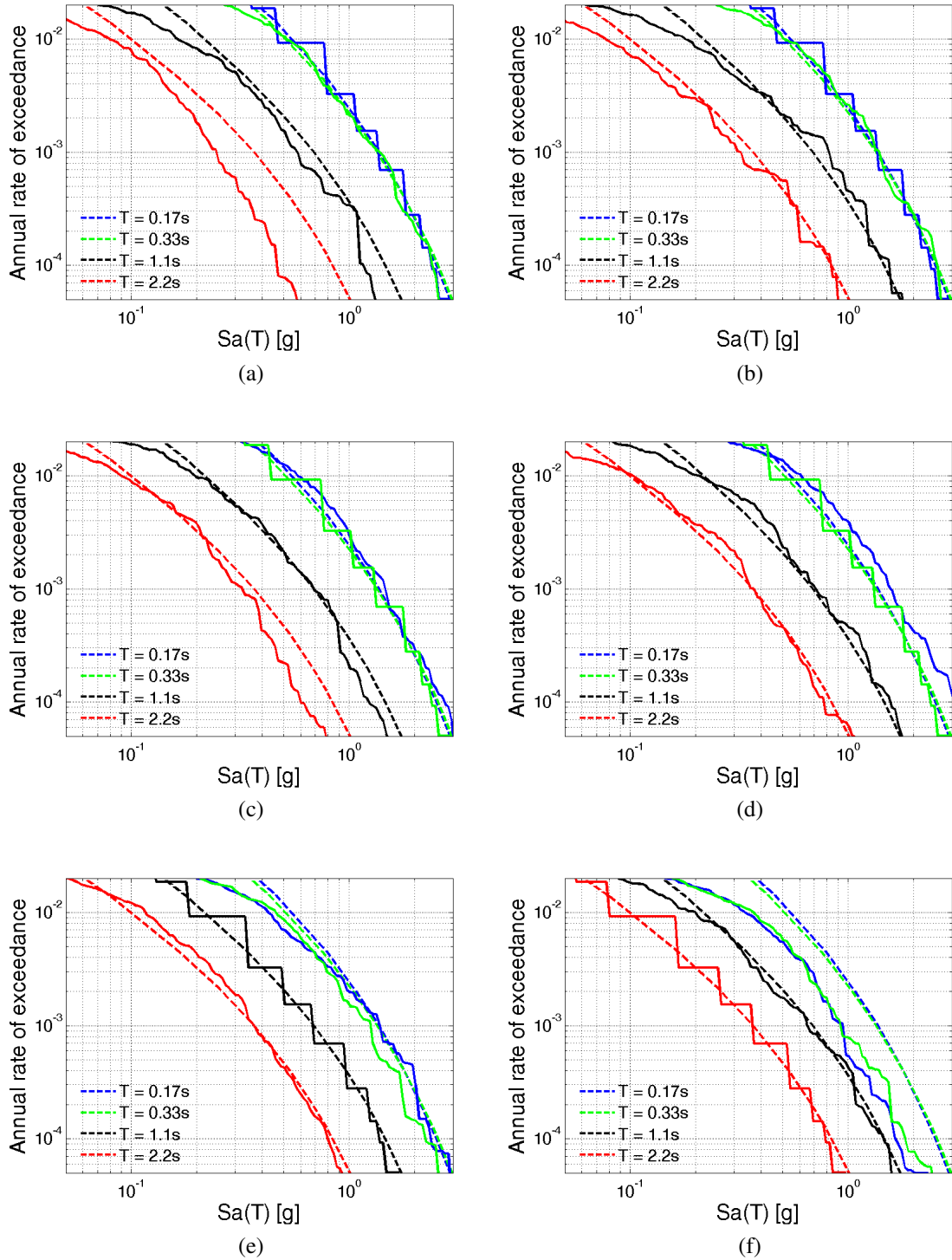


Figure A.46: 4-story space frame (Building No.1003) Sa distribution at four periods for ground motions selected at (a) $T^* = T_3$, CS μ and σ , (b) $T^* = T_3$, CS μ and 1.2σ , (c) $T^* = T_2$, CS μ and σ , (d) $T^* = T_2$, CS μ and 1.2σ , (e) $T^* = T_1$, CS μ and σ , and (f) $T^* = 2T_1$, CS μ and σ .

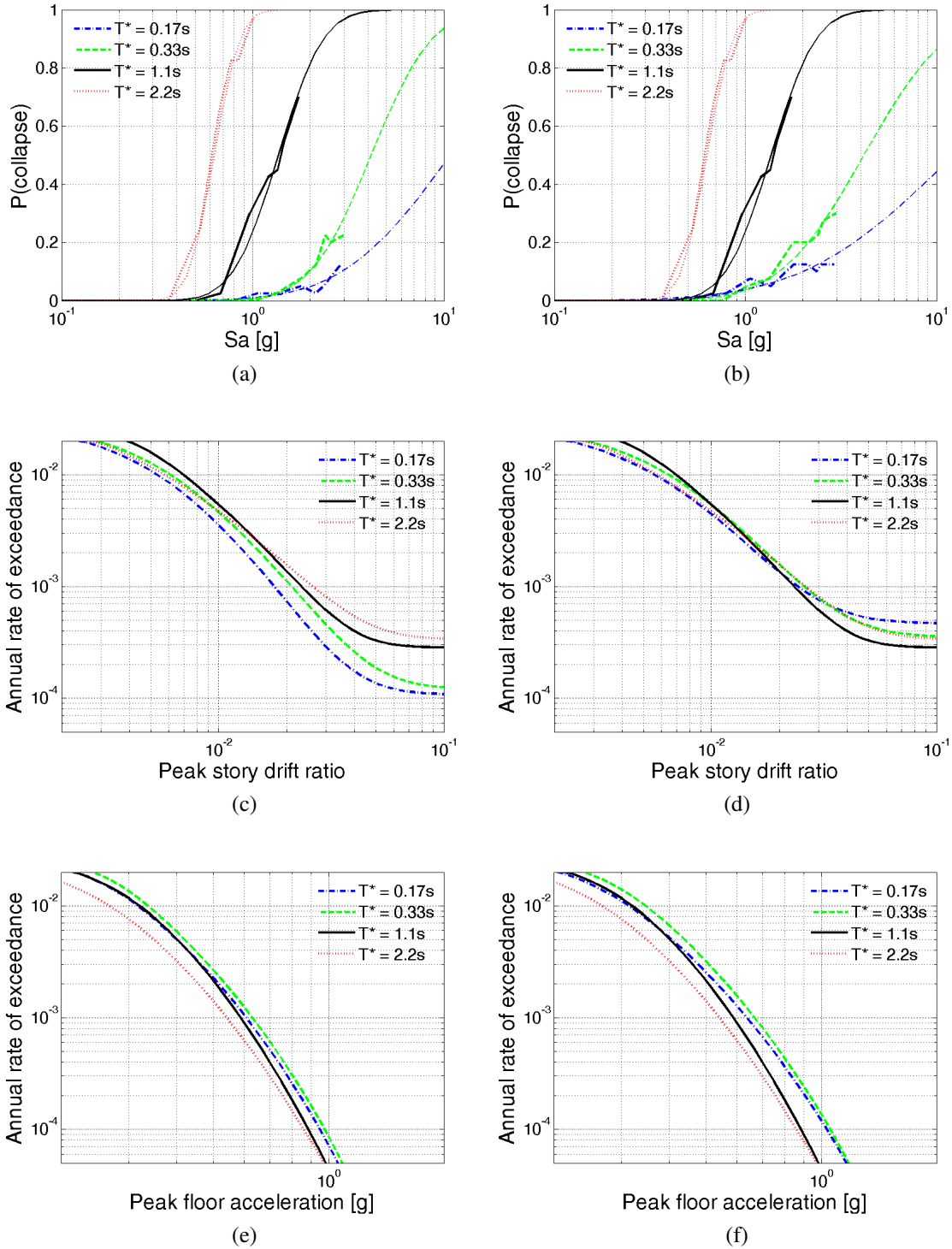


Figure A.47: 4-story space frame (Building No.1003) (a-b) probability of collapse, (c-d) *PSDR* hazard, and (e-f) *PFA* hazard for “basic” ground motions selected to match CS μ and σ ($T_3, T_2, T_1, 2T_1$) at (a, c, e) and “improved” ground motions selected to match CS μ and σ ($T_1, 2T_1$) and CS μ and 1.2σ (T_3, T_2) at (b, d, f).

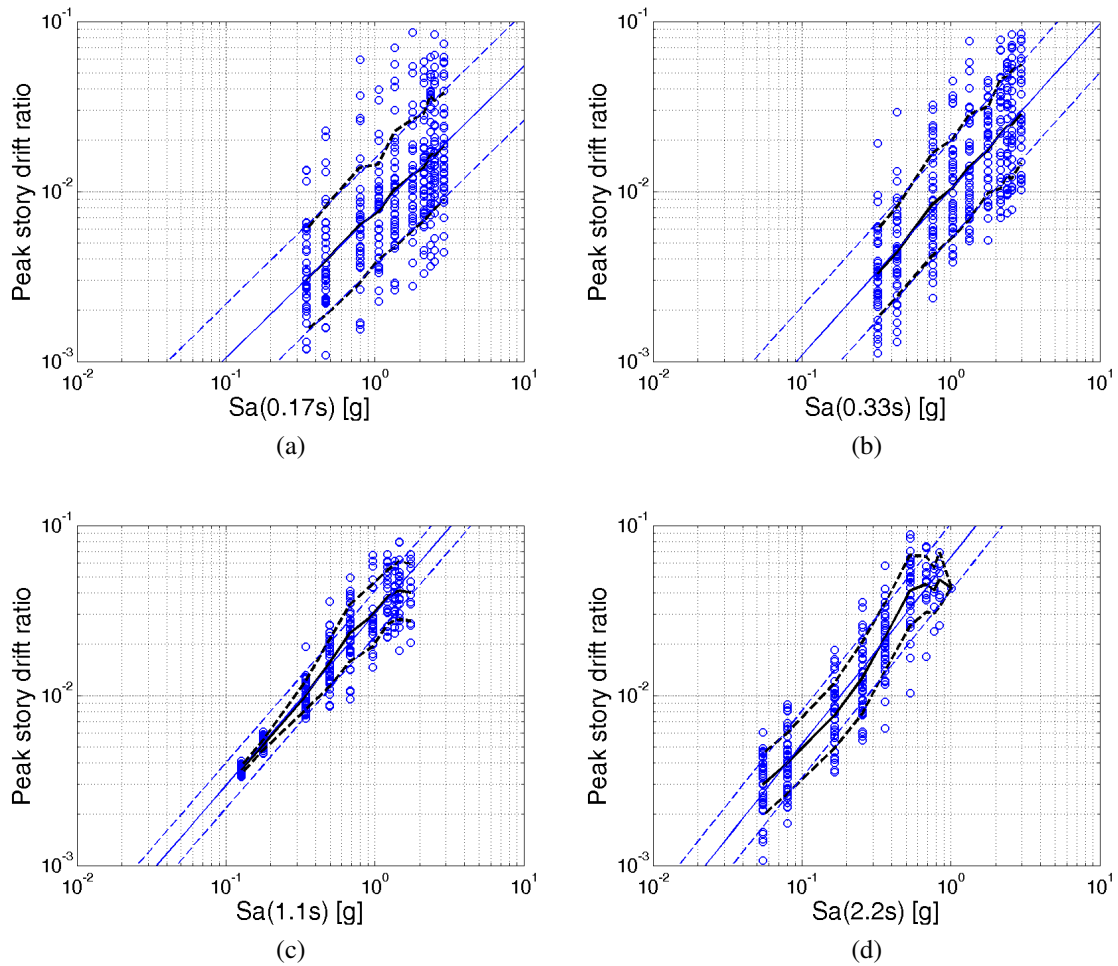


Figure A.48: 4-story space frame (Building No.1003) *PSDR* at (a) $T^* = T_3$, (b) $T^* = T_2$, (c) $T^* = T_1$, and (d) $T^* = 2T_1$ for “improved” ground motions selected to match CS μ and σ ($T_1, 2T_1$) and CS μ and 1.2σ (T_3, T_2).

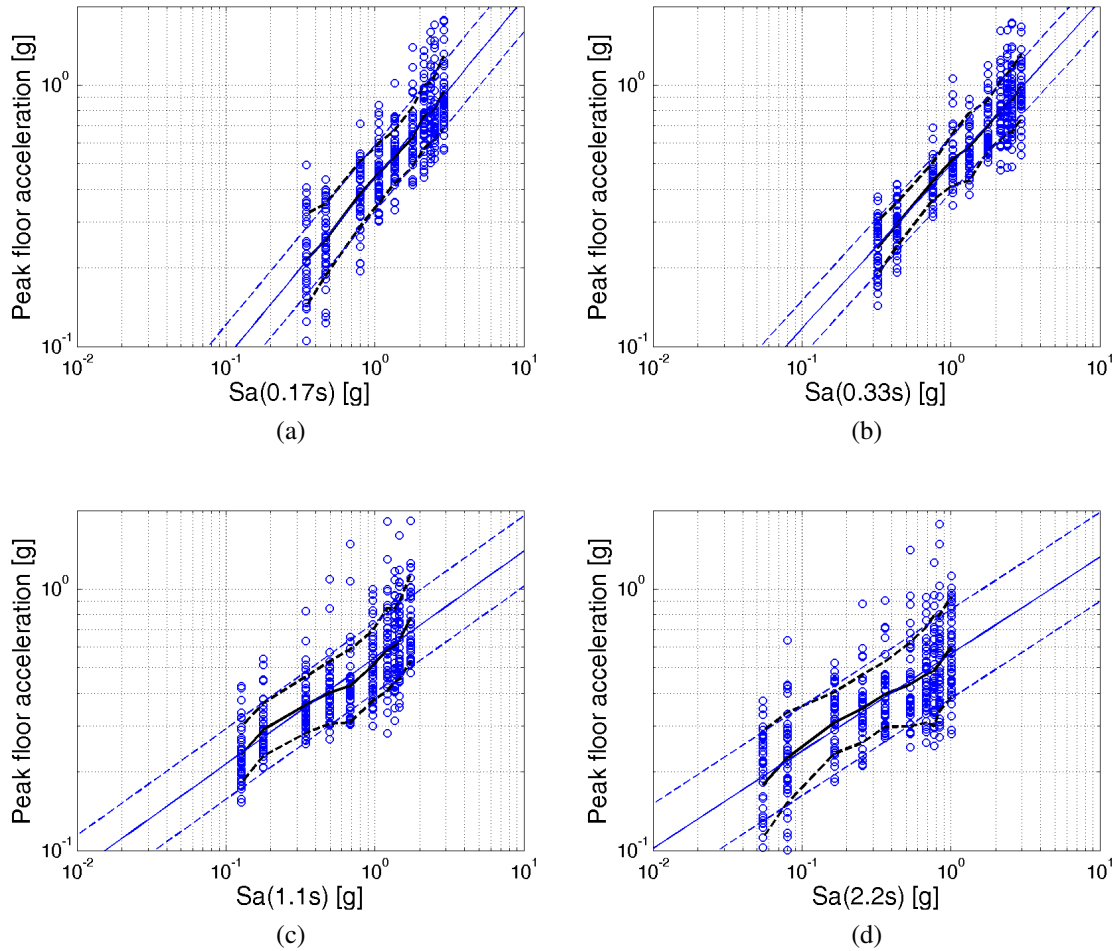


Figure A.49: 4-story space frame (Building No.1003) PFA at (a) $T^* = T_3$, (b) $T^* = T_2$, (c) $T^* = T_1$, and (d) $T^* = 2T_1$ for “improved” ground motions selected to match CS μ and σ ($T_1, 2T_1$) and CS μ and 1.2σ (T_3, T_2).

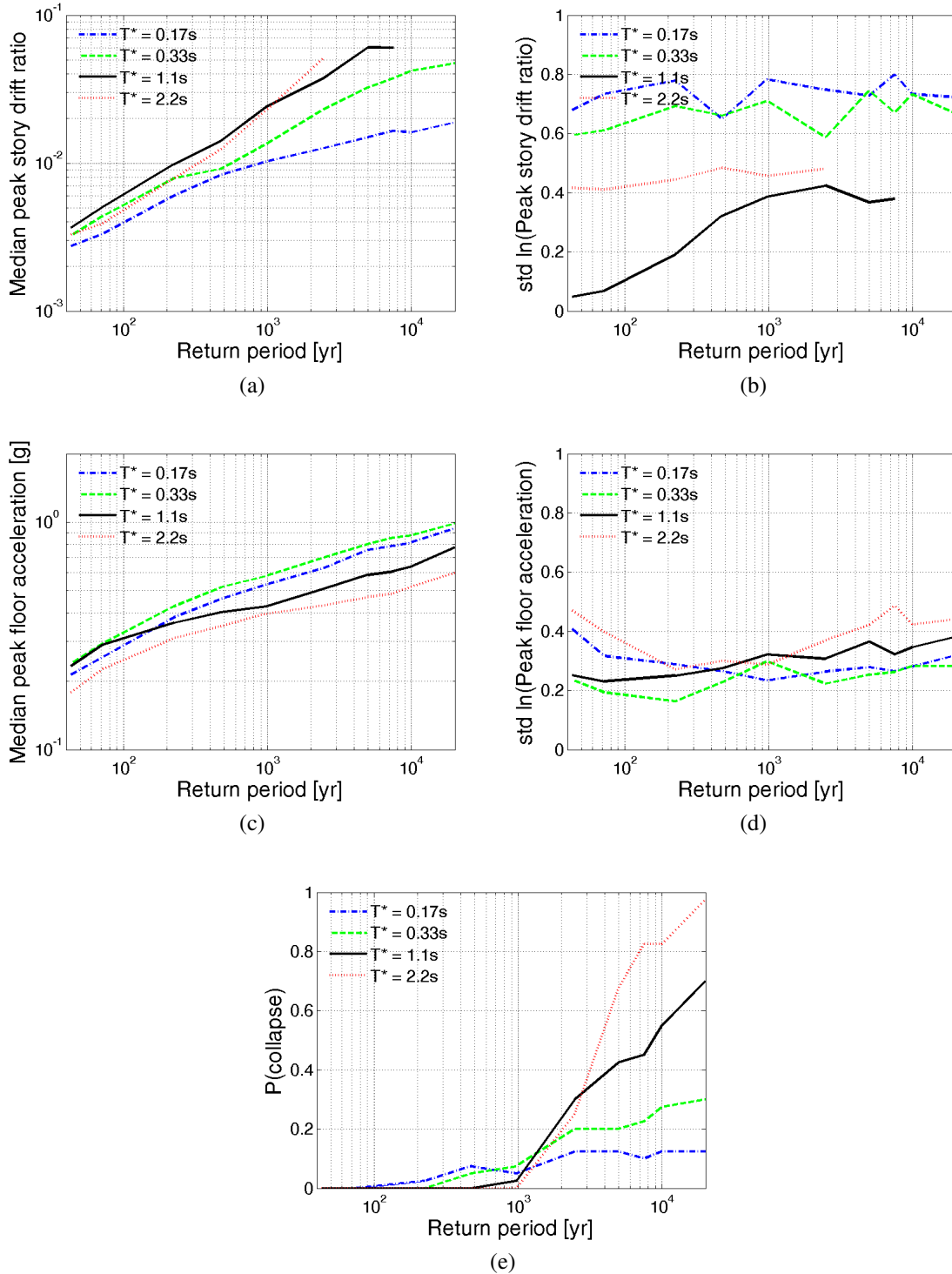


Figure A.50: 4-story space frame (Building No.1003) (a) median *PSDR*, (b) logarithmic standard deviation of *PSDR*, (c) median *PFA*, (d) logarithmic standard deviation of *PFA*, and (e) probability of collapse given return period for “improved” ground motions selected to match CS μ and σ ($T_1, 2T_1$) and CS μ and 1.2σ (T_3, T_2).

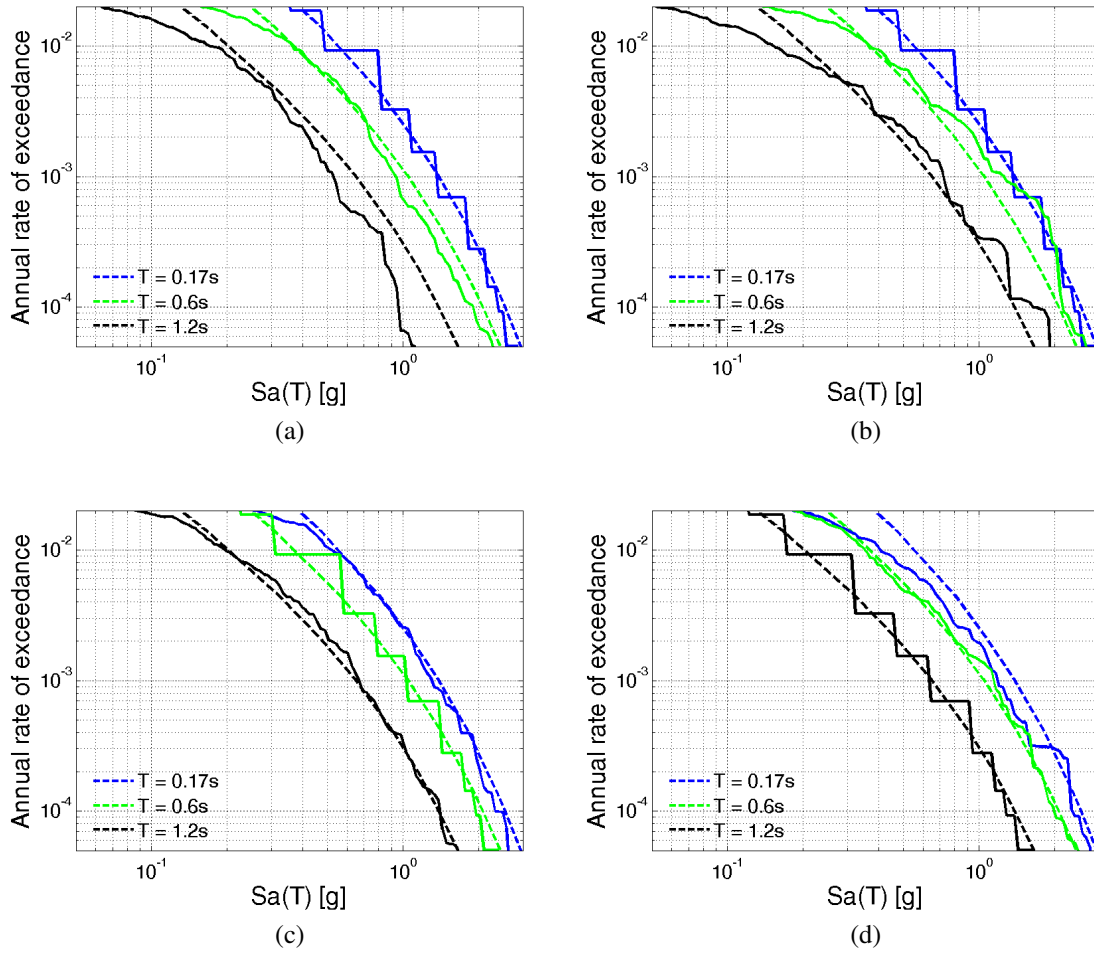


Figure A.51: 2-story space frame (Building No.1001) Sa distribution at three periods for ground motions selected at (a) $T^* = T_2$, CS μ and σ , (b) $T^* = T_2$, CS μ and 1.3σ , (c) $T^* = T_1$, CS μ and σ , and (d) $T^* = 2T_1$, CS μ and σ .

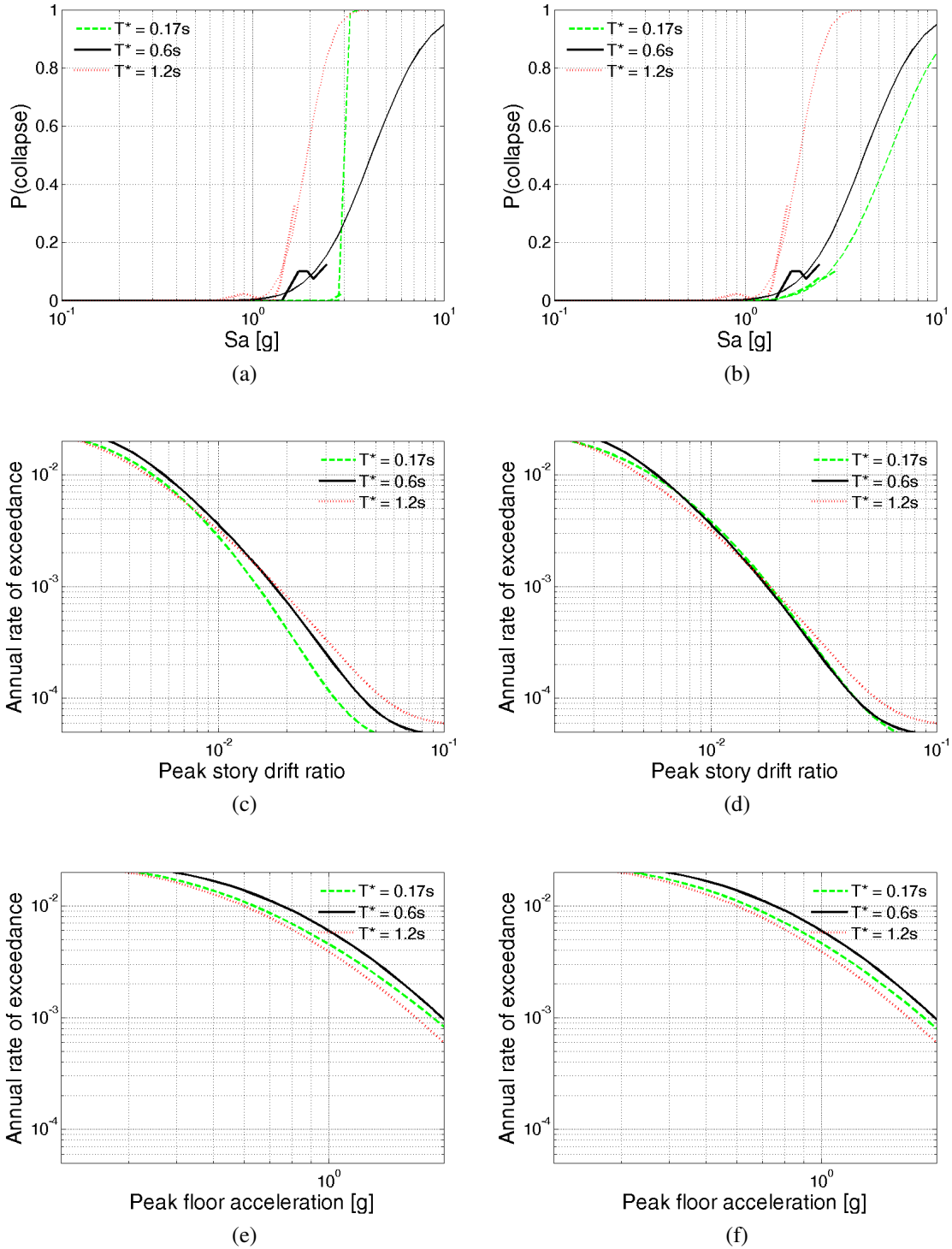


Figure A.52: 2-story space frame (Building No.1001) (a-b) probability of collapse, (c-d) *PSDR* hazard, and (e-f) *PFA* hazard for “basic” ground motions selected to match CS μ and σ ($T_2, T_1, 2T_1$) at (a, c, e) and “improved” ground motions selected to match CS μ and σ ($T_1, 2T_1$) and CS μ and 1.3σ (T_2) at (b, d, f).

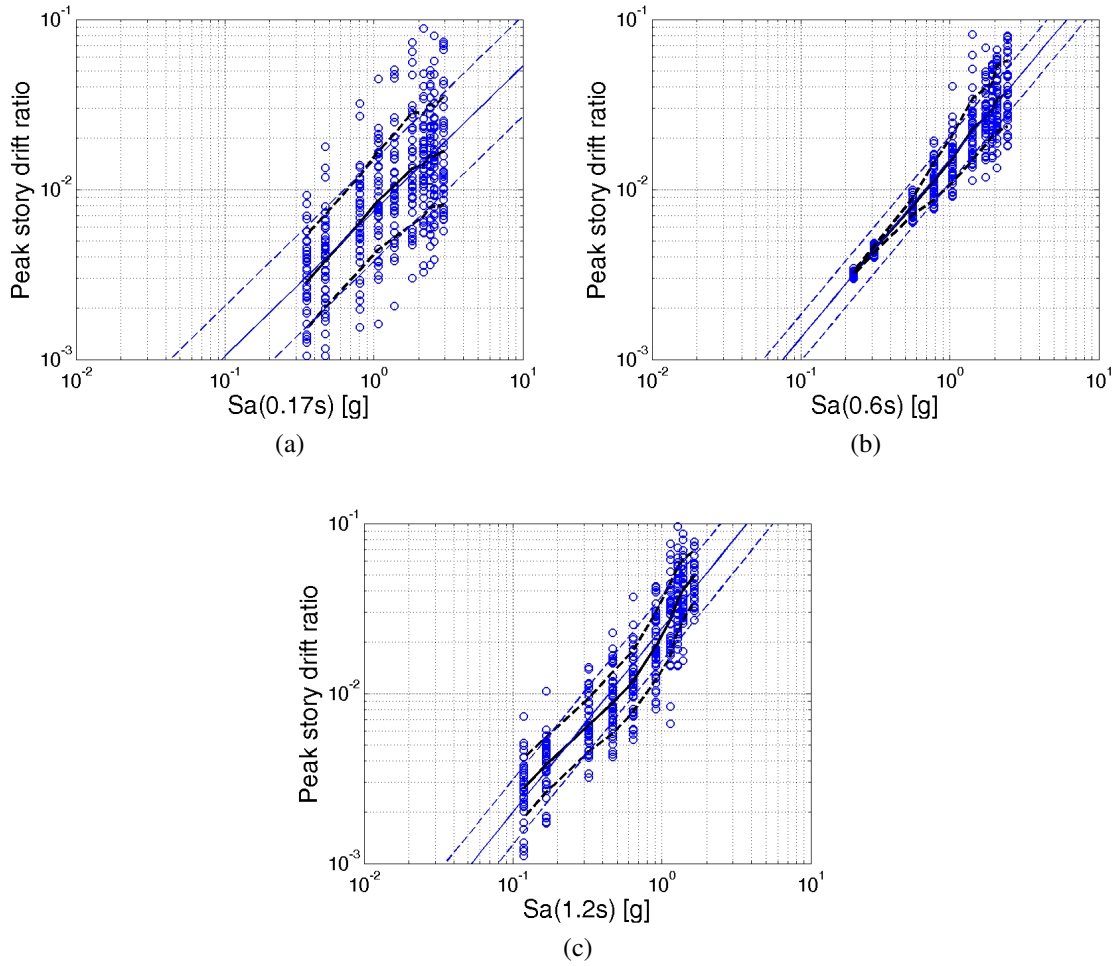


Figure A.53: 2-story space frame (Building No.1001) *PSDR* at (a) $T^* = T_2$, (b) $T^* = T_1$, and (c) $T^* = 2T_1$ for “improved” ground motions selected to match CS μ and σ ($T_1, 2T_1$) and CS μ and 1.3σ (T_2).

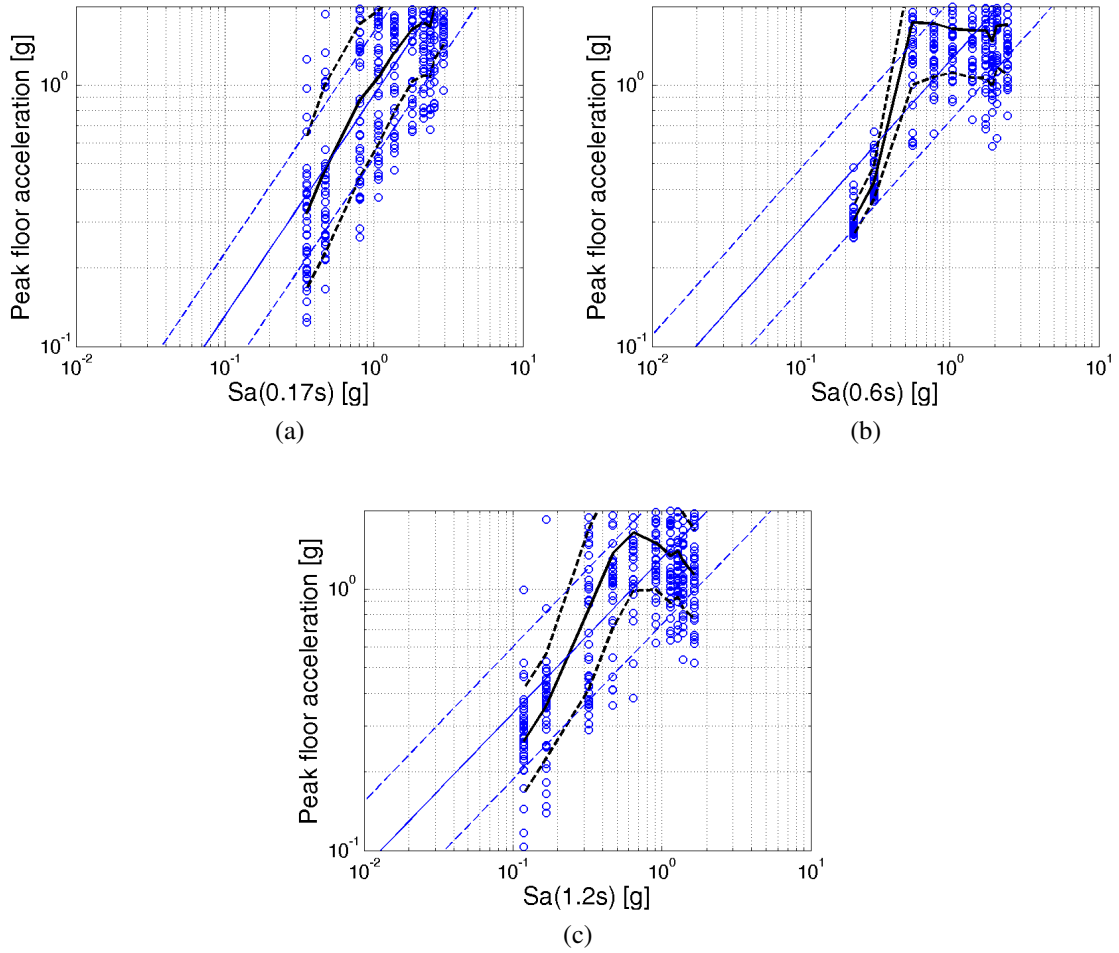


Figure A.54: 2-story space frame (Building No.1001) PFA at (a) $T^* = T_2$, (b) $T^* = T_1$, and (d) $T^* = 2T_1$ for “improved” ground motions selected to match CS μ and σ ($T_1, 2T_1$) and CS μ and 1.3σ (T_2).

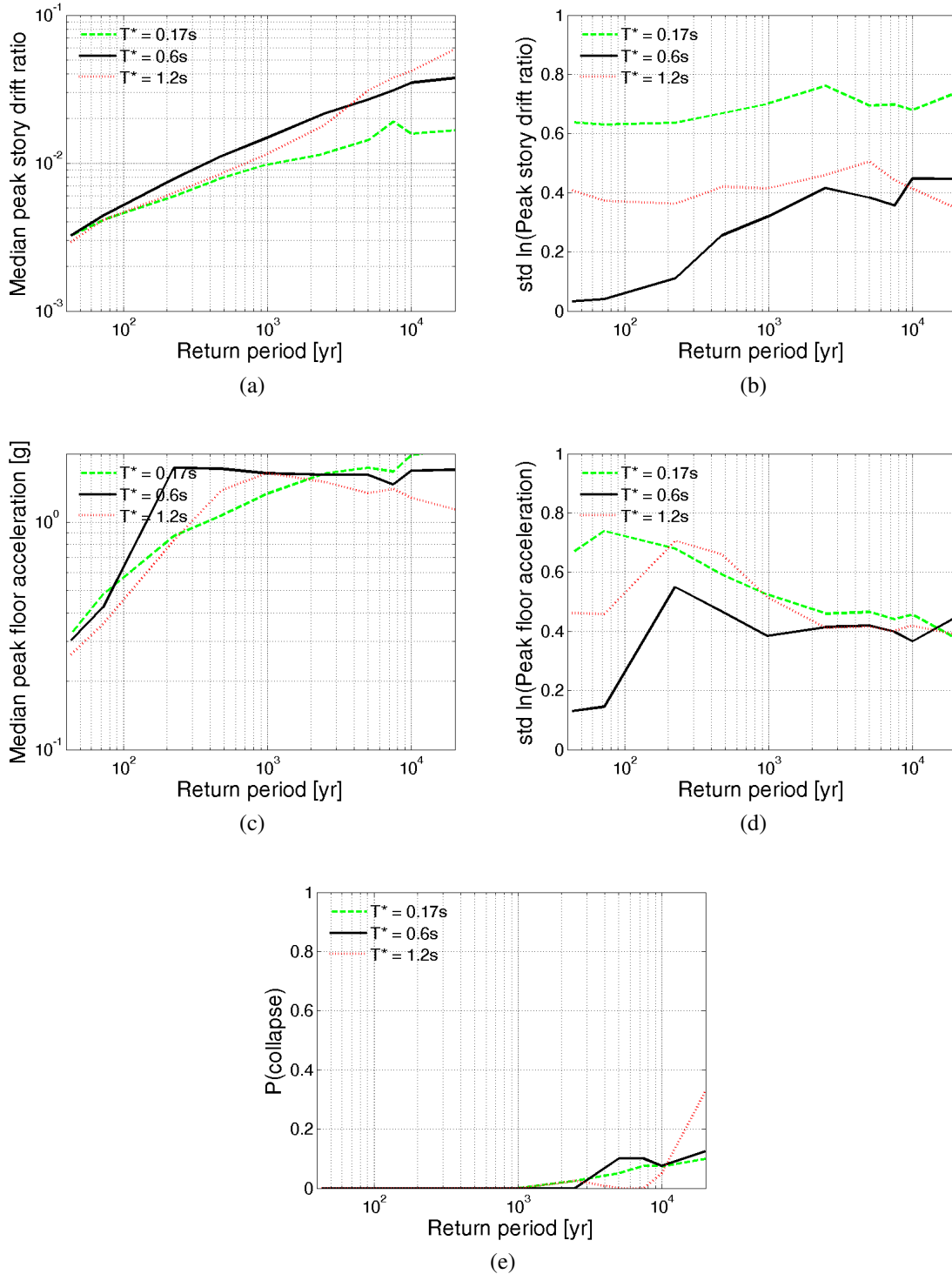


Figure A.55: 2-story space frame (Building No.1001) (a) median *PSDR*, (b) logarithmic standard deviation of *PSDR*, (c) median *PFA*, (d) logarithmic standard deviation of *PFA*, and (e) probability of collapse given return period for “improved” ground motions selected to match CS μ and σ ($T_1, 2T_1$) and CS μ and 1.3σ (T_2).

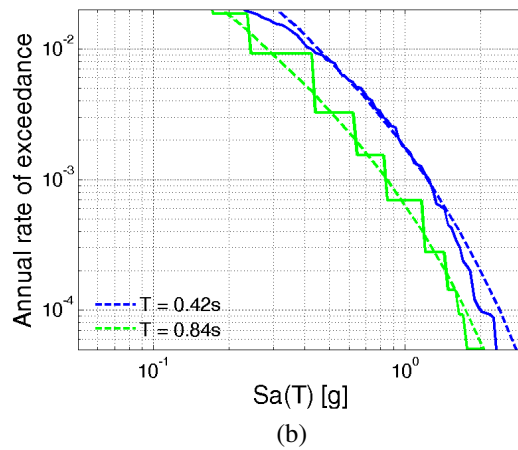
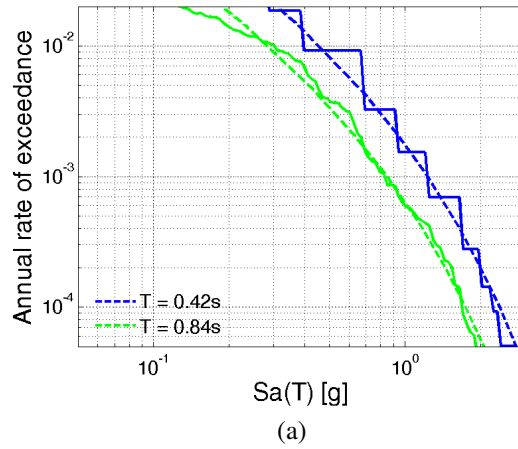


Figure A.56: 1-story space frame (Building No.2061) S_a distribution at two periods for ground motions selected at (a) $T^* = T_1$, CS μ and σ and (b) $T^* = 2T_1$, CS μ and σ .

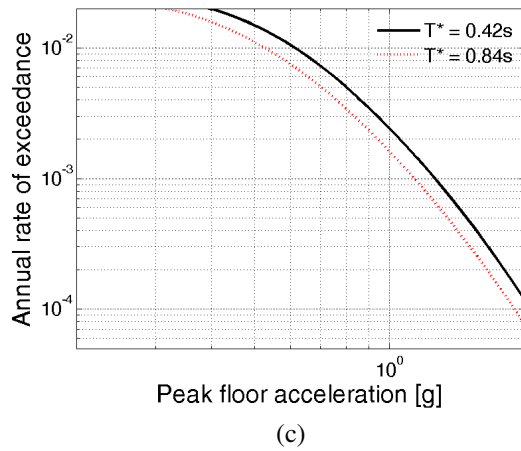
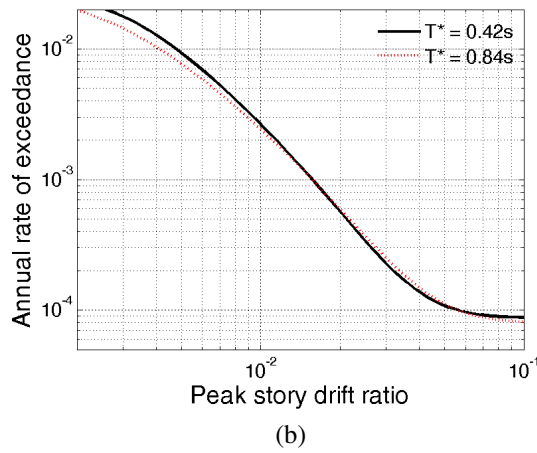
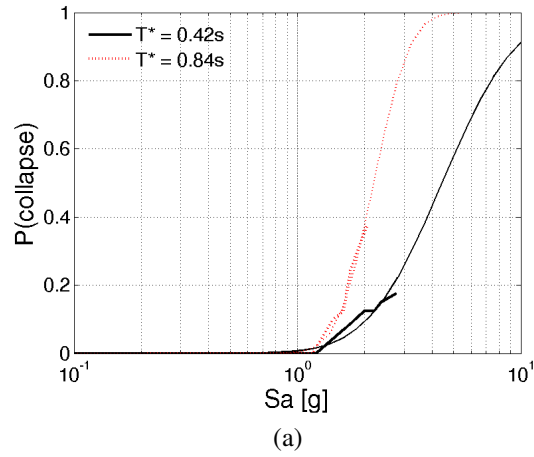


Figure A.57: 1-story space frame (Building No.2061) (a) probability of collapse, (b) *PSDR* hazard, and (c) *PFA* hazard for “basic” ground motions selected to match CS μ and σ .

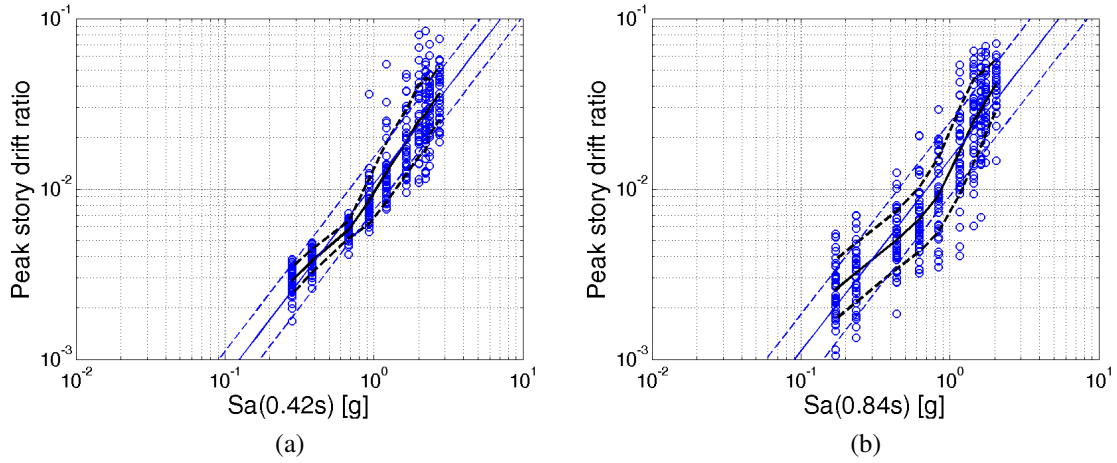


Figure A.58: 1-story space frame (Building No.2061) *PSDR* at (a) $T^* = T_1$ and (b) $T^* = 2T_1$ for “basic” ground motions selected to match CS μ and σ .

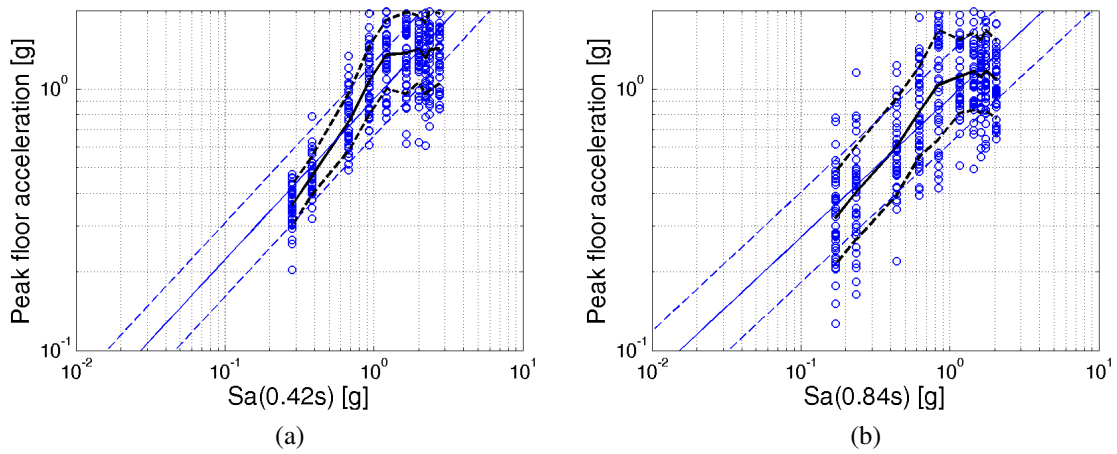


Figure A.59: 1-story space frame (Building No.2061) *PFA* at (a) $T^* = T_1$ and (b) $T^* = 2T_1$ for “basic” ground motions selected to match CS μ and σ .

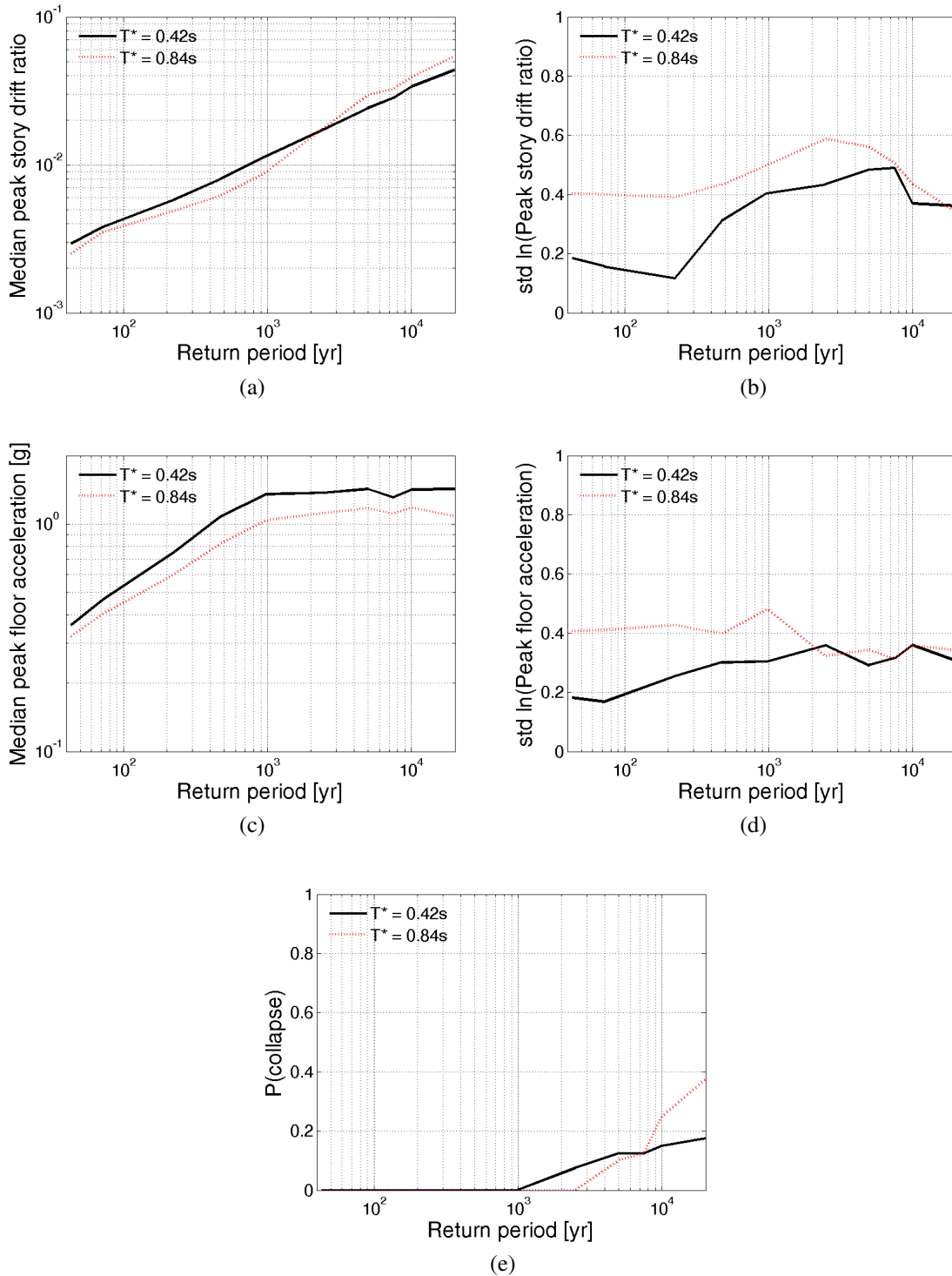


Figure A.60: 1-story space frame (Building No.2061) (a) median *PSDR*, (b) logarithmic standard deviation of *PSDR*, (c) median *PFA*, (d) logarithmic standard deviation of *PFA*, and (e) probability of collapse given return period for “basic” ground motions selected to match CS μ and σ .

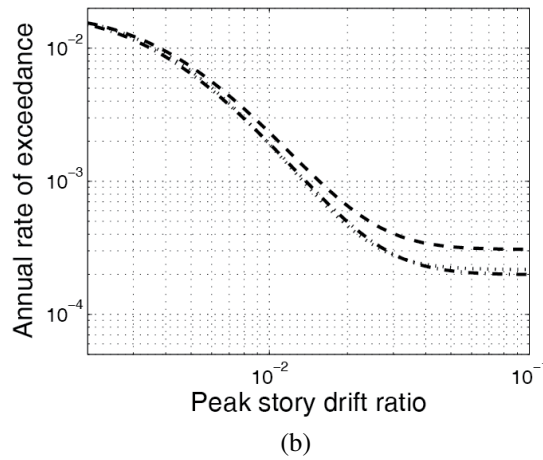
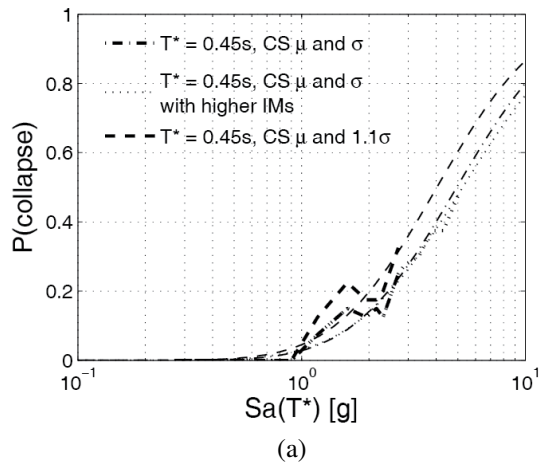


Figure A.61: 20-story perimeter frame (Building No.1020) (a) probability of collapse and (b) *PSDR* hazard for “basic” ground motions selected to match CS μ and σ ($T_3, T_2, T_1, 2T_1$), additional ground motions selected to match CS μ and σ ($T_3, T_2, T_1, 2T_1$) with higher Intensity Measures (IMs), i.e., higher spectral amplitudes, and “improved” ground motions selected to match CS μ and σ ($T_2, T_1, 2T_1$) and CS μ and 1.1σ (T_3).

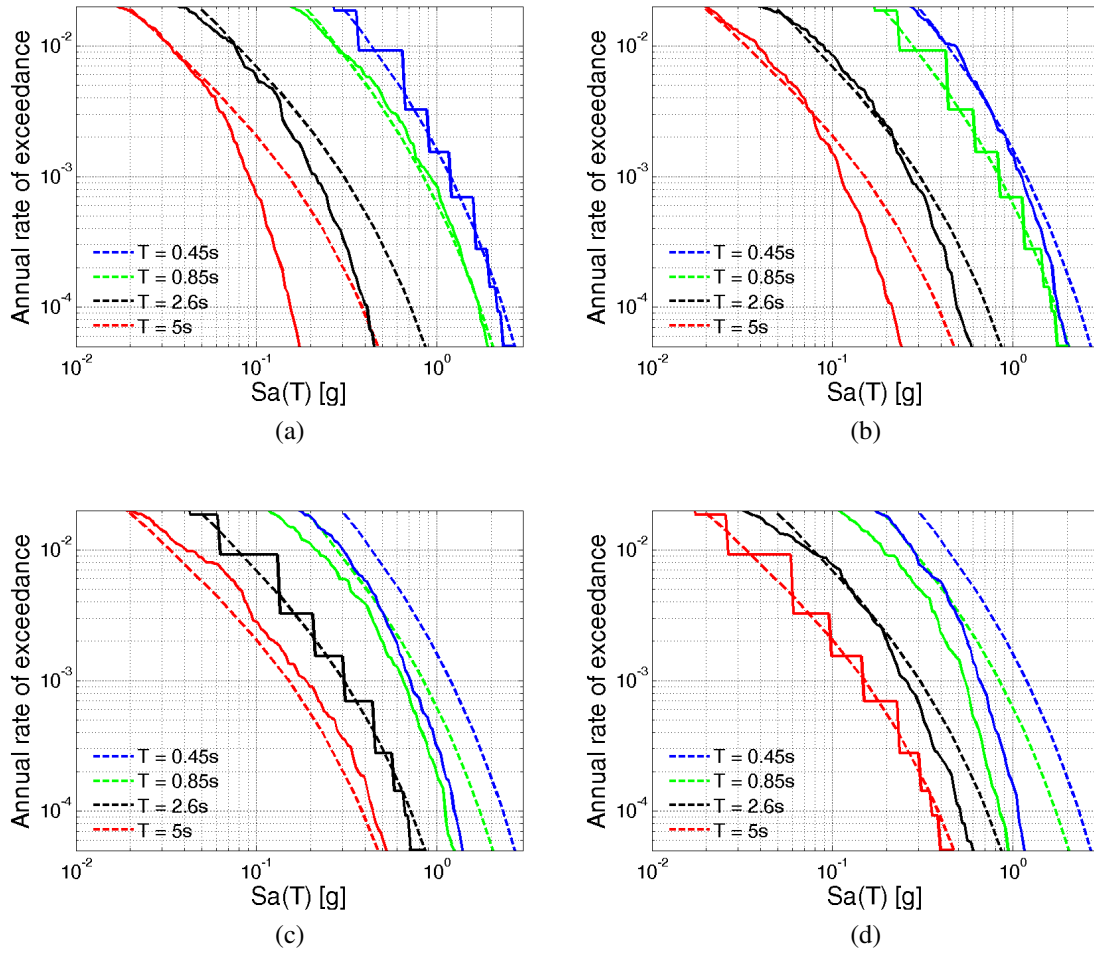


Figure A.62: 20-story perimeter frame (Building No.1020) Sa distribution at four periods for (a) $T^* = T_3$, (b) $T^* = T_2$, (c) $T^* = T_1$ and (d) $T^* = 2T_1$ for ground motions selected to match Conditional Mean Spectrum (CMS), i.e., $CS \mu (T_3, T_2, T_1, 2T_1)$.

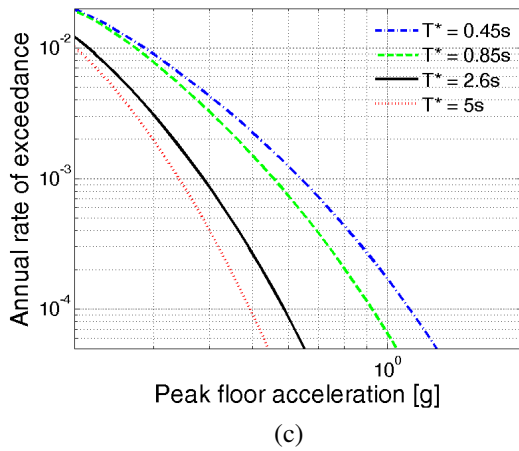
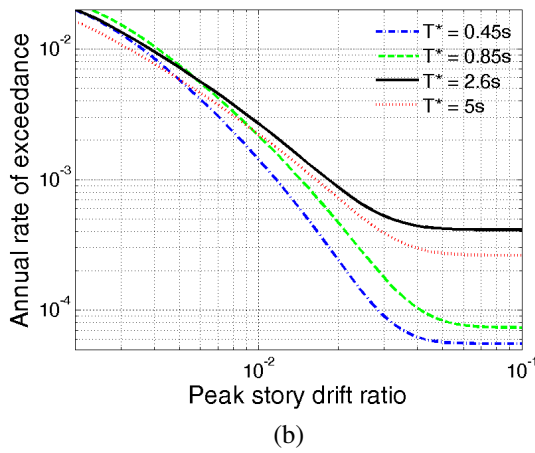
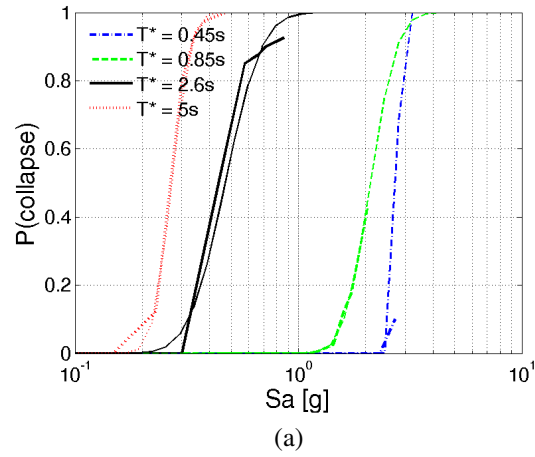


Figure A.63: 20-story perimeter frame (Building No.1020) (a) probability of collapse, (b) $PSDR$ hazard, and (c) PFA hazard for ground motions selected to match CMS, i.e., $CS \mu (T_3, T_2, T_1, 2T_1)$.

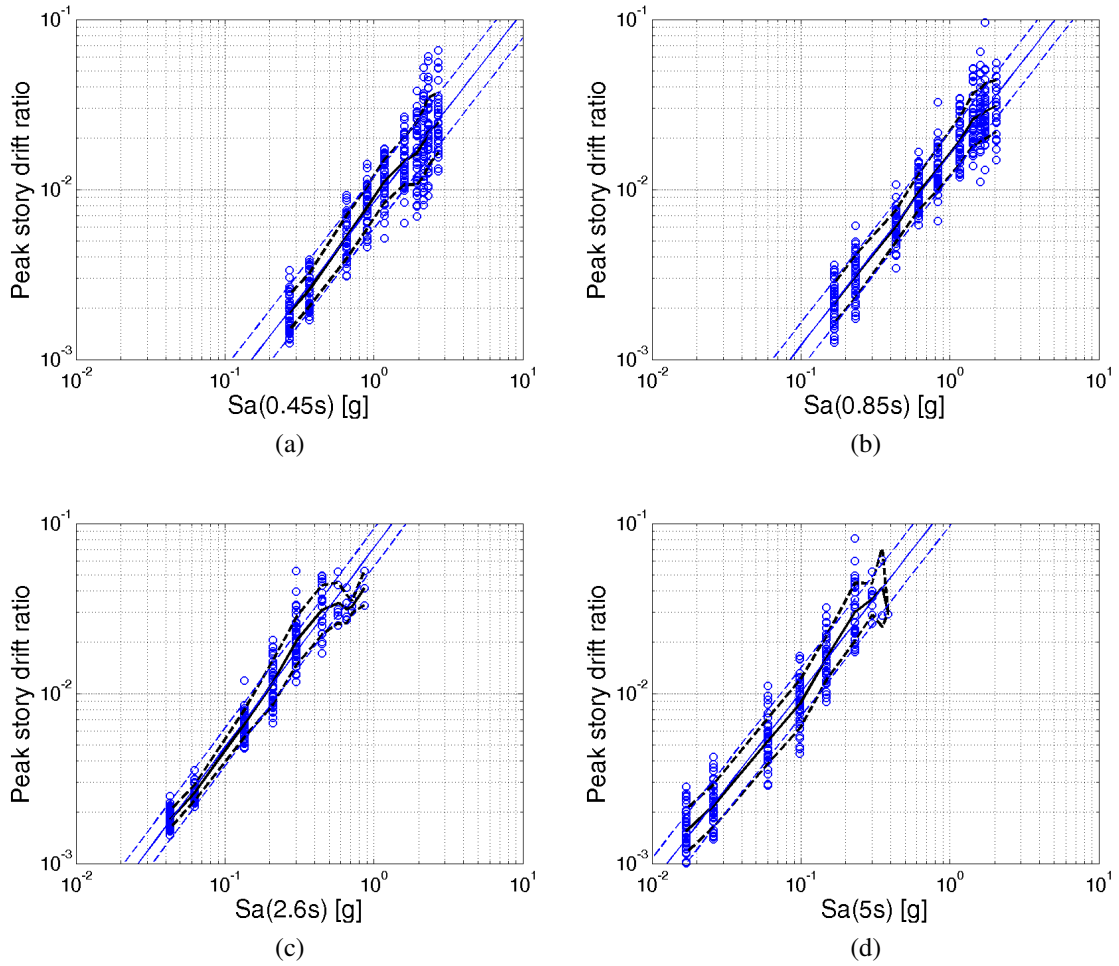


Figure A.64: 20-story perimeter frame (Building No.1020) *PSDR* at (a) $T^* = T_3$, (b) $T^* = T_2$, (c) $T^* = T_1$, and (d) $T^* = 2T_1$ for ground motions selected to match CMS, i.e., CS μ ($T_3, T_2, T_1, 2T_1$).

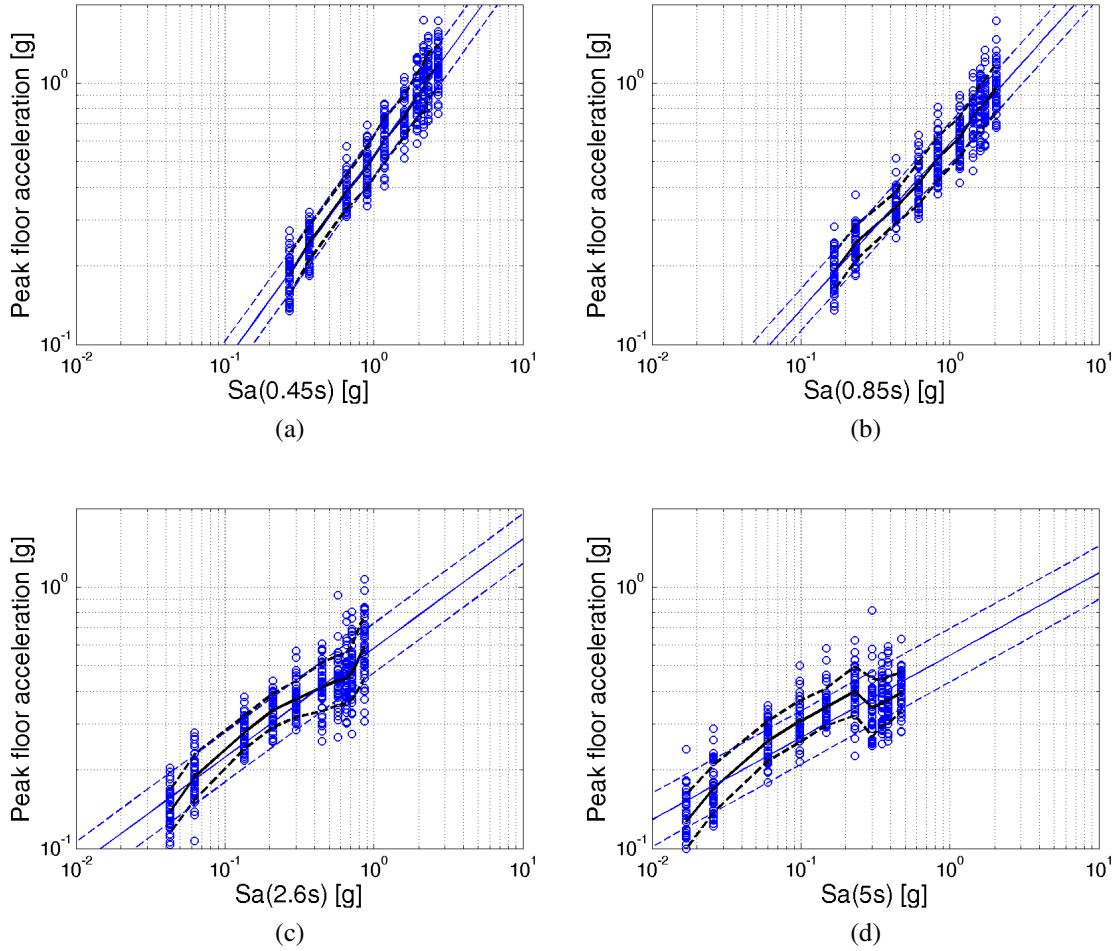


Figure A.65: 20-story perimeter frame (Building No.1020) PFA at (a) $T^* = T_3$, (b) $T^* = T_2$, (c) $T^* = T_1$, and (d) $T^* = 2T_1$ for ground motions selected to match CMS, i.e., CS μ ($T_3, T_2, T_1, 2T_1$).

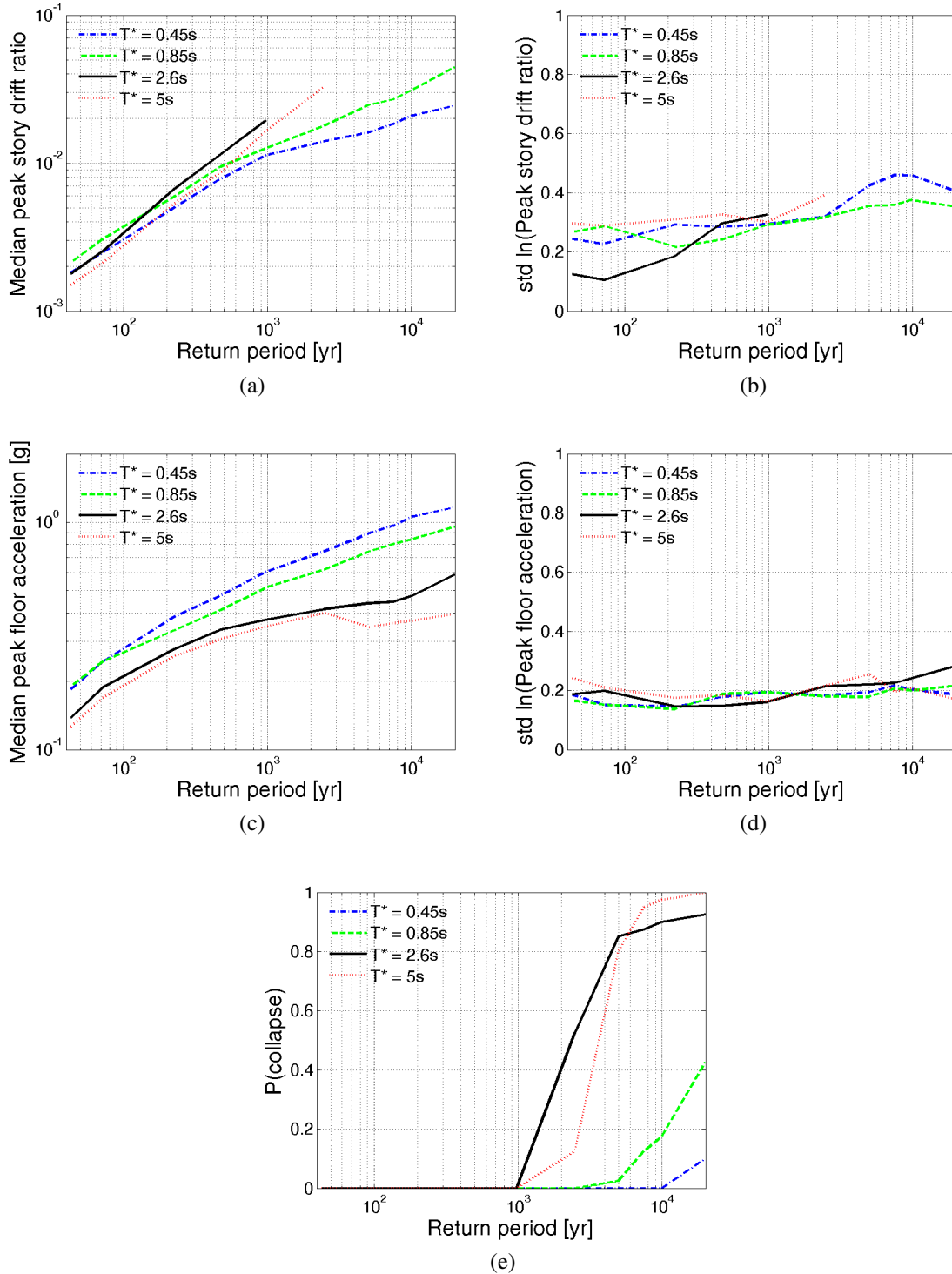


Figure A.66: 20-story perimeter frame (Building No.1020) (a) median *PSDR*, (b) logarithmic standard deviation of *PSDR*, (c) median *PFA*, (d) logarithmic standard deviation of *PFA*, and (e) probability of collapse given return period for ground motions selected to match CMS, i.e., $CS \mu (T_3, T_2, T_1, 2T_1)$.

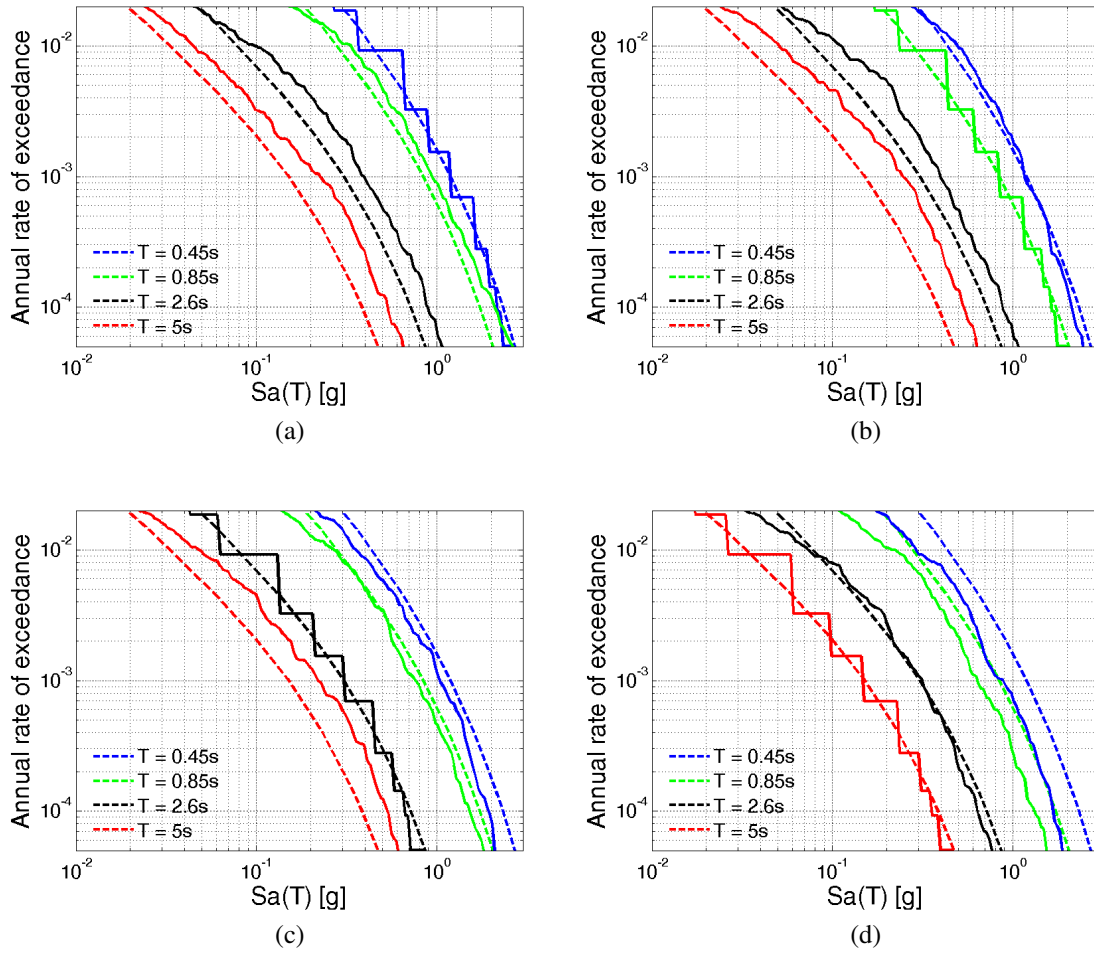


Figure A.67: 20-story perimeter frame (Building No.1020) S_a distribution at four periods for (a) $T^* = T_3$, (b) $T^* = T_2$, (c) $T^* = T_1$ and (d) $T^* = 2T_1$ for ground motions selected to match Uniform Hazard Spectrum (UHS).

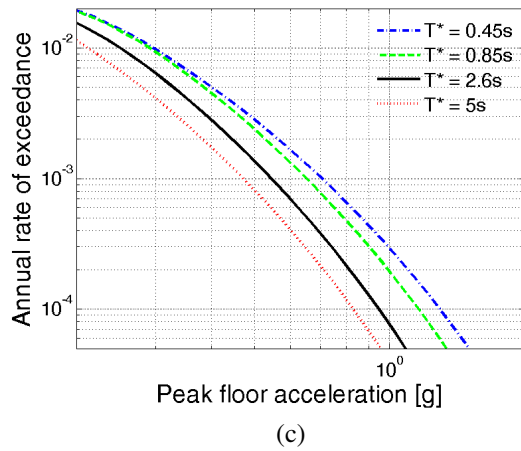
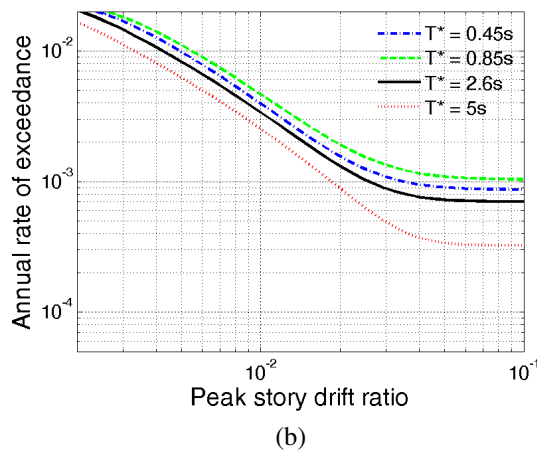
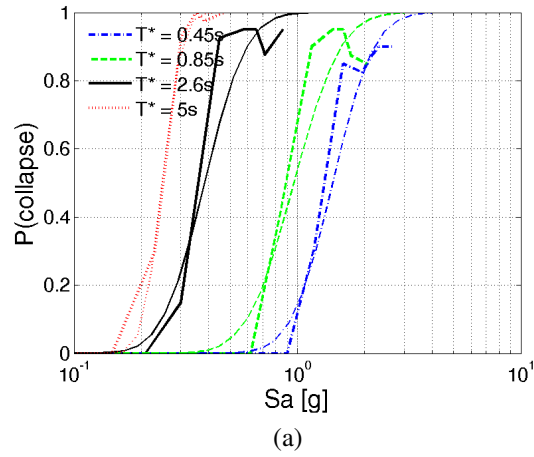


Figure A.68: 20-story perimeter frame (Building No.1020) (a) probability of collapse, (b) $PSDR$ hazard, and (c) PFA hazard for ground motions selected to match UHS.

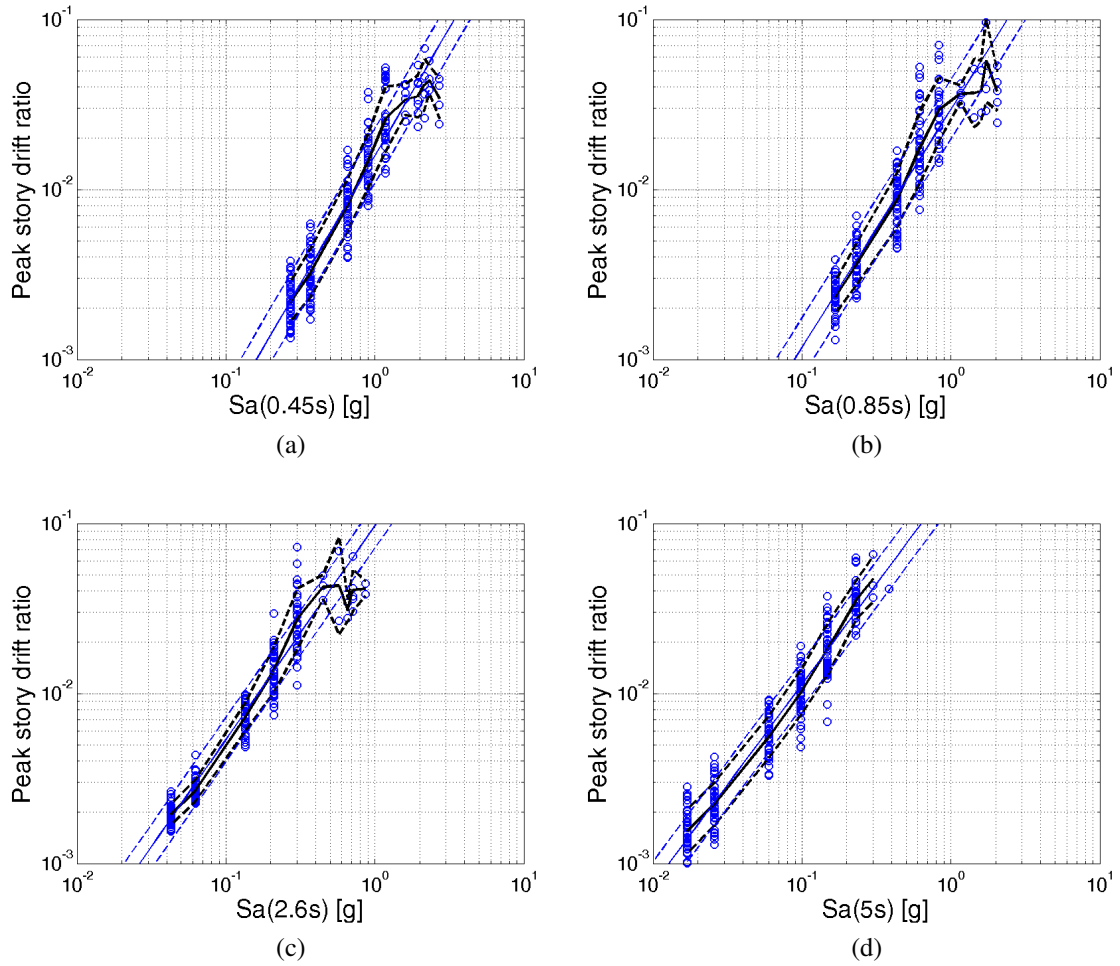


Figure A.69: 20-story perimeter frame (Building No.1020) *PSDR* at (a) $T^* = T_3$, (b) $T^* = T_2$, (c) $T^* = T_1$, and (d) $T^* = 2T_1$ for ground motions selected to match UHS.

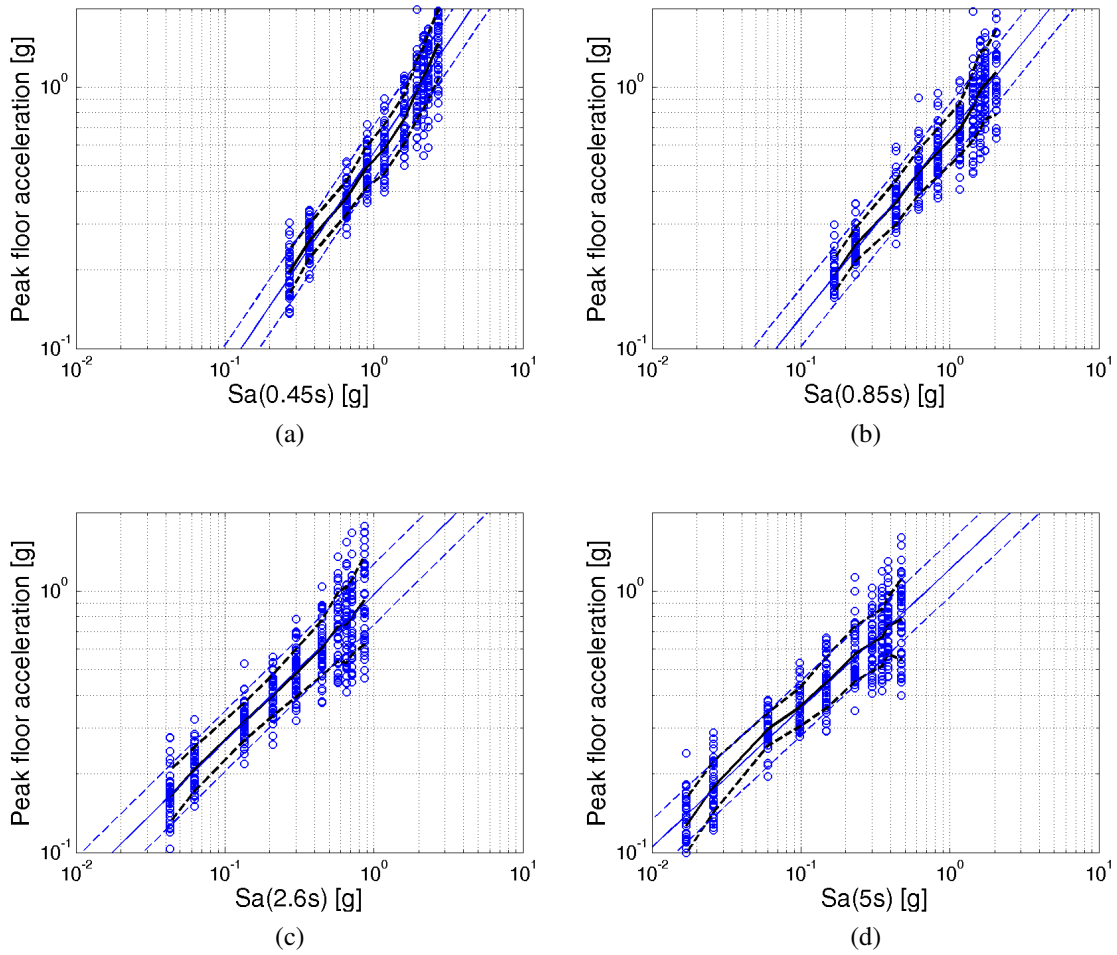


Figure A.70: 20-story perimeter frame (Building No.1020) PFA at (a) $T^* = T_3$, (b) $T^* = T_2$, (c) $T^* = T_1$, and (d) $T^* = 2T_1$ for ground motions selected to match UHS.

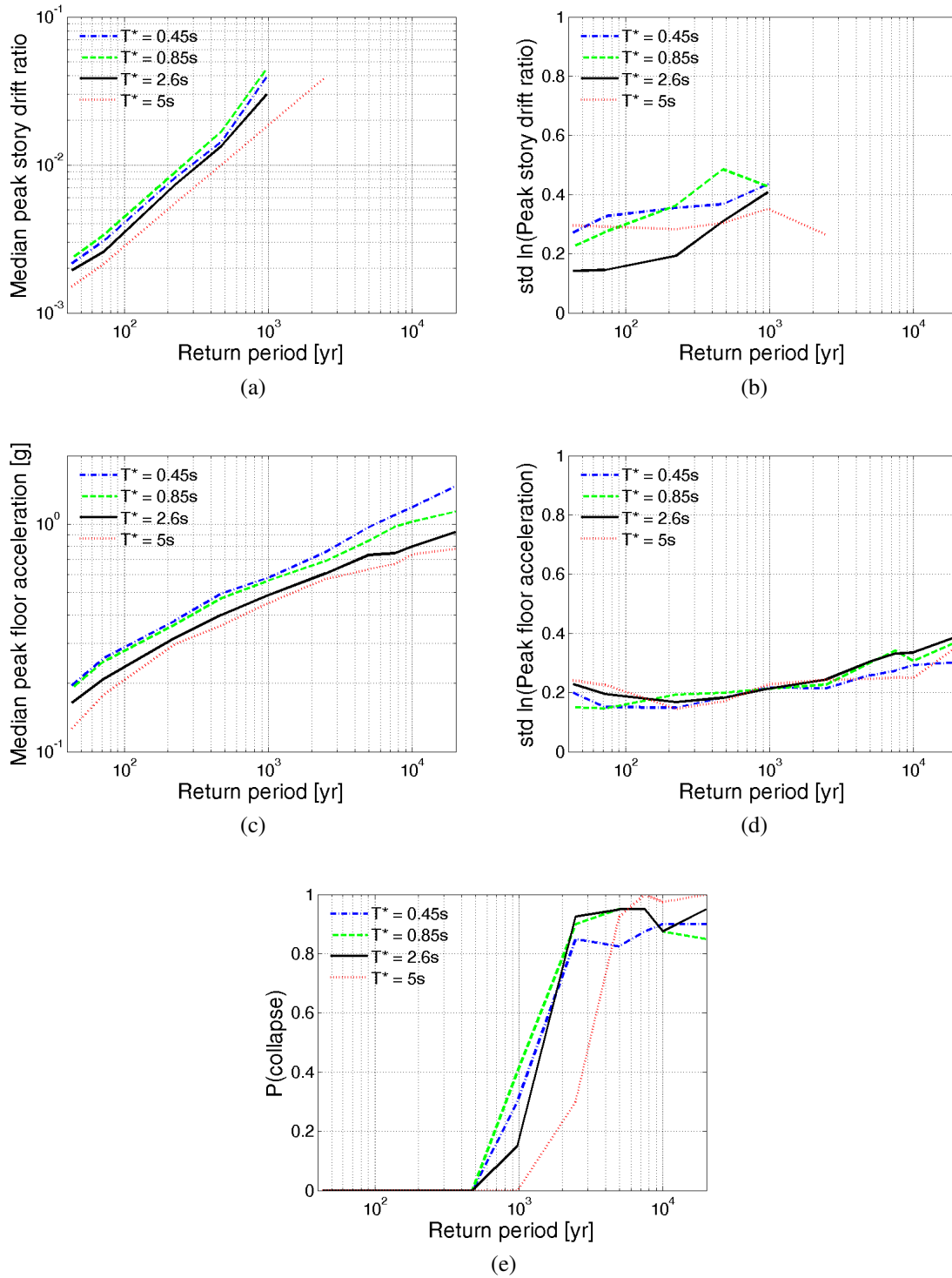


Figure A.71: 20-story perimeter frame (Building No.1020) (a) median *PSDR*, (b) logarithmic standard deviation of *PSDR*, (c) median *PFA*, (d) logarithmic standard deviation of *PFA*, and (e) probability of collapse given return period for ground motions selected to match UHS.

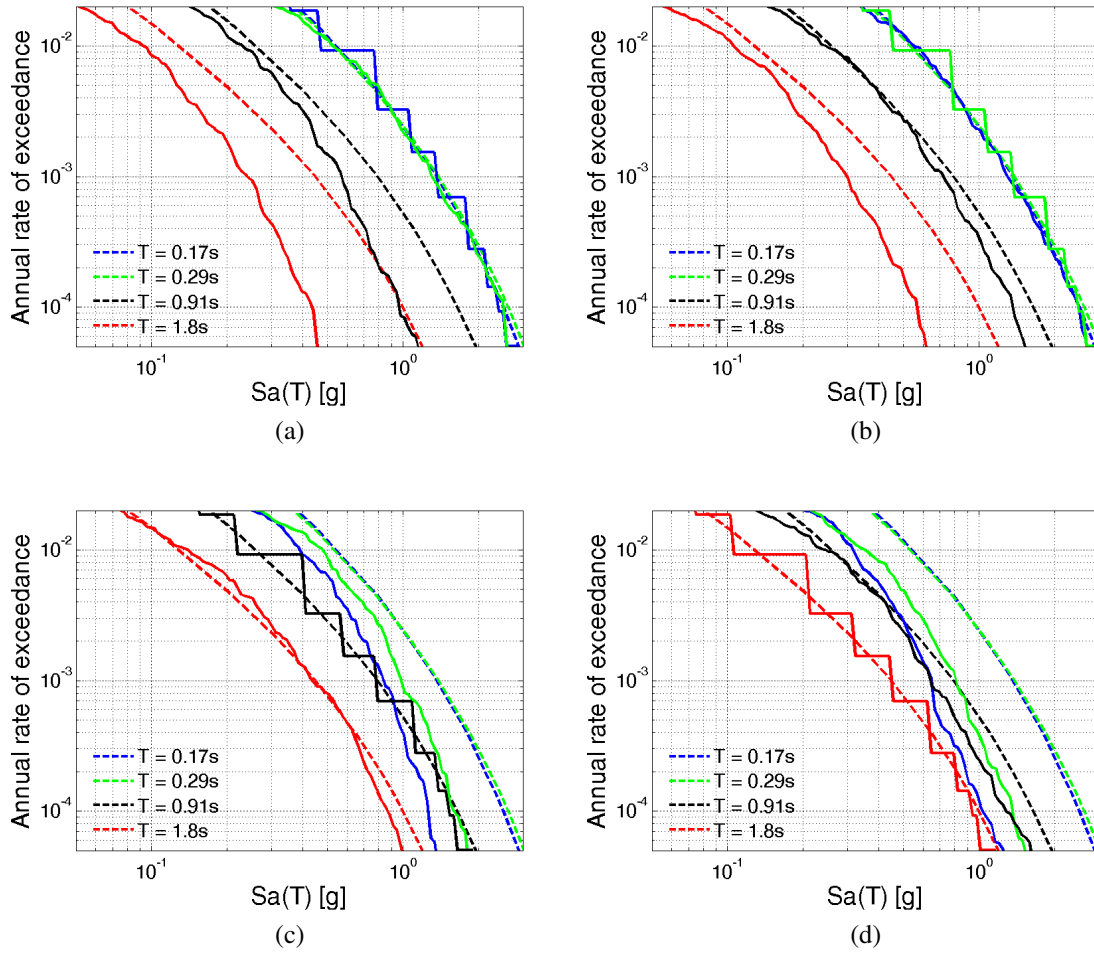


Figure A.72: 4-story perimeter frame (Building No.1008) Sa distribution at four periods for (a) $T^* = T_3$, (b) $T^* = T_2$, (c) $T^* = T_1$ and (d) $T^* = 2T_1$ for ground motions selected to match CMS, i.e., CS μ ($T_3, T_2, T_1, 2T_1$).

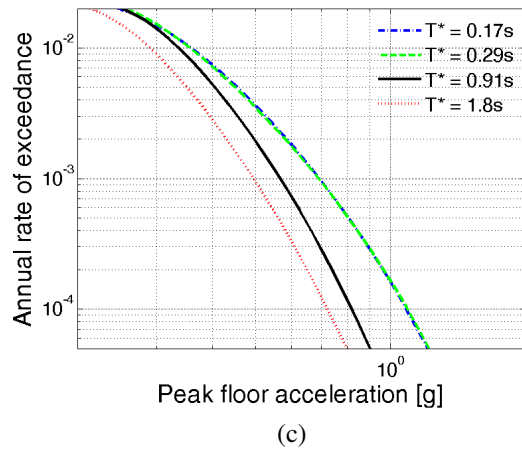
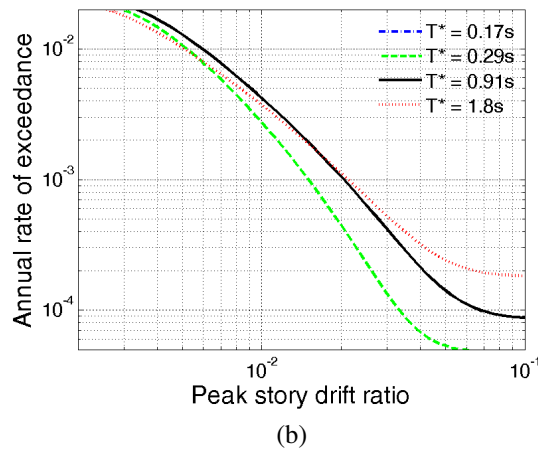
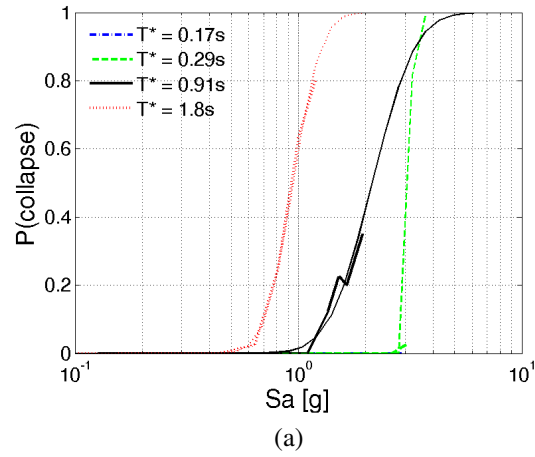


Figure A.73: 4-story perimeter frame (Building No.1008) (a) probability of collapse, (b) *PSDR* hazard, and (c) *PFA* hazard for ground motions selected to match CMS, i.e., $CS \mu (T_3, T_2, T_1, 2T_1)$.

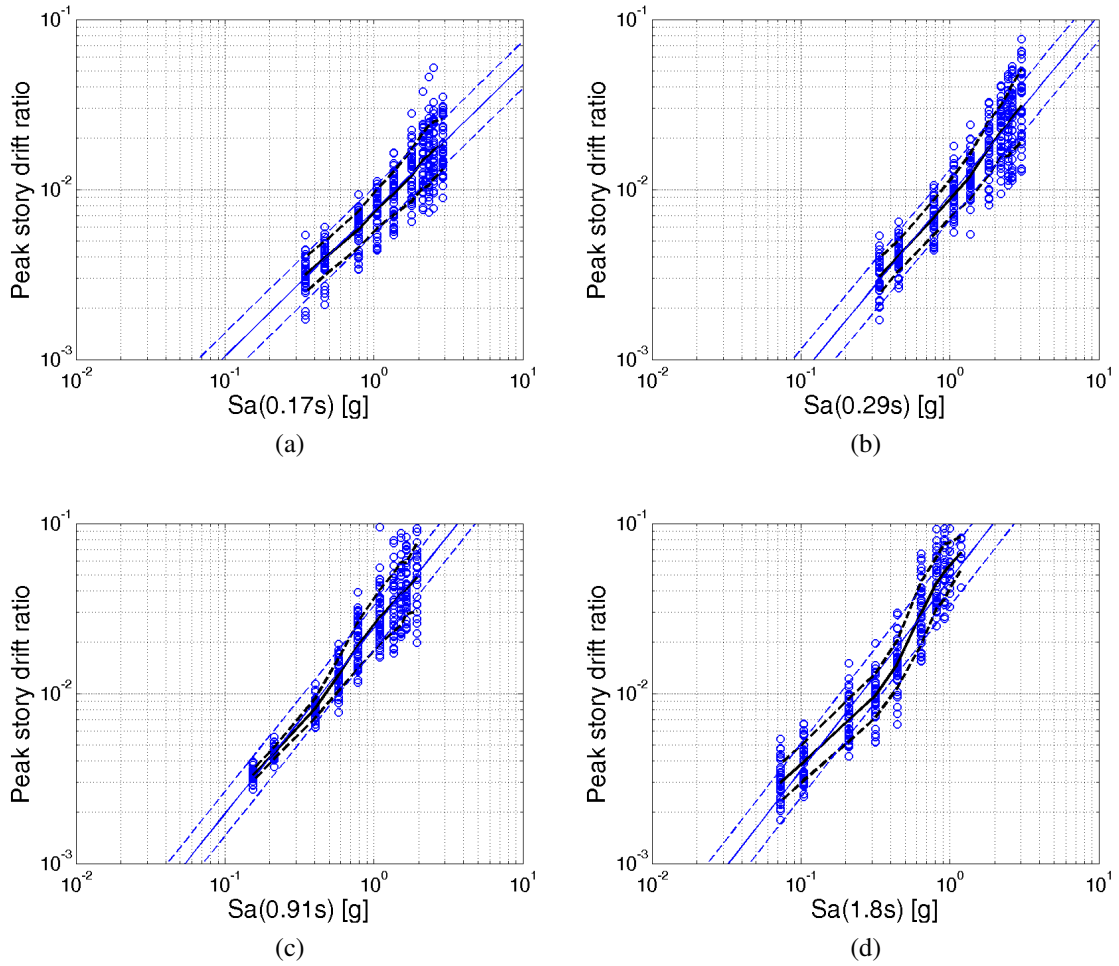


Figure A.74: 4-story perimeter frame (Building No.1008) *PSDR* at (a) $T^* = T_3$, (b) $T^* = T_2$, (c) $T^* = T_1$, and (d) $T^* = 2T_1$ for ground motions selected to match CMS, i.e., CS μ ($T_3, T_2, T_1, 2T_1$).

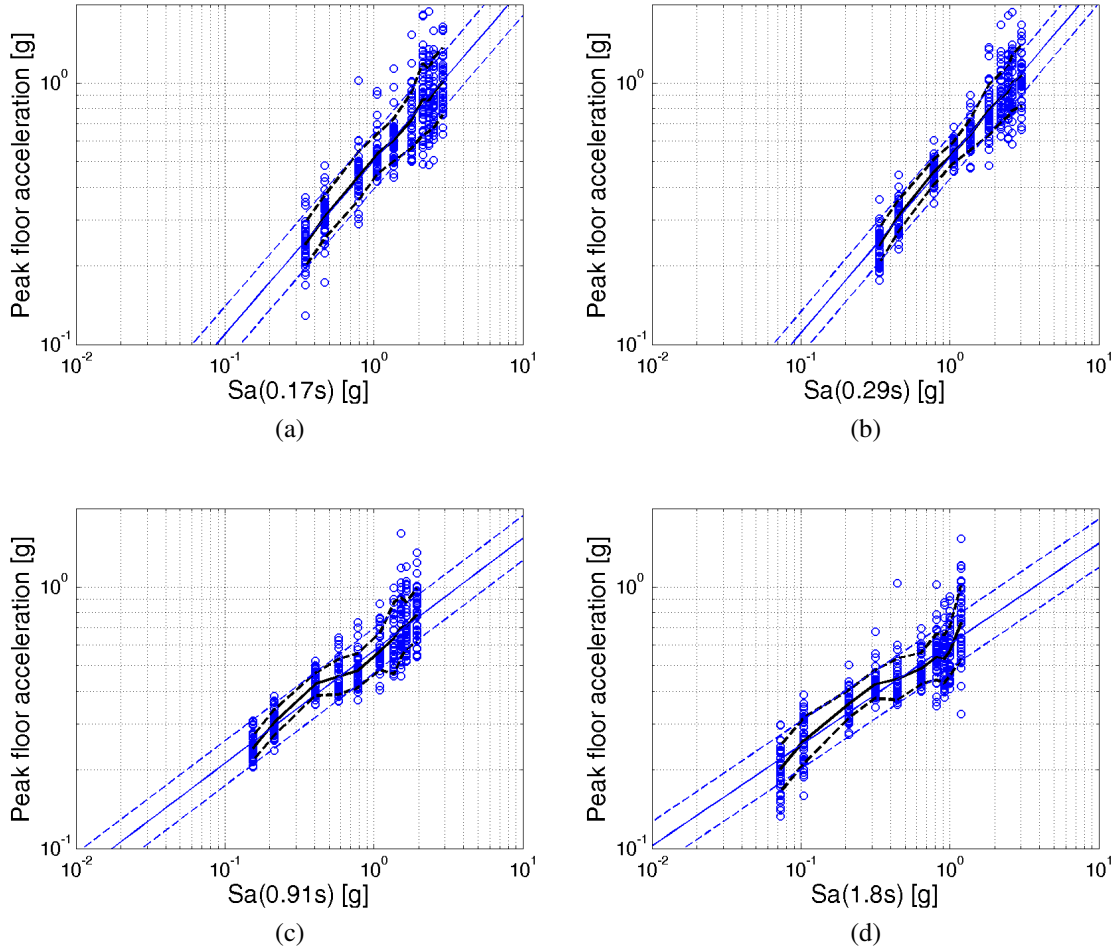


Figure A.75: 4-story perimeter frame (Building No.1008) PFA at (a) $T^* = T_3$, (b) $T^* = T_2$, (c) $T^* = T_1$, and (d) $T^* = 2T_1$ for ground motions selected to match CMS, i.e., CS μ ($T_3, T_2, T_1, 2T_1$).

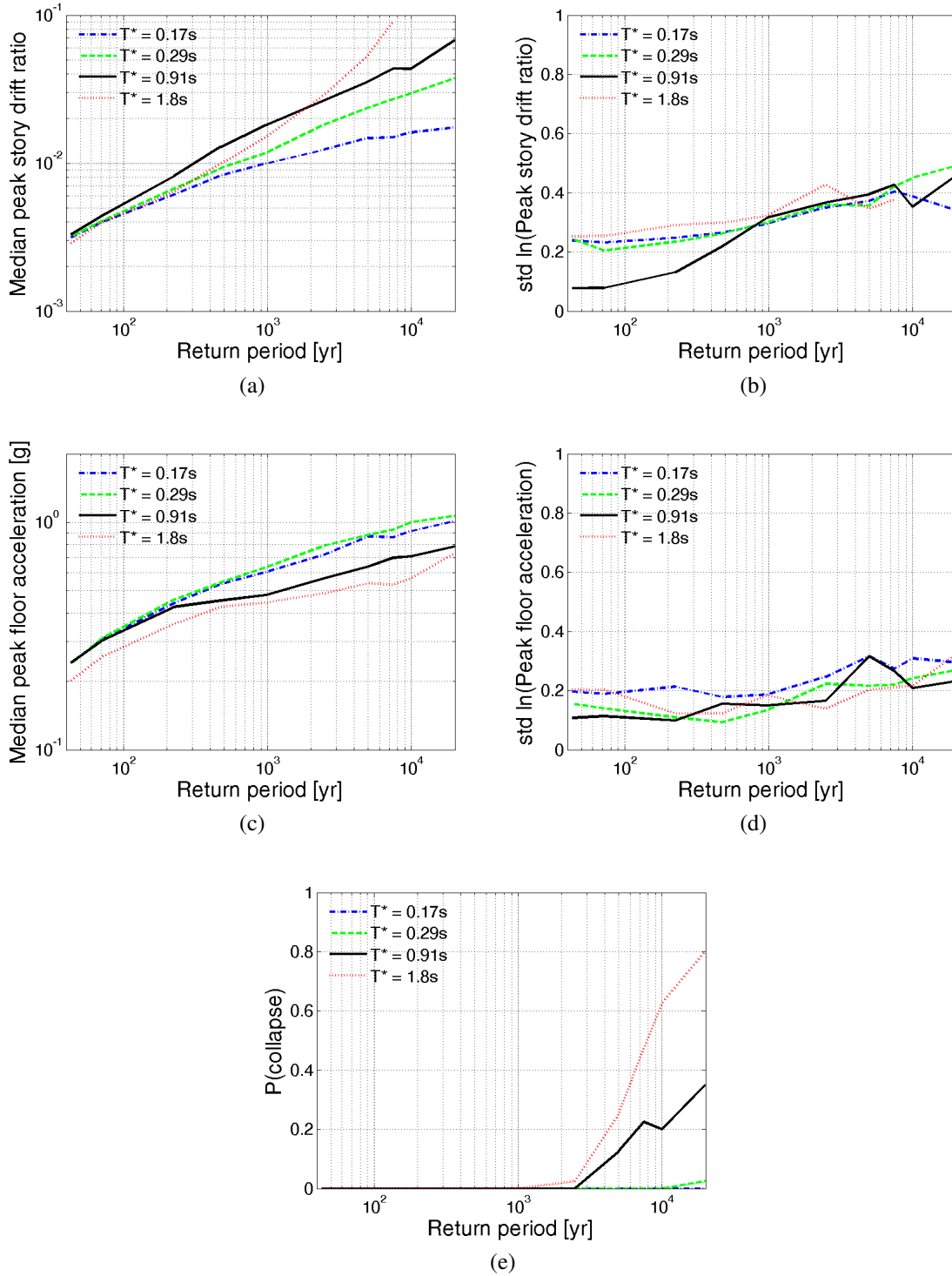


Figure A.76: 4-story perimeter frame (Building No.1008) (a) median $PSDR$, (b) logarithmic standard deviation of $PSDR$, (c) median PFA , (d) logarithmic standard deviation of PFA , and (e) probability of collapse given return period for ground motions selected to match CMS, i.e., $CS \mu (T_3, T_2, T_1, 2T_1)$.

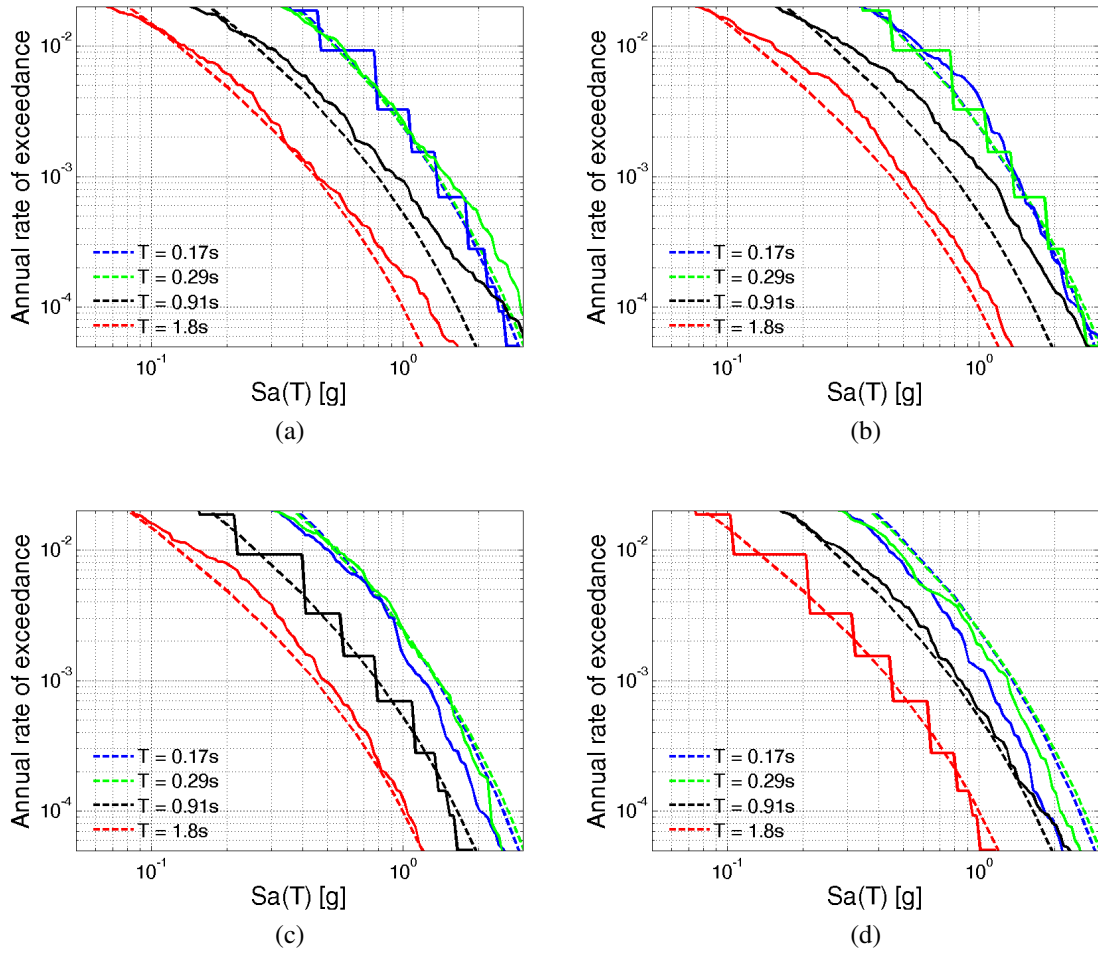


Figure A.77: 4-story perimeter frame (Building No.1008) Sa distribution at four periods for (a) $T^* = T_3$, (b) $T^* = T_2$, (c) $T^* = T_1$ and (d) $T^* = 2T_1$ for ground motions selected to match UHS.

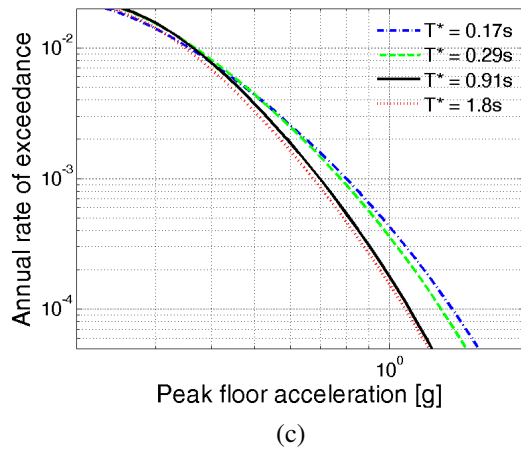
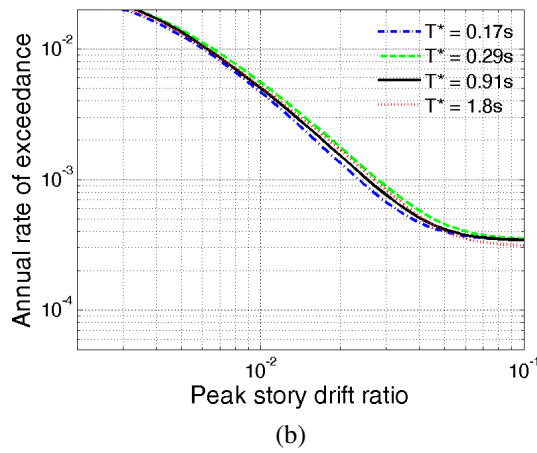
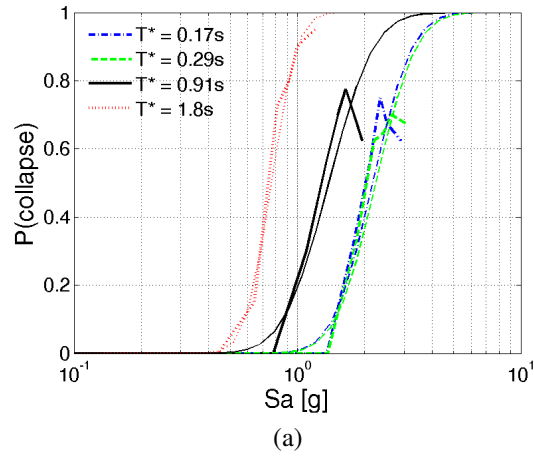


Figure A.78: 4-story perimeter frame (Building No.1008) (a) probability of collapse, (b) *PSDR* hazard, and (c) *PFA* hazard for ground motions selected to match UHS.

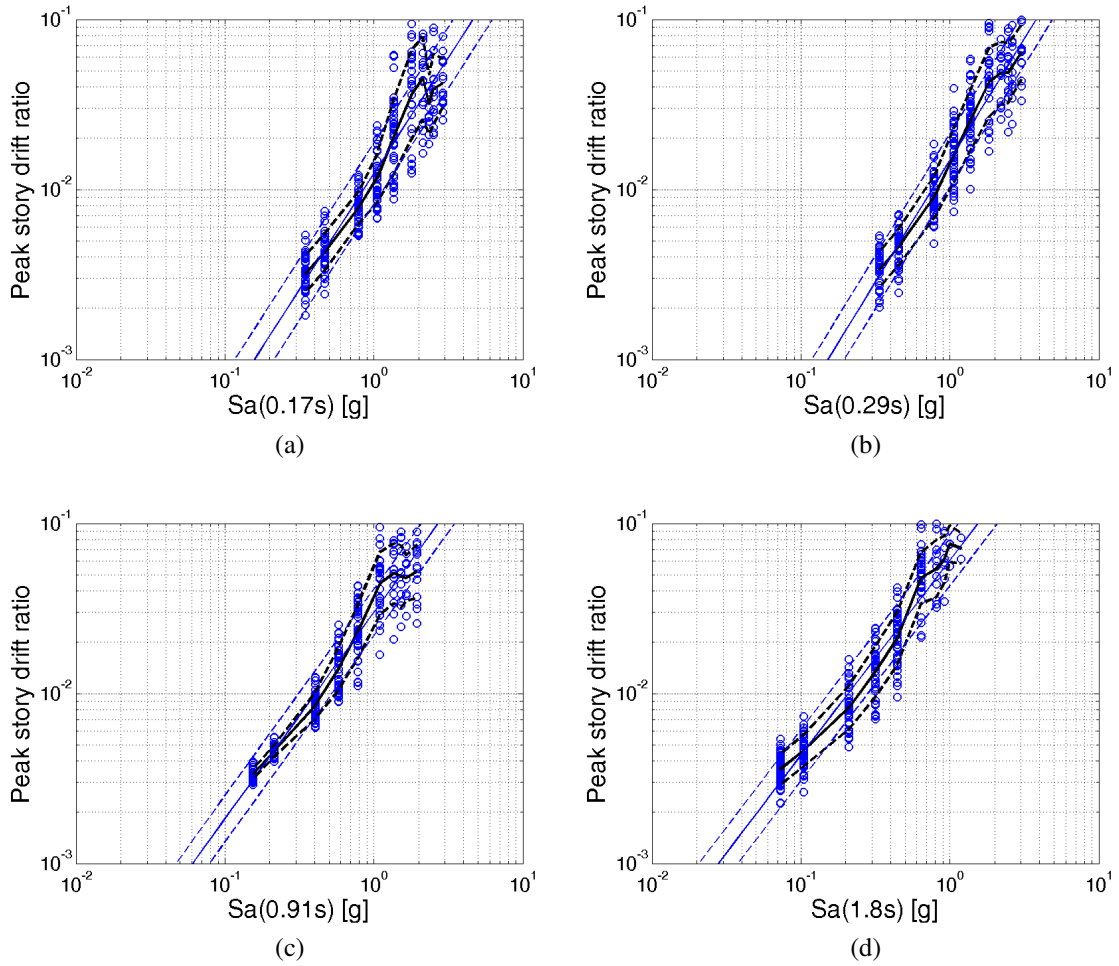


Figure A.79: 4-story perimeter frame (Building No.1008) *PSDR* at (a) $T^* = T_3$, (b) $T^* = T_2$, (c) $T^* = T_1$, and (d) $T^* = 2T_1$ for ground motions selected to match UHS.

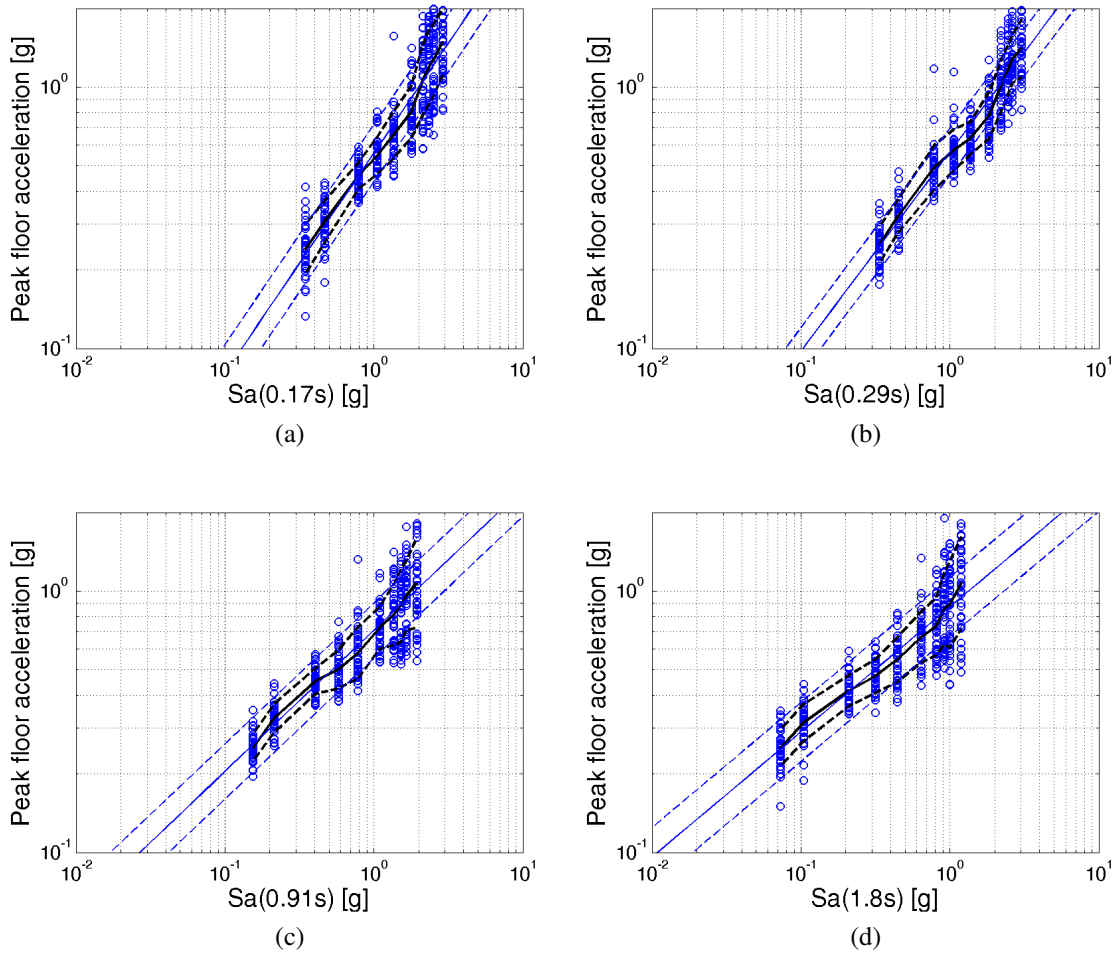


Figure A.80: 4-story perimeter frame (Building No.1008) PFA at (a) $T^* = T_3$, (b) $T^* = T_2$, (c) $T^* = T_1$, and (d) $T^* = 2T_1$ for ground motions selected to match UHS.

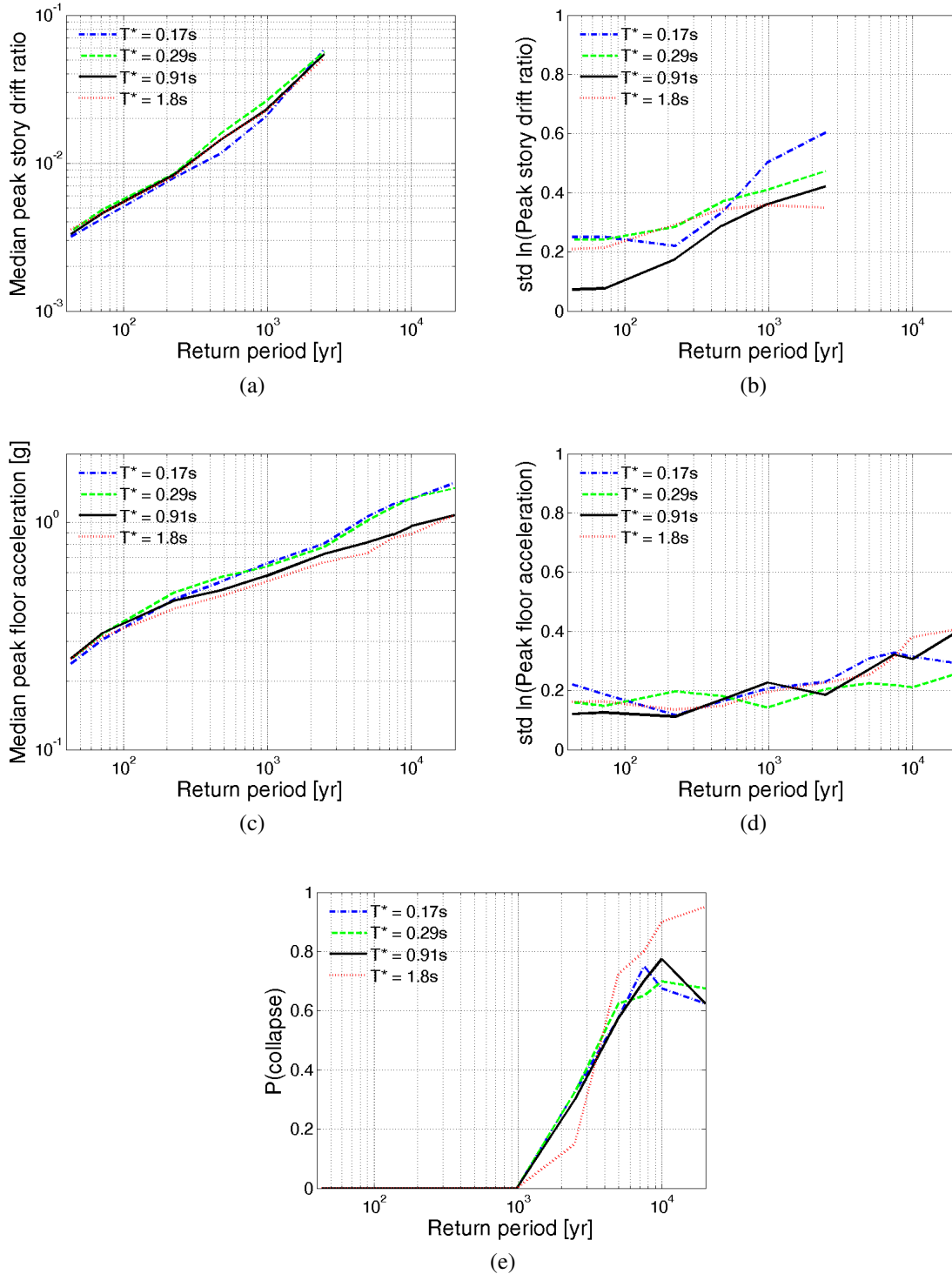


Figure A.81: 4-story perimeter frame (Building No.1008) (a) median *PSDR*, (b) logarithmic standard deviation of *PSDR*, (c) median *PFA*, (d) logarithmic standard deviation of *PFA*, and (e) probability of collapse given return period for ground motions selected to match UHS.

Bibliography

- Aagaard, B. T., R. W. Graves, A. Rodgers, T. M. Brocher, R. W. Simpson, D. Dreger, N. A. Petersson, S. C. Larsen, S. Ma, and R. C. Jachens (2010). Ground-motion modeling of hayward fault scenario earthquakes, Part II: simulation of Long-Period and broadband ground motions. *Bulletin of the Seismological Society of America* 100(6), 2945–2977.
- Abrahamson, N., Y. Bozorgnia, D. Boore, G. Atkinson, K. Campbell, W. Silva, B. Chiou, I. M. Idriss, and R. Youngs (2008). Comparisons of the NGA Ground-Motion relations. *Earthquake Spectra* 24(1), 45–66.
- Abrahamson, N. A. and L. Al Atik (2010). Scenario spectra for design ground motions and risk calculation. In *9th US National and 10th Canadian Conference on Earthquake Engineering*, Toronto, Canada.
- Abrahamson, N. A. and A. A. Yunatci (2010). Ground motion occurrence rates for scenario spectra. In *Fifth International Conference on Recent Advances in Geotechnical Earthquake Engineering and Soil Dynamics*, San Diego, CA, pp. 6.
- Aoi, S., T. Kunugi, H. Nakamura, and H. Fujiwara (2011). Deployment of new strong motion seismographs of K-net and KiK-net. In S. Akkar, P. Gulkan, T. van Eck, and A. Ansal (Eds.), *Earthquake Data in Engineering Seismology*, Volume 14 of *Geotechnical, Geological and Earthquake Engineering*, pp. 167–186. Springer Netherlands.
- ASCE (2010). *Minimum Design Loads for Buildings and Other Structures*. ASCE 7-10. Reston, VA: American Society of Civil Engineers/Structural Engineering Institute.
- Aslani, H. and E. Miranda (2005). Probability-based seismic response analysis. *Engineering Structures* 27(8), 1151–1163.

- ATC (1982). An investigation of the correlation between earthquake ground motion and building performance, ATC-10. Technical report, Applied Technology Council, Palo Alto, California.
- ATC (2009). Quantification of building seismic performance factors, FEMA P695. Technical report, Applied Technology Council, Redwood City, California.
- ATC (2011). Guidelines for seismic performance assessment of buildings, ATC-58 100% draft. Technical report, Applied Technology Council, Redwood City, California.
- Atkinson, G. M. and D. M. Boore (2003). Empirical ground-motion relations for subduction-zone earthquakes and their application to Cascadia and other regions. *Bulletin of the Seismological Society of America* 93(4), 1703–1729.
- Baker, J. W. (2005). *Vector-valued ground motion intensity measures for probabilistic seismic demand analysis*. Ph. D. thesis, Stanford University.
- Baker, J. W. (2007). Measuring bias in structural response caused by ground motion scaling. In *8th Pacific Conference on Earthquake Engineering*, Nanyang Technological University, Singapore.
- Baker, J. W. (2011). Conditional mean spectrum: Tool for ground motion selection. *Journal of Structural Engineering* 137(3), 322–331.
- Baker, J. W. and C. A. Cornell (2006a). Spectral shape, epsilon and record selection. *Earthquake Engineering & Structural Dynamics* 35(9), 1077–1095.
- Baker, J. W. and C. A. Cornell (2006b). Which spectral acceleration are you using? *Earthquake Spectra*, 22(2), 293–312.
- Baker, J. W. and C. A. Cornell (2008). Uncertainty propagation in probabilistic seismic loss estimation. *Structural Safety* 30(3), 236–252.
- Baker, J. W. and N. Jayaram (2008). Correlation of spectral acceleration values from NGA ground motion models. *Earthquake Spectra* 24(1), 299–317.

- Bazzurro, P. and C. A. Cornell (1999). Disaggregation of seismic hazard. *Bulletin of the Seismological Society of America* 89(2), 501–520.
- Benjamin, J. R. and C. A. Cornell (1970). *Probability, Statistics, and Decision for Civil Engineers*. New York: McGraw-Hill.
- Beyer, K. and J. J. Bommer (2007). Selection and scaling of real accelerograms for Bi-Directional loading: A review of current practice and code provisions. *Journal of Earthquake Engineering* 11, 13–45.
- Bommer, J. J. and F. Scherbaum (2008). The use and misuse of logic trees in probabilistic seismic hazard analysis. *Earthquake Spectra* 24(4), 997–1009.
- Bommer, J. J., S. Scott, and S. Sarma (2000). Hazard-consistent earthquake scenarios. *Soil Dynamics and Earthquake Engineering* 19, 219–231.
- Boore, D. M. and G. M. Atkinson (2008). Ground-motion prediction equations for the average horizontal component of PGA, PGV, and 5%-damped PSA at spectral periods between 0.01 s and 10.0 s. *Earthquake Spectra* 24(1), 99–138.
- Bradley, B. A. (2010a). A generalized conditional intensity measure approach and holistic ground-motion selection. *Earthquake Engineering & Structural Dynamics* 39(12), 1321–1342.
- Bradley, B. A. (2010b). OpenSHA implementation of the GCIM approach for ground motion selection. In *Southern California Earthquake Center (SCEC) Annual Meeting*, Palm Springs, CA.
- Bradley, B. A. (2012a). A ground motion selection algorithm based on the generalized conditional intensity measure approach. *Soil Dynamics and Earthquake Engineering* 40(0), 48–61.
- Bradley, B. A. (2012b). The seismic demand hazard and importance of the conditioning intensity measure. *Earthquake Engineering & Structural Dynamics* 41(11), 1417–1437.

- Bradley, B. A., R. P. Dhakal, G. A. MacRae, and M. Cubrinovski (2010a). Prediction of spatially distributed seismic demands in specific structures: Ground motion and structural response. *Earthquake Engineering & Structural Dynamics* 39(5), 501–520.
- Bradley, B. A., R. P. Dhakal, G. A. MacRae, and M. Cubrinovski (2010b). Prediction of spatially distributed seismic demands in specific structures: Structural response to loss estimation. *Earthquake Engineering & Structural Dynamics* 39(6), 591–613.
- Buratti, N., P. J. Stafford, and J. J. Bommer (2011). Earthquake accelerogram selection and scaling procedures for estimating the distribution of structural response. *Journal of structural engineering* 137(3), 345–357.
- Campbell, K. W. and Y. Bozorgnia (2008). NGA ground motion model for the geometric mean horizontal component of PGA, PGV, PGD and 5% damped linear elastic response spectra for periods ranging from 0.01 to 10 s. *Earthquake Spectra* 24(1), 139–171.
- CEN (2005). Eurocode 8: Design of structures for earthquake Resistance—Part 1: General rules, seismic actions and rules for buildings. *European Standard NF EN 1998*.
- Chiou, B., R. Darragh, N. Gregor, and W. Silva (2008). NGA project Strong-Motion database. *Earthquake Spectra* 24(1), 23.
- Chiou, B. S. J. and R. R. Youngs (2008). An NGA model for the average horizontal component of peak ground motion and response spectra. *Earthquake Spectra* 24(1), 173–215.
- Chopra, A. K. (2012). *Dynamics of structures: theory and applications to earthquake engineering* (4th ed.). Englewood Cliffs, NJ: Prentice Hall.
- Cornell, C. A. (1968). Engineering seismic risk analysis. *Bulletin of the Seismological Society of America* 58(5), 1583–1606.
- Cornell, C. A. and H. Krawinkler (2000). Progress and challenges in seismic performance assessment. *PEER Center News* 3(2).

- Deierlein, G. G. (2004). Overview of a comprehensive framework for earthquake performance assessment. In *International Workshop on Performance-Based Seismic Design Concepts and Implementation*, Bled, Slovenia, pp. 15–26.
- Ditlevsen, O. (1981). *Uncertainty modeling: with applications to multidimensional civil engineering systems*. New York; London: McGraw-Hill International Book Co.
- Dolsek, M. (2009). Incremental dynamic analysis with consideration of modeling uncertainties. *Earthquake Engineering & Structural Dynamics* 38(6), 805–825.
- Douglas, J. and H. Aochi (2008). A survey of techniques for predicting earthquake ground motions for engineering purposes. *Surv. Geophys.* 29(3), 187–220.
- Ebrahimian, H., A. Azarbakht, A. Tabandeh, and A. Akbar Golafshani (2012). The exact and approximate conditional spectra in the multi-seismic-sources regions. *Soil Dynamics and Earthquake Engineering* 39(0), 61–77.
- Esteva, L. and S. E. Ruiz (1989). Seismic failure rates of multistory frames. *Journal of Structural Engineering* 115(2), 268–283.
- GEM (2012). Global earthquake model. GEM Foundation, <http://www.globalquakemodel.org/>. Last accessed on Aug 9, 2012.
- Goda, K. and G. M. Atkinson (2011). Seismic performance of wood-frame houses in south-western british columbia. *Earthquake Engineering & Structural Dynamics* 40(8), 903–924.
- Graves, R., T. Jordan, S. Callaghan, E. Deelman, E. Field, G. Juve, C. Kesselman, P. Maechling, G. Mehta, K. Milner, D. Okaya, P. Small, and K. Vahi (2011). Cyber-Shake: A physics-based seismic hazard model for southern california. *Pure and Applied Geophysics* 168, 367–381.
- Graves, R. W. and A. Pitarka (2010). Broadband Ground-Motion simulation using a hybrid approach. *Bulletin of the Seismological Society of America* 100(5A), 2095–2123.

- Grigoriu, M. (2010). To scale or not to scale seismic ground-acceleration records. *Journal of Engineering Mechanics* 137(4), 284–293.
- Gulerce, Z. and N. A. Abrahamson (2011). Site-specific design spectra for vertical ground motion. *Earthquake Spectra* 27(4), 1023–1047.
- Han, S. W. and Y. K. Wen (1994). Method of reliability-based calibration of seismic structural parameters. Technical report, University of Illinois and Urbana-Champaign, Champaign, IL.
- Hancock, J., J. Watson-Lamprey, N. A. Abrahamson, J. J. Bommer, A. Markatis, E. McCoy, and R. Mendis (2006). An improved method of matching response spectra of recorded earthquake ground motion using wavelets. *Journal of Earthquake Engineering* 10, 67–89.
- Harmsen, S. C. (2001). Mean and modal epsilon in the deaggregation of probabilistic ground motion. *Bulletin of the Seismological Society of America* 91(6), 1537–1552.
- Hartzell, S., S. Harmsen, A. Frankel, and S. Larsen (1999). Calculation of broadband time histories of ground motion: Comparison of methods and validation using strong-ground motion from the 1994 northridge earthquake. *Bulletin of the Seismological Society of America* 89(6), 1484–1504.
- Haselton, C., J. Baker, Y. Bozorgnia, C. Goulet, E. Kalkan, N. Luco, T. Shantz, N. Shome, J. Stewart, P. Tothong, J. Watson-Lamprey, and F. Zareian (2009). Evaluation of ground motion selection and modification methods: Predicting median interstory drift response of buildings. Technical Report 2009/01, Pacific Earthquake Engineering Research Center, Berkeley, CA.
- Haselton, C. B. and J. W. Baker (2006). Ground motion intensity measures for collapse capacity prediction: choice of optimal spectral period and effect of spectral shape. In *8th National Conference on Earthquake Engineering*, San Francisco, California.
- Haselton, C. B. and G. G. Deierlein (2007). Assessing seismic collapse safety of modern reinforced concrete moment frame buildings. Technical Report 2007/08, Pacific Earthquake Engineering Research Center, Berkeley, CA.

- Ibarra, L. F. and H. Krawinkler (2005). Global collapse of frame structures under seismic excitations. Technical Report 152, John A. Blume Earthquake Engineering Center, Stanford, CA.
- Ibarra, L. F., R. A. Medina, and H. Krawinkler (2005). Hysteretic models that incorporate strength and stiffness deterioration. *Earthquake Engineering & Structural Dynamics* 34(12), 1489–1511.
- ICC (2003). *International Building Code 2003*. International Code Council.
- Iervolino, I. and C. A. Cornell (2005). Record selection for nonlinear seismic analysis of structures. *Earthquake Spectra* 21(3), 685–713.
- Jayaram, N. and J. W. Baker (2008). Statistical tests of the joint distribution of spectral acceleration values. *Bulletin of the Seismological Society of America* 98(5), 2231–2243.
- Jayaram, N., J. W. Baker, H. Okano, H. Ishida, M. W. McCann, and Y. Mihara (2011). Correlation of response spectral values in Japanese ground motions. *Earthquakes and Structures* 2(4), 357–376.
- Jayaram, N., T. Lin, and J. W. Baker (2011). A computationally efficient ground-motion selection algorithm for matching a target response spectrum mean and variance. *Earthquake Spectra* 27(3), 797–815.
- Katsanos, E. I., A. G. Sextos, and G. D. Manolis (2010). Selection of earthquake ground motion records: A state-of-the-art review from a structural engineering perspective. *Soil Dynamics and Earthquake Engineering* 30(4), 157–169.
- Kottke, A. and E. M. Rathje (2008). A Semi-Automated procedure for selecting and scaling recorded earthquake motions for dynamic analysis. *Earthquake Spectra* 24(4), 911–932.
- Kramer, S. L. (1996). *Geotechnical earthquake engineering*. Prentice-Hall International Series in Civil Engineering and Engineering Mechanics. Upper Saddle River, N.J.: Prentice Hall.

- Krawinkler, H. (2005). Van Nuys hotel building testbed report: Exercising seismic performance assessment. Technical Report 2005/11, Pacific Earthquake Engineering Research Center, Berkeley, CA.
- Krawinkler, H., R. Medina, and B. Alavi (2003). Seismic drift and ductility demands and their dependence on ground motions. *Engineering Structures* 25(5), 637–653.
- Krawinkler, H. and E. Miranda (2004). Performance-based earthquake engineering. In Y. Bozorgnia and V. V. Bertero (Eds.), *Earthquake engineering: from engineering seismology to performance-based engineering*. Boca Raton: CRC Press.
- Liel, A., C. Haselton, G. G. Deierlein, and J. W. Baker (2009). Incorporating modeling uncertainties in the assessment of seismic collapse risk of buildings. *Structural Safety* 31(2), 197–211.
- Lin, T. (2012). Probabilistic sea-level rise hazard analysis. In *Asian-Pacific Symposium on Structural Reliability and its Applications (APSSRA 2012)*, Singapore, Singapore.
- Lin, T. and J. W. Baker (2011). Probabilistic seismic hazard deaggregation of ground motion prediction models. In *5th International Conference on Earthquake Geotechnical Engineering*, Santiago, Chile.
- Lin, T., S. C. Harmsen, J. W. Baker, and N. Luco (2012). Conditional Spectrum computation incorporating multiple causal earthquakes and ground motion prediction models. *Bulletin of the Seismological Society of America* (in press).
- Lin, T., C. B. Haselton, and J. W. Baker (2012a). Conditional-Spectrum-based ground motion selection. Part I: Hazard consistency for risk-based assessments. *Earthquake Engineering & Structural Dynamics* (in review).
- Lin, T., C. B. Haselton, and J. W. Baker (2012b). Conditional-Spectrum-based ground motion selection. Part II: Intensity-based assessments and evaluation of alternative target spectra. *Earthquake Engineering & Structural Dynamics* (in review).
- Luco, N. and P. Bazzurro (2005). Effects of earthquake record scaling on nonlinear structural response. Technical report, PEER Lifelines Program.

- Luco, N. and C. A. Cornell (2007). Structure-Specific scalar intensity measures for Near-Source and ordinary earthquake ground motions. *Earthquake Spectra* 23(2), 357–392.
- Mai, P. M. and G. C. Beroza (2003). A hybrid method for calculating near-source, broadband seismograms: application to strong motion prediction. *Physics of the earth and planetary interiors* 137(1), 18.
- McGuire, R. K. (1995). Probabilistic seismic hazard analysis and design earthquakes: Closing the loop. *Bulletin of the Seismological Society of America* 85(5), 1275–1284.
- McGuire, R. K. (2004). *Seismic hazard and risk analysis*. Oakland, CA: Earthquake Engineering Research Institute.
- Moczo, P., J. O. Robertsson, L. Eisner, V. M. Ru-Shan Wu, and R. Dmowska (2007). The Finite-Difference Time-Domain method for modeling of seismic wave propagation. In *Advances in Wave Propagation in Heterogenous Earth*, Volume 48, pp. 421–516. Elsevier.
- Moehle, J. and G. G. Deierlein (2004). A framework methodology for performance-based earthquake engineering. 13th World Conference on Earthquake Engineering, Vancouver, BC, Canada.
- Naeim, F. and M. Lew (1995). On the use of design spectrum compatible time histories. *Earthquake Spectra* 11(1), 111–127.
- NIST (2011). Selecting and scaling earthquake ground motions for performing response-history analyses, NIST GCR 11-917-15. Technical report, prepared by the NEHRP Consultants Joint Venture for the National Institute of Standards and Technology, Gaithersburg, Maryland.
- OpenSEES (2011). Open system for earthquake engineering simulation. Pacific Earthquake Engineering Research Center, <http://opensees.berkeley.edu/>. Last accessed on Sep 9, 2011.
- Petersen, M. D., A. D. Frankel, S. C. Harmsen, C. S. Mueller, K. M. Haller, R. L. Wheeler, R. L. Wesson, Y. Zeng, O. S. D. M. Perkins, N. Luco, E. H. Field, C. J. Wills, and

- K. S. Rukstales (2008). Documentation for the 2008 update of the United States national seismic hazard maps: U.S. Geological Survey Open-File Report 2008–1128. Technical report.
- Porter, K. A., J. L. Beck, and R. Shaikhutdinov (2002). Sensitivity of building loss estimates to major uncertain variables. *Earthquake Spectra* 18(4), 719–743.
- Reiter, L. (1990). *Earthquake hazard analysis: Issues and insights*. New York: Columbia University Press.
- Rezaeian, S. and A. Der Kiureghian (2010). Simulation of synthetic ground motions for specified earthquake and site characteristics. *Earthquake Engineering & Structural Dynamics* 39(10), 1155–1180.
- Rezaeian, S. and A. D. Kiureghian (2008). A stochastic ground motion model with separable temporal and spectral nonstationarities. *Earthquake Engineering & Structural Dynamics* 37(13), 1565–1584.
- Sasani, M. and A. D. Kiureghian (2001). Seismic fragility of RC structural walls: Displacement approach. *Journal of Structural Engineering* 127(2), 219–228.
- Scherbaum, F., J. J. Bommer, H. Bungum, F. Cotton, and N. A. Abrahamson (2005). Composite ground-motion models and logic trees: Methodology, sensitivities, and uncertainties. *Bulletin of the Seismological Society of America* 95(5), 1575–1593.
- Scherbaum, F., J. Schmedes, and F. Cotton (2004). On the conversion of source-to-site distance measures for extended earthquake source models. *Bulletin of the Seismological Society of America* 94(3), 1053–1069.
- Shahi, S. K. and J. W. Baker (2011). An empirically calibrated framework for including the effects of near-fault directivity in probabilistic seismic hazard analysis. *Bulletin of the Seismological Society of America* 101(2), 742–755.
- Shantz, T. (2006). Selection and scaling of earthquake records for nonlinear dynamic analysis of first model dominated bridge structures. In *8th U.S. National Conference on Earthquake Engineering*, San Francisco, CA.

- Shinozuka, M., M. Q. Feng, J. Lee, and T. Naganuma (2000). Statistical analysis of fragility curves. *Journal of Engineering Mechanics* 126(12), 1224–1231.
- Shome, N. and C. A. Cornell (1999). Probabilistic seismic demand analysis of nonlinear structures. Technical Report RMS-35, RMS Program, Stanford, CA.
- Shome, N., C. A. Cornell, P. Bazzurro, and J. E. Carballo (1998). Earthquakes, records, and nonlinear responses. *Earthquake Spectra* 14(3), 469–500.
- Shome, N. and N. Luco (2010). Loss estimation of multi-mode dominated structures for a scenario of earthquake event. In *9th US National and 10th Canadian Conference on Earthquake Engineering*, Toronto, Canada, pp. 10.
- Silva, W. J. and K. Lee (1987). WES RASCAL code for synthesizing earthquake ground motions. Technical Report Report 24, Dept. of the Army, US Army Corps of Engineers.
- Somerville, P. G. and R. O. Hamburger (2009). Development of ground motion time histories for design. In *Seismic Mitigation for Museum Collection: Papers from the J. Paul Getty Museum - National Museum of Western Art (Tokyo) Jointly Sponsored Symposium*, Tokyo, Japan.
- Somerville, P. G. and H. K. Thio (2011). Development of ground motion time histories for seismic design. In *Proceedings of the Ninth Pacific Conference on Earthquake Engineering*, Auckland, New Zealand.
- Song, J. and B. R. Ellingwood (1999). Seismic reliability of special moment steel frames with welded connections: I. *Journal of Structural Engineering* 125(4), 357–371.
- Stewart, J. P., S. Chiou, J. D. Bray, R. W. Graves, P. G. Somerville, and N. A. Abrahamson (2001). Ground motion evaluation procedures for Performance-Based design. Technical Report 2001/09, Pacific Earthquake Engineering Research Center, Berkeley, CA.
- Stoica, M., R. A. Medina, and R. H. McCuen (2007). Improved probabilistic quantification of drift demands for seismic evaluation. *Structural Safety* 29(2), 132–145.

- Strasser, F. O., J. J. Bommer, and N. A. Abrahamson (2008). Truncation of the distribution of ground-motion residuals. *Journal of Seismology* (12), 79–105.
- Straub, D. and A. D. Kiureghian (2008). Improved seismic fragility modeling from empirical data. *Structural Safety* 30(4), 320–336.
- Taghavi, S. and E. Miranda (2003). Response assessment of nonstructural building elements. Technical Report 2003/05, Pacific Earthquake Engineering Research Center, Berkeley, CA.
- Thrainsson, H. and A. S. Kiremidjian (2002). Simulation of digital earthquake accelerograms using the inverse discrete fourier transform. *Earthquake Engineering & Structural Dynamics* 31(12), 2023–2048.
- USGS (2012). 2008 Interactive Deaggregations (Beta). Earthquake Hazards Program, <http://eqint.cr.usgs.gov/deaggint/2008/>. Last accessed on Jun 18, 2012.
- Vamvatsikos, D. and C. A. Cornell (2002). Incremental dynamic analysis. *Earthquake Engineering & Structural Dynamics* 31(3), 491–514.
- Vamvatsikos, D. and C. A. Cornell (2004). Applied incremental dynamic analysis. *Earthquake Spectra* 20(2), 523–533.
- Vetter, C. and A. A. Taflanidis (2012). Global sensitivity analysis for stochastic ground motion modeling in seismic-risk assessment. *Soil Dynamics and Earthquake Engineering* 38(0), 128–143.
- Wang, G. (2011). A ground motion selection and modification method capturing response spectrum characteristics and variability of scenario earthquakes. *Soil Dynamics and Earthquake Engineering* 31(4), 611–625.
- Watson-Lamprey, J. and N. A. Abrahamson (2006). Selection of ground motion time series and limits on scaling. *Soil Dynamics and Earthquake Engineering* 26(5), 477–482.
- Winterstein, S. R., T. Ude, and C. A. Cornell (1993). Environmental parameters for extreme response: Inverse FORM with omission factors. In *6th International Conference on Structural Safety and Reliability*, Innsbruck, Austria, pp. 551–557.

- Yamamoto, Y. and J. W. Baker (2011). Stochastic model for earthquake ground motions using wavelet packets. In *11th International Conference on Applications of Statistics and Probability in Soil and Structural Engineering (ICASP11)*, Zurich, Switzerland, pp. 8.
- Youngs, R. R., S.-J. Chiou, W. Silva, and J. Humphrey (1997). Strong ground motion attenuation relationships for subduction zone earthquakes. *Seismological Research Letters* 68(1), 58–73.
- Zhao, J. X., J. Zhang, A. Asano, Y. Ohno, T. Oouchi, T. Takahashi, H. Ogawa, K. Irikura, H. K. Thio, P. G. Somerville, Y. Fukushima, and Y. Fukushima (2006). Attenuation relations of strong ground motion in Japan using site classification based on predominant period. *Bulletin of the Seismological Society of America* 96(3), 898–913.